LOAD-DISPLACEMENT BEHAVIOR OF FRAME STRUCTURES COMPOSED OF FIBER REINFORCED POLYMERIC COMPOSITE MATERIALS

A Thesis
Presented to
The Academic Faculty

by

Gwang-Seok Na

In Partial Fulfillment
of the Requirements for the Degree
Doctor of Philosophy in the
School of Civil and Environmental Engineering

Georgia Institute of Technology
December 2008

LOAD-DISPLACEMENT BEHAVIOR OF FRAME STRUCTURES COMPOSED OF FIBER REINFORCED POLYMERIC COMPOSITE MATERIALS

Approved by:

Dr. Leroy Z. Emkin, Co-advisor
School of Civil and Environmental Engineering
Georgia Institute of Technology

Dr. Abdul-Hamid Zureick, Co-advisor
School of Civil and Environmental Engineering
Georgia Institute of Technology

Dr. Kenneth M. Will
School of Civil and Environmental Engineering
Georgia Institute of Technology

Dr. Rami M. Haj-Ali
Civil and Environmental Engineering
Georgia Institute of Technology

Dr. Dewey H. Hodges
School of Aeospace Engineering
Georgia Institute of Technology

Date Approved: November 10, 2008

ACKNOWLEDGEMENTS

The author wishes to express his sincere appreciation and profound gratitude to Dr. Leroy Z. Emkin and Dr. Abdul-Hamid Zureick for their guidance, encouragement, patience and support during the course of this study. The author would also like to acknowledge the invalueable comments and suggestions provided by the members of his reading committee, Dr. Kenneth M. Will, Dr. Dewey H. Hodges and Dr. Rami Haj-Ali.

Deep thanks go to the author's fellow colleagues at the Georgia Institute of Technology for providing a stimulating and fun environment in which to learn and grow.

The author wishes to thank his wife Hye-Sook, and his two daughters, Hyun-Jin and Yu-Jin, for their endless patience, support, and love that they provided through many difficult times. The author would have never achieved his goals without their being an integral part of his life. Most of all, deep thanks and love go out to the author's parents, Seoung-Duk Na and Soon-Re Kim, for their unconditional love, sacrifice and support through good and bad times. To them the author dedicates this thesis.

TABLE OF CONTENTS

LIST OF TABLES

LIST OF FIGURES

NOMENCLATURE

GENERAL

a	Loading location of concentrated loading
a_s, a_e	Start-point and end-point of distributed loading
d_X	Joint displacement in global X direction
Δd_X	Change of joint displacement in global X direction
E^{CSM}	Young's modulus of CSM layers
E_L^{RL}	Longitudinal modulus of roving layers
E_T^{RL}, E_N^{RL}	Transverse, normal moduli of roving layers
E_f	Longitudinal modulus of anisotropic fiber
E_L	Longitudinal modulus of component of cross-section
E_L^t, E_L^c	Longitudinal moduli of component of cross-section measured from tension, compression tests, respectively
$E_{L,0.05}^t, E_{L,0.05}^c$	$x_{0.05}$ of E_L^t, E_L^c, respectively
$E_{L,0.05}^t, E_{L,0.05}^c$	x_{char} of E_L^t, E_L^c, respectively
E_m	Young's modulus of matrix system
E_T	Transverse modulus of component of cross-section
e_x	Axial deformation measure along axis x
e_y, e_z	Shear deformation measure along axes y, z
$\mathbf{F}_{BB}$	6 by 6 flexibility matrix for a cantilever with free joint 'B'
$\overline{F}_B$	Translation member end forces vector at joint B sides (3 by 1)
F_L^{ut}, F_L^{uc}	Longitudinal strengths of component of cross-section measured from tension, compression tests, respectively
$F_{L,char}^t, F_{L,char}^c$	x_{char} of F_L^{ut}, F_L^{uc}, respectively
F_{LT}	In-plane shear strength
F_x	Axial force resultant along axis x
F_y, F_z	Shear force resultants about axes y, z
G^{CSM}	Shear modulus of CSM layers
G_{LT}	In-plane shear modulus of component of cross-section
G_{LT}^{RL}	In-plane shear modulus of roving layer
$G_{LT,0.05}$	$x_{0.05}$ of G_{LT}
$G_{LT,char}$	x_{char} of G_{LT}
G_m, G_{filler}, G_r	Shear moduli of the matrix, filler, and resin, respectively
$\mathbf{K}$	Space frame natural stiffness matrix

$\mathbf{K_{BB}}$	6 by 6 stiffness matrix for a cantilever with free joint 'B'
K_m, K_{filler}, K_r	Bulk modulus of the matrix, filler, and resin
k_x	Rotation rate about axis x
k_y, k_z	Curvatures about axes y and z
L	Member total length
L	Longitudinal direction in local reference frame of the component of a cross section of member
$\overline{M}_B$	Moment member end forces vector at joint B sides (3 by 1)
M_x	Torsional force resultant about axis x
M_y, M_z	Moment resultant about axes y, z
N	Normal direction in local reference frame of the component of a cross section of member
n	Number of connector
P	Applied loading
$P_x,\ P_y,\ P_z$	Member end concentrated forces x, y, and z components, respectively
P_1	Maximum axial member force in diagonal members
$\overline{P}_a$	Concentrated member translational loading vector at $x = a$
$Q_x,\ Q_y,\ Q_z$	Member end concentrated moments x, y, and z components, respectively
$\overline{Q}_a$	Concentrated member moment loading vector at $x = a$ (3 by1)
R	Sub matrix of sectional flexibility matrix (3 by 3)
S	Sectional stiffness
sc_y, sc_z	Shear center location in terms of axes y an z
T	Sub matrix of sectional flexibility matrix (3 by 3)
T	Transverse direction in local reference frame of the component of a cross section of member
t	Thickness of a plate
U	Reduction factor
$u_x,\ u_y,\ u_z$	Member end displacements
$\overline{u}_a$	Displacement vector at $x = a$ (3 by1)
$\overline{u}_B$	Displacement vector of joint B (3 by1)
$\mathrm{v}^m_{\mathrm{filler}}, \mathrm{v}^m_{\mathrm{void}}, \mathrm{v}^m_{\mathrm{resin}}$	Volume fractions of filler, void, and resin in the matrix system, respectively
$\mathrm{v}_{\mathrm{RL}},\ \mathrm{v}_{\mathrm{CSM}}$	Volume fractions of roving and CSM layers, respectively
$\mathrm{v}^{\mathrm{CSM}}_{\mathrm{f}},\ \mathrm{v}^{\mathrm{CSM}}_{\mathrm{m}}$	Volume fractions of fiber and matrix in CSM layer, respectively
$\mathrm{v}^{\mathrm{RL}}_{\mathrm{f}},\ \mathrm{v}^{\mathrm{RL}}_{\mathrm{m}}$	Volume fractions of fiber and matrix in roving layer, respectively
$x_{0.05}$	Nominal value of the sample data as the 5^{th} percentile of two-parameter Weibull distribution
x_{char}	Characteristic value

X, Y, Z	X, Y, Z directions in global reference frame, respectively
x, y, z	x, y, z directions in local reference frame, respectively
Z	Sub matrix of sectional flexibility matrix (3 by 3)
1, 2, 3	Local reference frame of a single layer of FRP materials

GREEK SYMBOLS

$\hat{\alpha}$	Estimated Weibull scale parameter
$\hat{\beta}$	Estimated Weibull shape parameter
γ	Shear strain
γ_{LT}	In-plane shear at failure
ε	Strain
$\varepsilon_L^t, \varepsilon_L^c$	Tension, compression ultimate strains in longitudinal direction, respectively
κ_x	Rotation rate about axis x
κ_y, κ_z	Curvatures about axes y, z
ξ	Empirical parameter for Halpin-Tsai equation
ν^{CSM}	Poisson's ratio of CSM layers
ν_{LT}	Poisson's ratios of component of cross section
ν_{LT}^t, ν_{LT}^c	Poisson's ratios measured from tension, compression tests, respectively
ν_m	Poisson's ratios of matrix
σ	Stress
τ	Shear stress
Φ	Sectional flexibility matrix
Ω	Data confidence factor that account for the uncertainty associated with a finite sample size
$\overline{\varpi}_a$	Rotation vector at $x = a$ (3 by1)
$\overline{\varpi}_B$	Rotation vector of joint B (3 by1)
ξ	Empirical parameter

SUMMARY

This thesis addresses the results of an experimental and analytical investigation aimed at examining the static load-displacement response of braced plane frame structures composed of fiber reinforced polymeric (FRP) composite material structural members manufactured by the pultrusion process.

In the experimental part of this investigation, 18 full-scale lateral loading tests for FRP composite frames with different brace configurations and beam column connection types were performed. The load-displacement responses of such frames were measured and are reported herein.

In the analytical part of this investigation, a frame analysis method that accounts for the anisotropic nature of FRP composite material structural members was investigated.

The results from the experimental work are compared with the results from the analytical procedures. The effects of various structural parameters of the frame, such as (1) effective mechanical material properties of members, (2) beam-column connection types, and (3) the influence of diagonal structural members on the lateral load-displacement response of the braced plane frames, are also investigated.

The numerical load-displacement results from the proposed FRP composite frames analysis procedure provided good agreement with the results from the full-scale laboratory tests.

CHAPTER 1
INTRODUCTION AND PREVIOUS RESEARCH

1.1 Introduction

As a result of a great need for materials that have desirable characteristics such as high strength to weight ratio, excellent corrosion resistance, and tailorability of engineering material properties, the study of structural members composed of fiber reinforced polymeric (FRP) composite materials in general civil engineering frame structures has been growing (Zureick, 1998).

As FRP composite structural members are used as load bearing members in structural frames (Figure 1.1), the load-displacement response under lateral loads (e.g., wind or earthquake) becomes an important factor in the design process. However, structural analysis techniques currently used to analyze structures whose members are composed of FRP composite materials have not been adequately developed. As the use of FRP composite materials in civil engineering frame structures continues to grow, there is a need to develop a practical frame analysis methodology that accounts for the influence of such anisotropic materials on the behavior of members and the structures assembled from such members.

Figure 0.1: Example of building construction using FRP composite structural members (Courtesy of Creative Pultrusion)

1.2 Objectives

The objective of this work is to experimentally and analytically examine the load-displacement response of a braced frame structure whose members are composed of FRP composite material structural members manufactured by the pultrusion process. The load-displacement response results from full-scale lateral loading frame tests of eighteen braced frame configurations are compared with the results from analytical procedures that account for the anisotropic nature of the FRP composite structural member components.

The effect of various parameters such as the (1) effective mechanical material properties of members, (2) beam-column connection types, and (3) presence of diagonal members on the load-displacement response of the FRP composite frames will be examined. Understanding the relationship among the various parameters and the load-displacement behavior is expected to provide practical analysis and design procedures.

1.3 Previous Research

This section reviews the previous research that has been conducted to understand the load-displacement responses of FRP composite frames.

Section 1.3.1 reviews the analytical methods which are fundamental to analytically predict the load-displacement response of an isolated FRP structural member. This section summarizes research associated with predicting load-displacement behavior of isolated structural members composed of isotropic and also anisotropic materials.

Section 1.3.2 reviews previous research related to the load-displacement behavior of a frame composed of multiple FRP composite material structural members and their connections

1.3.1 Analytical Methods Related to the Load-Displacement Behavior of an Isolated Structural Member

The Bernoulli beam assumptions (Timoshenko, 1953) dating back to the 17th century, have long been recognized as a convenient approximation for the flexural behavior of slender structural members and served as a cornerstone for structural analysis. He assumed that plane sections normal to the centroidal axis of a member remain plane and normal to the centroidal axis after deformation, and suggested that the curvature of an elastic beam is always proportional to the bending moment of that point.

Another well known structural member theory was introduced by Timoshenko (Timoshenko, 1922). Timoshenko structural member theory accounted for the shear deformation effect of a structural member. This means that plane sections normal to the

centroidal axis of a member do not need to remain normal to the centroidal axis after deformation.

Cowper (1966) extended the theoretical work of Timoshenko by utilizing three dimensional elasticity solutions that present the shear correction factors of specific cross-sections in terms of the geometry of the cross-section and Poisson's ratio of the material.

For the torsional behavior of a structural member, Saint-Venant (Saint-Venant, 1855) assumed the following two important assumptions.

(1) Member cross-section warping is not constrained in the axial direction of the member. This assumption is frequently referred to as free warping of the cross section.

(2) Member cross-sections remain rigid in the plane during torsion.

(3) Axial deformation is assumed uniform along the member.

Gjelsvik (1981) summarized the following three assumptions commonly adopted in developing engineering theory of thin-walled members composed of isotropic materials (see Figure 0.2).

(1) The contour does not deform in its own plane

(2) Shear strain is zero in the components (e.g., web and flange) of member sections. This assumption was postulated in the explicit form by Vlasov (1961) and frequently referred to as the Vlasov assumption.

(3) Each component of a member cross section behaves as a thin shell. This means that the straight line remains normal to the middle plane during the deformation. For the member to qualify as thin walled, thickness must be small compared to the length of a component of the member cross section.

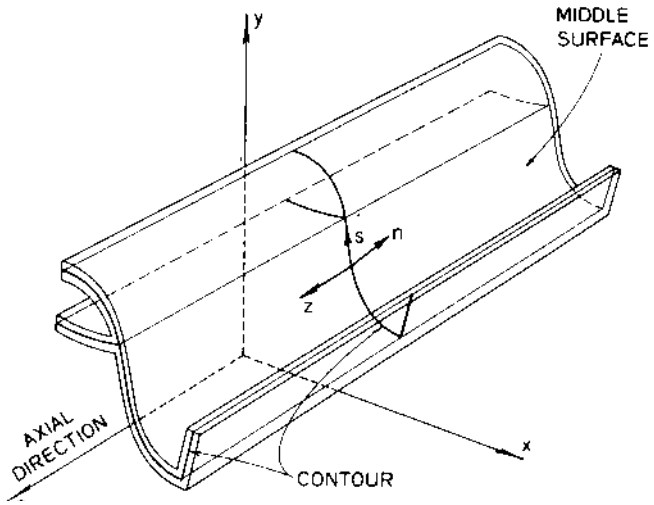

Fig. 1.1. General form of an open bar.

Figure 0.2: General form of a thin walled member (Gjelsvik, 1981)

Vlasov (1961) introduced a new stiffness term called 'warping stiffness' for the thin-walled structural members using the above assumption (2). If axial deformations of a cross-section are restrained at some specific location along a member, the torsional rigidity can be greatly modified due to the warping restraint.

However, the preceding analytical methods were formulated for structural members composed of isotropic materials. Those analytical methods were therefore useful when applied to the prediction of the load-deformation behavior of structural frame systems composed of isotropic materials. However, for structural frame systems composed of anisotropic materials, the above analytical methods are not applicable in their original form.

As anisotropic (e.g., fiber reinforced polymeric composite) materials have begun to be used widely in aerospace structural engineering applications, new analytical methods related to the load-deformation behavior of structural members also have been

developed. Rehfield (1982) accounted for additional stress components such as non-classical axial stresses and transverse-normal stress that were ignored in previously introduced structural member analytical methods for members composed of isotropic materials. Rehfield accounted for these two additional stress components to predict analytically the deflection behavior of anisotropic simple-beams and cantilever beams with uniform loading configurations.

Bauld and Tzeng (1983) tried to extend Vlasov (1961)'s analytical method of predicting deformation behavior of a thin walled isotropic material structural member for a structural member composed of FRP laminated plates. In addition to the three assumptions that Gjelsvik (1981) summarized, Bauld and Tzeng added the following two additional assumptions to account for the FRP laminate plates:

(1) Each component of a cross-section obeys classical lamination constitutive relationships

(2) Layer pattern of a component of a cross-section is always symmetric with respect to its middle plane.

Barbero (1993) derived a formula to construct the beam sectional stiffness of thin-walled structural members composed of laminated plates using Classical Lamination Theory (CLT) (Jones, 1975). First, the constitutive relations of each wall are determined by using CLT. By equating the sum of all cross-sectional strain energies of the walls to the total cross-sectional strain energy of the beam, unknown cross-sectional stiffness properties were determined by using the Variational method. In Barbero's approach, the Timoshenko beam assumption is utilized to account for the transverse shear strain of the member cross-section. Barbero's approach assumed that there is no strain along the

direction transverse to the member centroidal axis in the components (e.g., flange, web) of a member cross-section.

Two important procedures were subsequently developed to overcome the limitations of previously introduced anisotropic structural member analysis methods. First, Berdichevsky (1981) found that three-dimensional elasticity analysis for beam-like structure can be split into a one-dimensional analysis part and a two-dimensional analysis part that makes cross-sectional stiffness constants. Secondly, Danielson and Hodges (1987) presented a new beam kinematical description that can capture all possible displacement components (e.g., in-plane & out-of-plane displacements) in a member cross-section. These two procedures were combined to present a new structural member theory for general anisotropic structural members (Hodges et al., 1992). This new member theory was called the Variational Asymptotic Beam Sectional (VABS) analysis method. Hodges used a finite element technique in order to develop the cross-sectional stiffness of a member that relates beam resultant forces and centroidal deformation measures of a member cross-section, instead of simply combining the laminated plate stiffness terms[1] of each component (e.g., flange and webs) of the cross-section of the member to construct a member cross-sectional stiffness.

Hodges (2006) showed the close correlations of results from the previously published experimental results and the analytically predicted member load-deformation behavior using the VABS theory for a single member extensively.

Figures 1.3a and 1.3b show examples of cross-sections investigated by Hodges. Figure 0.3a shows an member cross-section used to find area properties of inverted T-

[1] Laminated plate stiffness terms represent A, B, and D stiffness terms for a laminated plate (See Jones, 1975). These three stiffness terms represent axial, coupling, and bending stiffness, respectively.

shape cross section composed of isotropic material (Yu et al., 2002). Figure 0.3b shows a member cross section used to obtain a sectional stiffness of the member cross section composed of laminated composite layers (Cesnik, 1994). By using the VABS finite element technique, a general cross-section can be modeled permitting a complex cross-section (e.g., helicopter blade) to be modeled for the stiffness calculation. The VABS analysis method can generate structural member cross-sectional stiffness that can be used for space frame member natural stiffness matrices for use in conventional space-frame analysis procedures. Cesnik (1994) successfully applied this method to the classical beam problem (i.e. without using transverse shear effect) for both isotropic and anisotropic materials. He also developed "alternative theory" to account for transverse shear effect. However, Yu and Hodges (2002) extended the VABS analysis method to account for shear deformation effects[3] and the Vlasov torsion effect with asymptotically correct theoretical basis.

Although the VABS analysis method is known to generate more refined results for a single isolated member (e.g., helicopter blade or turbine blade) than other analytical methods for the prediction load-displacement behavior, there has been no such study or application for full-scale frame structure composed of multiple FRP composite structural members for civil/structure applications. Therefore, a new study to apply and verify the application of the VABS method for civil engineering structural frameworks composed of FRP members would be of great value to civil/structural engineering.

[3] This beam type was named as a "Timoshenko like beam" in Hodges' literature

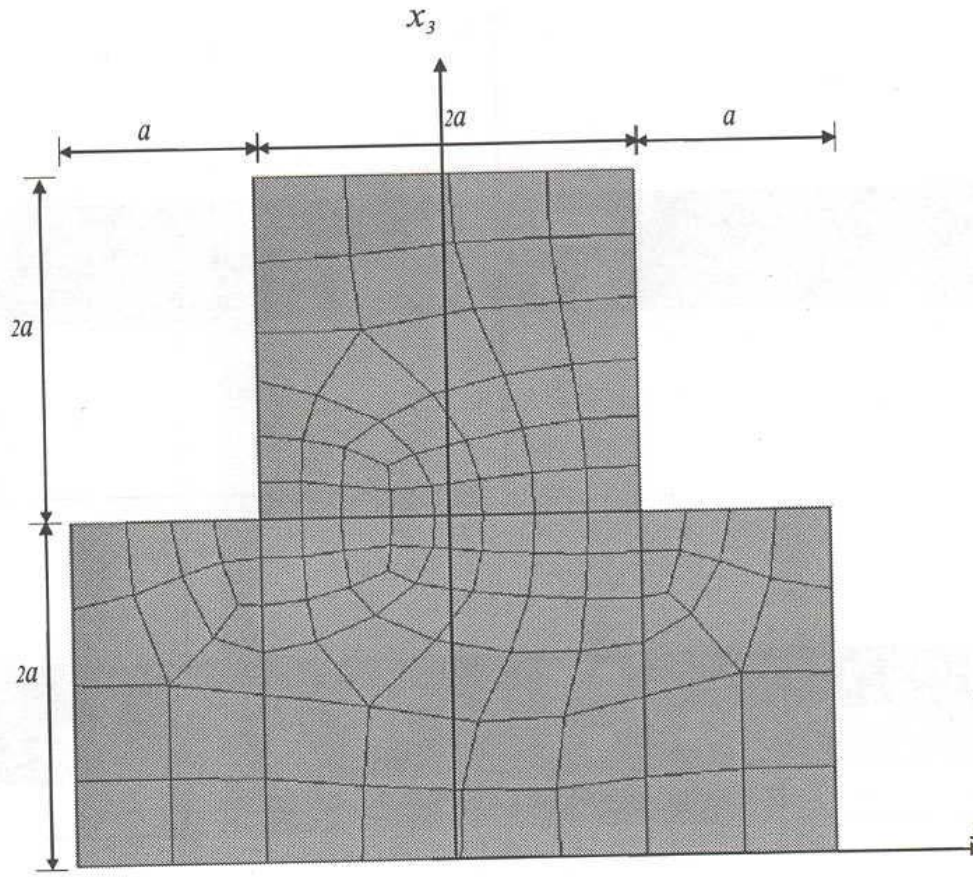

Figure 0.3a: Member cross-section examples - isotropic material (Yu and Hodges, 2005)

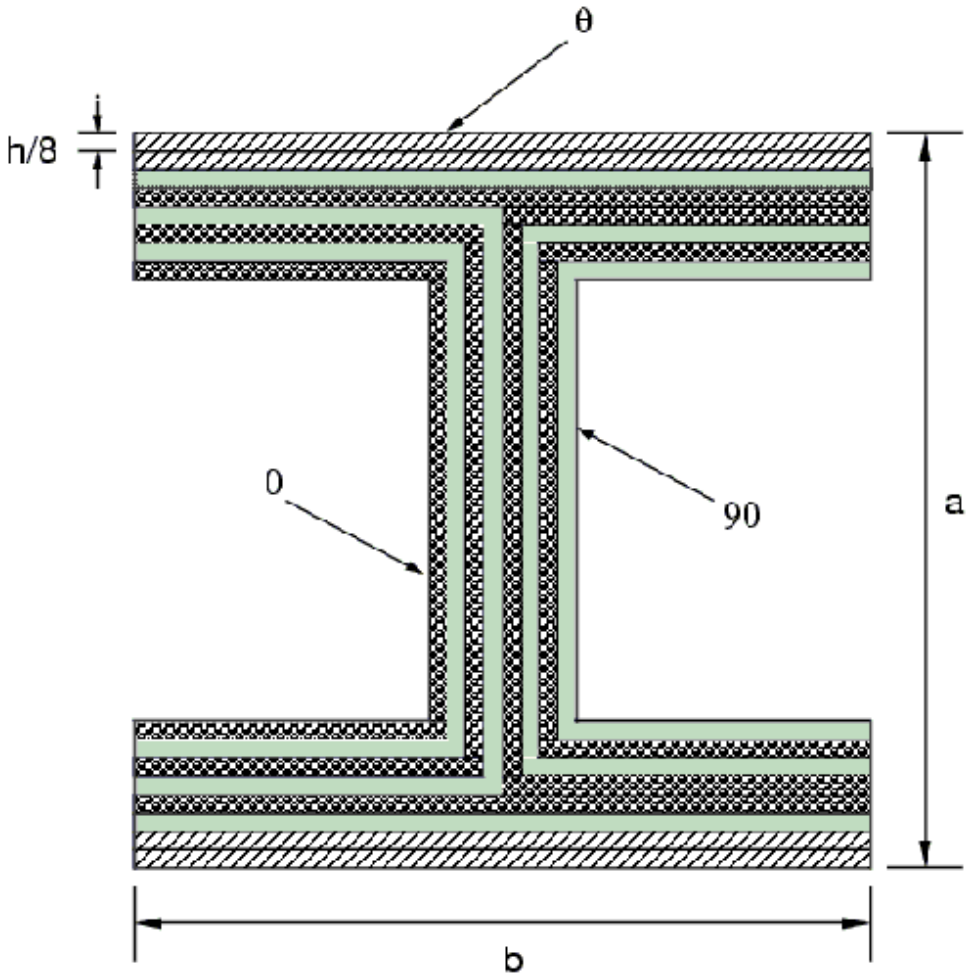

Figure 1.3b: Member cross-section examples - Anisotropic material (Cesnik, 1994)

The previously introduced analysis methods for anisotropic structural members assumed linear elastic material behavior. To overcome the limitations of linear anlysis, Haj-Ali et al. (2001) proposed a 3D micromechanical modeling framework for general nonlinear analysis of pultruded composite FRP material frame structures (Figure 0.4). The pultruded FRP materials were modeled by using multi-scale micro-mechanics models. A 'sublaminate model' was used to generate the 3D effective behavior of the material. The proposed multi-scale micro-mechanics model was integrated into general finite element software for 2D and 3D finite elements. The method showed refined

correlations with experimental results for material nonlinear analysis of structural models composed of 2D and 3D finite elements (Haj-Ali et al., 2007). However, this approach was developed for structural models composed of 2D and 3D finite elements, but not for structural models composed of 1D members.

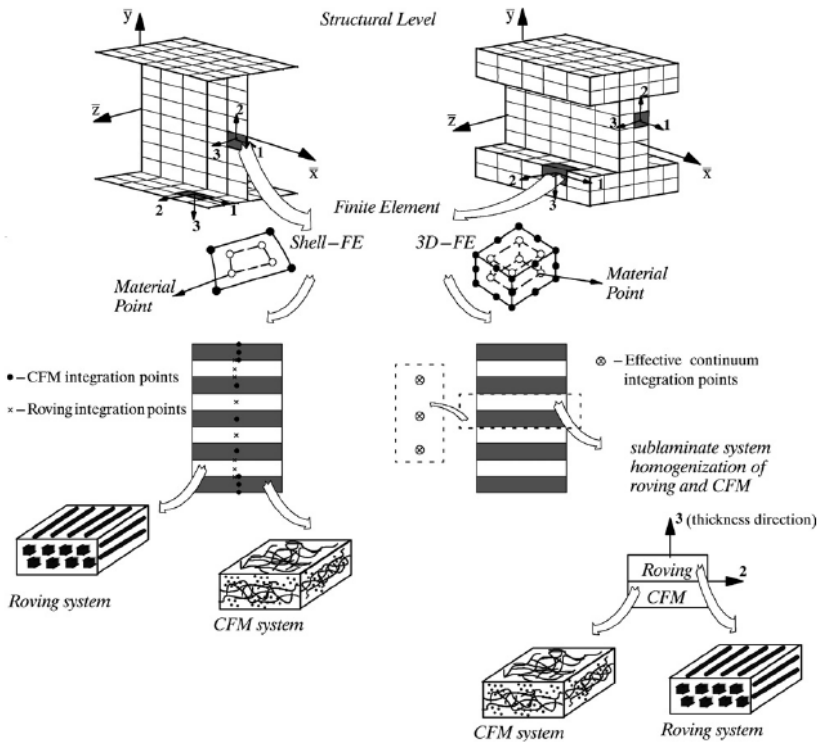

Figure 0.4: A framework for 3D nonlinear analysis of pultruded composite structures (Haj-Ali et al., 2007)

1.3.2 Static Load-Deformation Behavior of Structural Frames Composed of FRP Composite Materials

Little research has been reported on the load-deformation behavior of full-scale frames composed of fiber reinforced polymeric a composite material members. Bank (1989) conducted an analysis of portal frames constructed of pultruded FRP structural members. It was notable that, in the frame analytical study, Bank experimentally measured the member flexural rigidity and shear rigidity[4] of each member in order to construct the structural member stiffness of each member in the frame for the analysis. However, because Bank did not conduct the actual frame test to measure load-deformation behavior, analytically predicted load-deformation results of the frame could not be compared to the experimentally measured frame test results. Beam-column connections were assumed as rigid.

Mosallam and Bank (1992) performed the first experimental studies on the static load-displacement response of small FRP composite portal frames, 6 ft high by 9 ft wide, (Figure 0.5). The frames were subjected to static vertical loadings on the beams, and deflections and strains were measured. Mosallam's frame test results were compared to the frame analysis results that were based on an analytical method for single members presented by Bank (1987)[5]. Also, Mosallam and Bank (1992) considered the semi-rigid beam-column connections in the analysis models. Based on the test set-up as described by Mosallam and Bank (1992) as shown in Figure 0.5, out-of-plane displacement during loading such as those caused by lateral-torsional buckling only appears to be partially prevented.

[4] Bank used four point loading test to experimentally measure flexural rigidity and shear rigidity together.
[5] The method, which uses refined shear coefficient for laminated member, was discussed in Section 1.3.1, page 6.

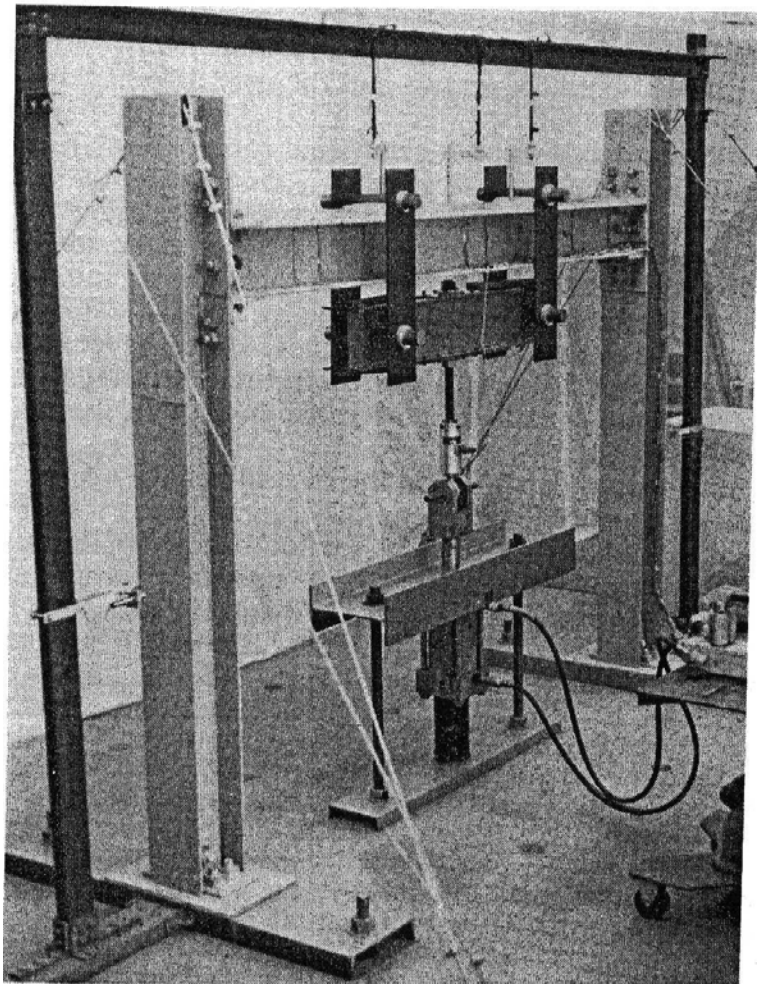

Figure 0.5: Mosallem's frame test setup (Mosallam and Bank, 1992)

Liu (1998) modeled the frames tested by Mosallam and Bank (1992) with NASTRAN by using its LAMINATE composite shell finite element in order to reflect the characteristics of composite materials (Figure 0.6). Liu compared these results with Mosallam's experimental and analytical results. The analytical results showed close correlations with experimental results.

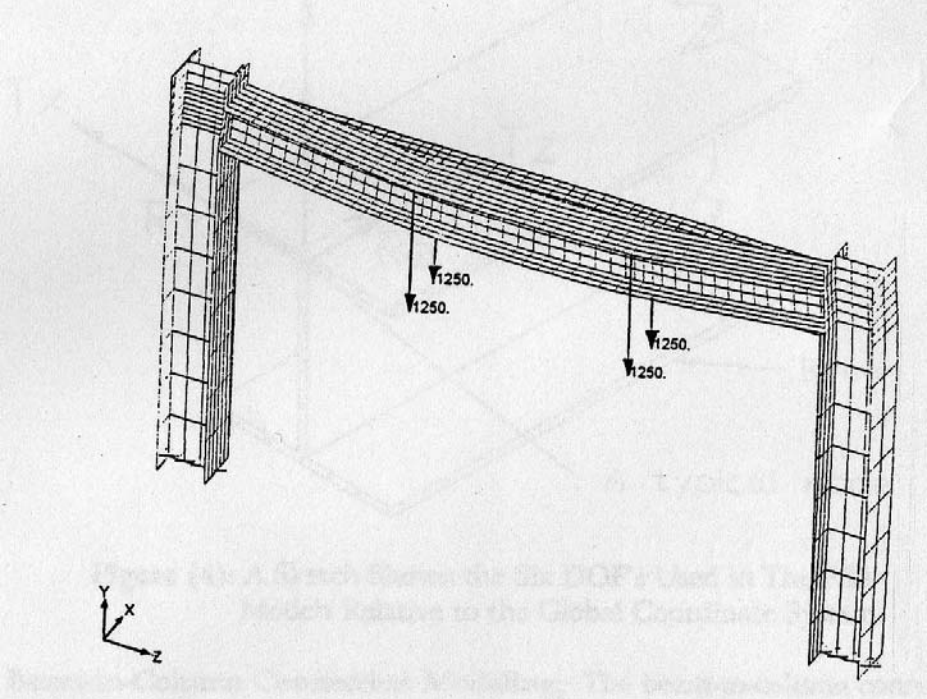

Figure 0.6: Liu's FEA model (Liu et al., 1998)

Turvey (1996) conducted experimental and analytical studies on the static behavior of FRP composite small portal frames (Figure 0.7). The portal frame was fabricated from W8×8×3/8 structural members, which are 8 inch in depth, 8 inch in width, and 3/8 inch web and flange thicknesses. The beam, of length 8.0 ft, was connected at its ends to two columns, each of length 7.5 ft. At the base of each column, the column support condition was pin connection. Two types of tests were performed separately. In the first test, a concentrated load was applied vertically at the beam mid-span up to a failure stage. In the second test, a lateral concentrated load was applied at the top of the column in the plane of the frame. To obtain the analytical results, Turvey adopted Mosallam's (1992) approach for the analytical predictions. Turvey's test was a first experimental test for sway deformation of FRP composite frames. However, in Turvey's analytical studies, the comparison results showed that the analytical model significantly

underestimated the sway deformation of the frames by as much as 15% to 45% of the measured displacements.

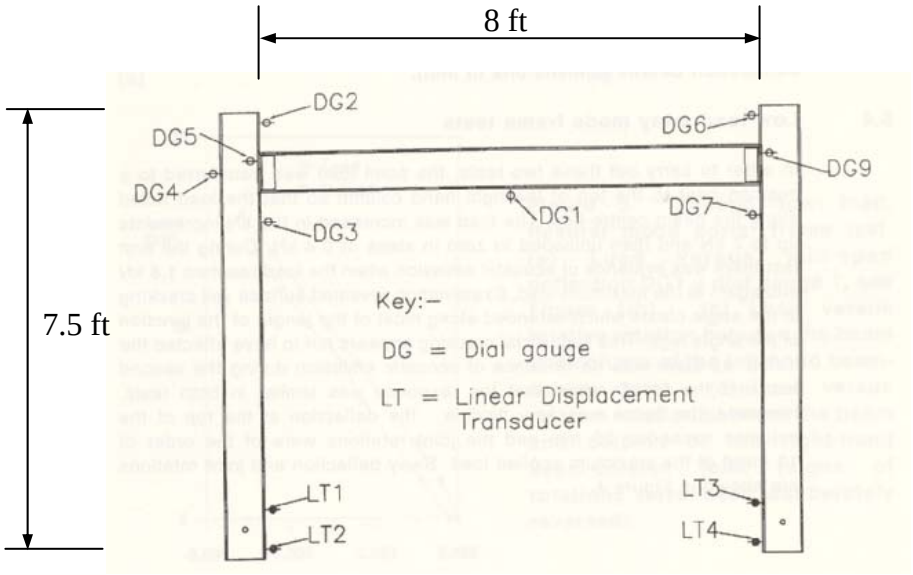

Figure 0.7: Turvey's frame test setup (Turvey, 1996)

Mottram (1996) conducted an analytical study to examine the elastic load-displacement behavior of plane frames composed of FRP structural members considering shear deformation of members and semi-rigid member connection conditions. The analytical model consisted of a three-story single-bay frame composed of FRP structural members (W8×8×3/8) (Figure 0.8). The column support conditions were assumed to be fixed in the analytical model, and uniform loads are applied on each beam. Unfortunately, there appear to be no published experimental studies associated with the analytical models.

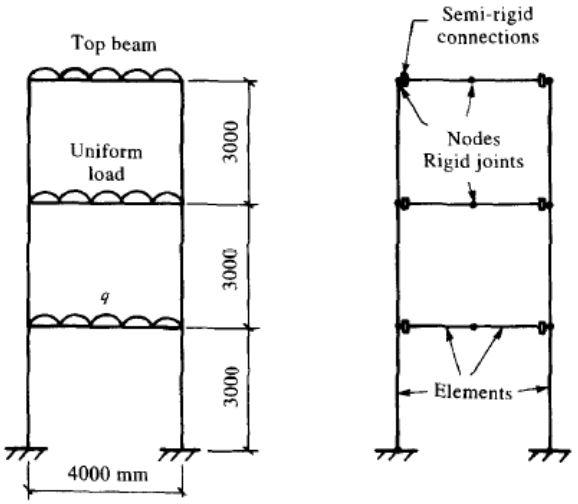

Fig. 11. Example of plane frame with semi-rigid connections.

Figure 0.8: Mottram's analytical model for a plane frame (Mottram and Zheng, 1996)

Turvey (2001) presented summaries of work on the testing of composite frames composed of pultruded FRP members having simple/semi-rigid beam-column connections. Turvey pointed out that there have been few composite frame test cases and criticized that most of the tests used the same size wide flange profiles for the columns and beams and there has been no research on the effects of various diagonal member arrangements to minimize sway deformations.

Regarding the modeling of beam-column connections, many researchers have focused on experimentally measuring the rotation-stiffness of beam-column connections for FRP structural frames. After the first series of moment-rotation tests on bolted joints connecting pultruded FRP structural members was carried out by Bank and Mosallam (1990), various types of beam-column connections were tested and the rotational stiffness properties were measured. Bass and Mottram (1994), Smith *et al* (1999) and Turvey (2000) carried out beam-column connection tests to measure the rotational stiffness of

FRP beam-column connections for different types of beam-column connections. Turvey (2004) summarized the beam-column moment-rotation tests performed by many researchers from 1984 to 2004, and showed that the stiffness characteristics of FRP beam-column connections are neither a pin connection nor a fixed connection. Rather, for the tests performed, the stiffness characteristics of FRP beam-column connections were that of partial moment fixity.

CHAPTER 2

LABORATORY TESTS FOR FULL-SCALE PULTRUDED FRP COMPOSITE MATERIAL FRAME STRUCTURES

This chapter summarizes the full-scale pultruded FRP composite frame experimental test program and associated test results. The experimental test program included material coupon tests and full-scale pultruded FRP composite frame tests.

- Sections 2.1 through 2.3 provide basic and fundamental information such as reference frame definitions of FRP pultruded structural members.
- Section 2.4 provides the detailed descriptions of the full-scale FRP frame configurations that were tested.
- Section 2.5 describes the experimental and analytical methodology to obtain mechanical properties of structural components of frames. The material test results are reported and examined herein.
- Section 2.6 describes the full-scale frame test setups and reports the measured load-displacements results of the FRP composite frames.

2.1 Reference Frame Systems

Coordinate reference frames are required in order to uniquely define the geometric position of structural members in a space frame model. Because of the inherent variability and manner in which FRP materials are fabricated for pultruded FRP members (see Section 2.2), several reference frames are required and used through this thesis.

Figure 2.1 shows both the global reference frame (X, Y, Z) and the member local reference frames (x, y, z). Figure 2.2 shows both the member local reference frame (x, y, z) and the local reference frames of the components of the cross-section (L, T, N). Figure 2.4(d) shows both a local reference frame of a typical component of a member (L, T, N) and a local reference frame of a single layer of FRP materials (1, 2, 3).

In other words, the global reference frame is represented by the (X, Y, Z) axes, the local reference frame of a member is represented by the (x, y, z) axes, the local reference frame of a typical component of a member is represented by the (L, T, N) axes, and the local reference frame of a single layer of FRP material is represented by the (1, 2, 3) axes.

Note that the L axis is parallel to, and in the same positive direction, as the x-axis, and the 1-axis is parallel to the fiber direction (Figure 2.4d).

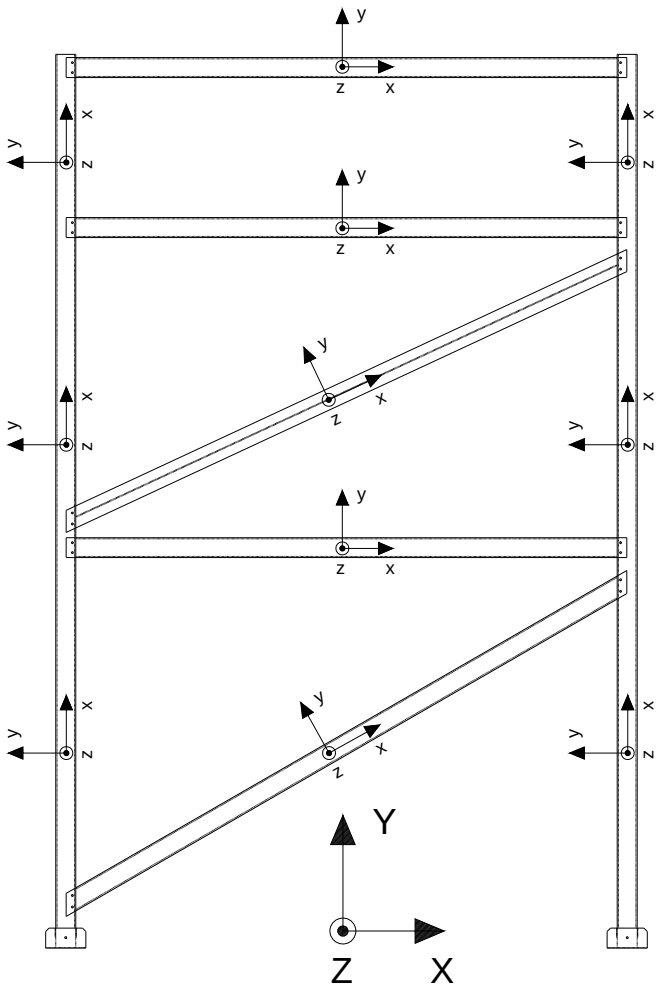

Figure 2.1: Global reference frame (X, Y, Z) and local member reference fames (x, y, z)

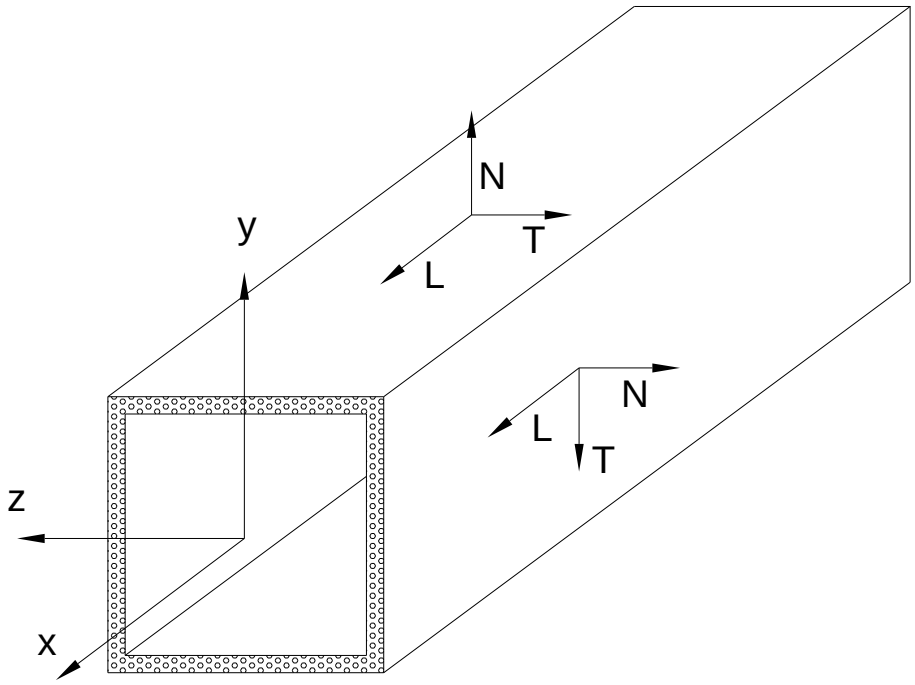

Figure 2.2: Member local reference frame (x, y, z) and local reference frames of the components of the members (L, T, N)

2.2 Pultruded FRP Test Member Components

Plate components (e.g., flanges and webs) of the cross-section of a pultruded FRP structural member can be assumed to be composed of multiple composite layers (Figure 2.3) for analysis purposes as follows:

a. Each layer is composed of a matrix and fiber reinforcement system (Figures 2.4(a) and (b)).

b. Fiber reinforcement systems can be categorized into several types such as a roving reinforcement system and/or continuous strand mat fiber reinforcement (Figure 2.4(c)).

c. Roving reinforced layers are composed of unidirectional fiber reinforcement (Figure 2.4(b)) and a matrix. Continuous strand mat fiber reinforced layers are composed of randomly oriented continuous fiber reinforcement (Figure 2.4(b)) and a matrix.

d. A roving reinforced layer is mainly used to provide a longitudinal stiffness for structural members, while a continuous strand mat fiber reinforced layer is mainly used to provide both a longitudinal and transverse stiffness for structural members.

e. Composite layers described in (c) and (d) above are stacked repeatedly to form a required thickness of components of a structural member (e.g., webs and flanges) (see Figure 2.3).

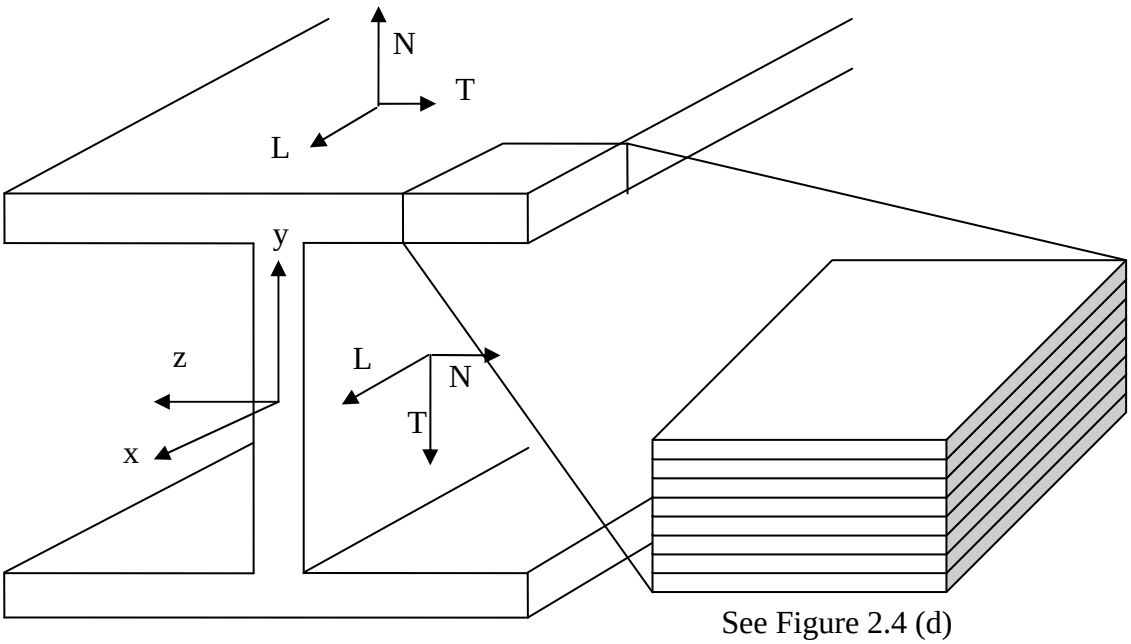

Figure 2.3: A member cross-section of W-shape FRP structural member

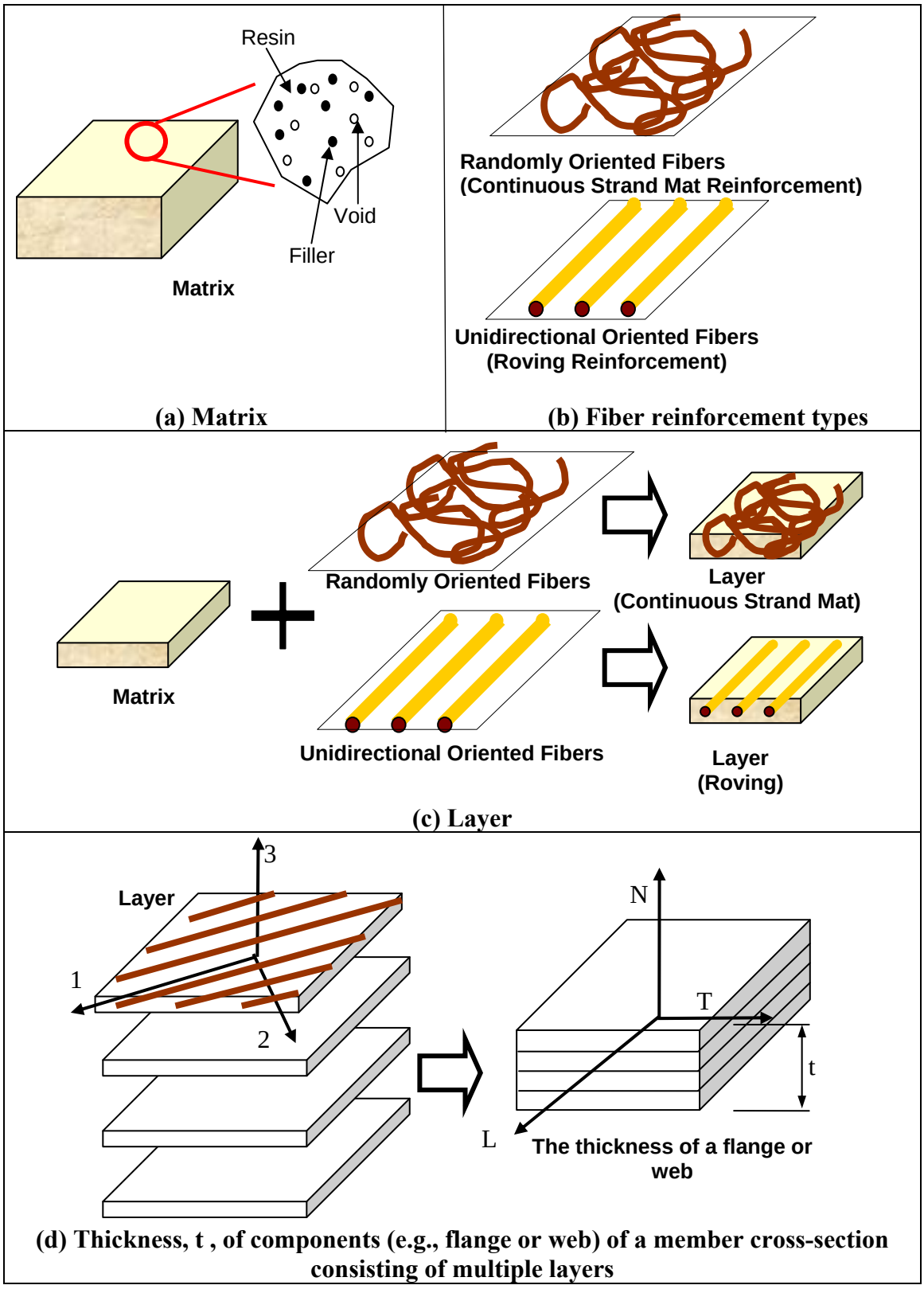

Figure 2.4: Illustration of a multi-scale homogenization approach

A matrix material in a composite layer can also be regarded as a composite material composed of multiple isotropic materials constituents such as resin, filler, and voids (see Figure 2.4(a)). A filler material is mixed with resin to modify the characteristics of the matrix.

Among many manufacturing techniques, pultrusion is a widely used technique and a cost-effective technique producing prismatic FRP structural members. In the pultrusion manufacturing process, continuous reinforcing fibers along with other additional fabric layers are pulled from creels and passed through a resin tank where fibers are impregnated with polymer resin. The saturated fibers are drawn through a performer and then pass through a heated die in which polymerization takes place. The hardened structural profiles are pulled and cut to the desired length.

2.3 Categorization of Frame Structures

In building code and criteria, frame structure can be divided into two major categories: moment frame and braced frame. The definition of each category can be adopted from IBC and ASCE code.

In accordance with the IBC 2003 and ASCE7-05 (ASCE, 2005) codes, a Braced Frame (Figure 2.5) is defined as a "*Frame that uses an essentially vertical truss, or its equivalent, of a concentric or eccentric type that is provided in a building frame system or dual frame system to resist lateral forces.*" In addition, a Moment Frame is defined as a "*Frame in which lateral forces are resisted primarily by the development of flexure in beams, columns and their connections.*"

Braced Frames are further categorized into two groups (Figure 2.5), which are a Concentrically Braced Frame (CBF) and an Eccentrically Braced Frame (EBF). The Concentrically Braced Frame (CBF) is again categorized into an Ordinary Concentrically Braced Frame (OCBF) and a Special Concentrically Braced Frame (SCBF).

It is of interest to note that all previously tested FRP composite frames (Section 1.3.2) have been only of the “Moment Frame” type.

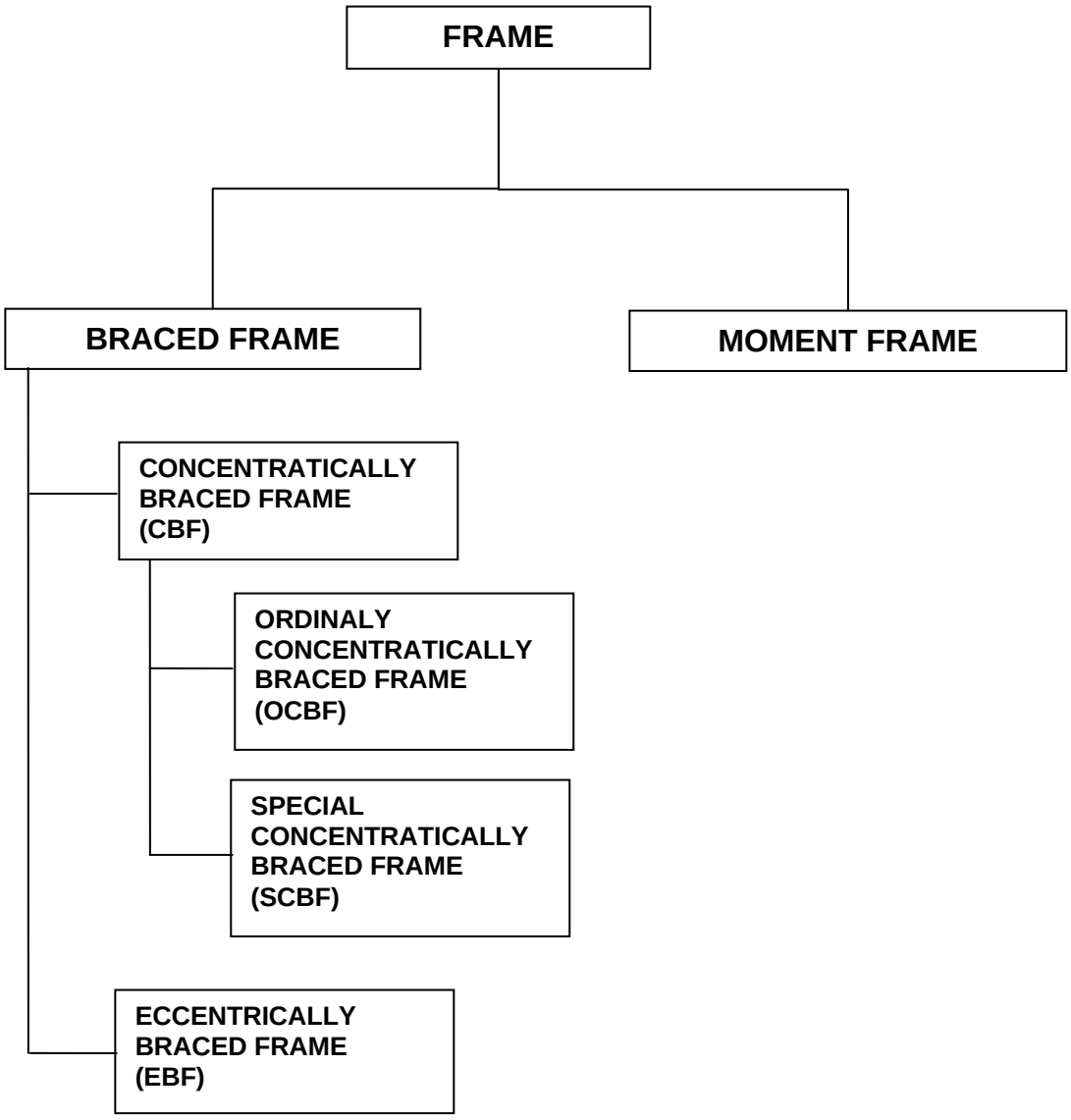

Figure 2.5: Categorization of a frame structures according to ASCE7-05

2.4 Test Portal Frames

An experimental investigation of the load-displacement response of plane braced frames whose members are made of FRP composite materials was conducted. In this section, physical characteristic of the test frames is presented. The physical information includes frame configurations and other details of the frame. A total of six frame configurations having different number of diagonal members and beam-column boundary conditions were tested (Table 2.1) and are described as follows:

a. The FRP members used to assemble the frames for the experimental tests were manufactured by Creative Pultrusion Co. (Creative Pultrusion, 2005)

b. The frames are 14 ft. wide and 22 ft. high and consist of three stories, each with two columns and one beam. Each column is three stories in length.

c. The six test frame configurations were examined. Table 2.1 summarized the six frame configurations. These six test frame configurations are:

   (1) FRAME-1-P: This frame (Figure 2.6) has one diagonal member in the bottom story. The beam-column connection is a "Type-P" connection as shown in detail (a) of Figure 2.10.

   (2) FRAME-1-FA: This frame (Figure 2.8) has one diagonal member in the bottom story. The beam-column connection is a "Type-FA" connection as shown in detail (b) of Figure 2.10.

(3) FRAME-1-SA: This frame (Figure 2.8) has one diagonal member in the bottom story. The beam-column connection is a "Type-SA" connection as shown in detail (c) of Figure 2.10.

(4) FRAME-2-P: This frame (Figure 2.7) has one diagonal member in the bottom two stories. The beam-column connection is a "Type-P" connection as shown in detail (a) of Figure 2.10.

(5) FRAME-2-FA: This frame (Figure 2.9) has one diagonal member in the bottom two stories. The beam-column connection is a "Type-FA" connection as shown in detail (b) of Figure 2.10.

(6) FRAME-2-SA: This frame (Figure 2.9) has one diagonal member in the bottom two stories. The beam-column connection is "Type-SA" connection as shown in detail (c) of Figure 2.10.

c. Except for member BR2, all members in the six frames are tubular box cross-sections. The exception is diagonal member BR2 in the FRAME-2 series (Table 2.1) which has a W-shape cross-section. Figure 2.11 shows the member cross-section nominal dimensions for each member in the six frames.

d. Three beam-column connection types were used in the tests. Figure 2.10 shows the three typical beam-column connection types. The connection type 'P' (Figure 2.10(a)) is the connection that only the side wall components (webs) of the box beam members are extended and connected to the column members and two ½-inch stainless steel bolts are used to grip the webs to the column members. The

connection type ‘FA’ (Figure 2.10(b)) is the connection where FRP angles are added to connect the top and bottom flanges of the box beam members to the columns in addition to the above connection type ‘P’. The connection type ‘SA’ (Figure 2.10(c)) has the same geometry of connection type ‘FA’ but instead of an FRP angle, steel angles are used.

e. Figures 2.12 to 2.21 show the details of the beam-column connections. Figures 2.16 to 2.22 show the connection details between the diagonal members and the columns in the frames.

f. Figure 2.22 shows the detail of the column base support with a stainless steel shoe. Two ½-inch stainless bolts are used to connect the column member to the stainless steel shoe. Two 1-inch steel bolts are used to anchor the column base shoe to the ground.

g. Considering the frame structure types categorization presented in IBC-2003 and ASCE7-05, the FRP composite frames in this thesis can be categorized as an Eccentrically Braced Frame (EBF), which is defined as a diagonally braced frame in which at least one end of each brace frames into a member a short distance from a beam-column connection or from another diagonal brace (see Section 2.3).

Table 2.1: Six tested frames

FRAME	Number of diagonal members	Beam-column connection types * (Figure 2.10)
FRAME-1-P	1	Connection type “P”
FRAME-1-FA	1	Connection type “FA”
FRAME-1-SA	1	Connection type “SA”
FRAME-2-P	2	Connection type “P”
FRAME-2-FA	2	Connection type “FA”
FRAME-2-SA	2	Connection type “SA”

* Note: Connection types:

“P” = Pin connection using bolts on side walls of beam members (Figure 2.10(a))

“FA” = Fixed connection using bolts on webs of beam members and FRP angles on flanges on beam members (Figure 2.10(b))

“SA” = Fixed connection using bolts on webs of beam members and steel angles on flanges on beam members (Figure 2.10(c))

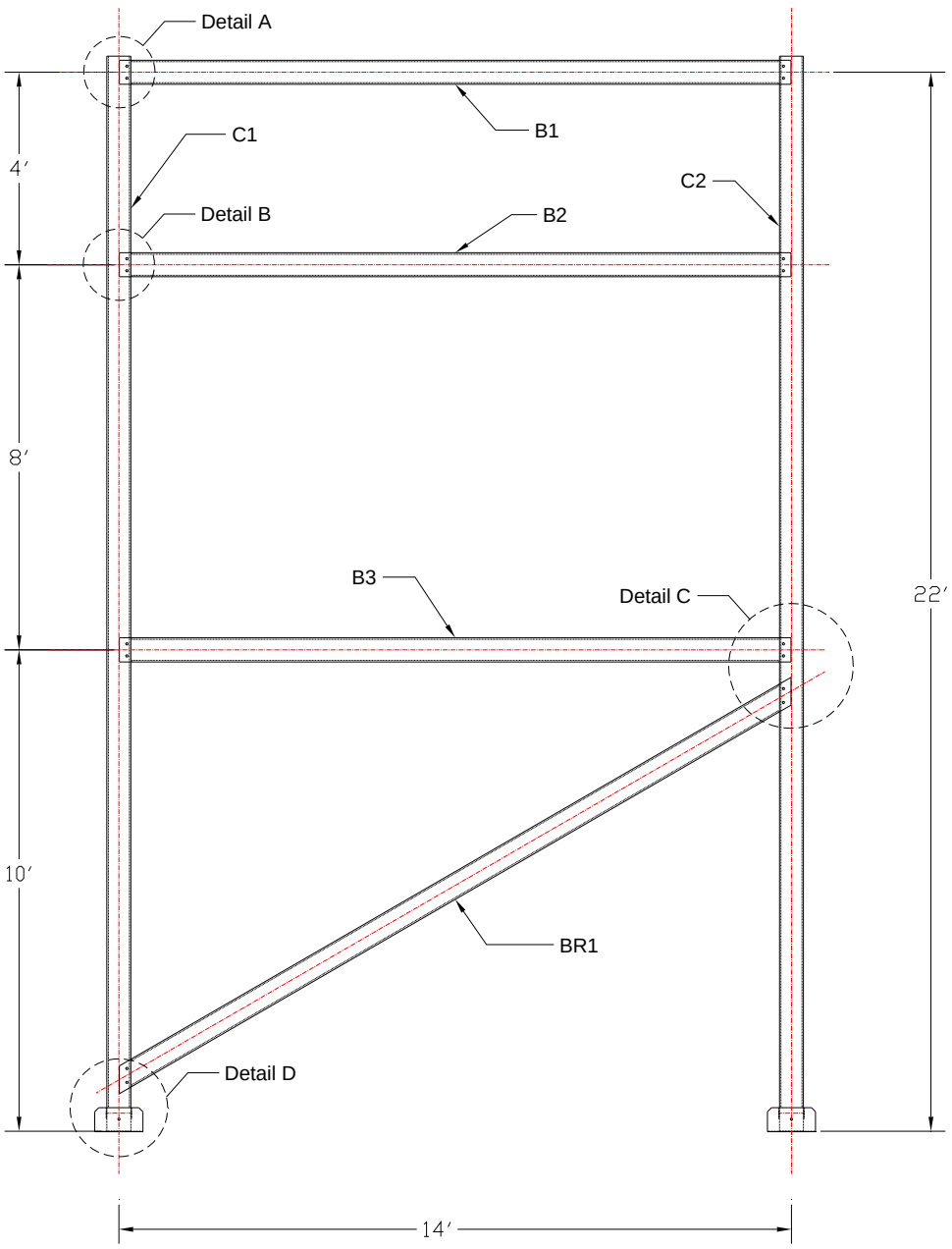

Figure 2.6: Elevation of the FRAME-1-P (simple connection using bolts only) with diagonal member in the bottom story

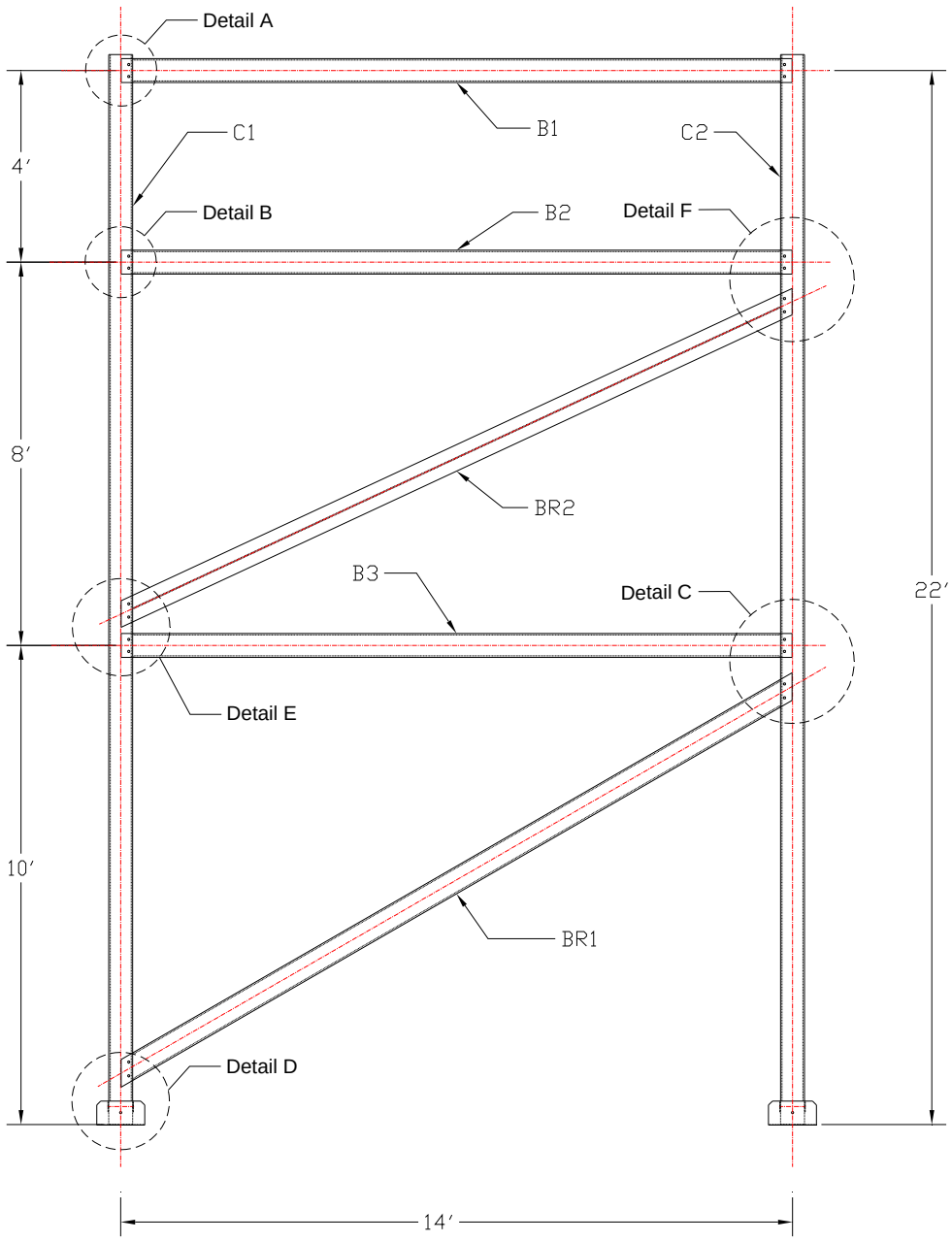

Figure 2.7: Elevation of the FRAME-2-P (simple connection using bolts only) with diagonal members in the bottom two stories

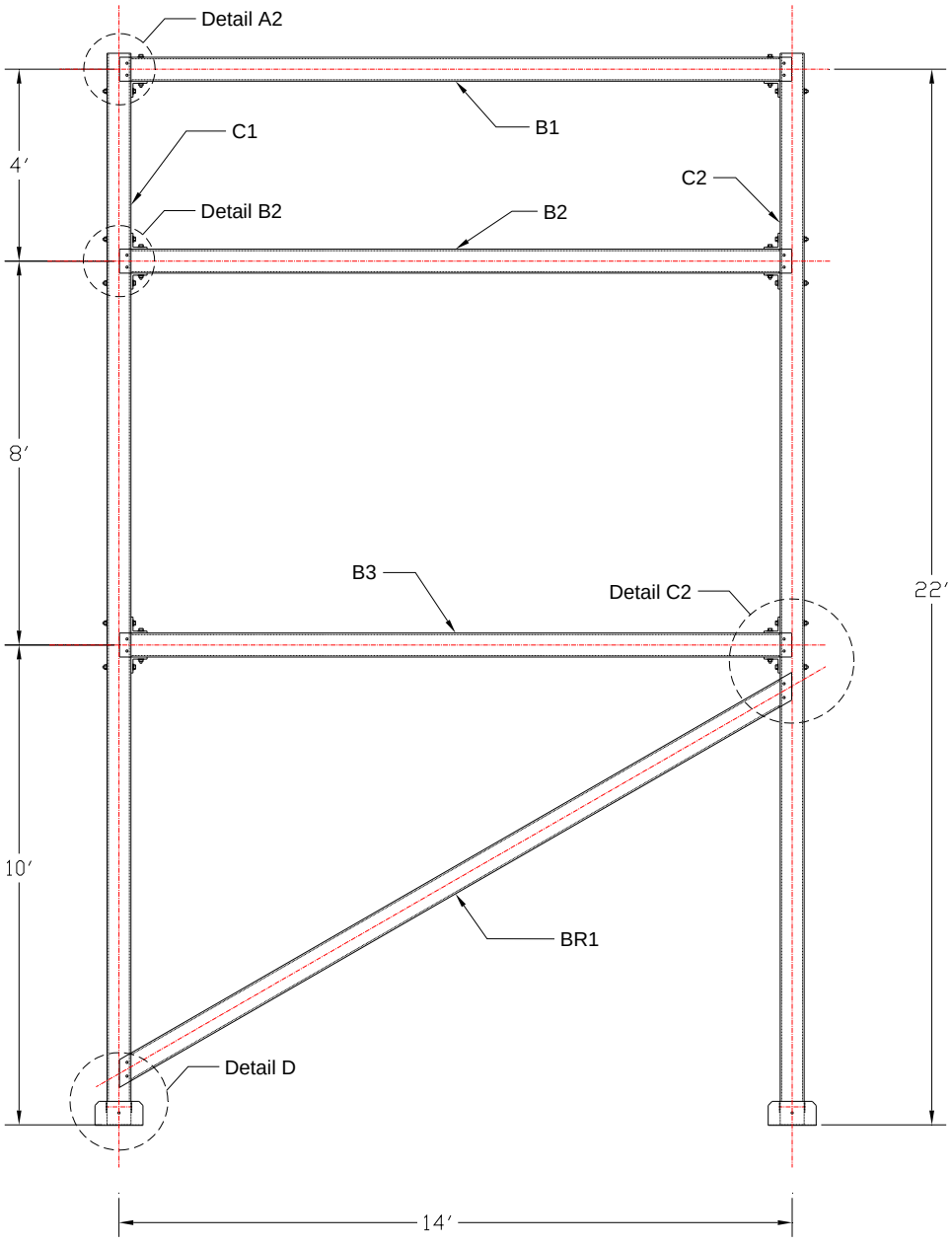

Figure 2.8: Elevation of the FRAME-1-FA (fixed connection using FRP angles) and FRAME-1-SA (fixed connection using steel angles) with one diagonal member in the bottom story

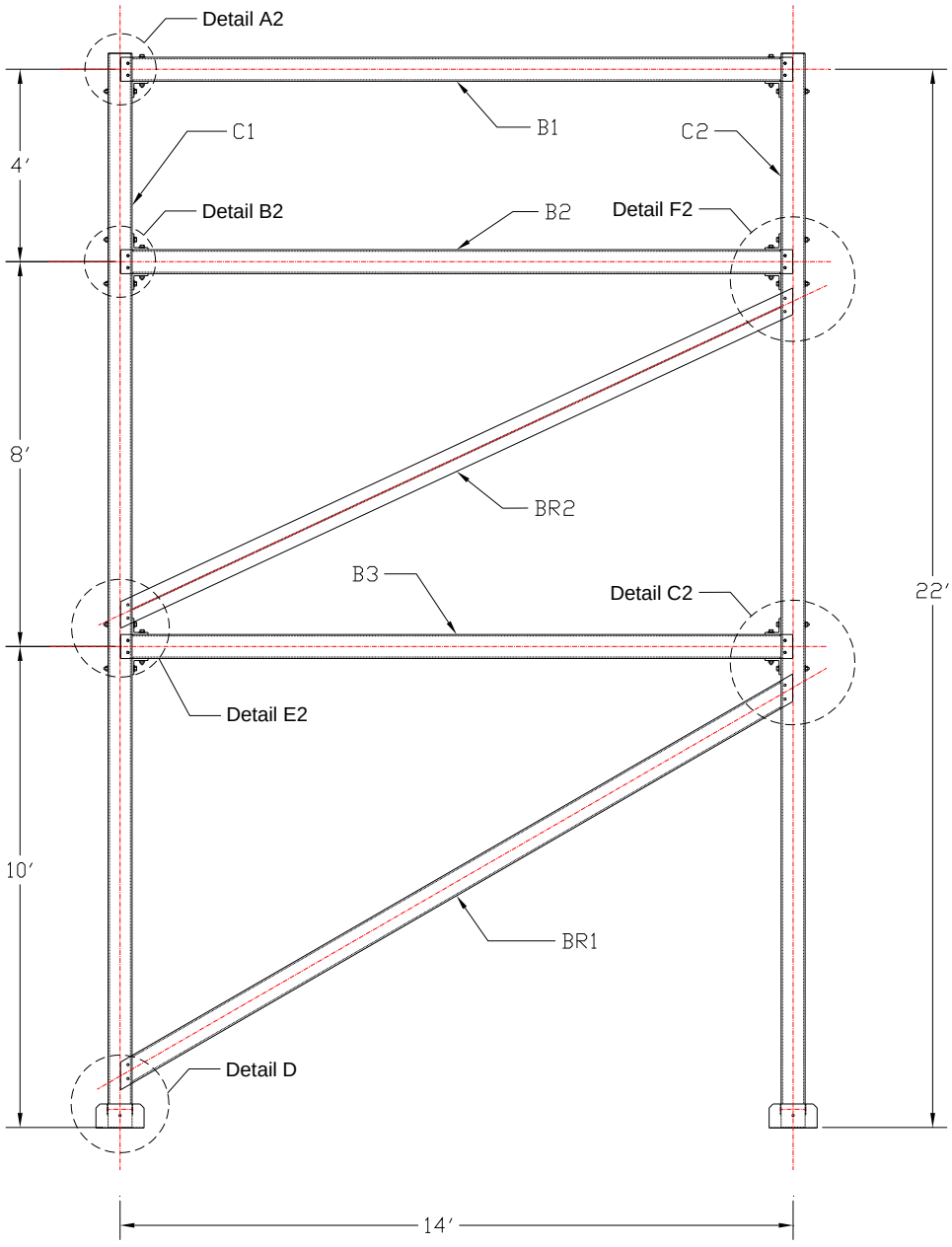

Figure 2.9: Elevation of the FRAME-2-FA (fixed connection using FRP angles) and FRAME-2-SA (fixed connection using steel angles) with diagonal members in the bottom two stories

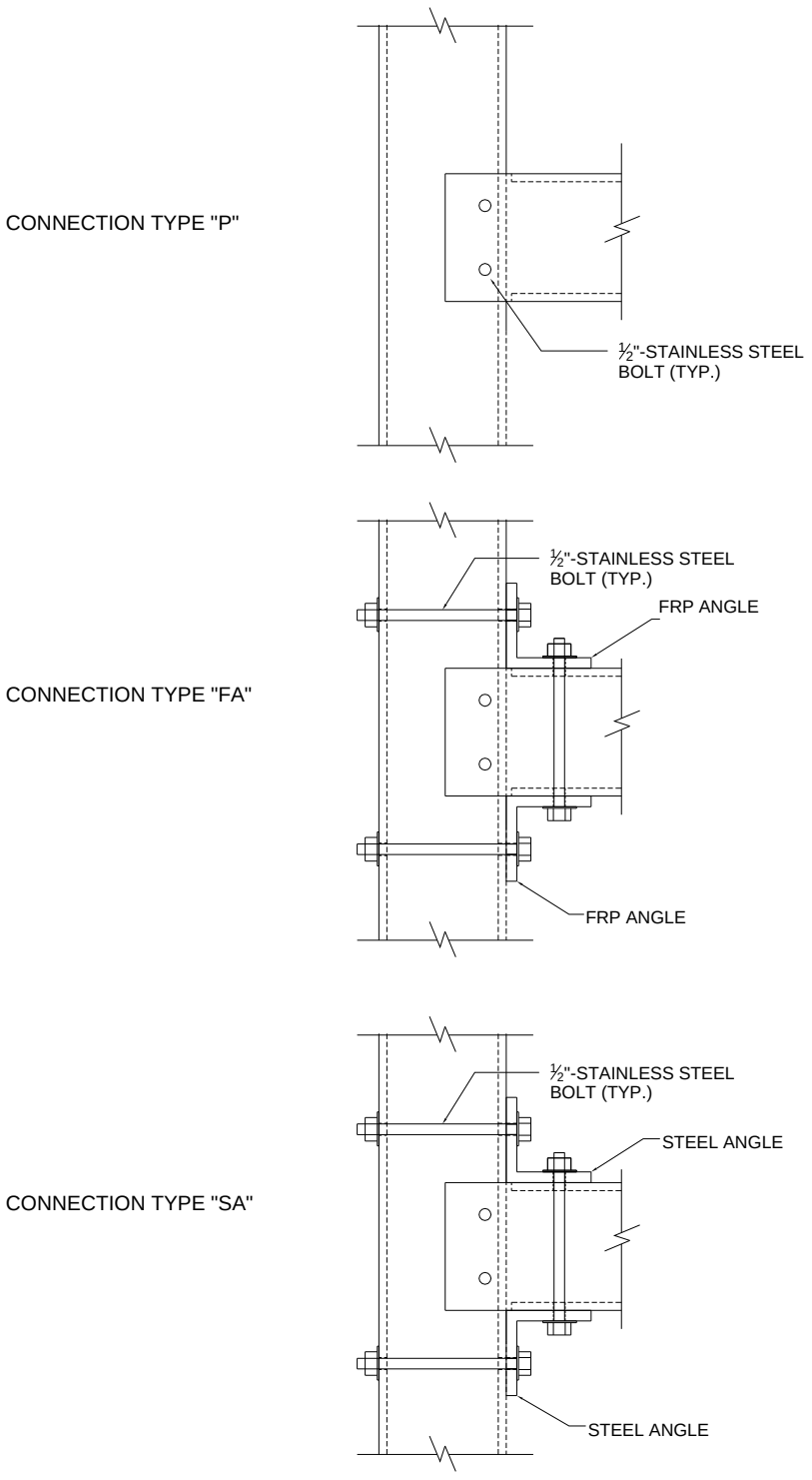

Figure 2.10: Illustrations of three connection types used in the tests

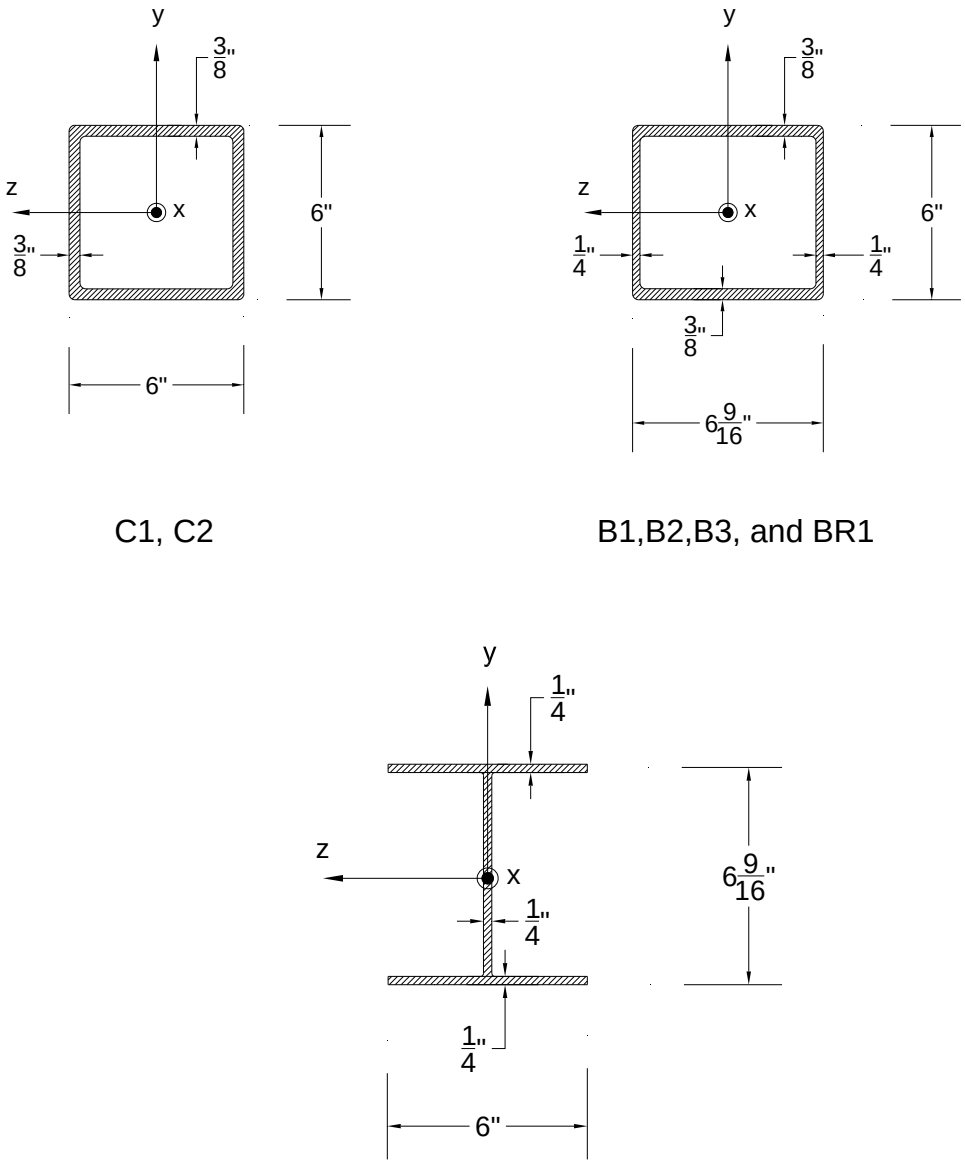

Figure 2.11: Cross-section nominal dimensions for columns, beams, and diagonal member

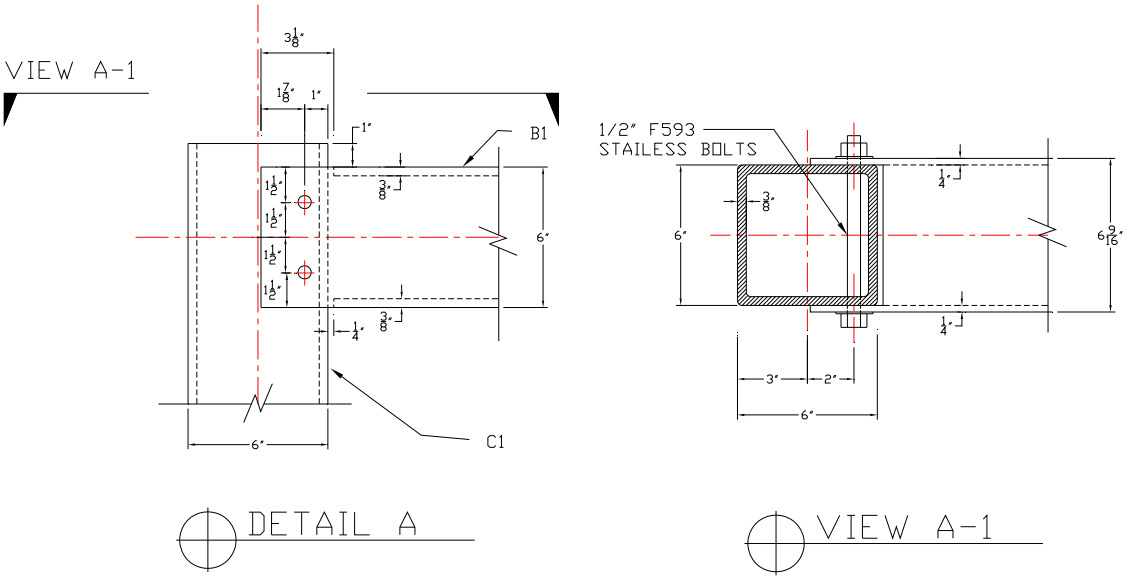

Figure 2.12a: Detail A*

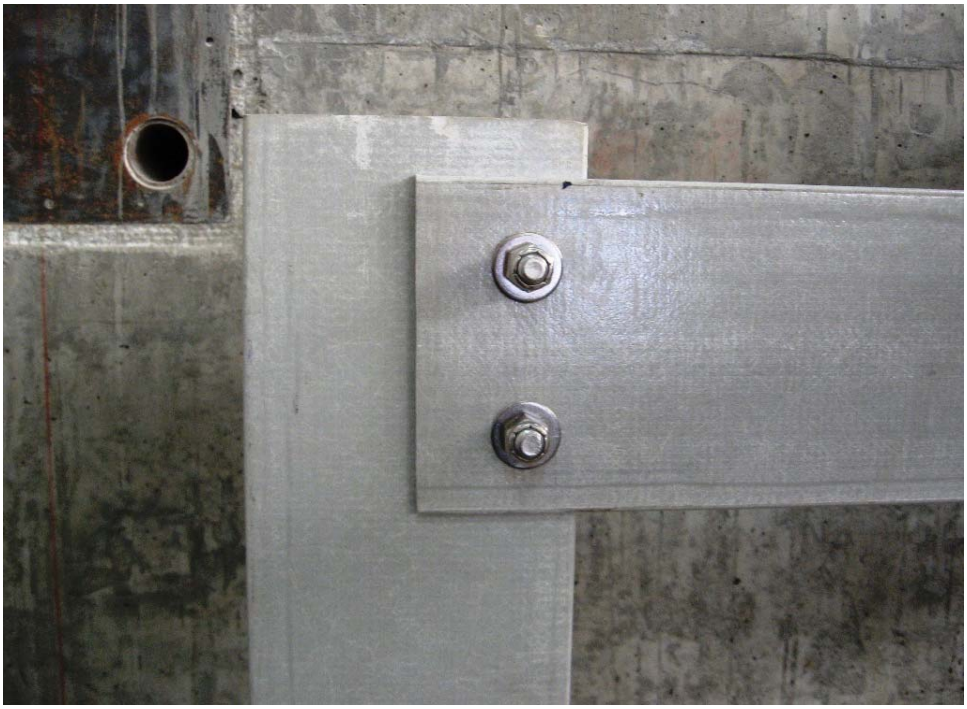

Figure 2.12b: Detail A Photo

* see Figures 2-6 and 2-7

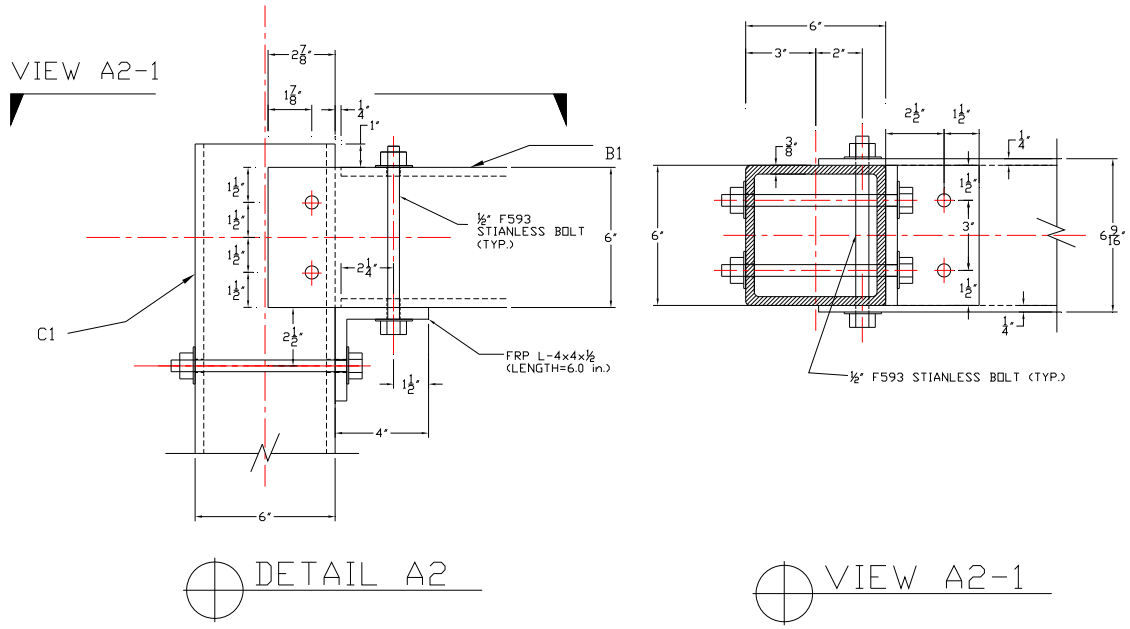

Figure 2.13a: Detail A2 *

* See Figures 2-8 and 2-9

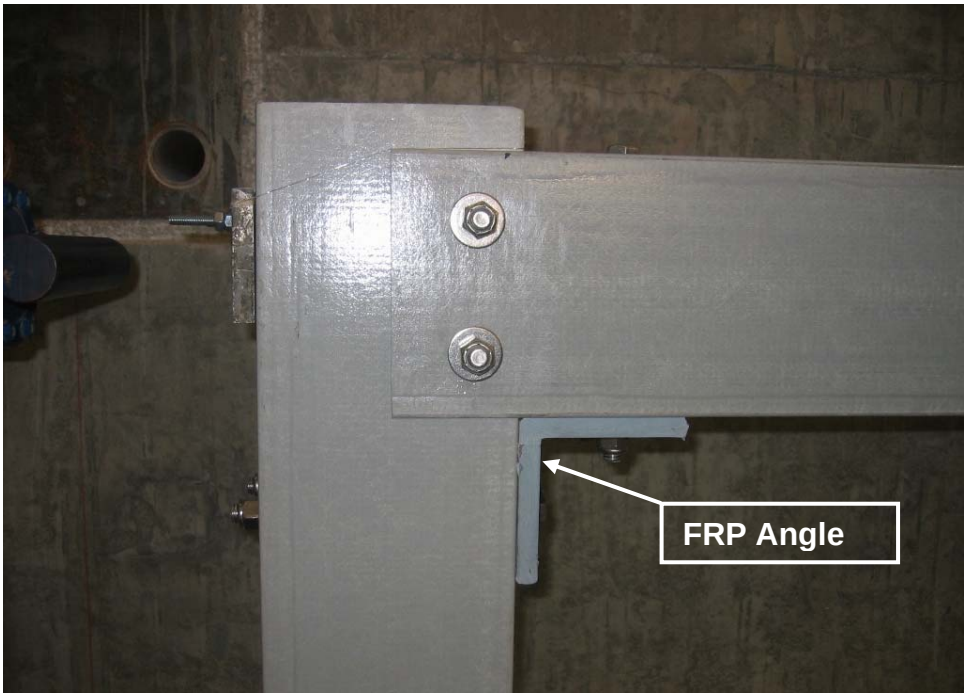

Figure 2.13b: Detail A2 Photo (FRP angle case) (see Figure 2.13a)

Figure 2.13c: Detail A2 Photo (Steel angle case) (see Figure 2.13a)

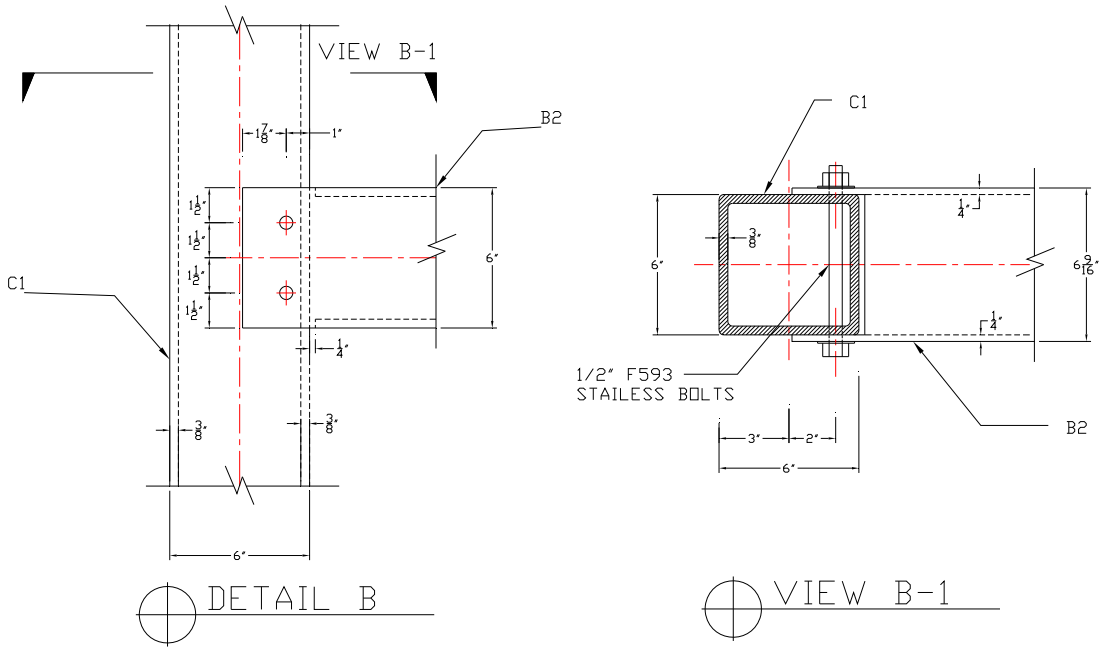

Figure 2.14a: Detail B *

Figure 2.14b: Detail B Photo

* See Figures 2-6 and 2-7

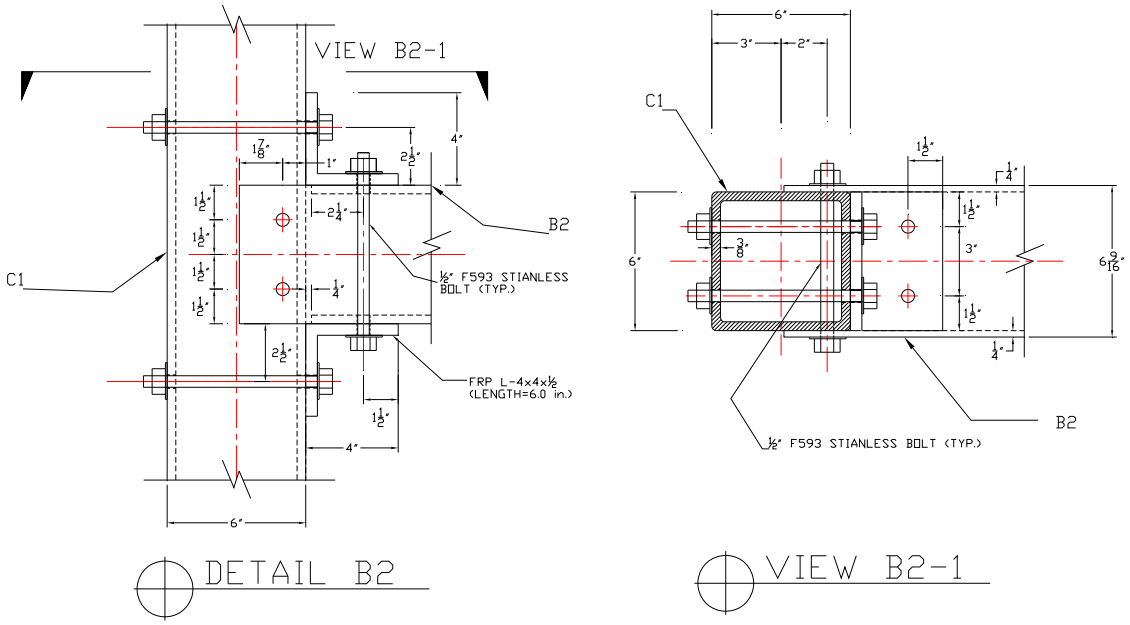

Figure 2.15a: Detail B2 *

* See Figures 2-8 and 2-9

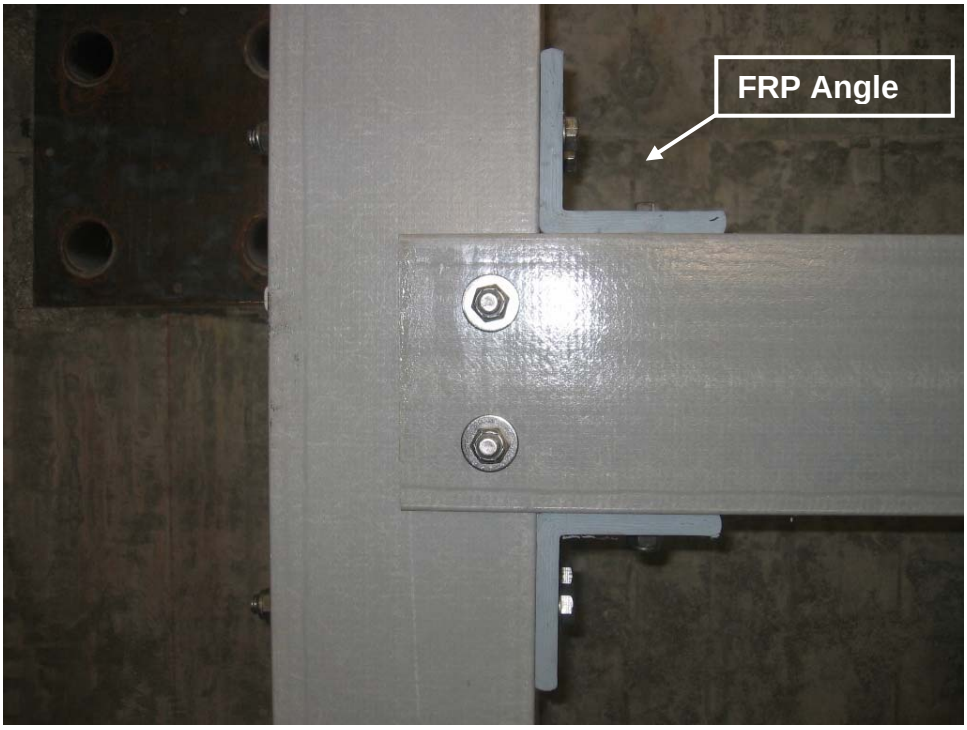

Figure 2.15b: Detail B2 Photo (FRP angle case) (see Figure 2.15a)

Figure 2.15c: Detail B2 Photo (Steel angle case) (see Figure 2.15a)

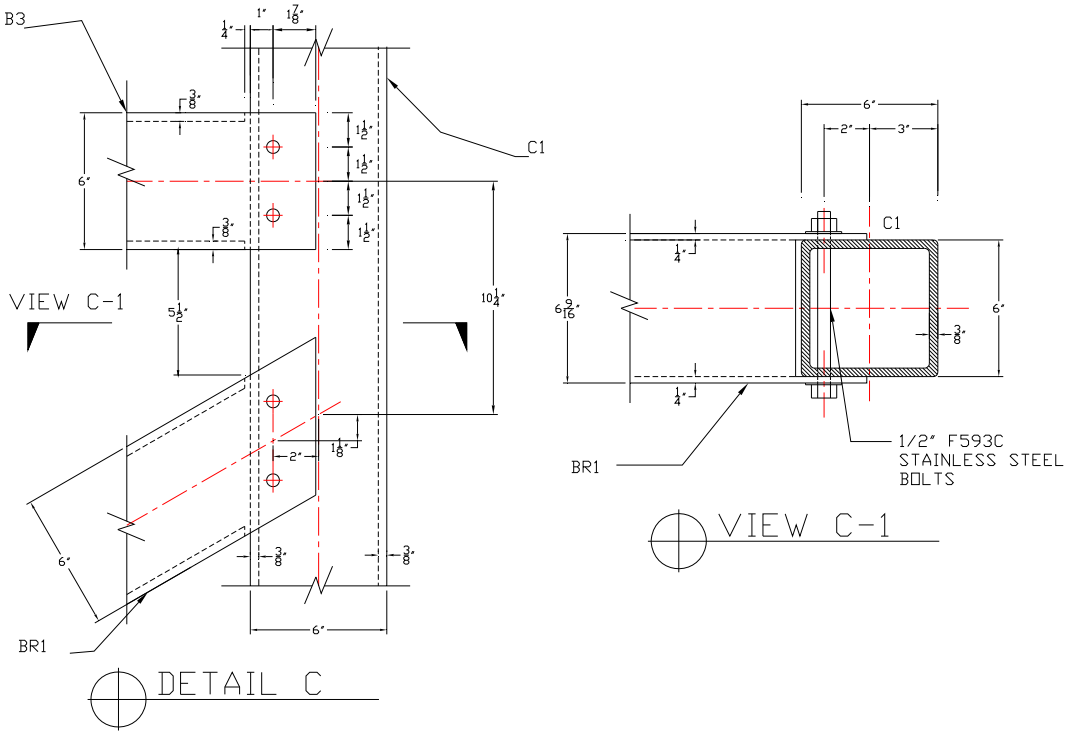

Figure 2.16a: Detail C*

Figure 2.16b: Detail C Photo

* see Figures 2-6 and 2-7

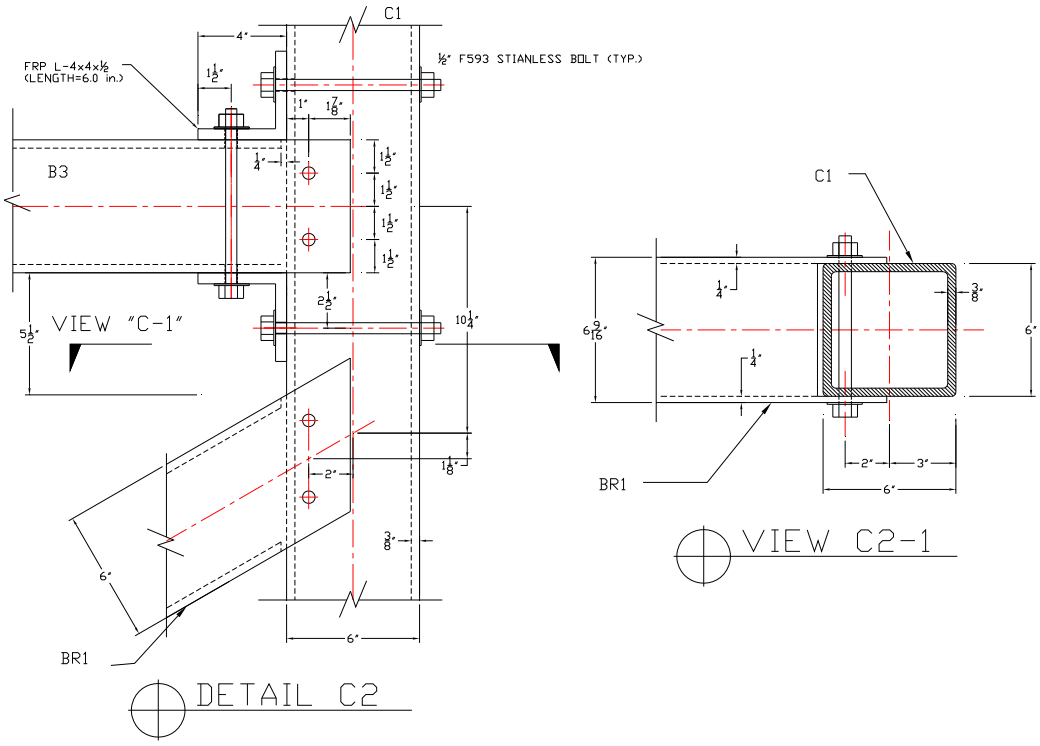

Figure 2.17a: Detail C2*

* see Figure 2-8 and 2-9

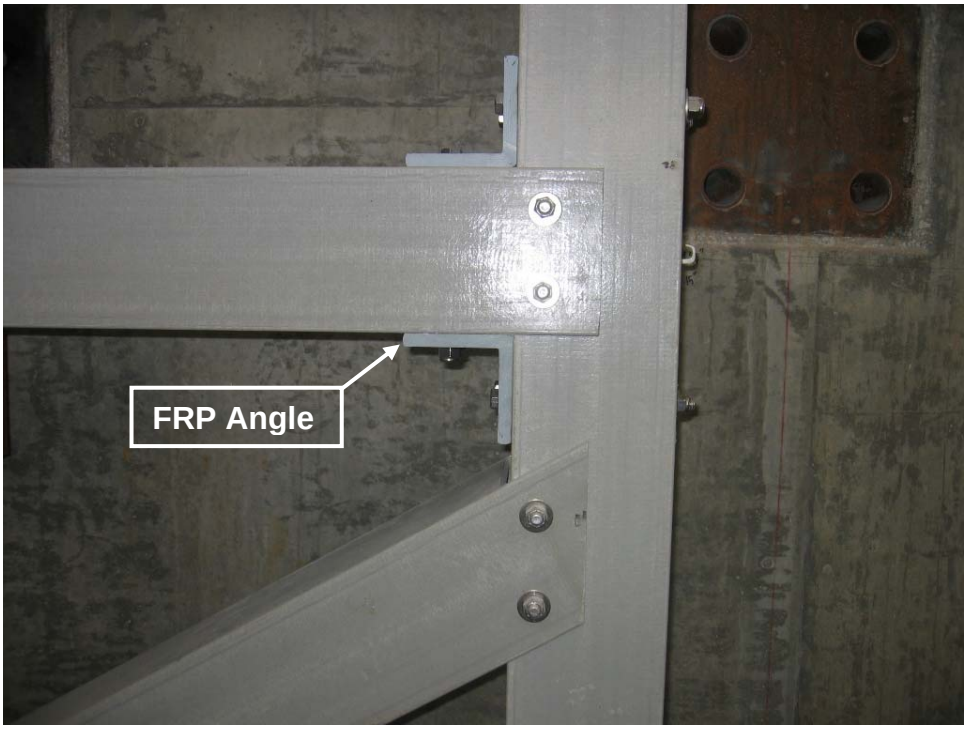

Figure 2.17b: Detail C2 Photo (FRP angle case) (see Figure 2.17a)

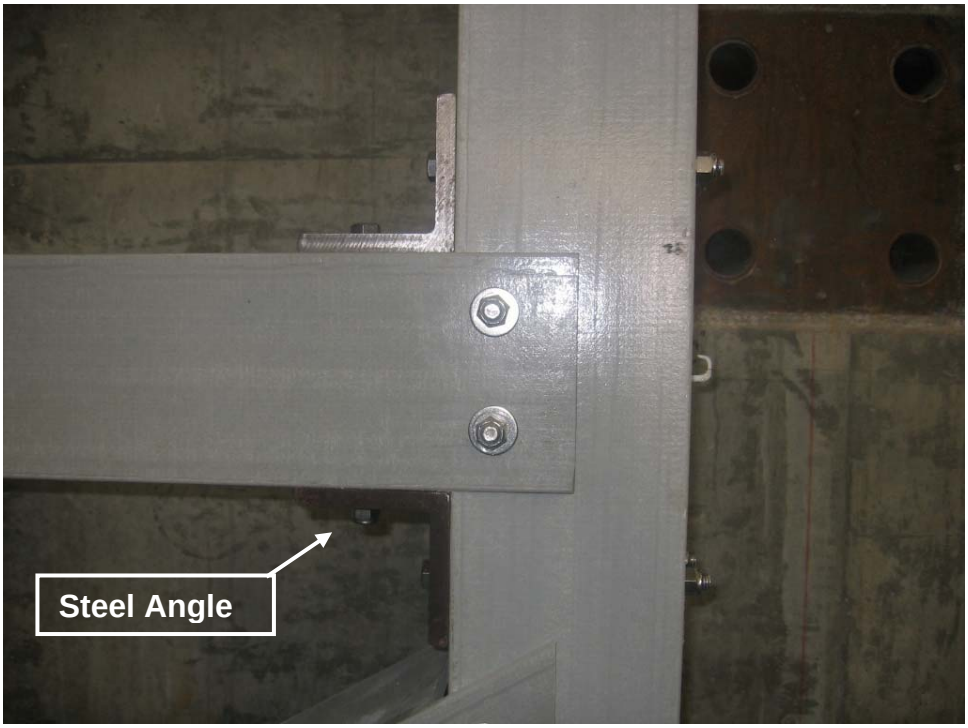

Figure 2.17c: Detail C2 Photo (Steel angle case) (see Figure 2.17a)

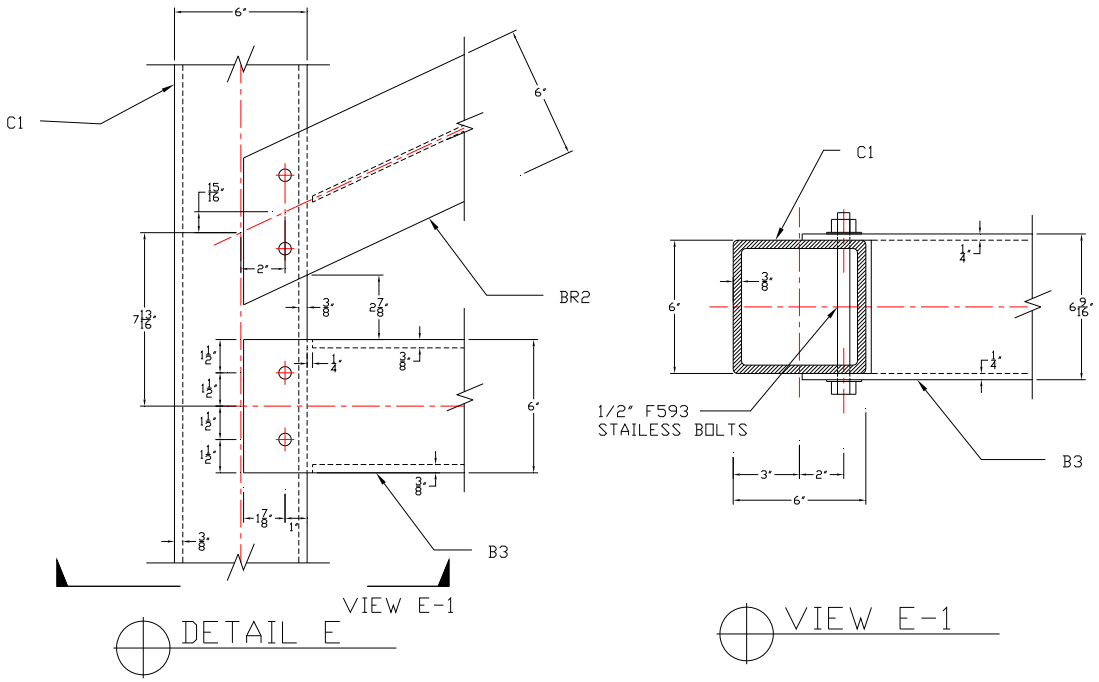

Figure 2.18a: Detail E*

Figure 2.18b: Detail E Photo

* see Figure 2-7

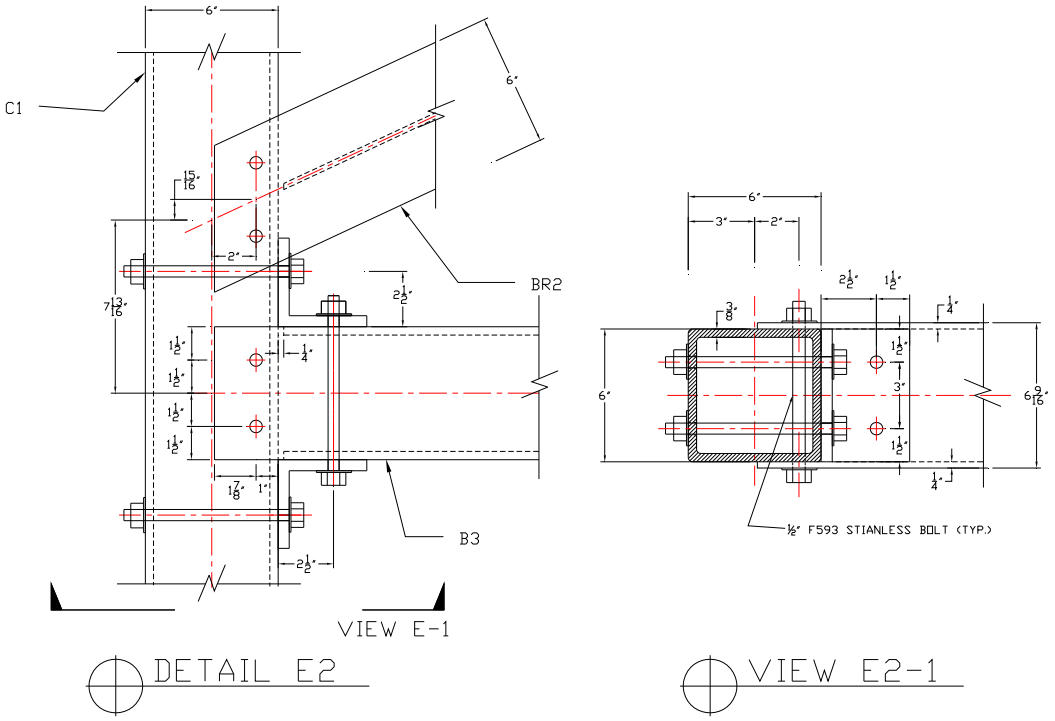

Figure 2.19a: Detail E2*

* see Figure 2-9

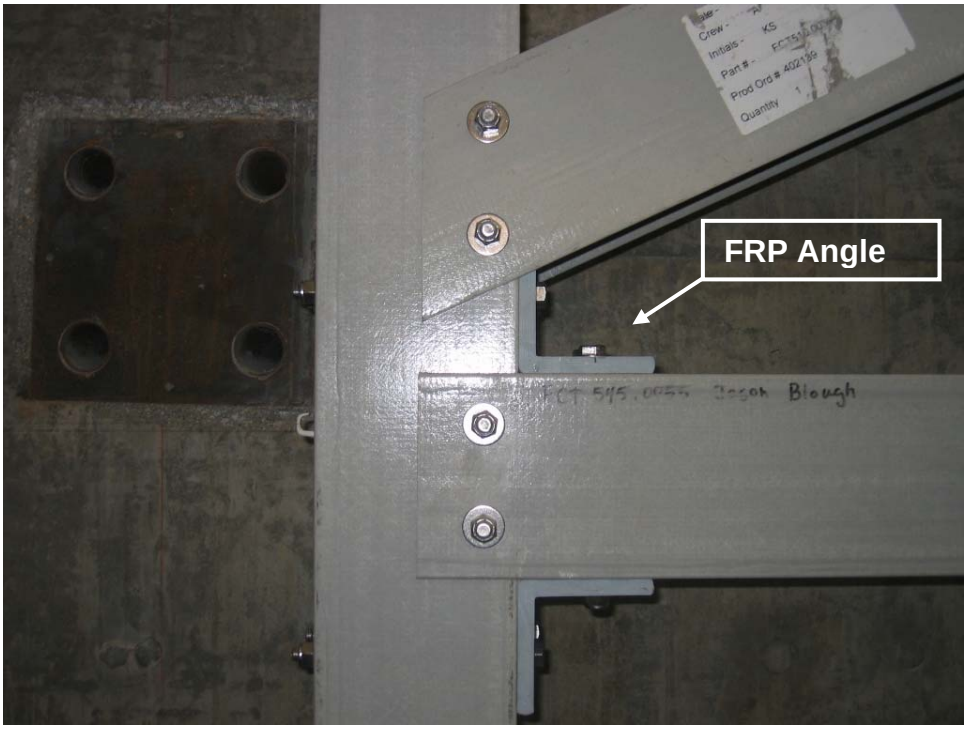

Figure 2.19b: Detail E2 Photo (FRP angle case) (see Figure 2.19a)

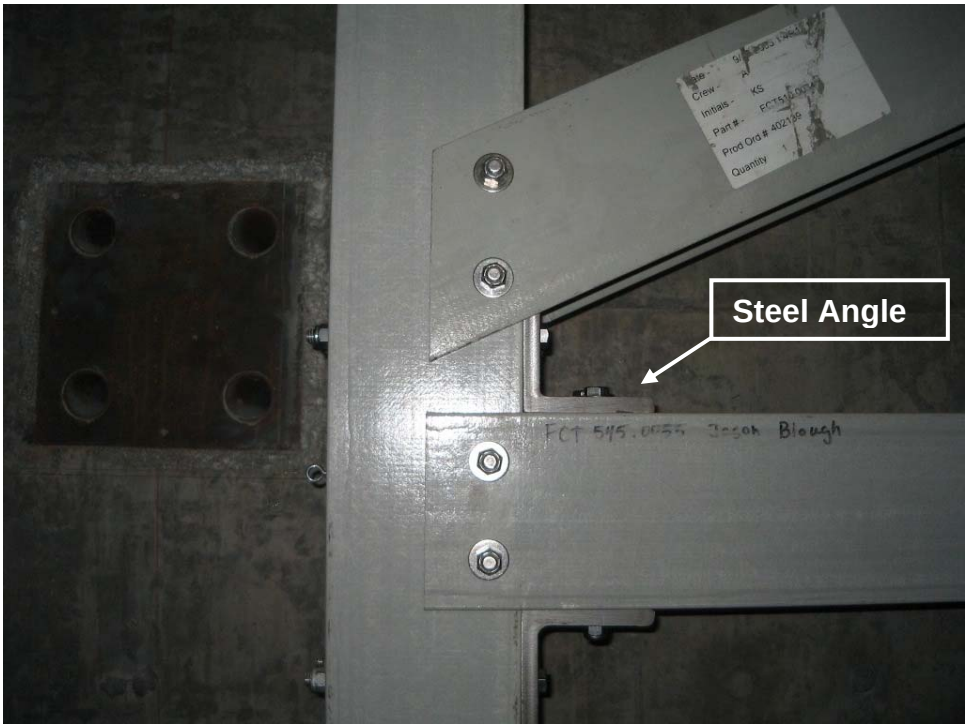

Figure 2.19c: Details E2 Photo (Steel angle case) (see Figure 2.19a)

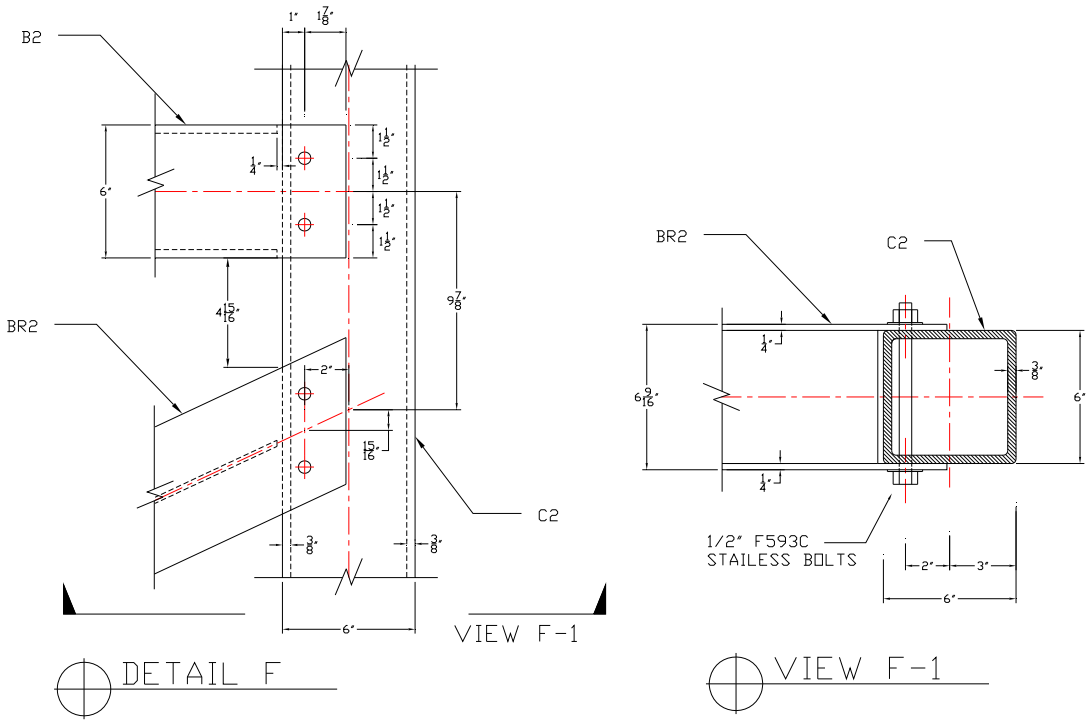

Figure 2.20a: Detail F*

Figure 2.20b: Detail F Photo

* See Figure 2-7

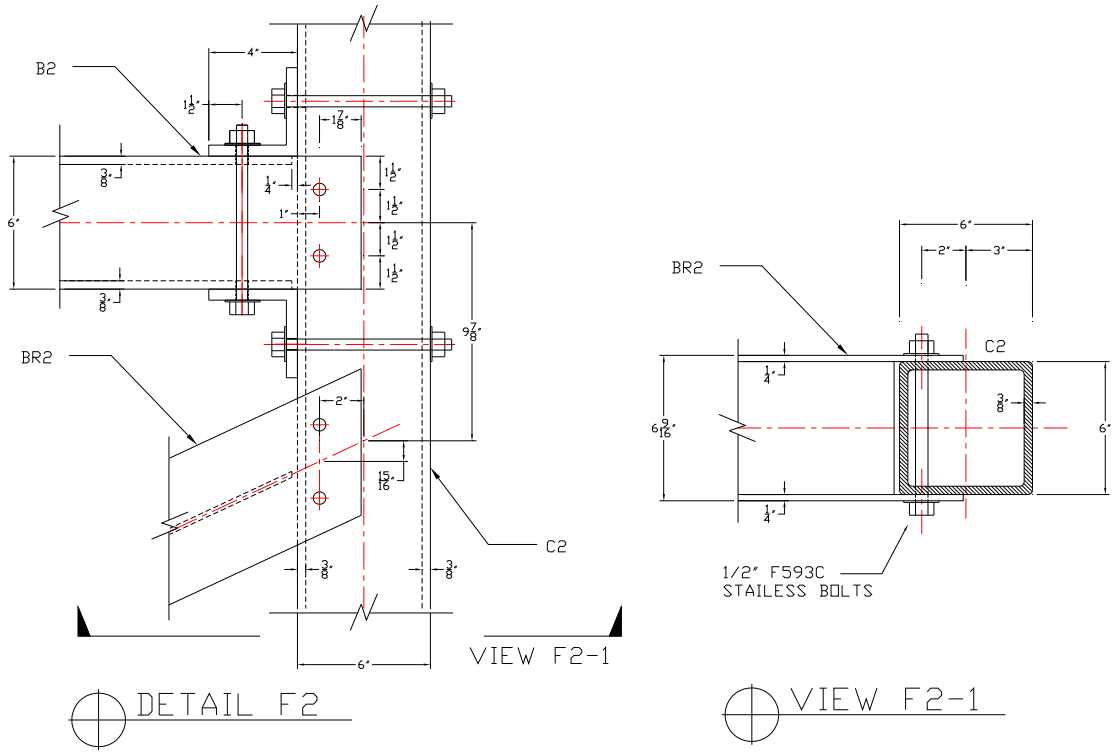

Figure 2.21a: Detail F2*

* See Figure 2-9

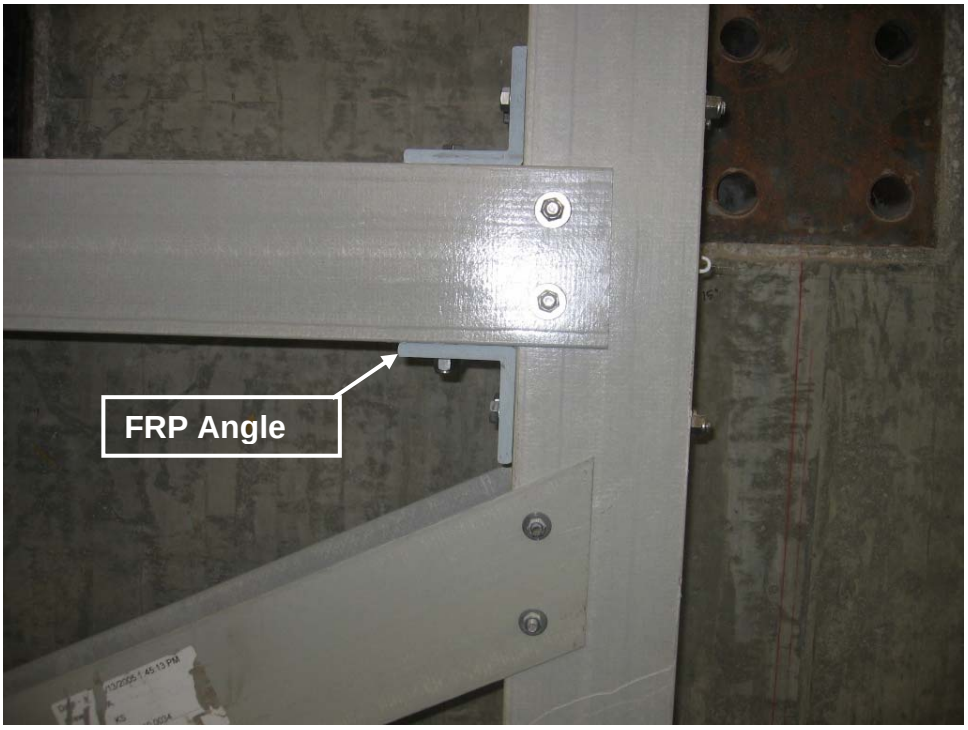

Figure 2.21b: Detail F2 Photo (FRP angle case) (see Figure 2.21a)

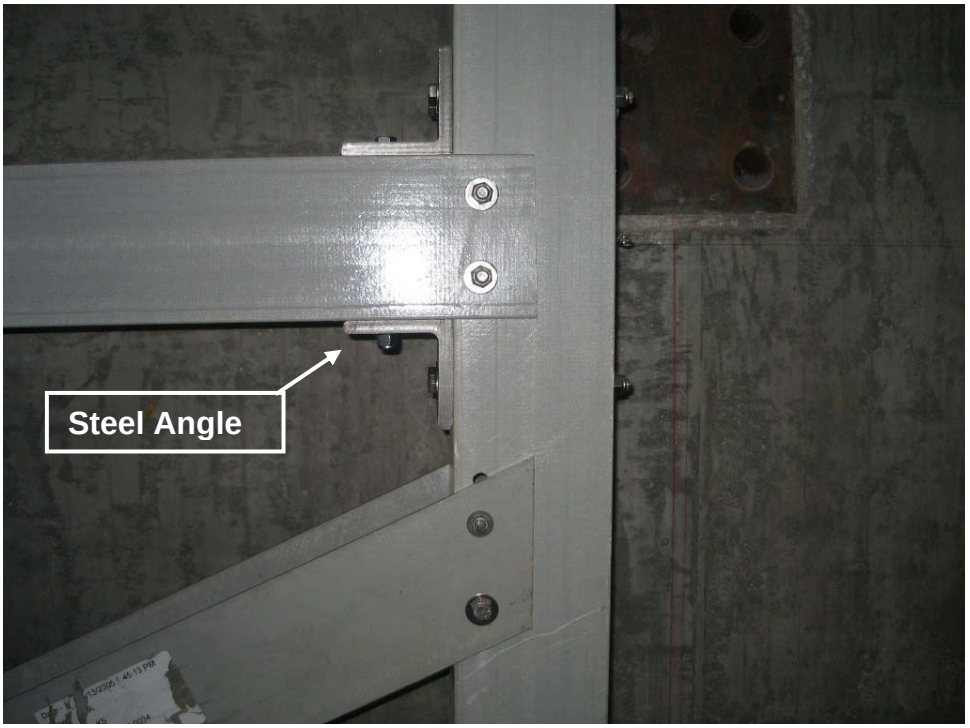

Figure 2.21c: Detail F2 Photo (Steel angle case) (see Figure 2.21a)

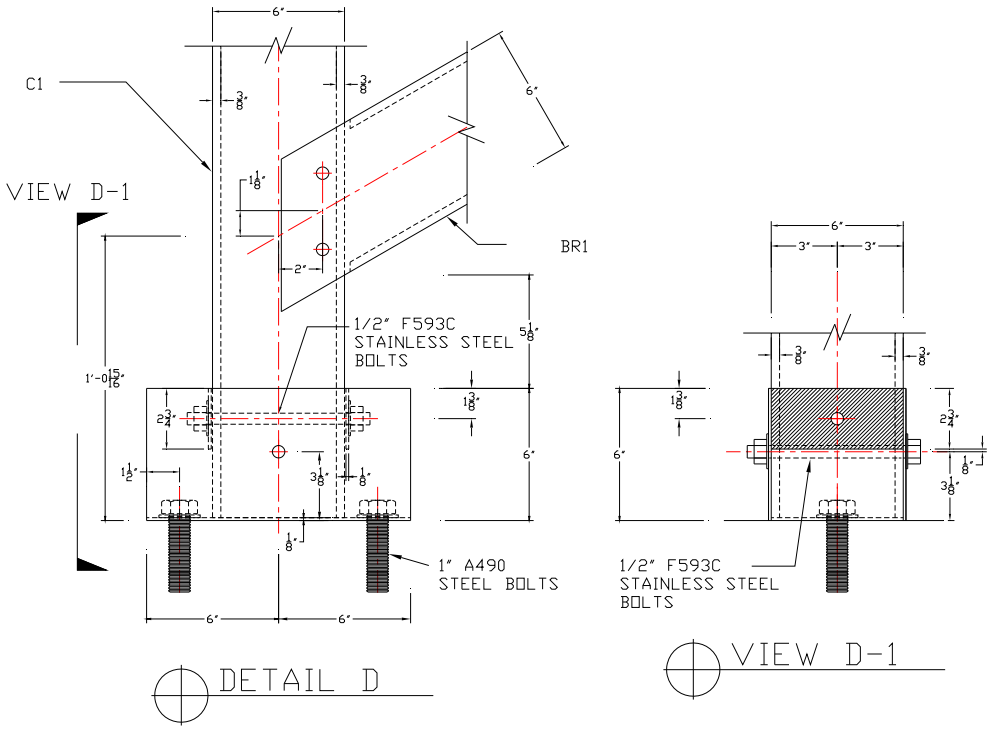

Figure 2.22a: Detail D[*]

[*] See Figures 2-6 through 2-9

Figure 2.22b: Detail D Photo - View from front (see Figure 2.22a)

Figure 2.22c: Detail D Photo - View from top-left (see Figure 2.22a)

2.5 Mechanical Material Properties

The mechanical material properties of each member were obtained experimentally using tension coupon tests (Section 2.5.1), compression coupon tests (Section 2.5.2), and shear coupon tests (Section 2.5.3). Coupons were taken from five locations in the frames. Table 2.2 shows the group numbers and corresponding locations where the coupons are taken.

Group-1 coupons were taken from the column members. Group-2 and Group-3 coupons were taken from top/bottom components (flanges) and side walls (webs) of box shape beams and brace members (B1, B2, B3, and BR1), respectively. Group-4 and Group-5 coupons were taken from flanges and webs of W-shape brace members (BR2), respectively. Member names of frames can be found in frame elevation drawings shown at Figures 2.6 through 2.9.

Table 2.2: Groups for mechanical material properties tests

Group number	Members in the Frames	Member Cross Section Type	Location	Coupon Thickness (in)
1	Columns C1, C2	Box	Column members	0.375
2	Beams B1,B2,B3 and Brace BR1	Box	Top/bottom components of cross-section (flanges) of beams and brace member BR-1	0.375
3			Side wall components of cross-section (Webs) of beams and brace member BR-1	0.250
4	Brace BR2	W	Flanges of brace member BR-2	0.250
5			Webs of brace member BR-2	0.250

An MTS-810 tension/compression servo-hydraulic testing system was used for the material tests. The applied loads and strains were recorded by an OPTIM MEGADAC 5180AC data acquisition system at the rate of one scan per second.

2.5.1 Tension Coupon Tests

Fifteen tension coupon tests were performed for each group of structural members according to the ASTM D3039 (1993) standard. Figure 2.23 shows a photo of a typical tension coupon test which is described as follows:

a. Prismatic coupons without end tabs were used in these tests. The coupons were 12.0 in. long and 1.0 in. wide in the x-direction. The grip length was set to 3.0 in. on both sides (Figure 2.26a).

b. A foil bi-directional strain gage from Micro-Measurements Group, CEA-06-062WT-350, was mounted at the center of each coupon to measure the strains in the L-direction and T-direction (see Figure 2.2).

c. The displacement rate was set as 0.02in/min up to failure of the coupons.

d. Tensile modulus (E_L^t), tensile strength (F_L^c), ultimate strain (ε_L^t), and Poisson's ratio (ν_{LT}^t) were measured through these tests. The modulus was determined from the slope of the linear regression line of the stress-strain curve in the L-direction between strains 0.1% and 0.3%. Poisson's ratio (ν_{LT}^t) was determined from the stress-strain curves in the L-direction and T-direction between strains 0.1% and 0.3%.

e. Test results are described in Section 2.5.4.

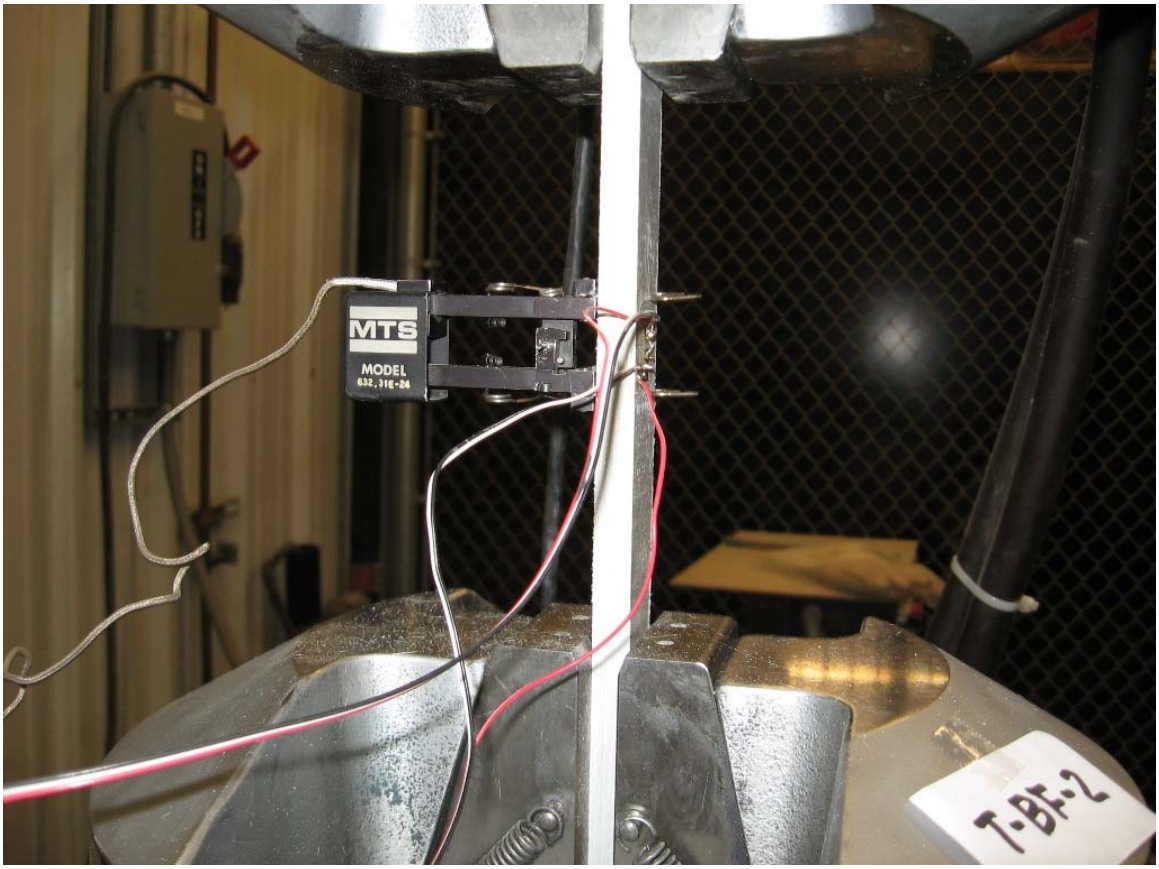

Figure 2.23: Typical tension coupon test setup

2.5.2 Compression Coupon Tests

Fifteen compression coupon tests were performed for each group of structural members utilizing a test protocol of ASTM D3410 (1995). Figure 2.24 shows a photo of a typical compression coupon test which is described as follows:

a. Prismatic coupons without end tabs were used in these tests. The coupons were 8.0 in. long and 1.0 in. wide in the L-direction. The grip length was set to 3.0 in. on both sides (Figure 2.26b).

b. A foil bi-directional strain gage from Micro-Measurements Group, CEA-06-062WT-350, was mounted at the center of each coupon to measure the strains in the L-direction and T-direction (see Figure 2.2).

c. The displacement rate was set as 0.02in/min up to failure of the coupons.

d. Compressive modulus (E_L^c), compressive strength (F_L^c), ultimate strain (ε_L^c), and Poisson's ratio (ν_{LT}^c) were measured through these tests. The modulus was determined from the slope of the linear regression line of the stress-strain curve between strains 0.1% and 0.3%. Poisson's ratio (ν_{LT}^c) was determined from the stress-strain curves in the L-direction and T-direction between strains 0.1% and 0.3%.

e. Test results are described in Section 2.5.4.

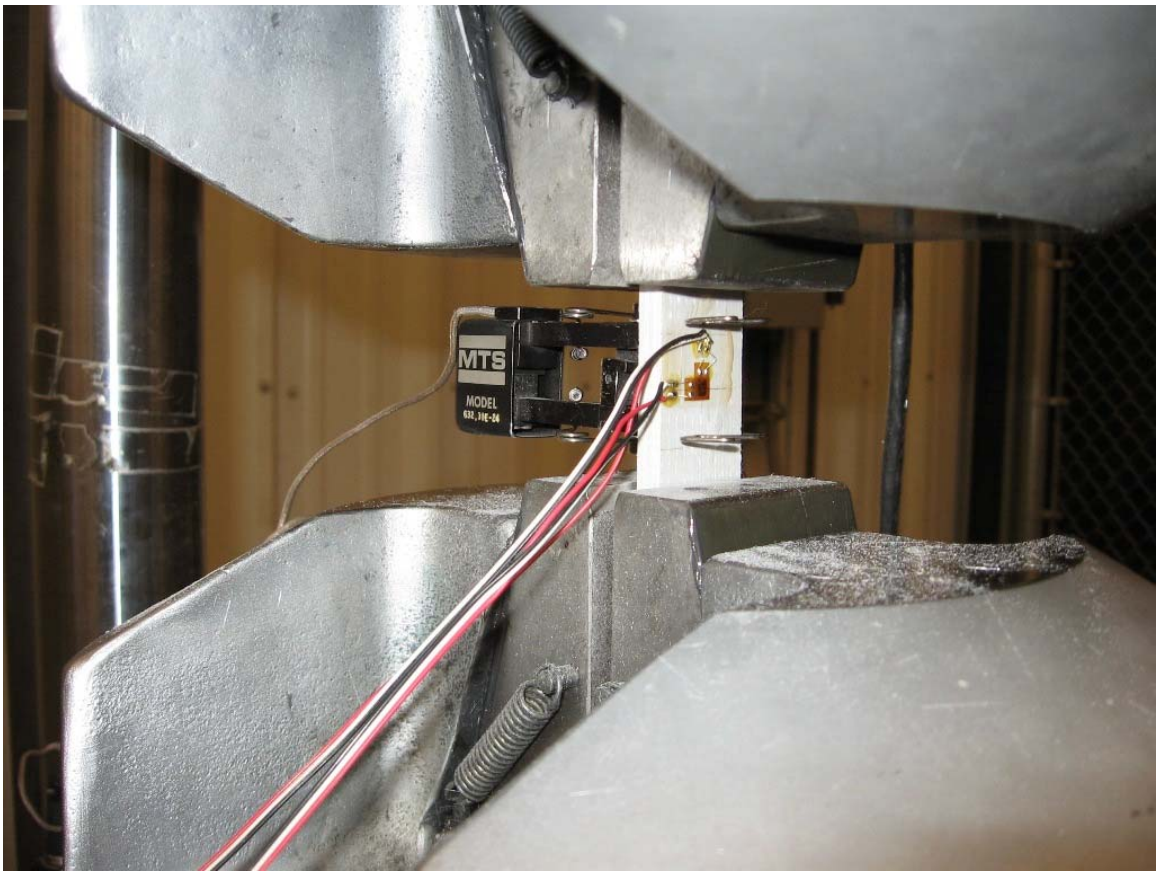

Figure 2.24: Typical compression coupon test setup

2.5.3 In-Plane Shear Coupon Tests

The in-plane shear properties were determined from tests performed using ten coupons for each group of structural members (Figure 2.25). These in-plane shear tests utilized the test protocols of ASTM D5379. However, the Georgia Tech shear fixture with large coupons was used instead of standard coupons in order to reduce inhomogenity of materials in pultruded coupons (Park, 2001):

a. The coupons were 8.0 in. long and 1.5 in. wide in the L-direction (Figure 2.26c).

b. The tensile load from a loading test system (MTS-810) was converted to an asymmetric four-point bending load by fixture.

c. The three strain-gage stacked rectangular rosettes from Micro-Measurements Group, CEA-06-125UR-350, were mounted at the center of the coupon specimens to measure the shear strains.

d. The displacement rate was set as 0.01in/min up to failure of the coupons.

e. Shear modulus, shear strength, ultimate shear strain were measured through these tests. The in-plane shear modulus was determined from the slope of the linear regression line of stress-strain curves between strains 0.1 % and 0.6 %.

f. Test results are described in Section 2.5.4.

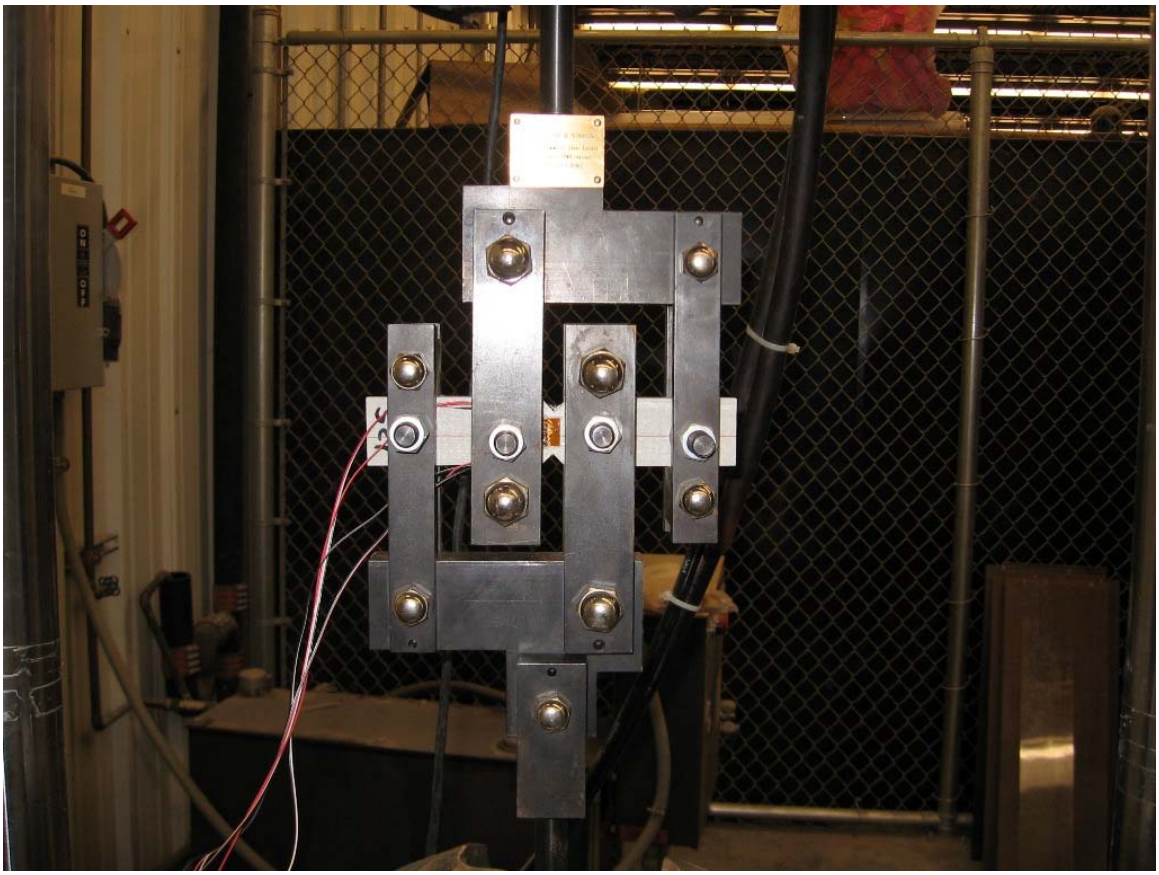

Figure 2.25: Typical in-plane shear coupon test setup

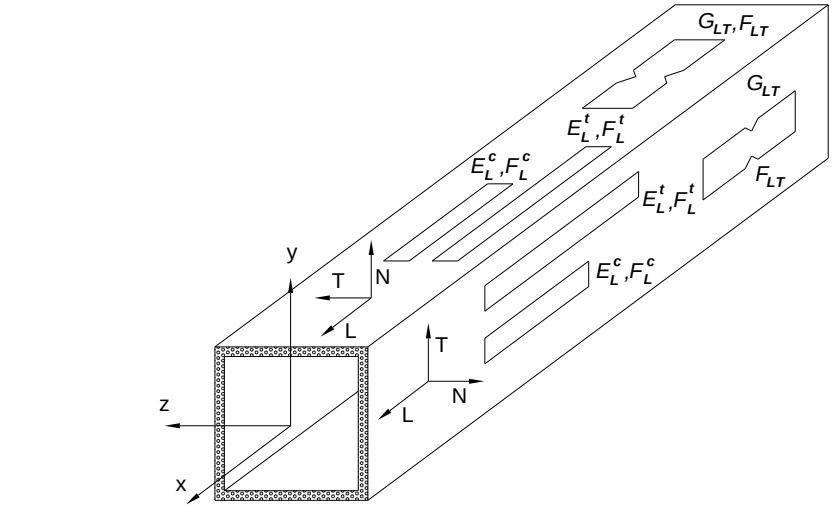

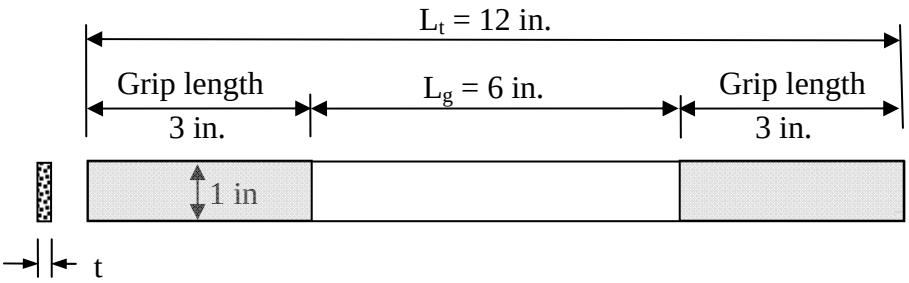

(a) Tension

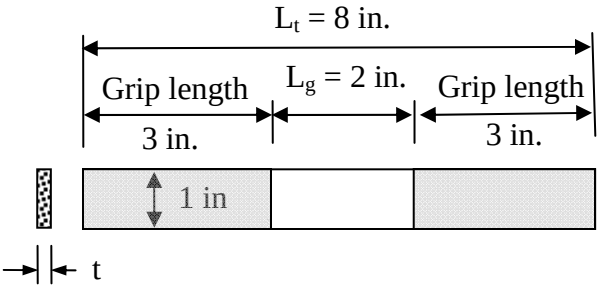

(b) Compression

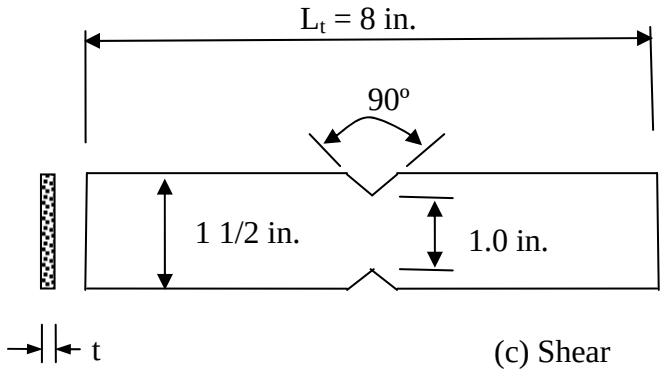

(c) Shear

Coupon Thickness
t = 3/8 in. (columns, flanges of beam & diagonal members)
t = 1/2 in. (Webs of beam & diagonal members)

Figure 2.26: Coupon dimensions for material tests

2.5.4 Mechanical Material Properties Tests Results

The measured mechanical material properties of each member are summarized in this Section. The following mechanical material properties were measured.

E_L^t: Tension modulus in the longitudinal-direction (ksi)

F_L^t: Tension strength in the longitudinal-direction (ksi)

ε_L^t: Tension ultimate strain in the longitudinal-direction

ν_{LT}^t: In-plane Poisson's ratio in tension test

E_L^c: Compression modulus in the longitudinal-direction (ksi)

F_L^c: Compression strength in the longitudinal-direction (ksi)

ε_L^c: Compression ultimate strain in the longitudinal-direction

ν_{LT}^c: In-plane Poisson's ratio in compression test.

G_{LT}: In-plane shear modulus (ksi)

F_{LT}: In-plane shear strength (ksi)

γ_{LT}: In-plane shear strain at failure

The measured mechanical material properties are presented in Tables 2.4 to 2.8. The following statistical results are presented in each table:

a. Arithmetic values of average (AVG), standard deviation (STD), and coefficient of variation (COV) of the population.

b. The characteristic value, x_{char}, of each material property was computed according to ASTM D7290 (ASTM, 2006) and the characteristic values and intermediate parameters are shown in each table. ASTM

D7290 standard defines the characteristic value as a statistically based property representing the 80% lower confidence bound on the 5th percentile of a specified population. The following parameters are used for the calculation of characteristic value, x_{char} :

$\hat{\alpha}$: Estimated Weibull scale parameter.

$\hat{\beta}$: Estimated Weibull shape parameter.

$x_{0.05}$: Nominal value of the sample data as the 5th percentile of two-parameter Weibull distribution

Ω : Data confidence factor that accounts for the uncertainty associated with a finite sample size

Tension/compression moduli (E_L^t and E_L^c) of coupons were obtained by using extensometers for measuring the strains up to 0.4%. The tension/compression strengths (F_L^t and F_L^c) of coupons were obtained directly from the machine.

Both the tension/compression 5th percentile moduli ($E_{L,0.05}^t$ and $E_{L,0.05}^c$) and tension/compression characteristic values of moduli ($E_{L,char}^t$ and $E_{L,char}^c$) were computed using all test data in accordance with ASTM7290 and presented in each table. In addition, the tensile/compression characteristic values of each strength properties ($F_{L,char}^t$ and $F_{L,char}^c$) were computed in accordance with ASTM7290 and presented in the tables. Failure strains (ε_L^t and ε_L^c) were not directly obtained because of limited numbers of strain-gage used.

For design point of view only, the characteristic values of failure strain for the coupons that did not have strains mounted at the center were estimated from the characteristic values of modulus and characteristic values of strength. Because the in-plane shear stress-strain curves of the composite are nonlinear, it was decided that ten strain gages be used so that the failure in-plane shear strains are obtained.

Tables 2.4 through 2.8 present the experimental results of the mechanical material properties obtained from five structural member groups shown in Table 2.2. Each table is followed by graphs showing tensile stress-strain curves, compression stress-strain curves, and in-plane stress-strain curves of coupons cut in Longitudinal-direction. In addition, each tension graph and compression graph show the predicted failure points as black dots. The following Table 2.3 shows table numbers and figure numbers for each material test group for reader's convenience.

Table 2.3: Tables and graphs for material properties test results

Group number	Location	Summary Table	Stress-Strain Curve		
			Tension Test	Compression Test	In-Plane Shear Test
1	Column members	Table 2.4	Figure 2.27	Figure 2.28	Figure 2.29
2	Top/bottom components of cross-section (flanges) of beams and diagonal member BR-1	Table 2.5	Figure 2.30	Figure 2.31	Figure 2.32
3	Side wall components of cross-section (Webs) of beams and diagonal member BR-1	Table 2.6	Figure 2.33	Figure 2.34	Figure 2.35
4	Flanges of diagonal member BR-2	Table 2.7	Figure 2.36	Figure 2.37	Figure 2.38
5	Webs of diagonal member BR-2	Table 2.8	Figure 2.39	Figure 2.40	Figure 2.41

Table 2.4: Mechanical material properties values of the column members (C1, C2) – GROUP1

Test	Const-ants	No. of samples	Unit				Characteristic Value Calculation					
				AVG	STD	COV	$\hat{\alpha}$	$\hat{\beta}$	COV	$x_{0.05}$	Ω	x_{char}
Tension *	E_L^t	15	ksi	5,050	150	3.0 %	5,125	32.8	4.0 %	4,681	0.963	4,508
	F_L^t	15	ksi	52.8	2.3	4.4	54.0	21.6	5.9 %	47.0	0.956	45.0
	$\varepsilon_L^{t\,**}$	-	%	-	-	-	-	-	-	1.004	-	0.998
	ν_{LT}^t	3	-	0.3	0.02	5.9	-	-	-	-	-	-
Compres-sion *	E_L^c	15	ksi	5,550	197	3.5 %	5,638	34.6	3.8 %	5,174	0.963	4,982
	F_L^c	15	ksi	59.4	5.4	9.1 %	61.7	13.6	9.1 %	49.9	0.933	46.2
	$\varepsilon_L^{c\,**}$	-	%	-	-	-	-	-	-	0.964	-	0.927
	ν_{LT}^c	3		0.25	0.03	12.2 %	-	-	-	-	-	-
In-Plane Shear	G_{LT}	10	ksi	541	29.2	5.4 %	55.5	20.1	6.3 %	479	0.937	449
	F_{LT}	10	ksi	9.8	0.32	3.3 %	99.4	30.1	4.4 %	9.0	0.950	8.5
	γ_{LT}	10	%	2.53	0.26	10.3 %	2.6	11.6	10.5 %	2.1	0.894	1.835

Note:

* Strain-gages were used for three samples.

** The ultimate strain is estimated based on the modulus and the strength.

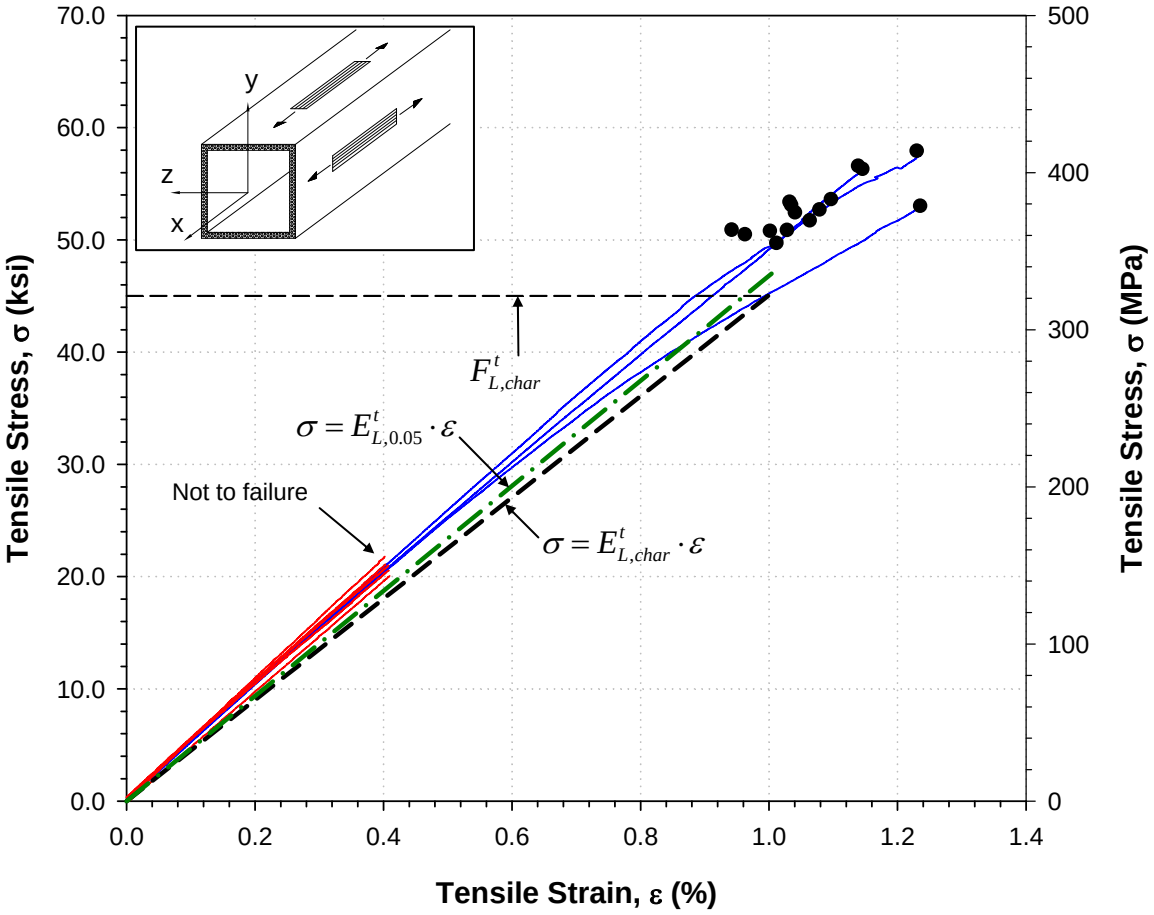

* Note

$E^t_{L,char}$	x_{char} of E^t_L (Characteristic value of E^t_L)
$E^t_{L,0.05}$	$x_{0.05}$ of E^t_L (5th percentile value of E^t_L based on two-parameter Weibull distribution)
$F^t_{L,char}$	x_{char} of F^t_L (Characteristic value of F^t_L)

Figure 2.27: Tension coupon test results for column members (C1, C2) in the L-direction

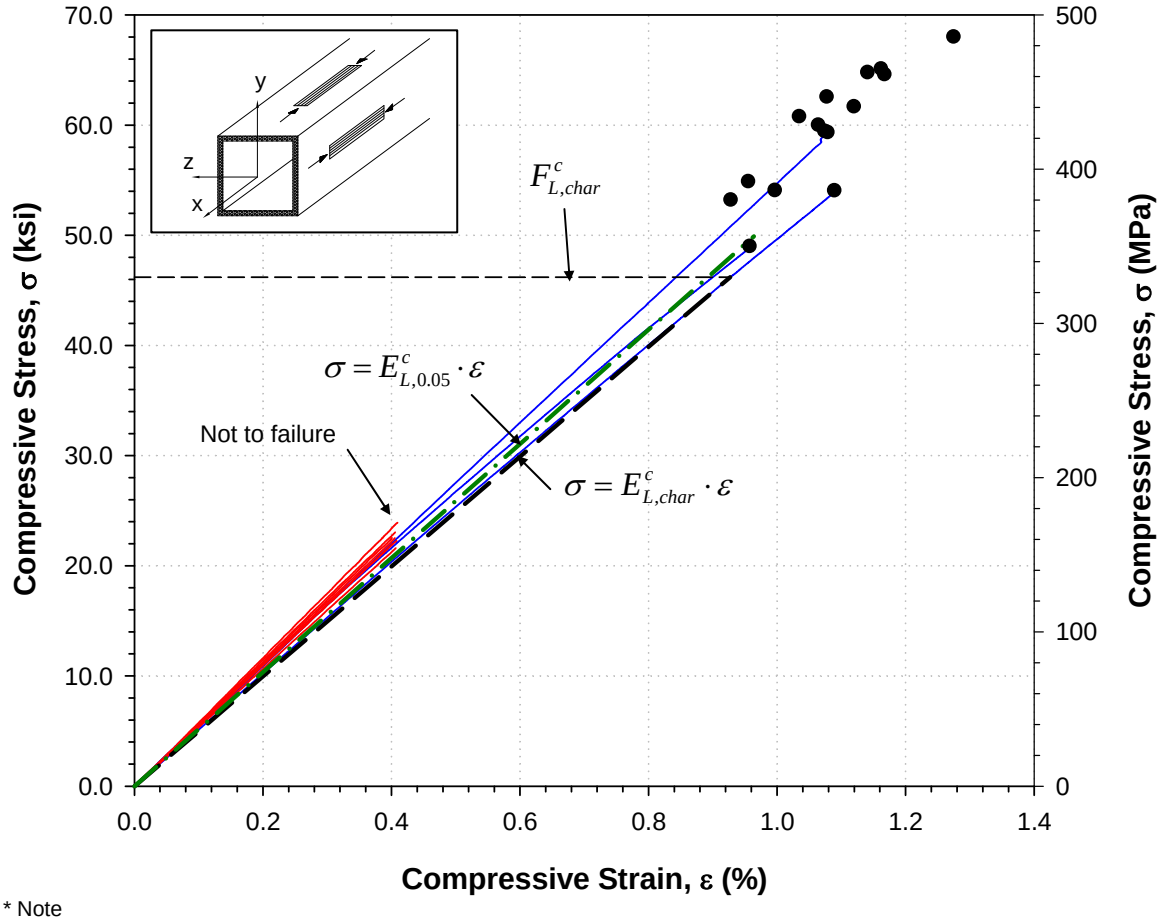

* Note

$E^c_{L,char}$	x_{char} of E^c_L (Characteristic value of E^c_L)
$E^c_{L,0.05}$	$x_{0.05}$ of E^c_L (5th percentile value of E^c_L based on two-parameter Weibull distribution)
$F^c_{L,char}$	x_{char} of F^c_L (Characteristic value of F^c_L)

Figure 2.28: Compression coupon test results for column members (C1, C2) in the L-direction

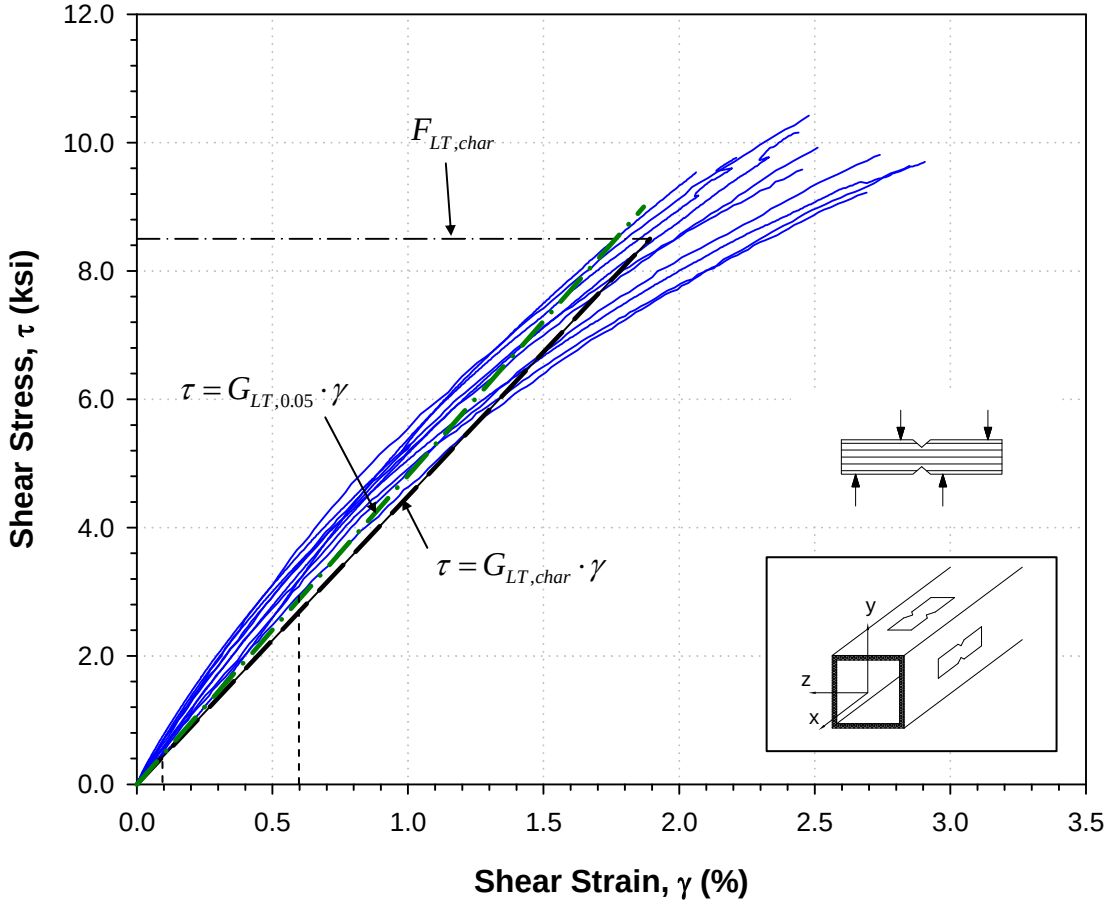

* Note

$G_{LT,char}$	x_{char} of G_{LT} (Characteristic value of G_{LT})
$G_{LT,0.05}$	$x_{0.05}$ of G_{LT} (5th percentile value of G_{LT} based on two-parameter Weibull distribution)
$F_{LT,char}$	x_{char} of F_{LT} (Characteristic value of F_{LT})

Figure 2.29: In-plane shear coupon test results for column members (C1, C2)

Table 2.5: Mechanical material properties values of the top & bottom wall components of beam and diagonal members (B1,B2,B3, BR1)–GROUP2

Test	Const-ants	No. of samples	Unit				Characteristic Value Calculation					
				AVG	STD	COV	$\hat{\alpha}$	$\hat{\beta}$	COV	$x_{0.05}$	Ω	x_{char}
Tension *	E_L^t	15	ksi	5,046	253	5.0 %	5,165	20.9	6.1 %	4,482	0.955	4,280
	F_L^t	15	ksi	48.3	2.6	5.4 %	49.5	23.9	5.4 %	43.7	0.960	41.9
	$\varepsilon_L^{t\,***}$	-	%	-	-	-	-	-	-	0.975	-	0.979
	ν_{LT}^t	3	-	0.25	0.02	8.0 %	-	-	-	-	-	-
Compres-sion **	E_L^c	15	ksi	5,351	187	3.5 %	5,442	29.3	4.5 %	4,917	0.963	4,736
	F_L^c	15	ksi	59.7	8.3	13.9 %	63.4	7.3	16.1 %	42.1	0.880	37.1
	$\varepsilon_L^{c\,***}$	-	%	-	-	-	-	-	-	0.856	-	0.783
	ν_{LT}^c	2	-	0.24	0.01	4.2 %	-	-	-	-	-	-
In-Plane Shear	G_{LT}	10	ksi	677	34.9	5.2 %	69.4	20.5	6.2 %	600	0.938	563
	F_{LT}	10	ksi	11.5	0.5	4.3 %	11.7	27.1	4.8 %	10.5	0.950	10.0
	γ_{LT}	10	%	2.72	0.30	11.0 %	2.9	9.3	12.9 %	2.1	0.870	1.8

Note:

* Strain-gage were used for three samples

** Strain-gage were used for two samples

*** The ultimate strains are estimated based on the modulus and the strength.

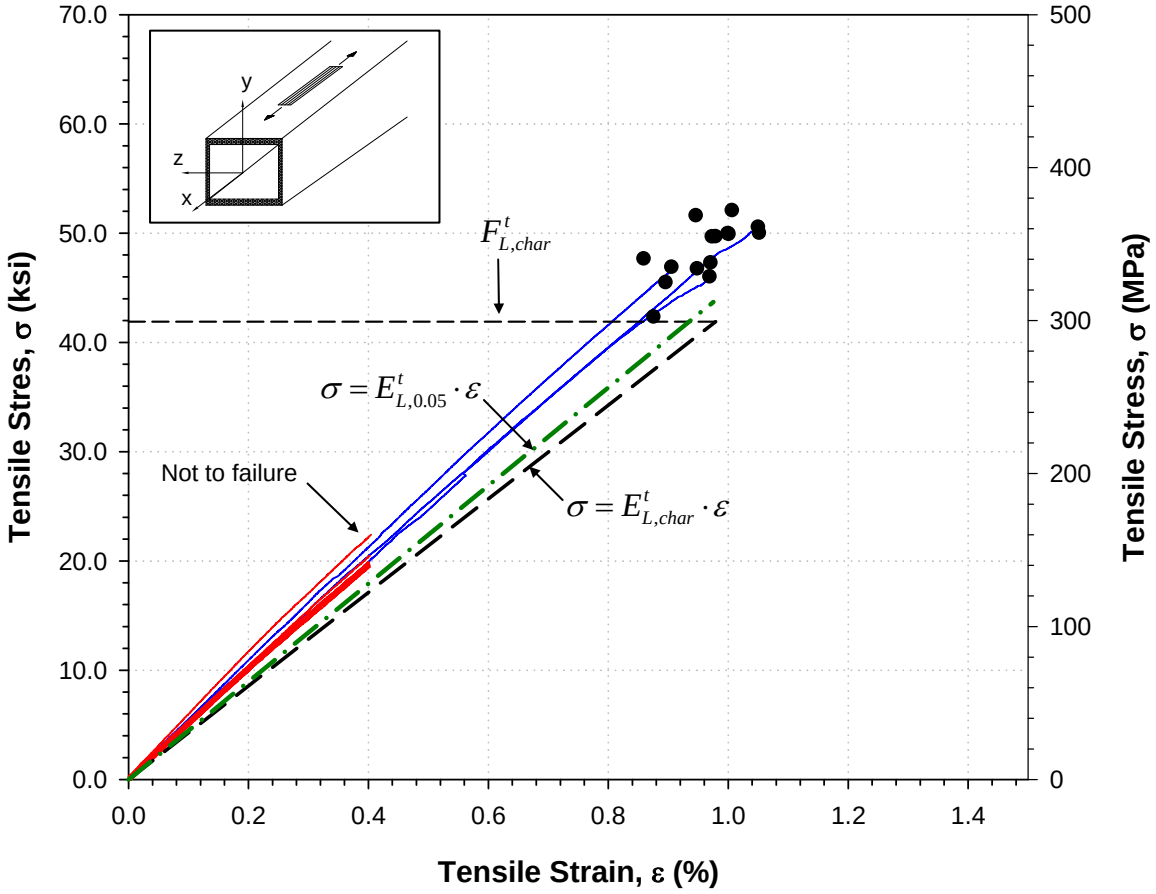

* Note

$E^t_{L,char}$	x_{char} of E^t_L (Characteristic value of E^t_L)
$E^t_{L,0.05}$	$x_{0.05}$ of E^t_L (5th percentile value of E^t_L based on two-parameter Weibull distribution)
$F^t_{L,char}$	x_{char} of F^t_L (Characteristic value of F^t_L)

Figure 2.30: Tension coupon test results for top & bottom walls of beam and diagonal members (B1,B2,B3, BR1) in the L-direction

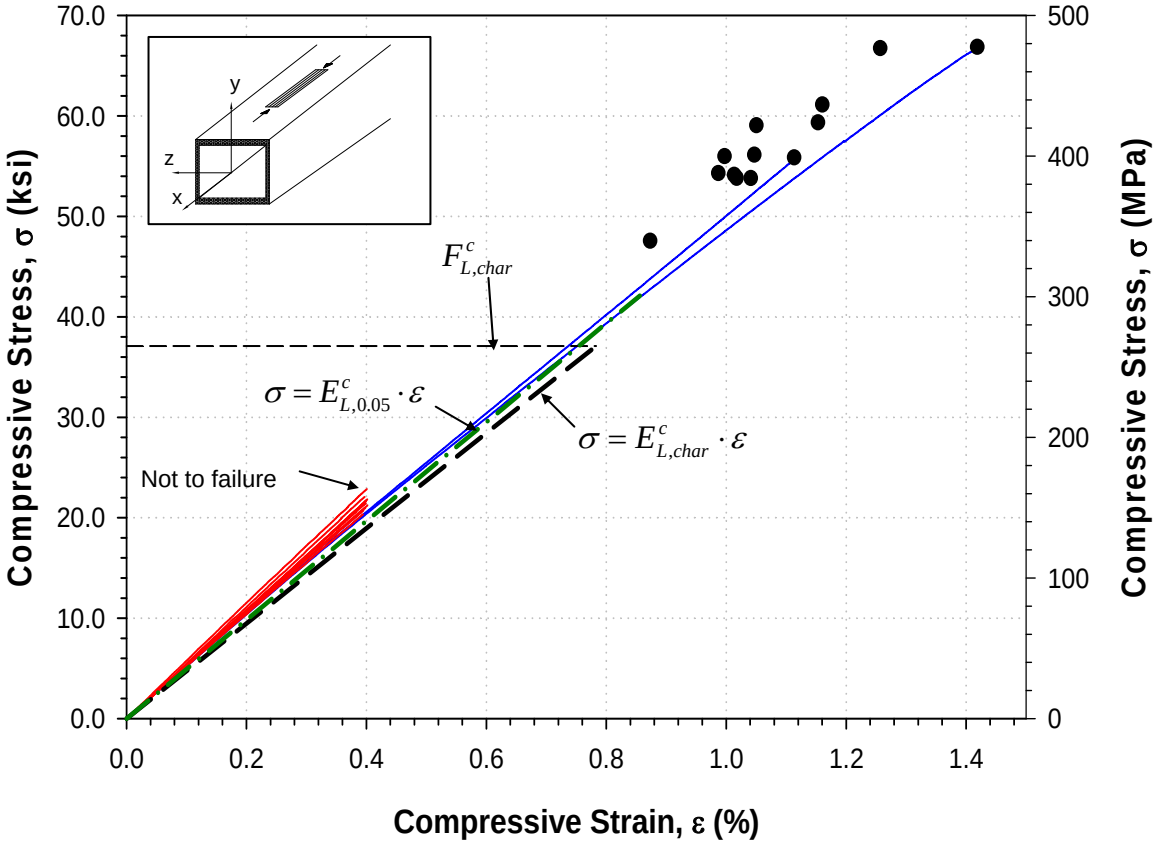

* Note

$E^c_{L,char}$	x_{char} of E^c_L (Characteristic value of E^c_L)
$E^c_{L,0.05}$	$x_{0.05}$ of E^c_L (5th percentile value of E^c_L based on two-parameter Weibull distribution)
$F^c_{L,char}$	x_{char} of F^c_L (Characteristic value of F^c_L)

Figure 2.31: Compression coupon test results for top & bottom wall components of beam and diagonal members (B1,B2,B3, BR1) in the L-direction

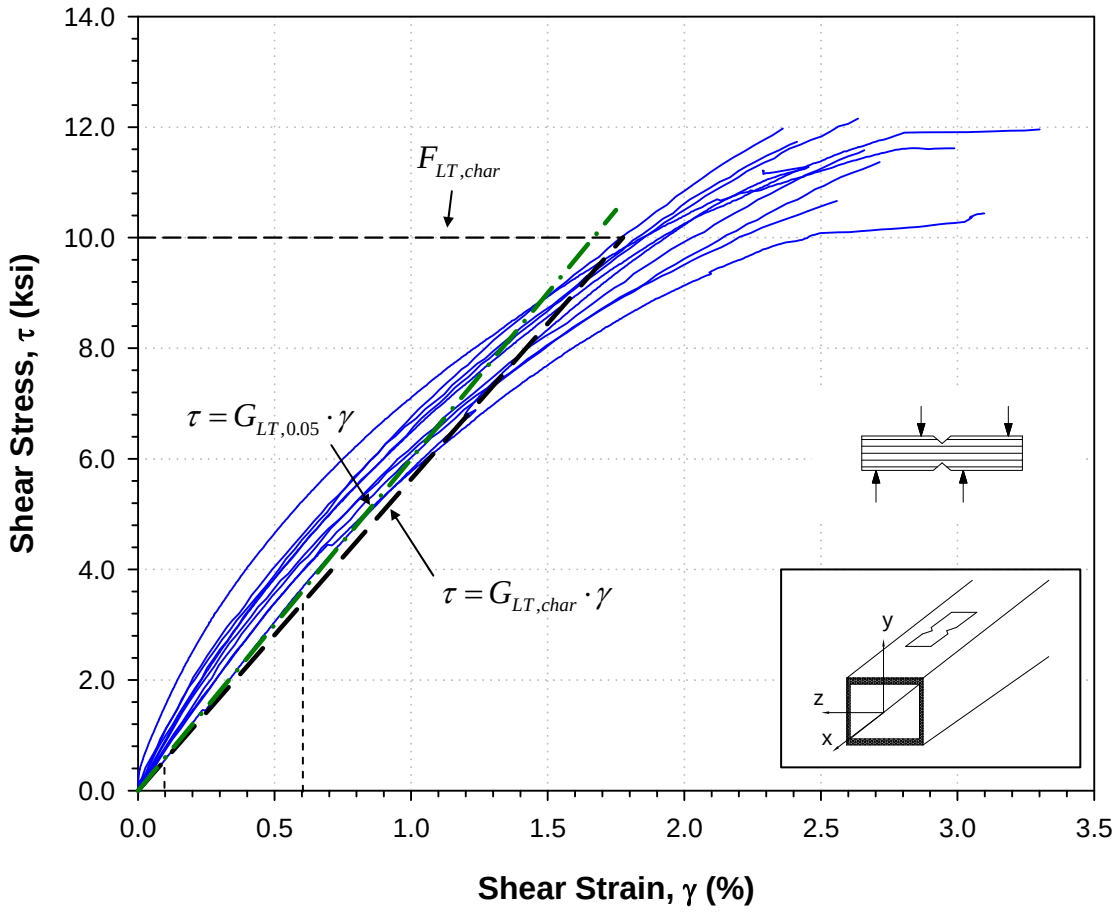

* Note

$G_{LT,char}$	x_{char} of G_{LT} (Characteristic value of G_{LT})
$G_{LT,0.05}$	$x_{0.05}$ of G_{LT} (5th percentile value of G_{LT} based on two-parameter Weibull distribution)
$F_{LT,char}$	x_{char} of F_{LT} (Characteristic value of F_{LT})

Figure 2.32: In-plane shear coupon test results for top & bottom walls of beam and diagonal members (B1,B2,B3, BR1)

Table 2.6: Mechanical material property value of the side wall component of beam and diagonal members (B1,B2,B3,BR1) – GROUP3

Test	Const-ants	No. of samples.	Unit				Characteristic Value Calculation					
				AVG	STD	COV	$\hat{\alpha}$	$\hat{\beta}$	COV	$x_{0.05}$	Ω	x_{char}
Tension *	E_L^t	15	ksi	4,225	309	7.3 %	4,370	13.4	9.2 %	3,499	0.932	3,260
	F_L^t	15	ksi	39.1	3.8	9.7 %	40.8	12.1	10.1 %	31.9	0.925	29.5
	$\varepsilon_L^{t\ ***}$	-	%	-	-	-	-	-	-	0.911	-	0.904
	ν_{LT}^t	3	-	0.25	0.02	8.0 %	-	-	-	-	-	-
Compres-sion **	E_L^c	15	ksi	4,304	339	7.9 %	4,456	14.9	8.3 %	3,655	0.939	3,431
	F_L^c	15	ksi	47.6	6.3	13.3 %	50.2	9.4	12.8 %	36.57	0.905	33.1
	$\varepsilon_L^{c\ ***}$	-	%	-	-	-	-	-	-	1.00	-	0.964
	ν_{LT}^c	2	-	0.25	0.01	4.0 %	-	-	-	-	-	-
In-Plane Shear	G_{LT}	10	ksi	694	39.2	5.7 %	71.2	19.1	6.6 %	610	0.933	569
	F_{LT}	10	ksi	11.6	0.8	6.9 %	11.9	18.8	6.7 %	10.2	0.933	9.5
	γ_{LT}	10	%	2.43	0.34	14.0 %	2.6	7.9	15.0 %	1.77	0.849	1.80

Note:

* Strain-gage were used for three samples

** Strain-gage were used for two samples

*** The ultimate strains are based on the modulus and the strength.

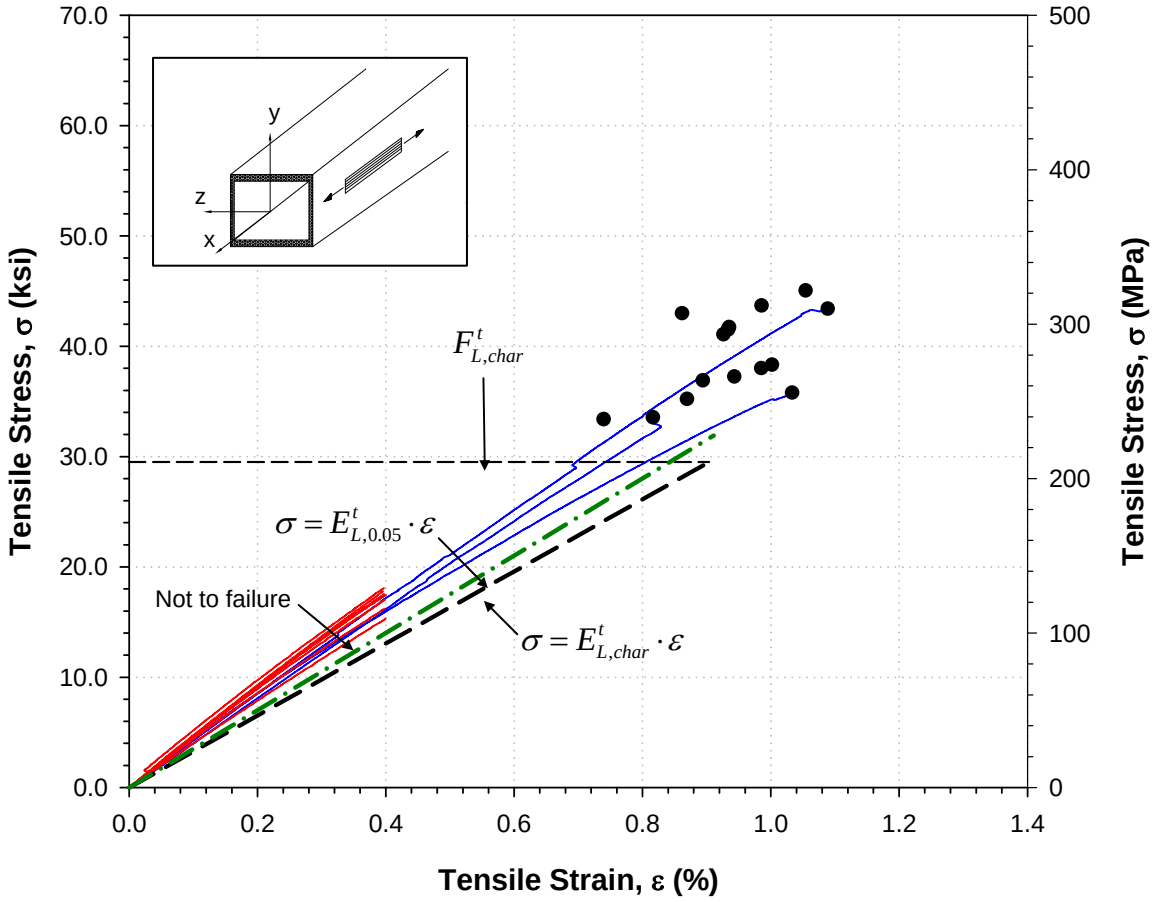

* Note

$E^t_{L,char}$	x_{char} of E^t_L (Characteristic value of E^t_L)
$E^t_{L,0.05}$	$x_{0.05}$ of E^t_L (5th percentile value of E^t_L based on two-parameter Weibull distribution)
$F^t_{L,char}$	x_{char} of F^t_L (Characteristic value of F^t_L)

Figure 2.33: Tension coupon test results for side walls of beam and diagonal members (B1, B2, B3, BR1) in the L-direction

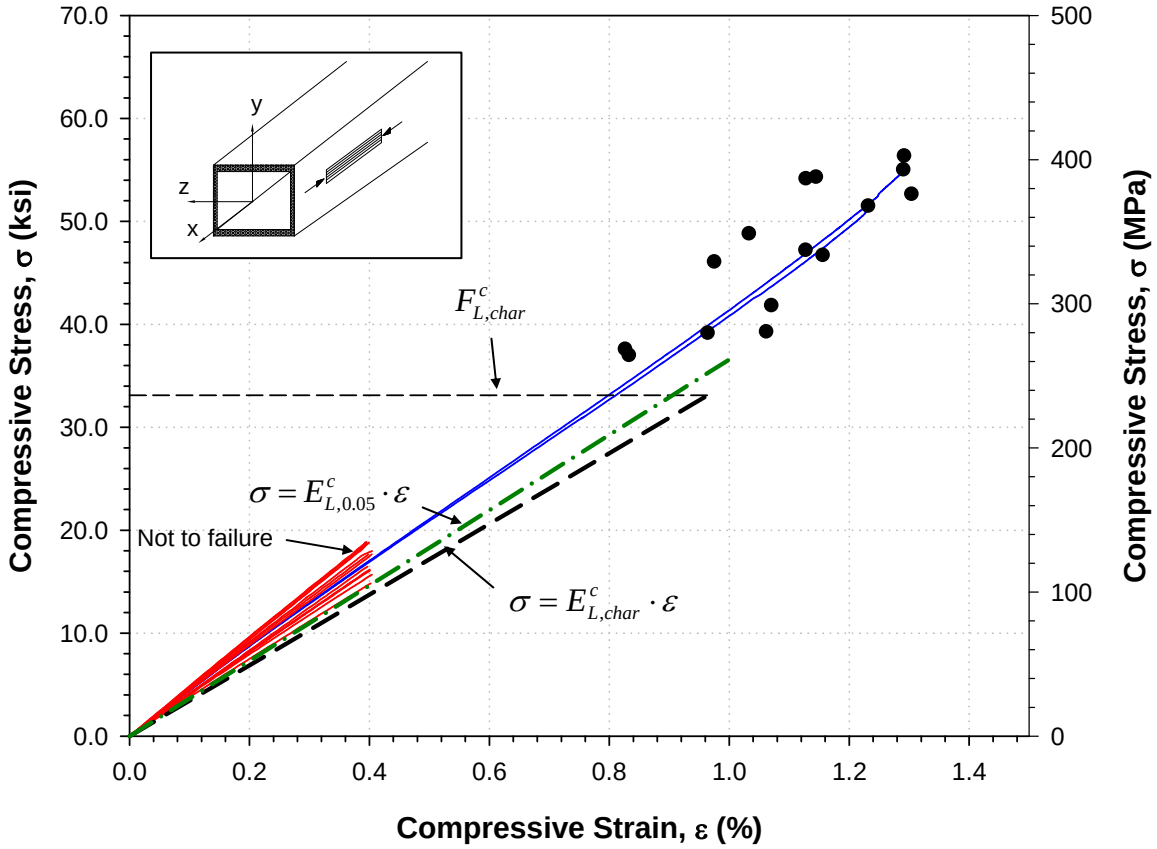

* Note

$E^c_{L,char}$	x_{char} of E^c_L (Characteristic value of E^c_L)
$E^c_{L,0.05}$	$x_{0.05}$ of E^c_L (5th percentile value of E^c_L based on two-parameter Weibull distribution)
$F^c_{L,char}$	x_{char} of F^c_L (Characteristic value of F^c_L)

Figure 2.34: Compression coupon test results for side walls of beam and diagonal members (B1, B2, B3, BR1) in the L-direction

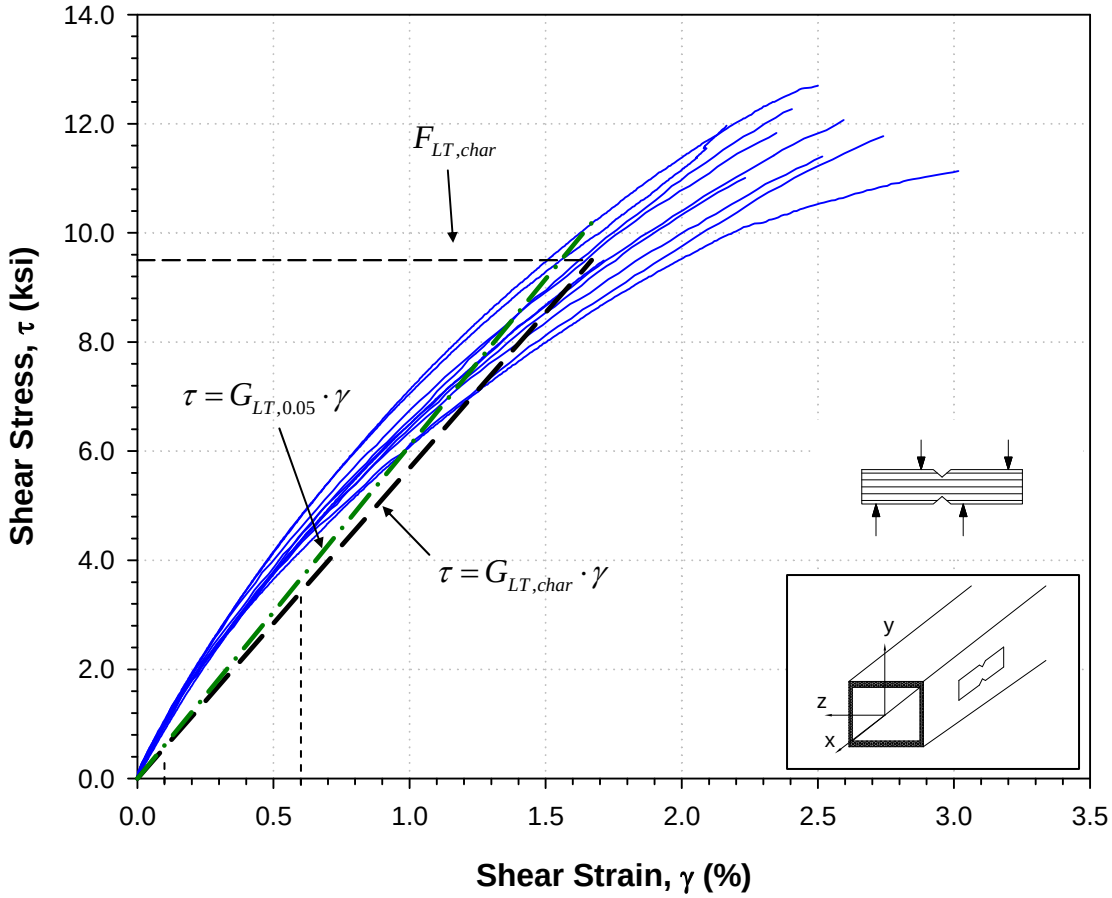

* Note

$G_{LT,char}$	x_{char} of G_{LT} (Characteristic value of G_{LT})
$G_{LT,0.05}$	$x_{0.05}$ of G_{LT} (5th percentile value of G_{LT} based on two-parameter Weibull distribution)
$F_{LT,char}$	x_{char} of F_{LT} (Characteristic value of F_{LT})

Figure 2.35: In-plane shear coupon test results for side walls of beam and diagonal members (B1,B2,B3, BR1)

Table 2.7: Mechanical material property value of the flange component of diagonal member (BR2) – GROUP4

Test	Const-ants	No. of samples	Unit				Characteristic Value Calculation					
				AVG	STD	COV	$\hat{\alpha}$	$\hat{\beta}$	COV	$x_{0.05}$	Ω	x_{char}
Tension *	E_L^t	15	ksi	3,928	190	4.8 %	4,011	27.8	4.7 %	3.605	0.963	3,472
	F_L^t	15	ksi	36.7	3.3	9.0 %	38.2	12.4	9.9 %	30.0	0.927	27.8
	$\varepsilon_L^{t\ ***}$	-	%	-	-	-	-	-	-	0.832	-	0.801
	ν_{LT}^t	3	-	0.25	0.02	8.0 %	-	-	-	-	-	-
Compres-sion **	E_L^c	15	ksi	4,230	249	5.9 %	4,349	17.4	7.2 %	3,666	0.947	3,470
	F_L^c	15	ksi	46.5	5.5	11.8 %	48.9	9.7	12.4 %	35.9	0.908	32.7
	$\varepsilon_L^{c\ ***}$	-	%	-	-	-	-	-	-	0.979	-	0.942
	ν_{LT}^c	2	-	0.25	0.01	4.0 %	-	-	-	-	-	-
In-Plane Shear	G_{LT}	10	ksi	526	31.6	6.0 %	540	21.4	6.0 %	470	0.940	442.8
	F_{LT}	10	ksi	9.3	0.3	3.3 %	9.4	37.5	3.6 %	8.71	0.950	8.3
	γ_{LT}	10	%	2.45	0.2	9.3 %	2.6	11.9	10.3	1.98	0.896	1.781

Note:

* Strain-gage were used for three samples

** Strain-gage were used for two samples

*** The ultimate strains are estimated from the modulus and the strength.

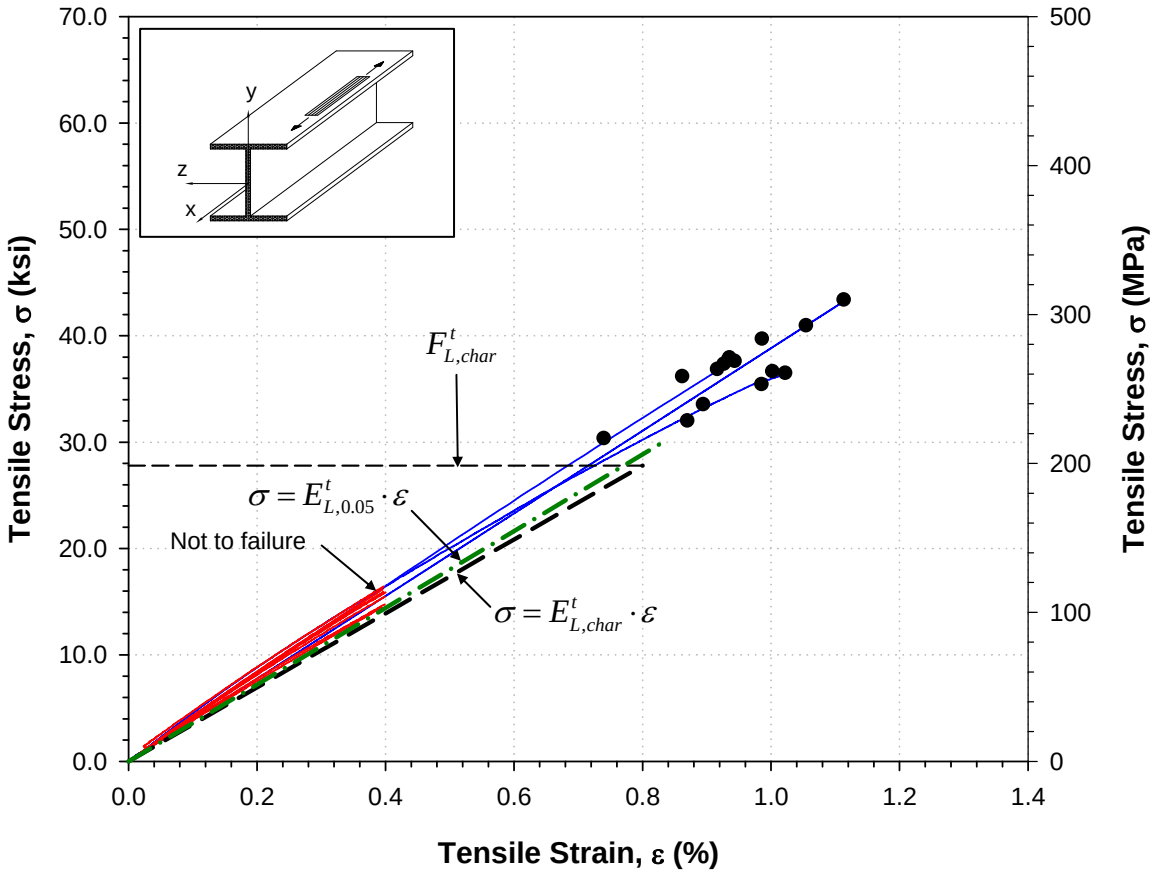

* Note

$E^t_{L,char}$	x_{char} of E^t_L (Characteristic value of E^t_L)
$E^t_{L,0.05}$	$x_{0.05}$ of E^t_L (5th percentile value of E^t_L based on two-parameter Weibull distribution)
$F^t_{L,char}$	x_{char} of F^t_L (Characteristic value of F^t_L)

Figure 2.36: Tension coupon test results for flanges of diagonal member (BR2) in the L-direction

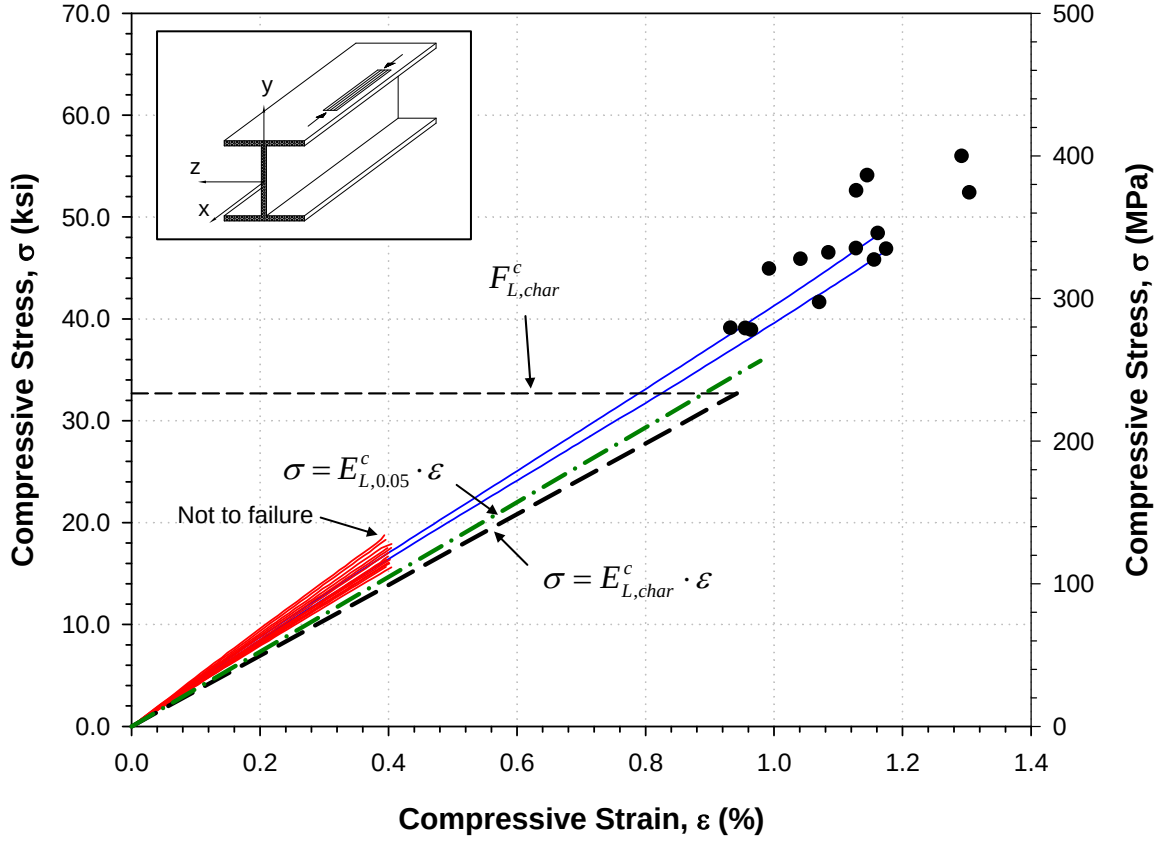

* Note

$E^c_{L,char}$	x_{char} of E^c_L (Characteristic value of E^c_L)
$E^c_{L,0.05}$	$x_{0.05}$ of E^c_L (5th percentile value of E^c_L based on two-parameter Weibull distribution)
$F^c_{L,char}$	x_{char} of F^c_L (Characteristic value of F^c_L)

Figure 2.37: Compression coupon test results for flanges of diagonal member (BR2) in the L-direction

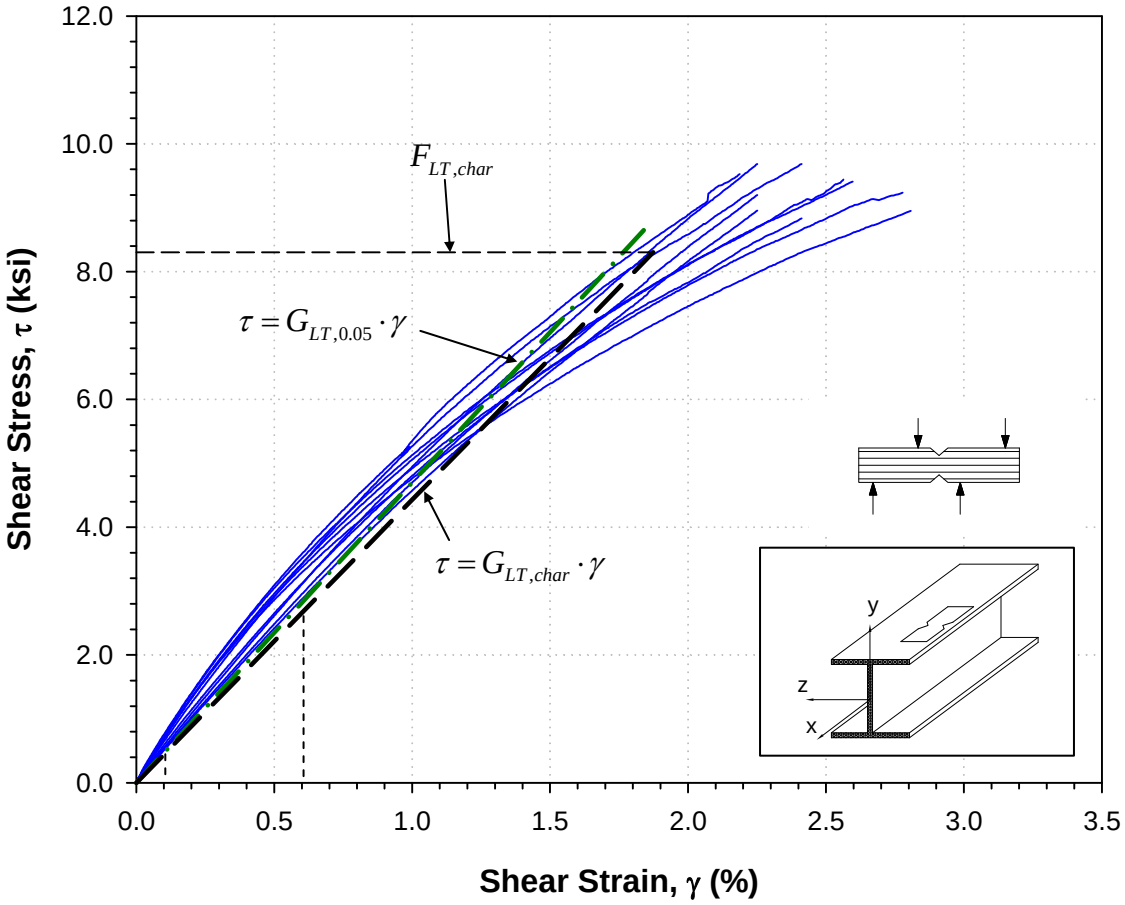

*** Note**

$G_{LT,char}$	x_{char} of G_{LT} (Characteristic value of G_{LT})
$G_{LT,0.05}$	$x_{0.05}$ of G_{LT} (5th percentile value of G_{LT} based on two-parameter Weibull distribution)
$F_{LT,char}$	x_{char} of F_{LT} (Characteristic value of F_{LT})

Figure 2.38: In-plane shear coupon test results for flanges of beam and diagonal members (BR2)

Table 2.8: Mechanical material property value of the web component of diagonal member (BR2) – GROUP 5

Test	Const-ants	No. of samples	Unit				Characteristic Value Calculation					
				AVG	STD	COV	$\hat{\alpha}$	$\hat{\beta}$	COV	$x_{0.05}$	Ω	x_{char}
Tension *	E_L^t	15	ksi	4,148	154	3.7	4,220	28.9	4.5 %	3,808	0.963	3,667
	F_L^t	15	ksi	39.2	3.7	9.4	40.7	12.5	9.8 %	32.1	0.928	29.8
	$\varepsilon_L^{t\,***}$	-	%	-	-	-	-	-	-	0.842	-	0.813
	ν_{LT}^t	3	-	0.25	0.02	8.0	-	-	-	-	-	-
Compres-sion **	E_L^c	15	ksi	4,227	266	6.3	4,351	17.1	7.3 %	3,658	0.946	3,460
	F_L^c	15	ksi	46.2	5.5	11.8	48.5	9.5	12.6 %	35.5	0.907	32.2
	$\varepsilon_L^{c\,***}$	-	%	-	-	-	-	-	-	0.970	-	0.931
	ν_{LT}^c	2	-	0.26	0.02	7.7	-	-	-	-	-	-
In-Plane Shear	G_{LT}	10	ksi	636	30.8	4.8 %	650	24.8	5.2 %	576	0.948	547
	F_{LT}	10	ksi	12.0	0.9	7.9 %	12.4	17.0	7.4 %	10.4	0.926	9.64
	γ_{LT}	10	%	2.57	0.17	6.8 %	2.6	16.4	7.6 %	2.20	0.923	2.03

Note:

* Strain-gage were used for three samples

** Strain-gage were used for two samples

*** The ultimate strains are estimated from the modulus and the strength.

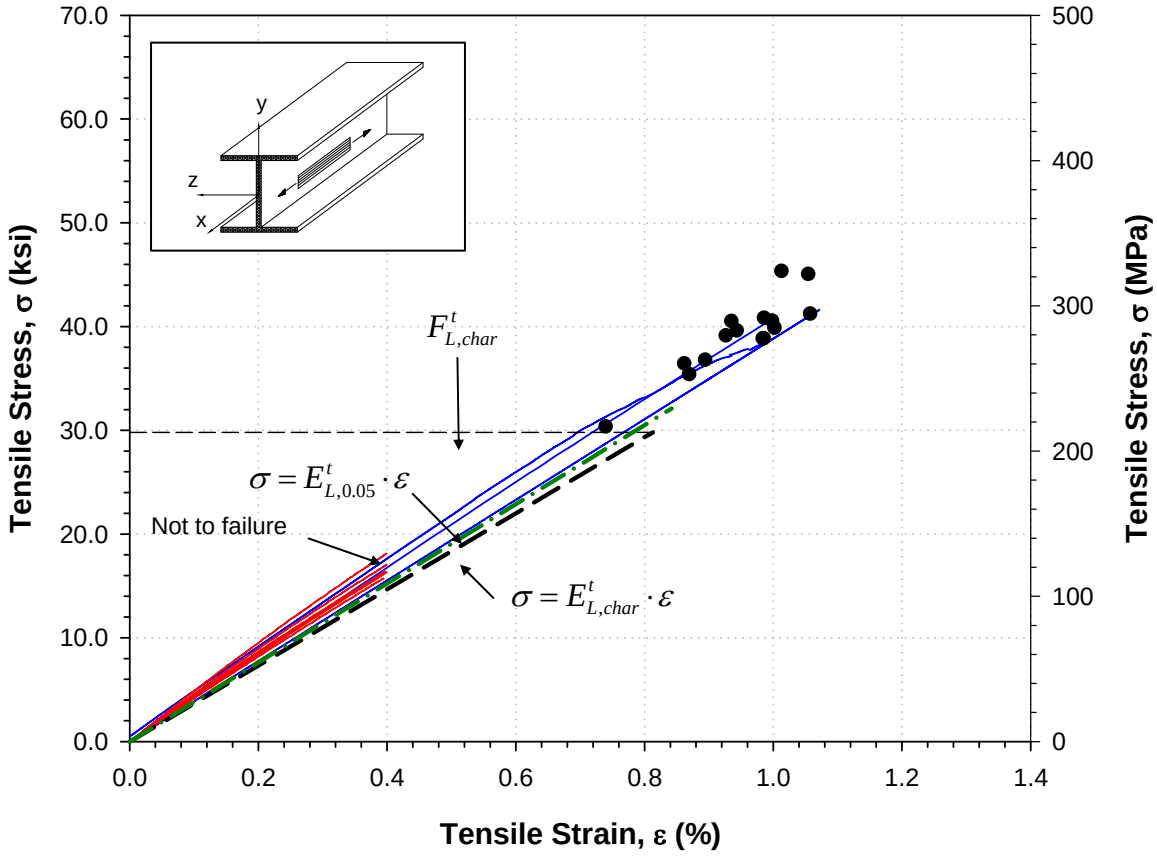

* Note

$E^t_{L,char}$	x_{char} of E^t_L (Characteristic value of E^t_L)
$E^t_{L,0.05}$	$x_{0.05}$ of E^t_L (5th percentile value of E^t_L based on two-parameter Weibull distribution)
$F^t_{L,char}$	x_{char} of F^t_L (Characteristic value of F^t_L)

Figure 2.39: Tension coupon test results for webs of diagonal member (BR2) in the L-direction

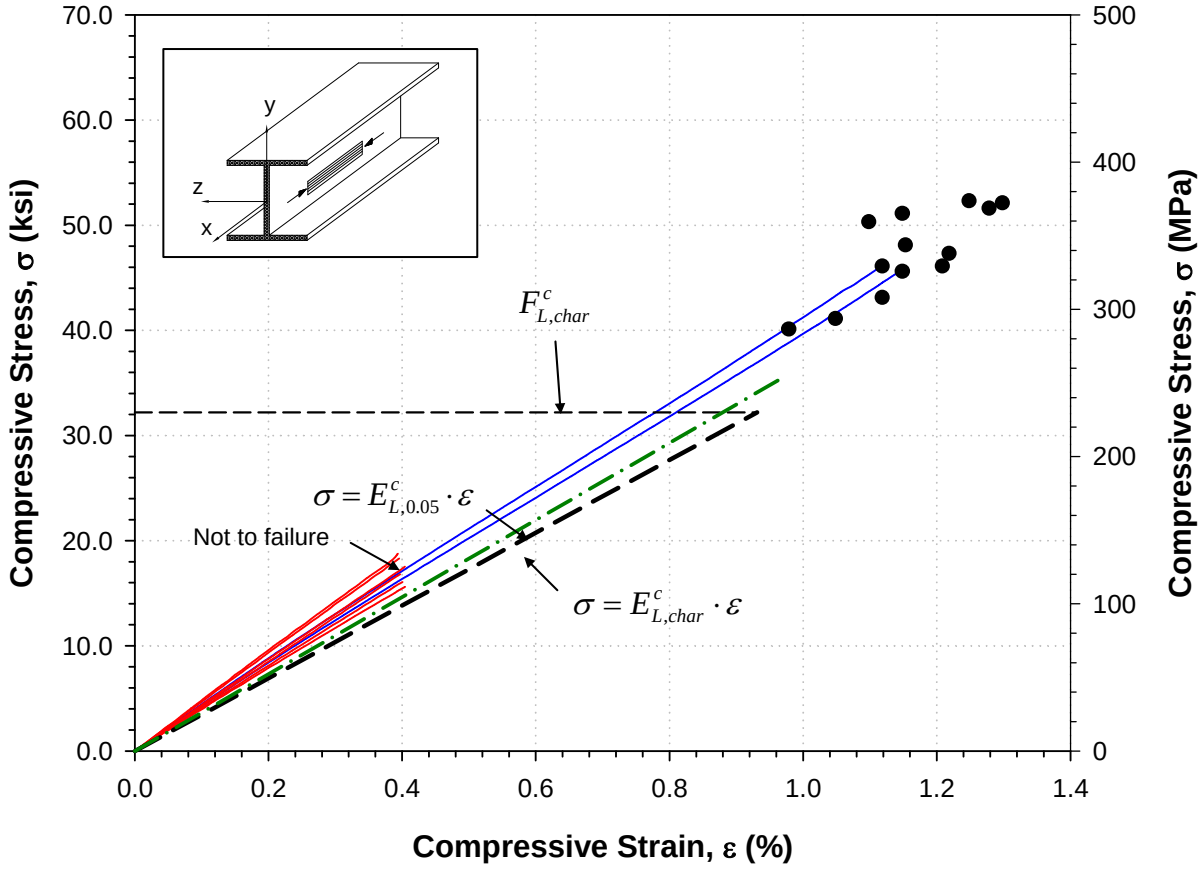

* Note

$E^c_{L,char}$	x_{char} of E^c_L (Characteristic value of E^c_L)
$E^c_{L,0.05}$	$x_{0.05}$ of E^c_L (5th percentile value of E^c_L based on two-parameter Weibull distribution)
$F^c_{L,char}$	x_{char} of F^c_L (Characteristic value of F^c_L)

Figure 2.40: Compression coupon test results for webs of diagonal member (BR2) in the L-direction

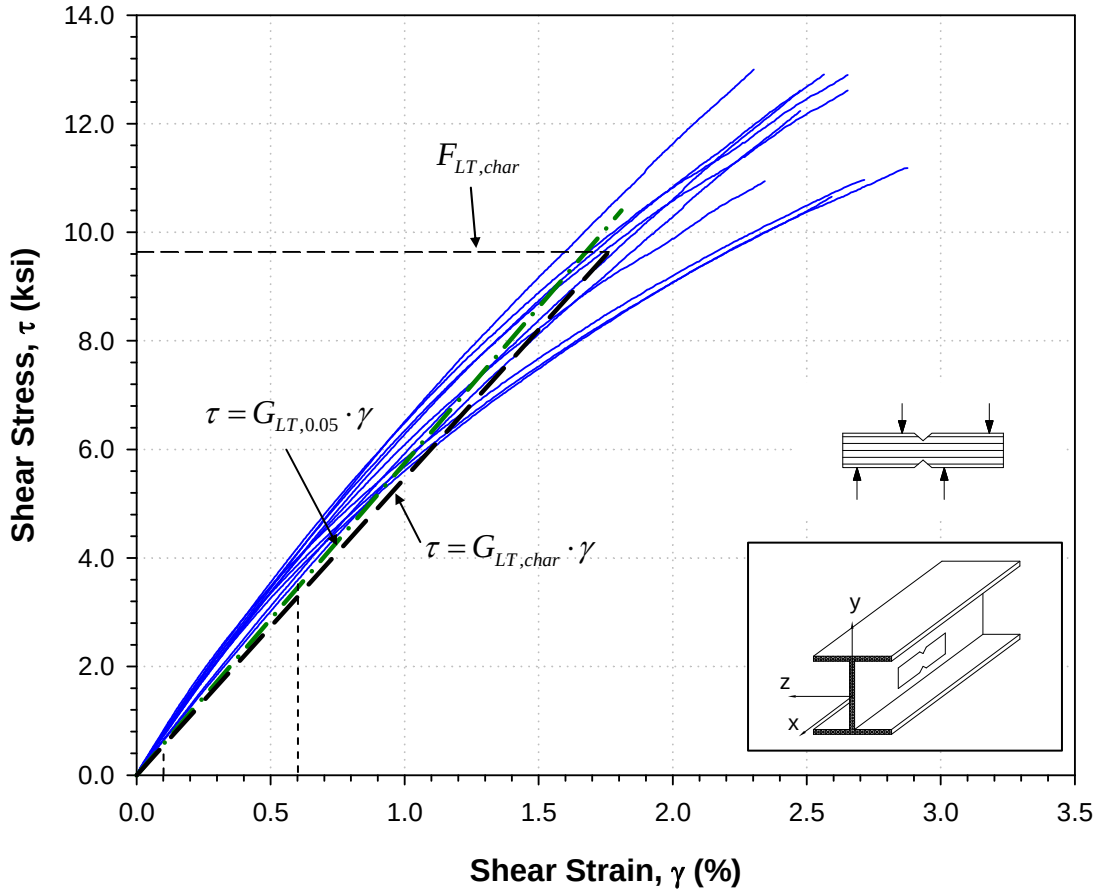

* Note

$G_{LT,char}$	x_{char} of G_{LT} (Characteristic value of G_{LT})
$G_{LT,0.05}$	$x_{0.05}$ of G_{LT} (5th percentile value of G_{LT} based on two-parameter Weibull distribution)
$F_{LT,char}$	x_{char} of F_{LT} (Characteristic value of F_{LT})

Figure 2.41: In-plane shear coupon test results for webs of beam and diagonal members (BR2)

2.6 Experimental Setups of Full-Scale Frame Tests

Six frame configurations with different number of diagonal members and beam-column boundary conditions were presented in Section 2.4. Three loading cases on each frame configuration result in a total of 18 test setup cases (Table 2.9). The test identification names of the 18 test cases are set as shown in Figure 2.42. Table 2.9 shows the 18 test cases used for the experimental investigation of this thesis. The experimental set-up associated with each test consisted of:

a. A hydraulic actuator installed on the reinforced concrete reaction wall in the same plane as that of the test frame so that an external concentrated force from the actuator could be applied to one joint of the frame.

b. Five potentiometers installed on each beam-column joint except the joint subjected to the external force. These potentiometers were used to measure the horizontal joint displacements of the frame.

c. Electronically, the force and displacement data are collected at the rate of one sample per second during the tests so that the force-displacement histories were obtained.

d. Six out-of-plane support fixtures (Figure 2.43) composed of steel tube members installed on the concrete reaction wall to prevent out-of-plane movement of the frames during the tests. Teflon pads were attached to the out-of-plane support fixtures to minimize friction between the composite frame and the out-of-plane support fixtures.

e. It should be noted that actual external force and joint displacements were measured at 'outer face' of columns, not a cross point of column centerline and beam centerline. Nevertheless, the measured data were regarded as an external load and displacements of the cross point of column centerline and beam centerline. The effects of local deflection of the locations for external force and displacements measurements were ignored.

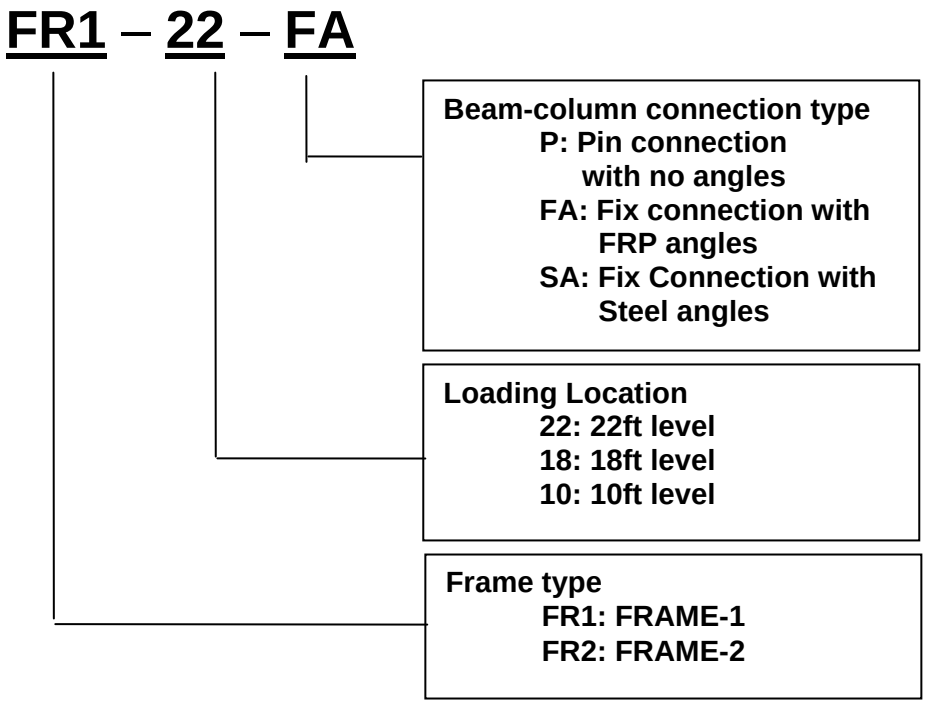

Figure 2.42: Test case identification name

Table 2.9: Full-scale frame test configurations summary

Test case ID. (Figure 2.42)	Frame (Table 2.1)	Loading Height	Test Layout	Set-up plan
FR1-22-P FR1-22-FA FR1-22-SA	FRAME-1 series	22 ft	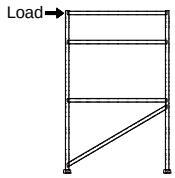	Figure 2.44
FR1-18- P FR1-18- FA FR1-18- SA		18 ft	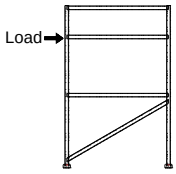	Figure 2.46
FR1-10- P FR1-10- FA FR1-10- SA		10 ft	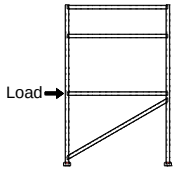	Figure 2.48
FR2-22- P FR2-22- FA FR2-22- SA	FRAME-2 series	22 ft	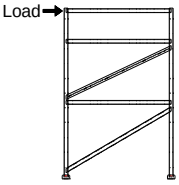	Figure 2.50
FR2-18- P FR2-18- FA FR2-18- SA		18 ft	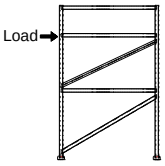	Figure 2.52
FR2-10- P FR2-10- FA FR2-10- SA		10 ft	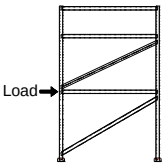	Figure 2.54

Note: Loading height is measured from bottom of column base plate.

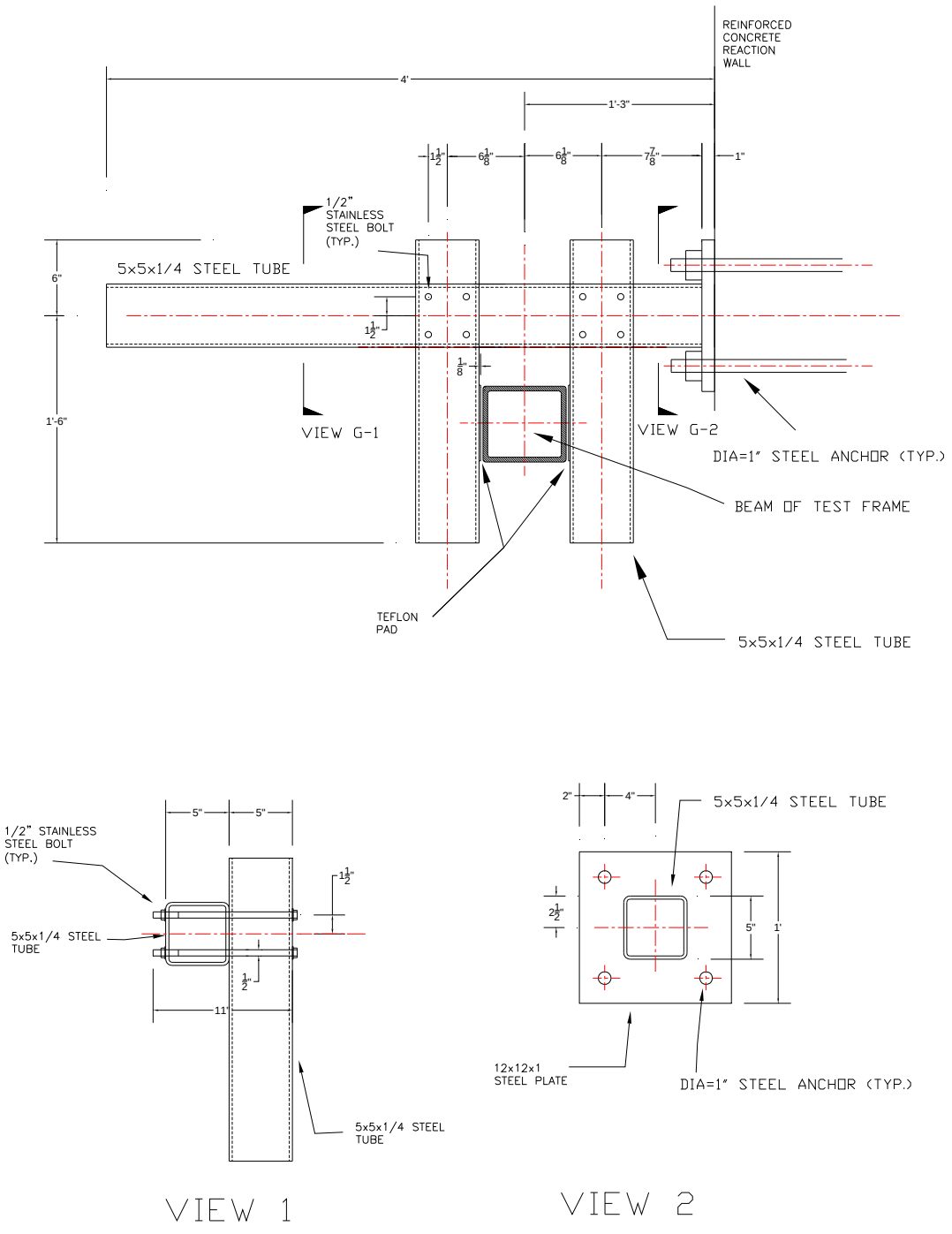

Figure 2.43: Out-of-plane support fixture drawing

2.6.1 'FR1-22' Test Series Setup

Figure 2.44 shows the experimental setup plan for the 'FR1-22' test series, and Figure 2.45 shows one test in progress for the 'FR1-22'test series. The manual-hydraulic jack for the FR1-22 test series was placed on the side of the frame at 22 ft. above the bottom of column base plate.

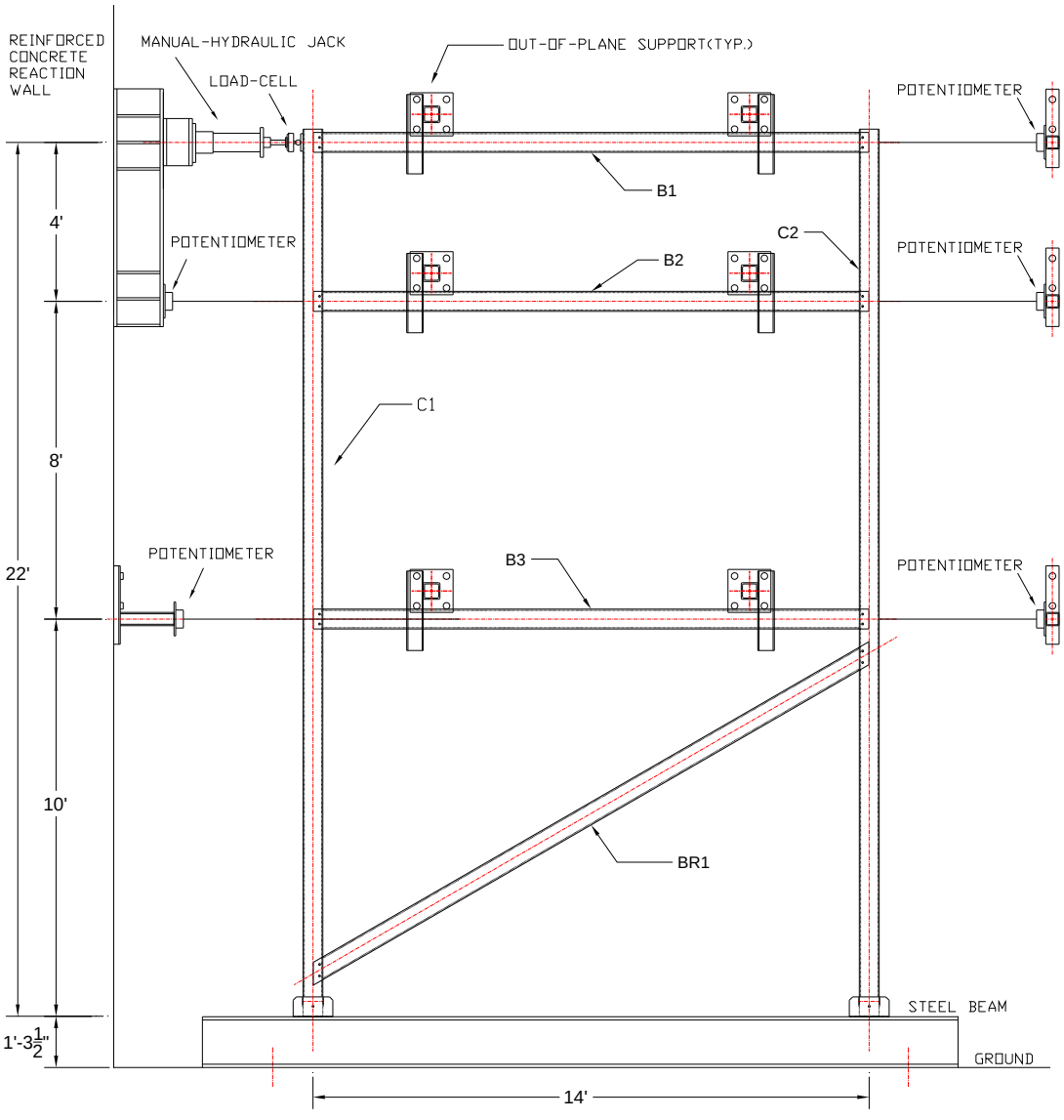

Figure 2.44: Test setup plan for the 'FR1-22' test series

Figure 2.45: Test setup for the 'FR1-22' test series

2.6.2 'FR1-18' Test Series Setup

Figure 2.46 shows the experimental setup plan for the 'FR1-18' test series, and Figure 2.47 shows one test in progress for the 'FR1-18' test series. The manual-hydraulic jack for the FR1-18 test series was placed on the side of the frame at 18 ft. above the bottom of column base plate.

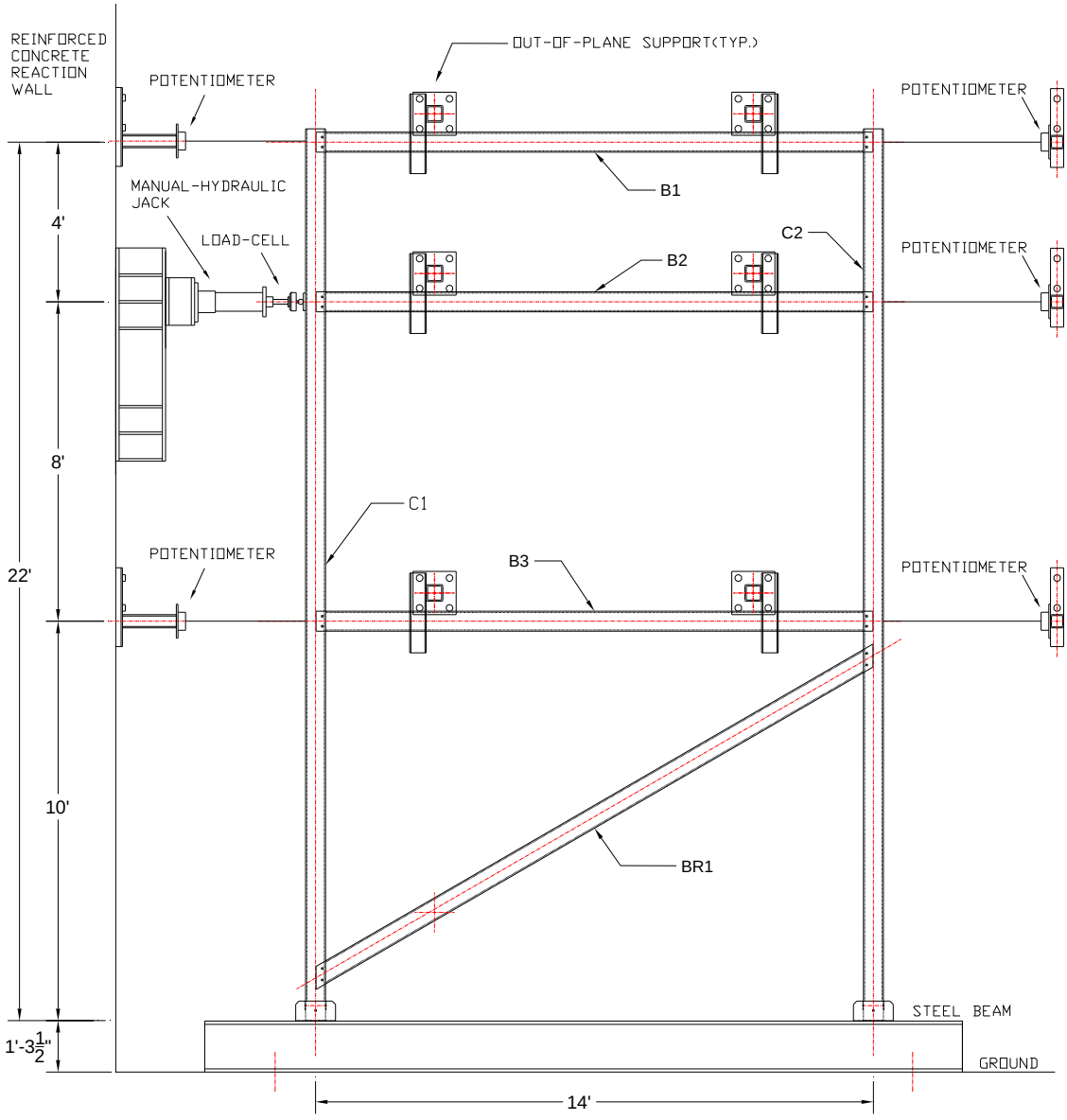

Figure 2.46: Test setup plan for the 'FR1-18' test series

Figure 2.47: Test setup for ‘FR1-18’ test series

2.6.3 'FR1-10' Test Series Setup

Figure 2.48 shows the experimental setup plan for the 'FR1-10' test series, and Figure 2.49 shows one test in progress for the 'FR1-10' test series. The manual-hydraulic jack for the FR1-10 test series was placed on the side of the frame at 10 ft. above the bottom of column base plate.

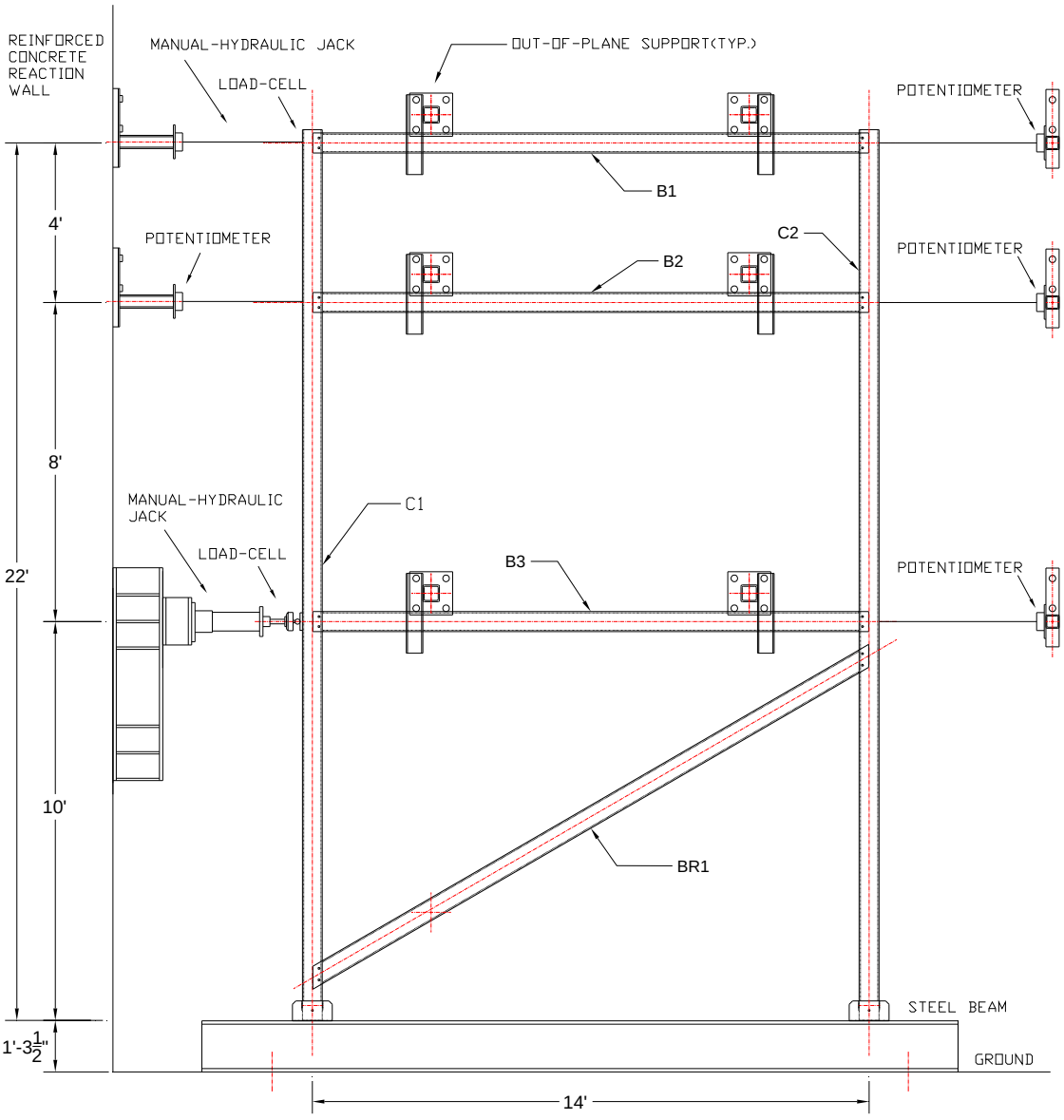

Figure 2.48: Test setup plan for the 'FR1-10' test series

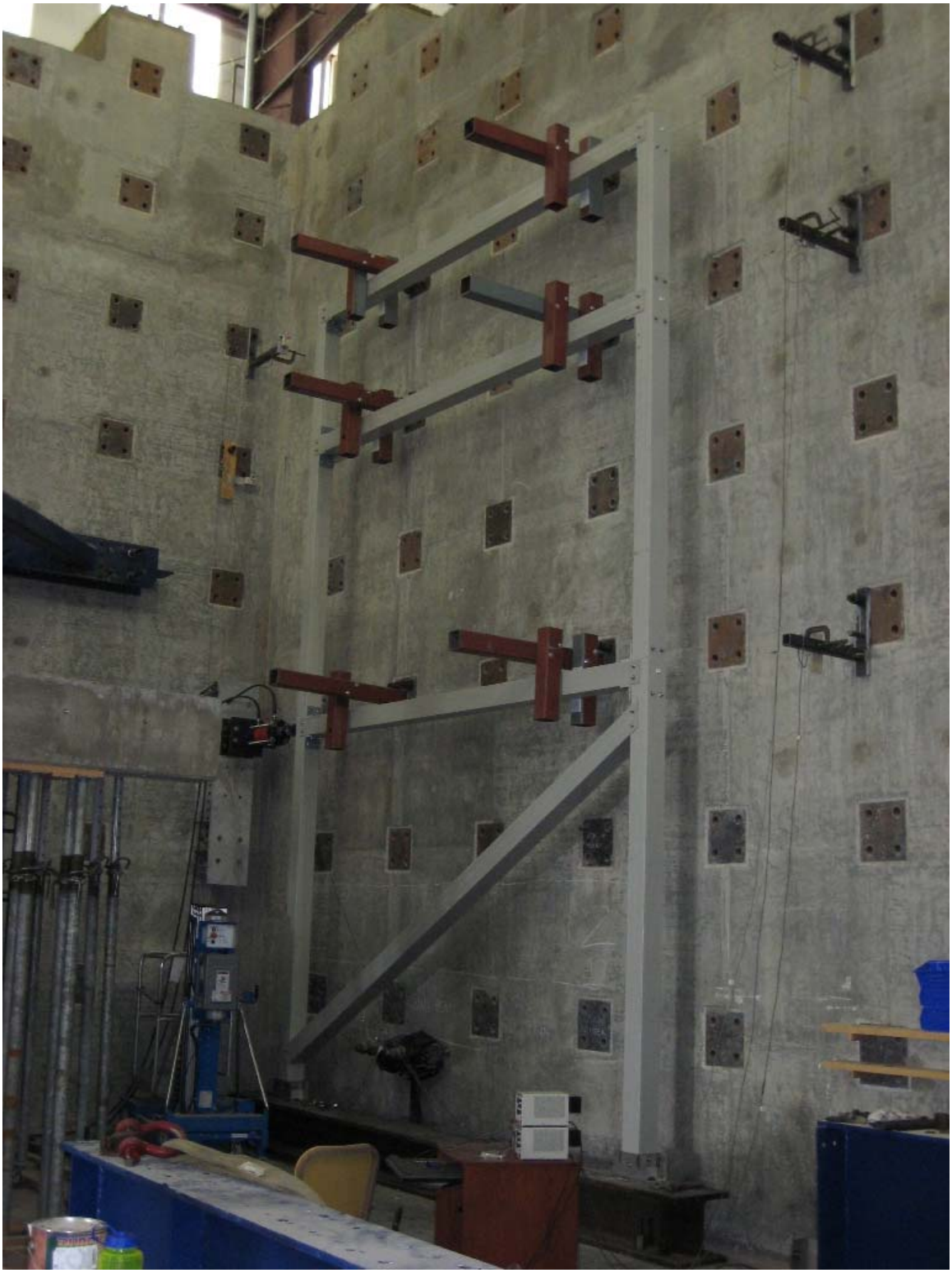

Figure 2.49: Test setup for the ‘FR1-10’ test series

2.6.4 'FR2-22' Test Series Setup

Figure 2.50 shows experimental setup plan of the 'FR2-22' test series, and Figure 2.51 shows one test in progress for the 'FR2-22' test series. The manual-hydraulic jack for the FR2-22 test series was placed on the side of the frame at 22 ft. above the bottom of column base plate.

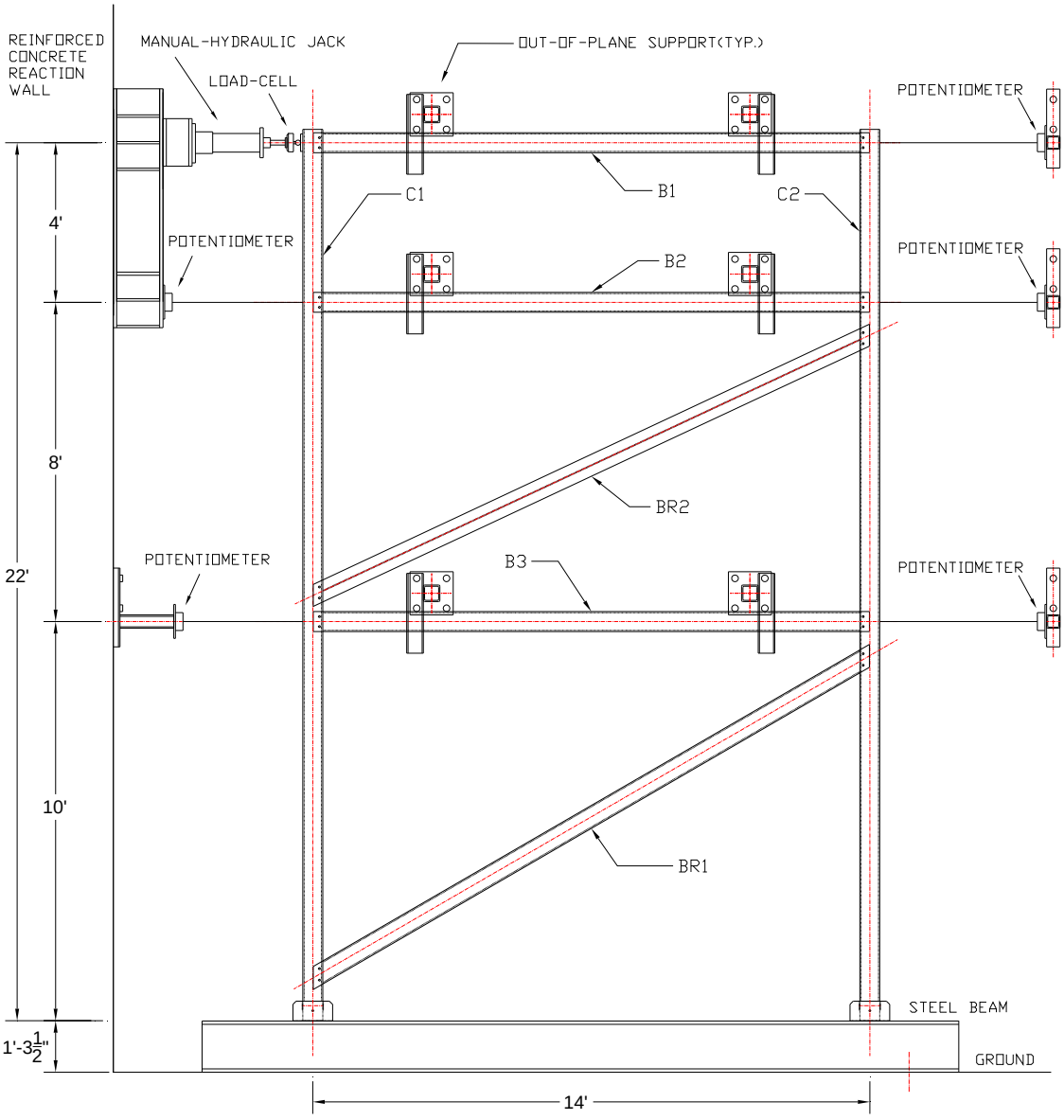

Figure 2.50: Test setup plan for the 'FR2-22' test series

Figure 2.51: Test setup for the 'FR2-22' test series

2.6.5 'FR2-18' Test Series Setup

Figure 2.52 shows experimental setup plan for the 'FR2-18' test series, and Figure 2.53 shows one test in progress for the 'FR2-18' test series. The manual-hydraulic jack for the FR2-18 test series was placed on the corner of the frame at 18 ft. above the bottom of column base plate.

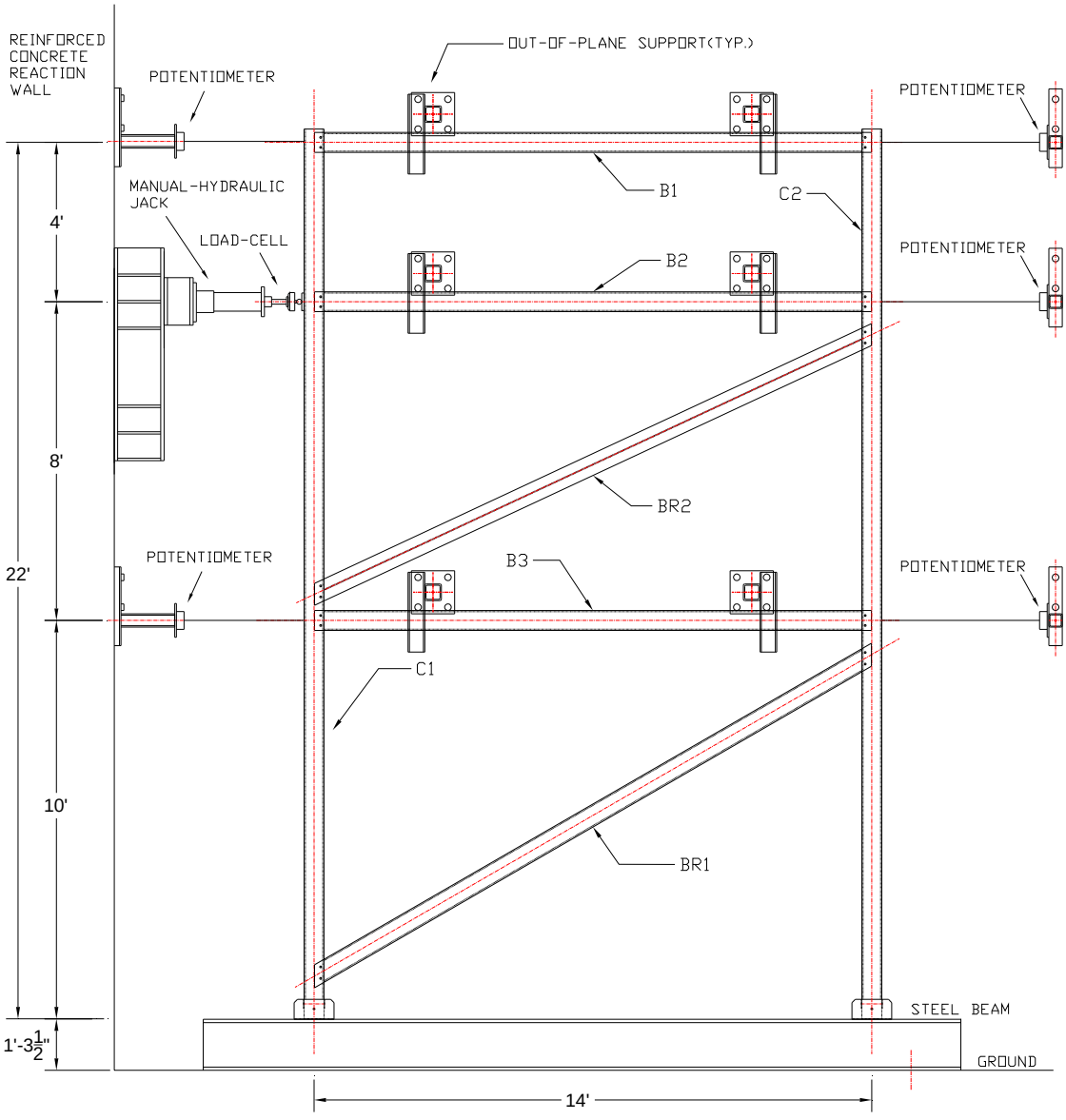

Figure 2.52: Test setup plan for the 'FR2-18' test series

Figure 2.53: Test setup for the 'FR2-18' test series

2.6.6 'FR2-10' Test Series Setup

Figure 2.54 shows experimental setup plan for the 'FR2-10' test series, and Figure 2.55 shows one test in progress for the 'FR2-10' test series. The manual-hydraulic jack for the FR2-10 test series was placed on the left corner of the frame at 10 ft. above the bottom of column base plate.

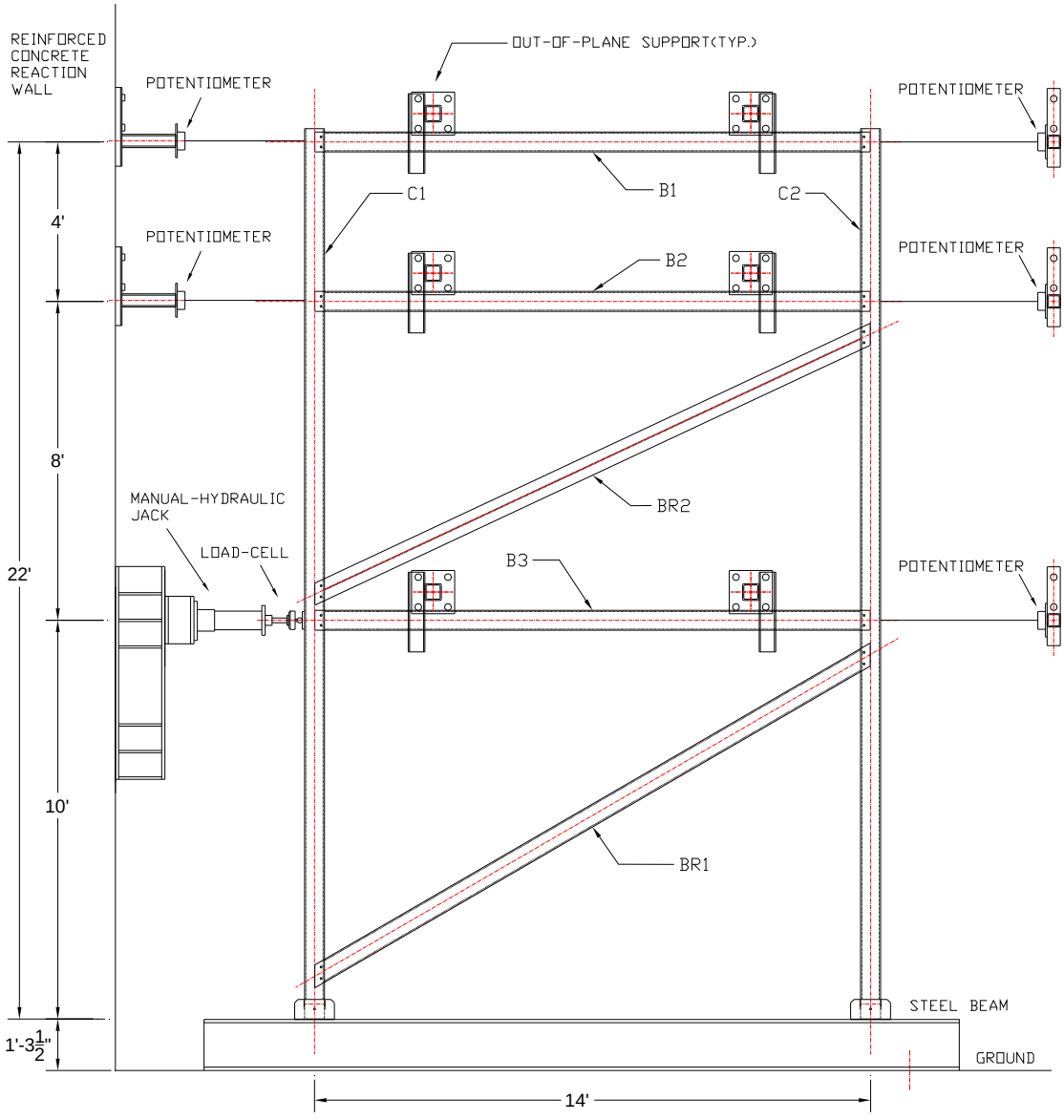

Figure 2.54: Test setup plan for the 'FR2-10' test series

Figure 2.55: Test setup for the ‘FR2-10’ test series

2.7 Maximum Applied Force

In order to assure that the test frames remain in an elastic state range during the tests, the maximum applied force was calculated for each test series. To determine the maximum loading for each test, the ultimate strength of the weakest location (beam-column connection) in the frame had to be calculated. Based on the detail drawings for member connections (Figures 2.12 to 2.22), and the applied load conditions, maximum experimental applied loads are estimated considering connection strengths and member strengths.

Table 2.10: Maximum applied force P calculation for each test setup

Test Configuration	Loading Height (ft.)	Maximum Applied Loading P for test (kips)
FR1-22-P FR1-22-FA FR1-22-SA	22	1.6
FR2-22-P FR2-22-FA FR2-22-SA		
FR1-18-P FR1-18-FA FR1-18-SA	18	2.4
FR2-18-P FR2-18-FA FR2-18-SA		
FR1-10-P FR1-10-FA FR1-10-SA	10	4.5
FR2-10-P FR2-10-FA FR2-10-SA		

Note: Loading height is measured from bottom of column base plate.

2.8 FRP Composite Frame Test Results

Results of static elastic loading tests of eighteen test configurations presented in Table 2.9 are reported herein. Load-displacement test for each configuration was reported ten times. Sections 2.8.1 through 2.8.6 reported the joint-displacement results of each test configuration. The following summarized the observed test results:

a. Joint displacements of frames with different beam-column connection types showed different results. Among the three different beam-column connection types (Type-P, Type-FA, and Type-SA), the joint displacements of a frame without any angle cleats (Type-P) showed the largest joint displacements. The joint displacements of a frame with steel angle cleats (Type-SA) showed the smallest joint displacements among all cases. These test results demonstrate that the behavior of the pultruded frame is influenced by the rotational stiffness of the beam-column connections.

b. It is interesting to note that the load-displacement relationship shown in the Figures in Sections 2.8.1 to 2.8.6 show linear elastic behavior in most of the loading range. However, at low applied force values, force-displacement responses are nonlinear. Figure 2.57 shows the initial nonlinear loading range from 0.0 kips up to 0.2 kips. Load-displacement results for the frames having FRP angles and steel angles showed somewhat wider load ranges of initial nonlinear behavior from 0.0 to 0.6 kips (Figures 2.58 and 2.59).

c. It should be noted that, when the frames experience large deflection (horizontal displacement of Joint A > 4.0 inch), clear nonlinear stage is observed in the early loading stage (e.g., Figures 2.57 and 2.61). Nonlinear in-plane shear modulus and nonlinear beam-column connections rotational stiffness are thought to affect such nonlinear load-displacement behavior of the frames.

2.8.1 'FR1-22' test series

Figure 2.56 shows loading and displacement measuring points for the 'FR1-22' test series (Table 2.9), where loading P was equal to 1.6 kips (Table 2.10). Tables 2.11, 2.12 and 2.13 present displacements of joints A, B, C, E, and F under a concentrated load P applied at joint D for three different beam-column connection types. Figures 2-57, 2-58 and 2-59 show typical load-displacement curves for 'FR1-22-P', 'FR1-22-FA', and 'FR1-22-SA' respectively.

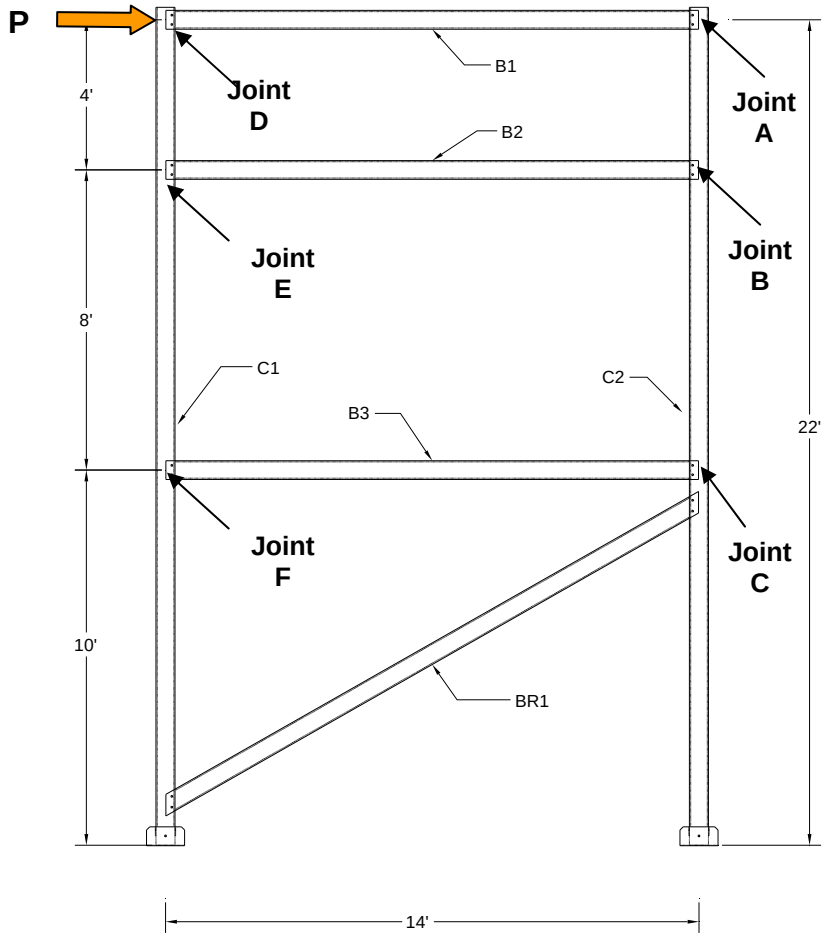

Figure 2.56: Loading and displacements measuring positions for 'FR1-22' test series

Table 2.11: Measured displacement results under load P =1.6 kips at level 22 ft. (Test 'FR1-22-P', connections use bolts only)

Test #	Displacement (inch) *		
	Joint A	Joint B	Joint C
1	5.822	3.797	0.413
2	5.696	3.688	0.390
3	5.713	3.700	0.380
4	5.719	3.706	0.384
5	5.695	3.688	0.384
6	5.738	3.719	0.384
7	5.732	3.710	0.382
8	5.707	3.697	0.376
9	5.673	3.682	0.373
10	5.627	3.647	0.384
Average	**5.712**	**3.703**	**0.385**
STD	0.050	0.038	0.011
COV (%)	0.876	1.035	2.835

* Displacements of Joints E and F were not measured.

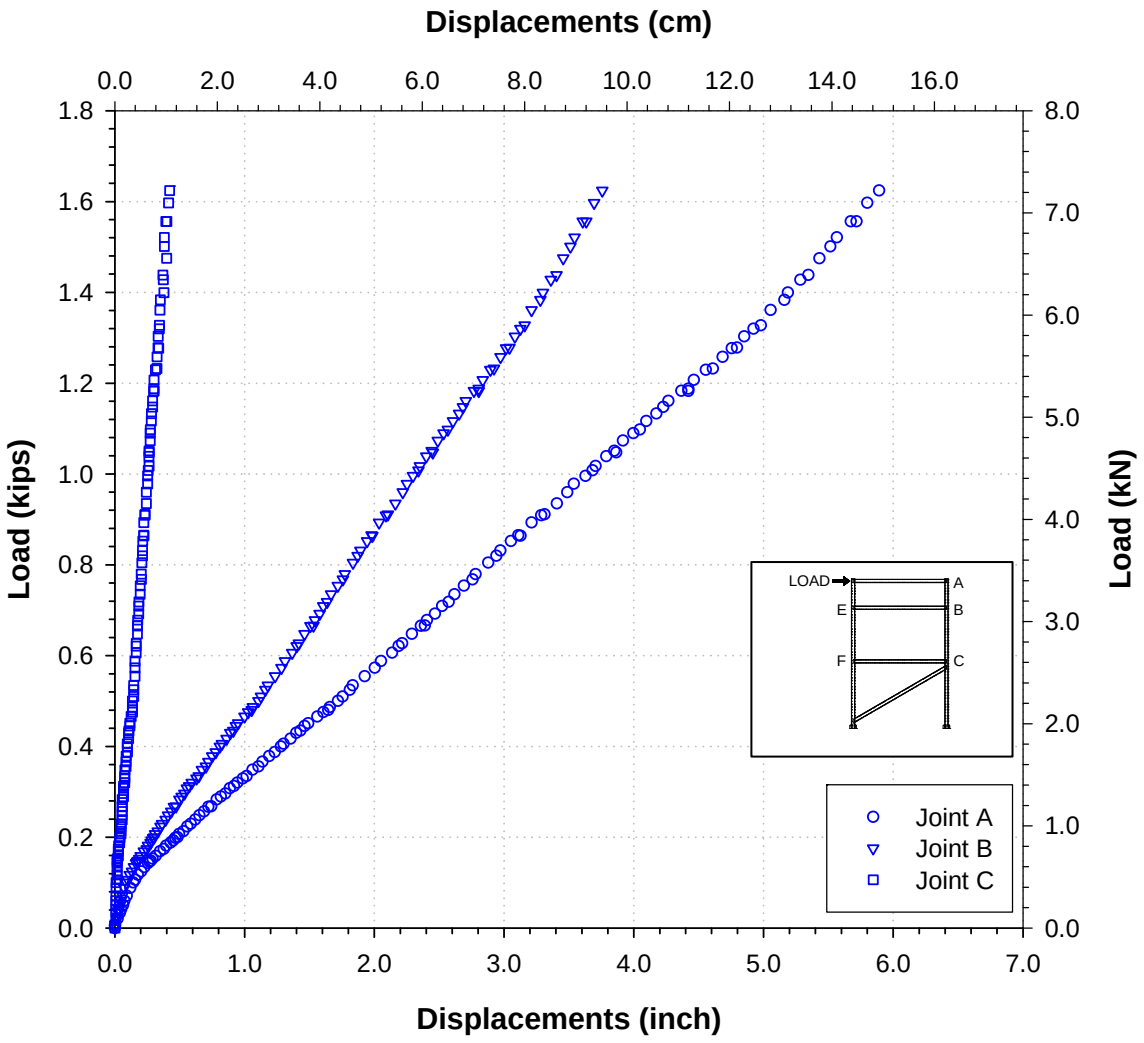

* Displacements of Joints E and F were not measured

Figure 2.57: Typical loading-displacement curves result for test 'FR1-22-P' (connections use bolts only)

Table 2.12: Measured displacement results under load P =1.6 kips at level 22 ft. (Test 'FR1-22-FA', connections use FRP angles)

Test #	Displacement (inch)				
	Joint A	Joint B	Joint C	Joint E	Joint F
1	4.671	2.967	0.334	3.039	0.319
2	4.792	3.050	0.337	3.119	0.332
3	4.760	3.016	0.328	3.114	0.337
4	4.790	3.033	0.330	3.116	0.333
5	4.662	2.960	0.327	3.040	0.324
6	4.772	3.025	0.325	3.115	0.319
7	4.643	2.943	0.327	3.018	0.321
8	4.771	3.024	0.336	3.094	0.323
9	4.747	3.025	0.332	3.107	0.333
10	4.668	2.960	0.330	3.028	0.316
Average	**4.727**	**3.000**	**0.331**	**3.079**	**0.326**
STD	0.059	0.038	0.004	0.042	0.007
COV (%)	1.251	1.277	1.196	1.361	2.234

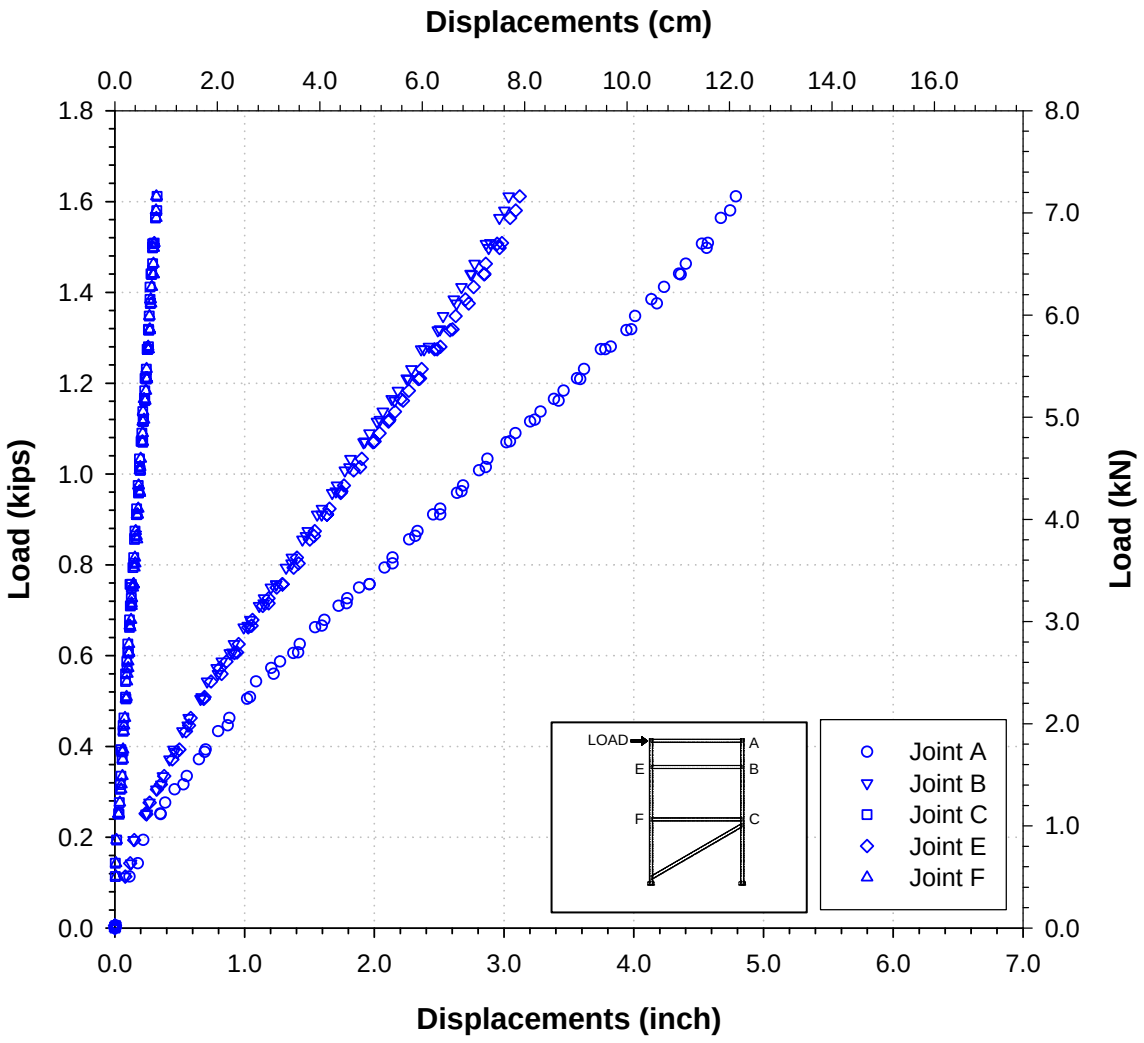

Figure 2.58: Typical loading-displacement curves result for test 'FR1-22-FA' (connections use FRP angles)

Table 2.13: Measured displacement results under load P =1.6 kips at level 22 ft. (Test 'FR1-22-SA', connections use steel angles)

Test #	Displacement (inch)				
	Joint A	Joint B	Joint C	Joint E	Joint F
1	3.793	2.454	0.341	2.537	0.353
2	3.286	2.153	0.294	2.235	0.292
3	3.252	2.130	0.288	2.180	0.294
4	3.231	2.110	0.281	2.179	0.288
5	3.273	2.132	0.291	2.210	0.289
6	3.289	2.140	0.290	2.203	0.282
7	3.329	2.168	0.285	2.258	0.281
8	3.315	2.160	0.283	2.221	0.284
9	3.286	2.154	0.294	2.245	0.294
10	3.337	2.183	0.292	2.253	0.298
Average	**3.339**	**2.178**	**0.294**	**2.252**	**0.295**
STD	0.163	0.099	0.017	0.104	0.021
COV (%)	4.876	4.552	5.803	4.614	7.056

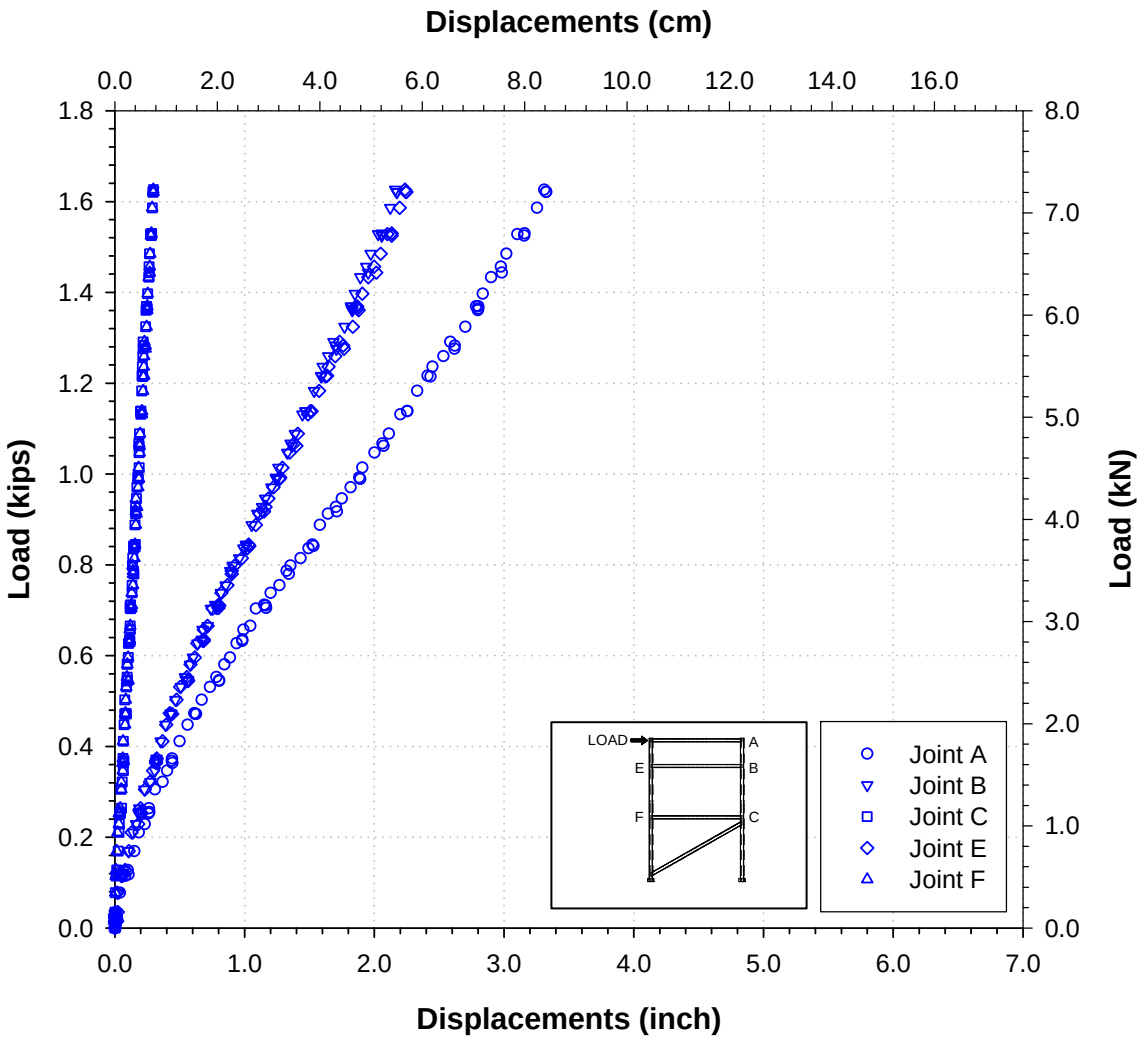

Figure 2.59: Typical loading-displacement curves result for test 'FR1-22-SA' (connections use steel angles)

2.8.2 'FR1-18' test series

Figure 2.60 shows loading and displacement measuring points for 'FR1-18' test series (Table 2.9), where loading P was equal to 2.4 kips (Table 2.10). Tables 2.14, 2.15 and 2.16 present horizontal displacements of joints A, B, C, D, and F under a concentrated load P applied at joint E for three different beam-column connection types. Figures 2-61, 2-62 and 2-63 show typical load-displacement curves for 'FR1-18-P', 'FR1-18-FA', and 'FR1-18-SA' respectively.

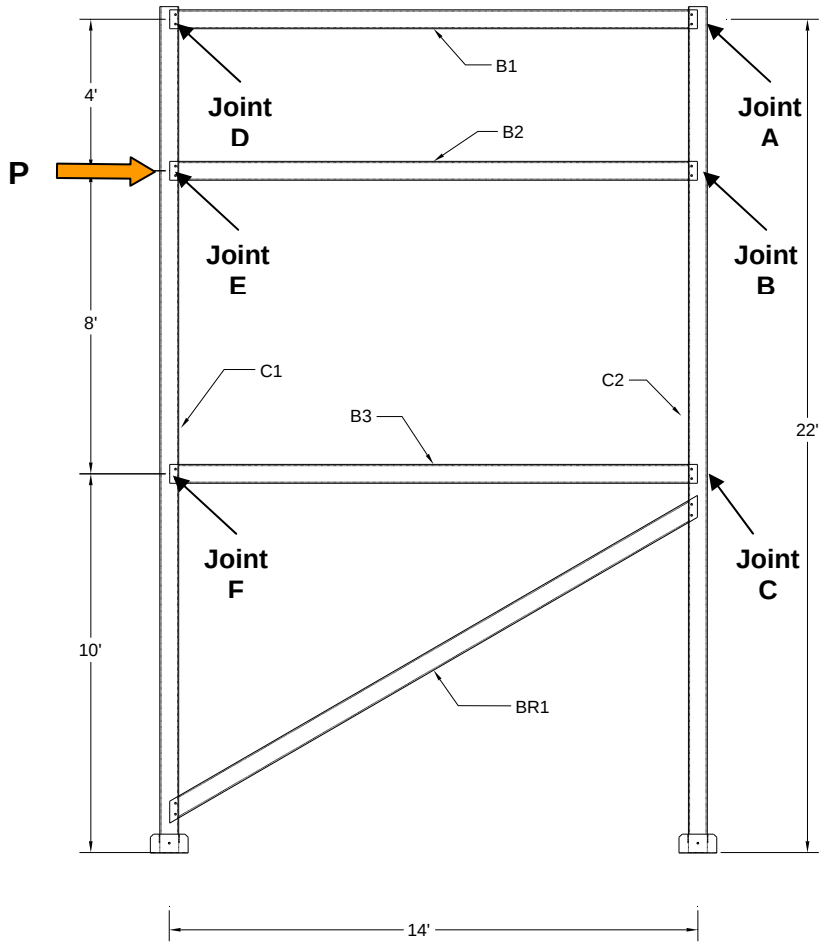

Figure 2.60: Loading and displacements measuring positions for 'FR1-18' test series

Table 2.14: Measured displacement results under load P =2.4 kips at level 18 ft. (Test 'F1-18-P', connections use bolts only)

Test #	Displacement (inch) *		
	Joint A	Joint B	Joint C
1	5.677	3.912	0.501
2	5.454	3.760	0.460
3	5.461	3.772	0.459
4	5.470	3.781	0.462
5	5.461	3.769	0.441
6	5.458	3.770	0.463
7	5.458	3.771	0.452
8	5.451	3.768	0.451
9	5.411	3.738	0.444
10	5.435	3.755	0.457
Average	**5.474**	**3.780**	**0.459**
STD	0.073	0.048	0.017
COV (%)	1.341	1.270	3.599

* Displacements of joints D and F were not measured.

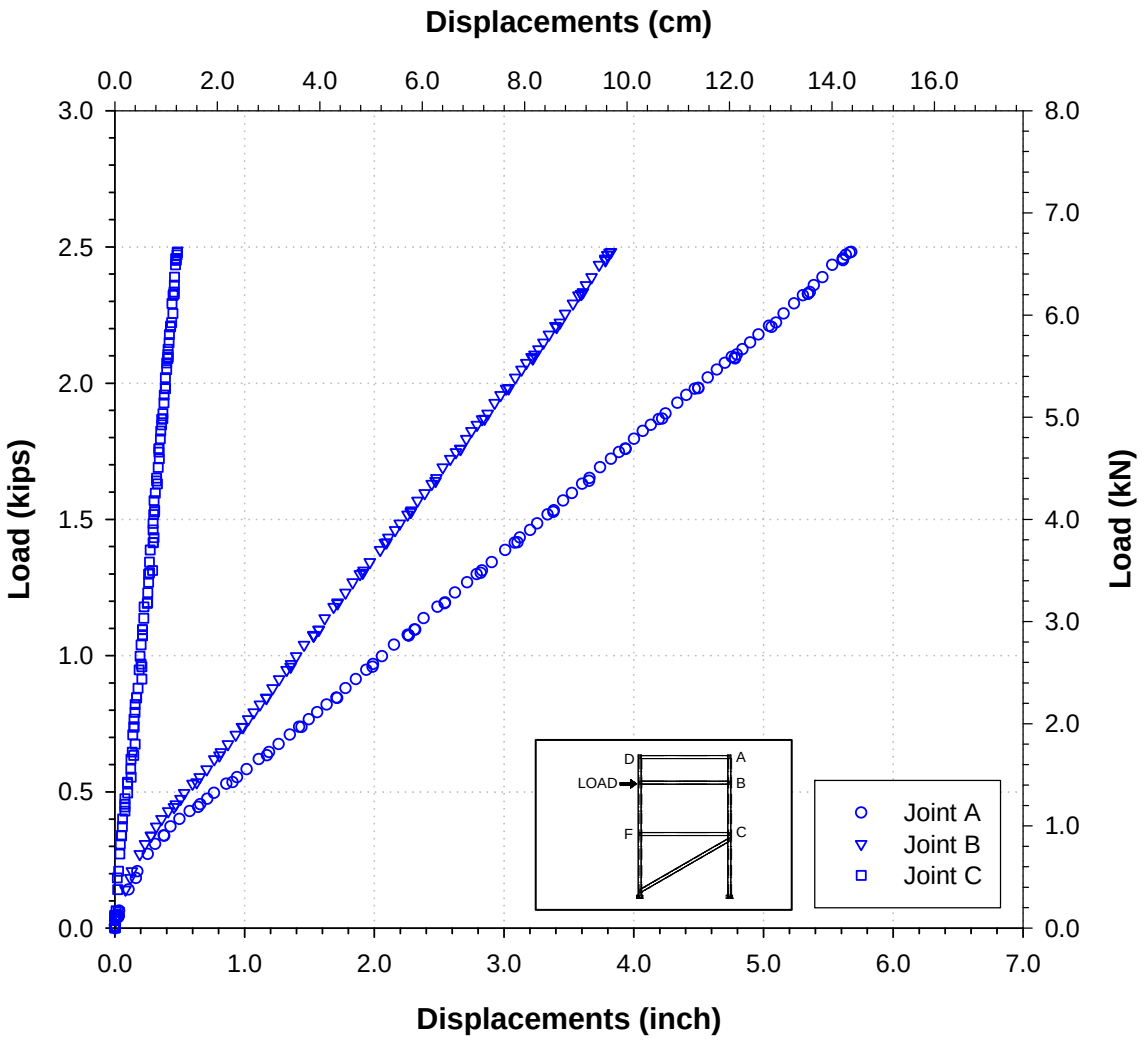

* Displacements of joints D and F were not measured

Figure 2.61: Typical loading-displacement curves result for test 'FR1-18-P' (connections use bolts only)

Table 2.15: Measured displacement results under load P =2.4 kips at level 18 ft. (Test 'FR1-18-FA', connections use FRP angles)

Test #	Displacement (inch)				
	Joint A	Joint B	Joint C	Joint D	Joint F
1	4.641	3.201	0.426	4.687	0.417
2	4.575	3.148	0.418	4.643	0.406
3	4.599	3.163	0.426	4.678	0.405
4	4.595	3.155	0.407	4.676	0.398
5	4.561	3.128	0.416	4.638	0.408
6	4.636	3.189	0.421	4.708	0.406
7	4.636	3.195	0.417	4.725	0.430
8	4.624	3.181	0.421	4.697	0.407
9	4.641	3.191	0.420	4.706	0.411
10	4.618	3.180	0.426	4.687	0.417
Average	**4.613**	**3.173**	**0.420**	**4.684**	**0.410**
STD	0.029	0.024	0.006	0.028	0.009
COV (%)	0.622	0.746	1.438	0.589	2.191

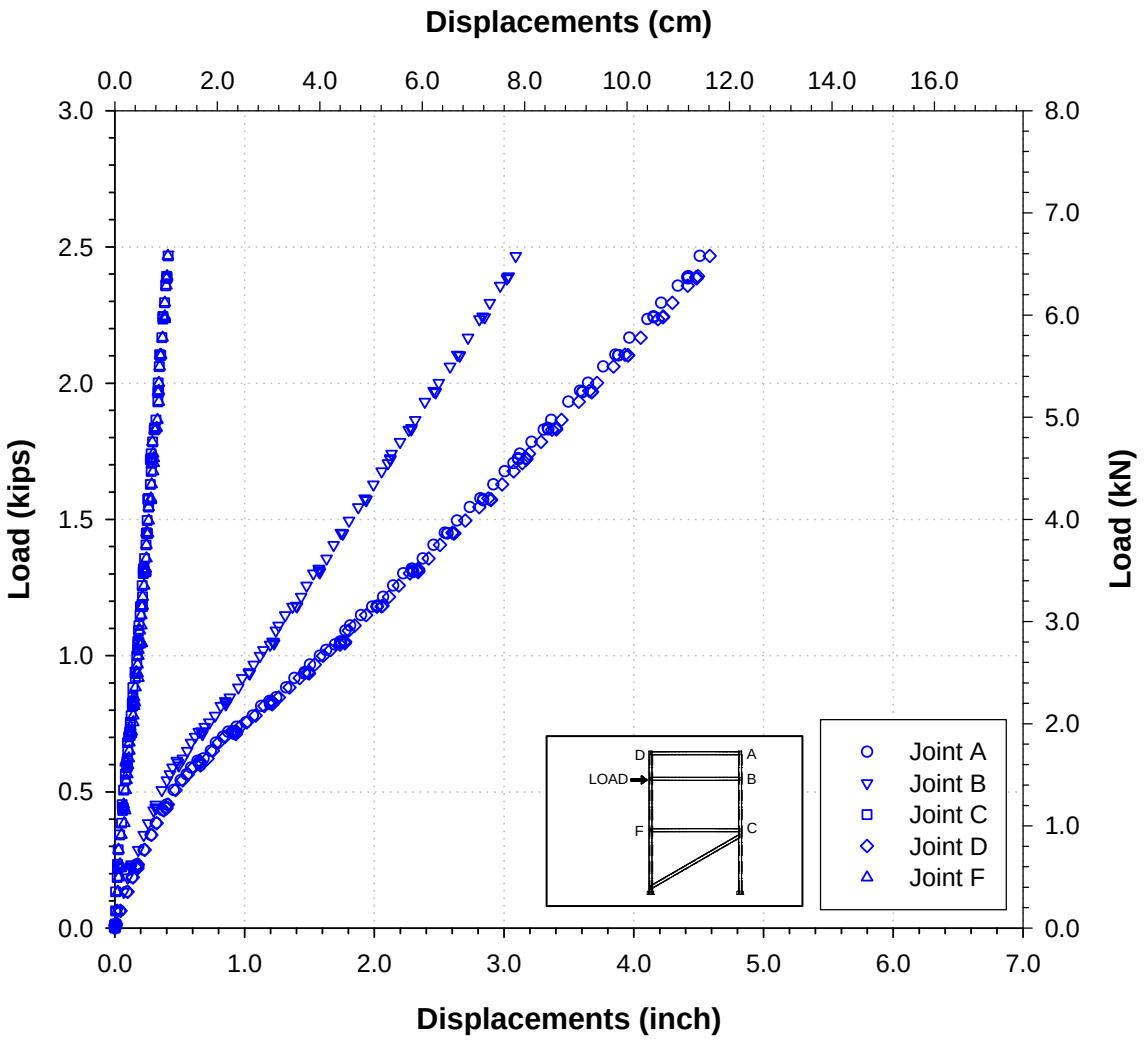

Figure 2.62: Typical loading-displacement curves result for test 'FR1-18-FA' (connections use FRP angles)

Table 2.16: Measured displacement results under load P = 2.4 kips at level 18 ft. (Test 'FR1-18-SA', connections use steel angles)

Test #	Displacement (inch)				
	Joint A	Joint B	Joint C	Joint E	Joint F
1	3.546	2.522	0.413	3.582	0.418
2	3.420	2.437	0.387	3.443	0.375
3	3.389	2.432	0.383	3.446	0.391
4	3.465	2.492	0.402	3.535	0.401
5	3.409	2.446	0.381	3.468	0.379
6	3.437	2.464	0.387	3.480	0.393
7	3.385	2.440	0.380	3.465	0.393
8	3.413	2.453	0.392	3.490	0.393
9	3.418	2.452	0.375	3.476	0.378
10	3.406	2.451	0.382	3.469	0.388
Average	**3.429**	**2.459**	**0.388**	**3.486**	**0.391**
STD	0.047	0.028	0.011	0.043	0.013
COV (%)	1.372	1.127	2.952	1.221	3.225

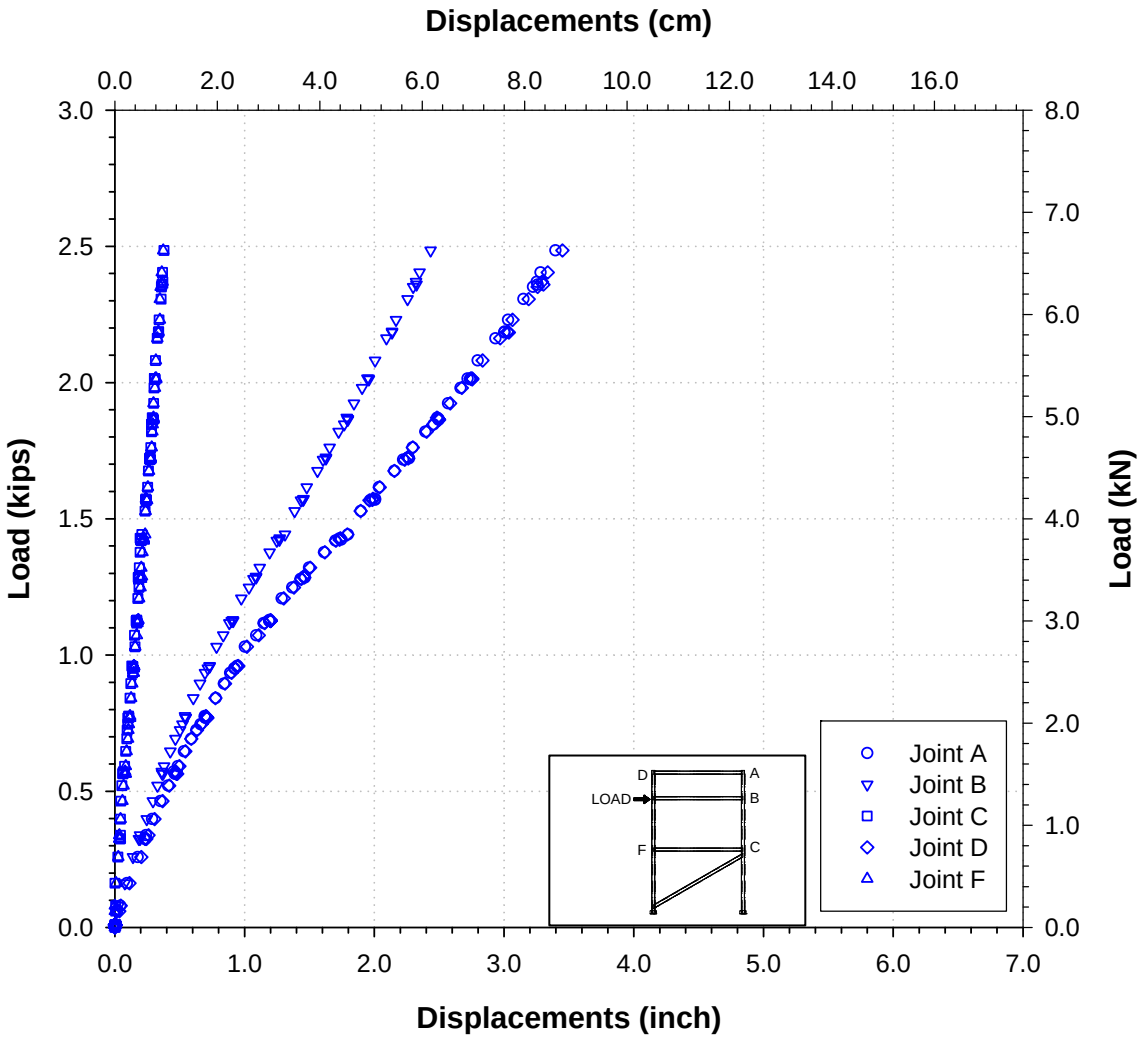

Figure 2.63: Typical loading-displacement curves result for test 'FR1-18-SA' (connections use steel angles)

2.8.3 'FR1-10' test series

Figure 2.64 shows loading and displacement measuring points for the 'FR1-10' test series (Table 2.9), where loading P was equal to 4.5 kips (Table 2.10). Tables 2.17, 2.18 and 2.19 present displacements of joints A, B, C, D, and E under a concentrated load P applied at joint F for three different beam-column connection types. Figures 2-65, 2-66 and 2-67 show typical load-displacement curves for 'FR1-10-P', 'FR1-10-FA', and 'FR1-10-SA' respectively.

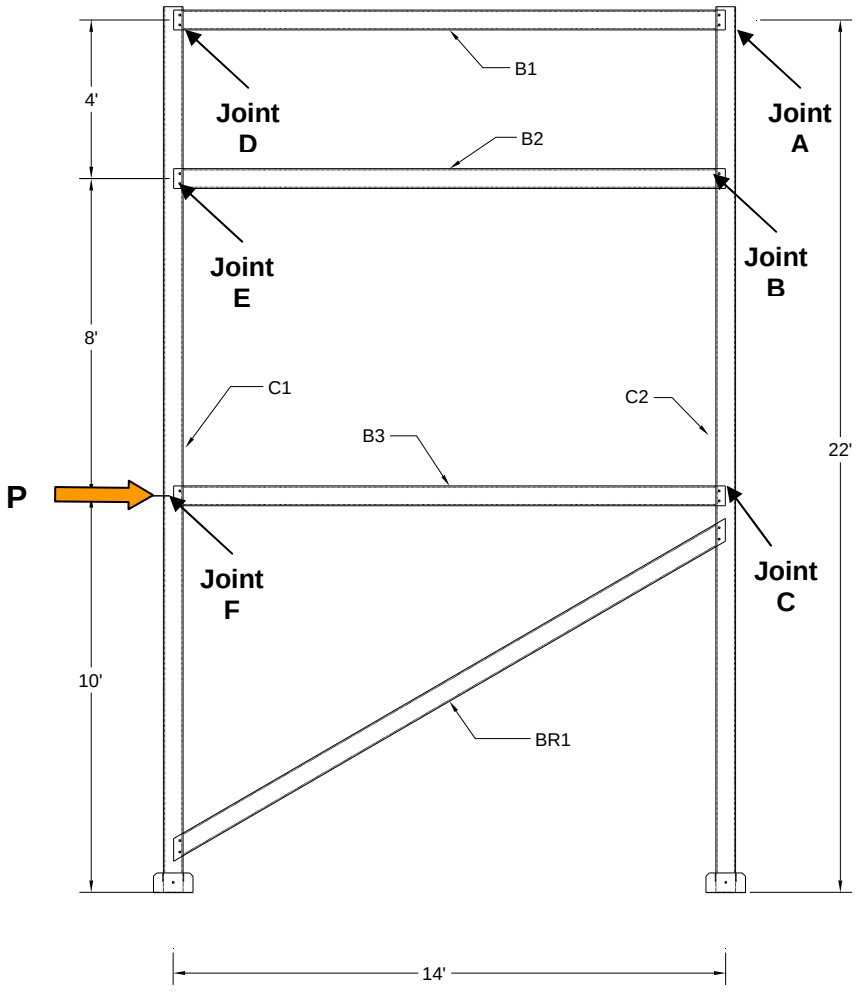

Figure 2.64: Loading and displacements measuring positions for 'FR1-10' test series

Table 2.17: Measured displacement results under load P =4.5 kips at level 10 ft. (Test 'FR1-10-P', connections use bolts only)

Test #	Displacement (inch) *		
	Joint A	Joint B	Joint C
1	0.880	0.791	0.470
2	0.780	0.707	0.421
3	0.768	0.697	0.401
4	0.764	0.699	0.407
5	0.756	0.693	0.413
6	0.759	0.692	0.410
7	0.764	0.683	0.405
8	0.752	0.682	0.403
9	0.753	0.686	0.363
10	0.742	0.683	0.401
Average	**0.772**	**0.701**	**0.409**
STD	0.039	0.032	0.026
COV (%)	5.102	4.625	6.426

* Displacements of joints D and E were not measured.

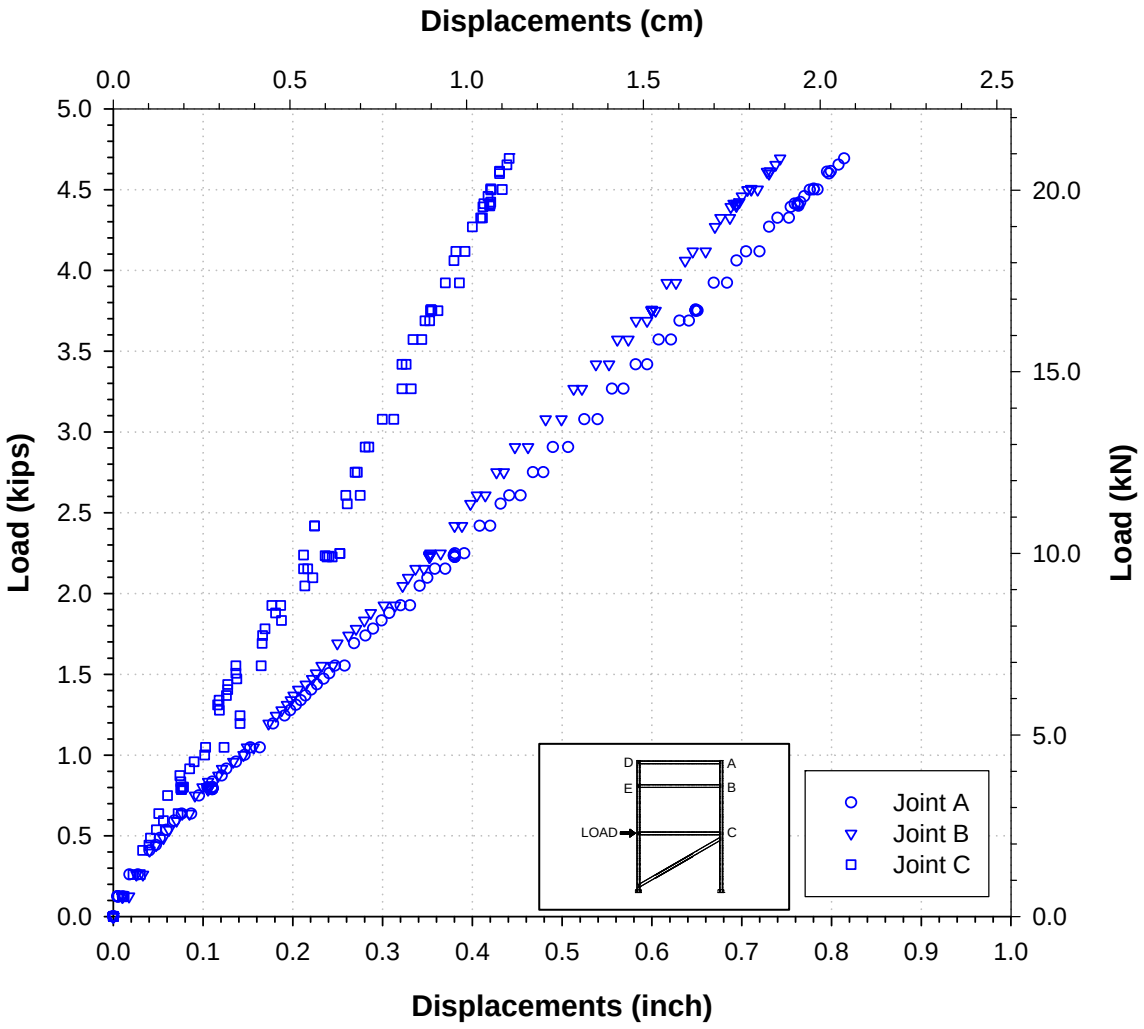

* Displacements of joints D and E were not measured

Figure 2.65: Typical loading-displacement curves result for test 'FR1-10-P' (connections use bolts only)

Table 2.18: Measured displacement results under load P = 4.5 kips at level 10 ft. (Test 'FR1-10-FA', connections use FRP angles)

Test #	Displacement (inch)				
	Joint A	Joint B	Joint C	Joint D	Joint E
1	0.766	0.687	0.440	0.768	0.677
2	0.732	0.657	0.417	0.742	0.648
3	0.742	0.668	0.416	0.759	0.672
4	0.731	0.668	0.417	0.747	0.674
5	0.728	0.654	0.409	0.738	0.677
6	0.736	0.660	0.410	0.737	0.660
7	0.739	0.661	0.407	0.739	0.645
8	0.732	0.649	0.406	0.741	0.664
9	0.731	0.655	0.408	0.742	0.672
10	0.741	0.665	0.423	0.749	0.661
Average	**0.738**	**0.662**	**0.416**	**0.746**	**0.665**
STD	0.011	0.011	0.010	0.010	0.012
COV (%)	1.497	1.593	2.489	1.357	1.739

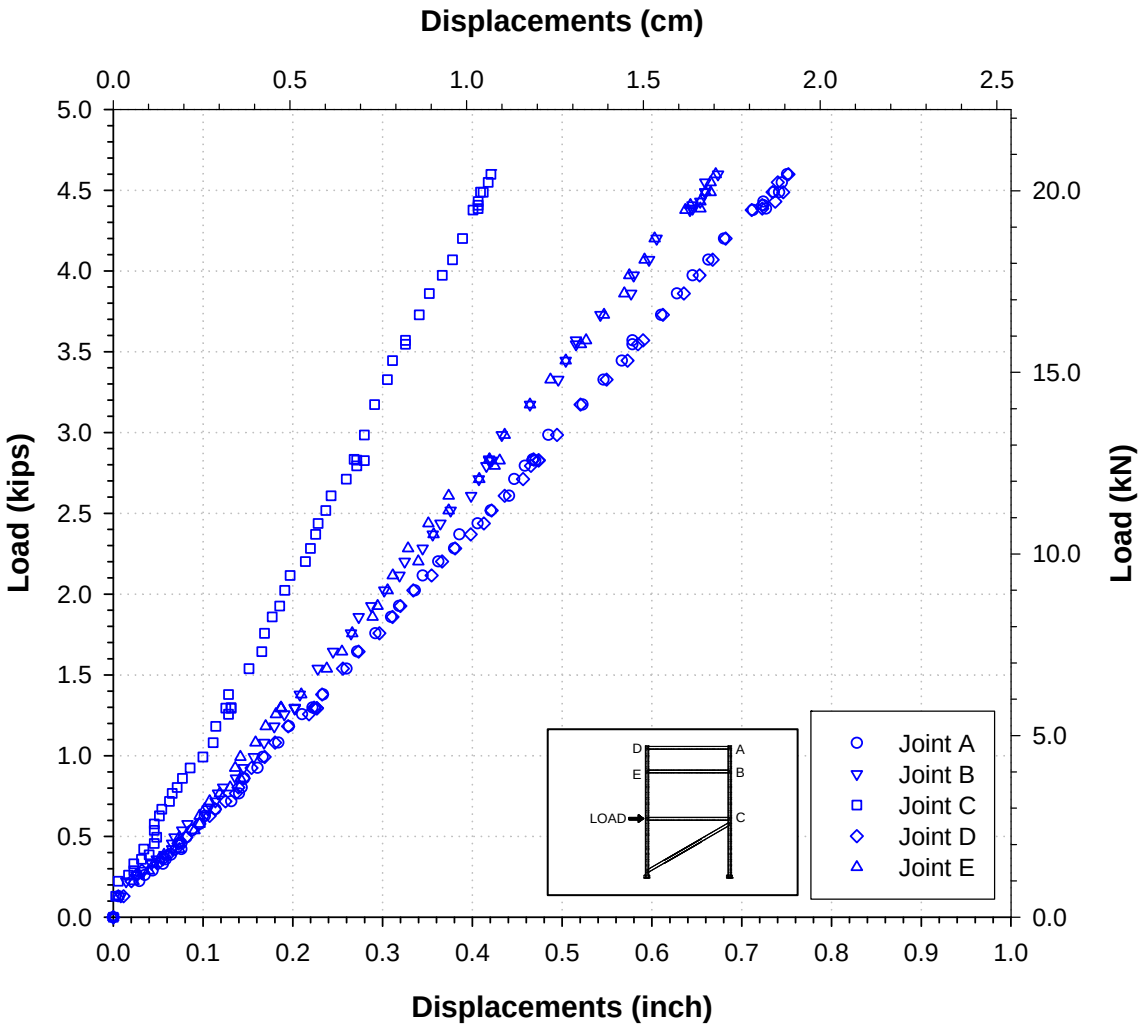

Figure 2.66: Typical loading-displacement curves result for test 'FR1-10-FA' (connections use FRP angles)

Table 2.19: Measured displacement results under load P = 4.5 kips at level 10 ft. (test 'FR1-10-SA', connections use steel angles)

Test #	Displacement (inch.)				
	Joint A	Joint B	Joint C	Joint D	Joint E
1	0.706	0.651	0.407	0.707	0.644
2	0.708	0.652	0.391	0.711	0.648
3	0.707	0.643	0.399	0.701	0.646
4	0.696	0.645	0.396	0.703	0.632
5	0.706	0.651	0.393	0.700	0.640
6	0.698	0.640	0.391	0.695	0.634
7	0.702	0.645	0.393	0.696	0.640
8	0.698	0.638	0.386	0.695	0.637
9	0.701	0.644	0.396	0.678	0.637
10	0.689	0.634	0.382	0.703	0.639
Average	**0.701**	**0.644**	**0.394**	**0.699**	**0.640**
STD	0.006	0.006	0.007	0.009	0.005
COV (%)	0.848	0.914	1.795	1.263	0.805

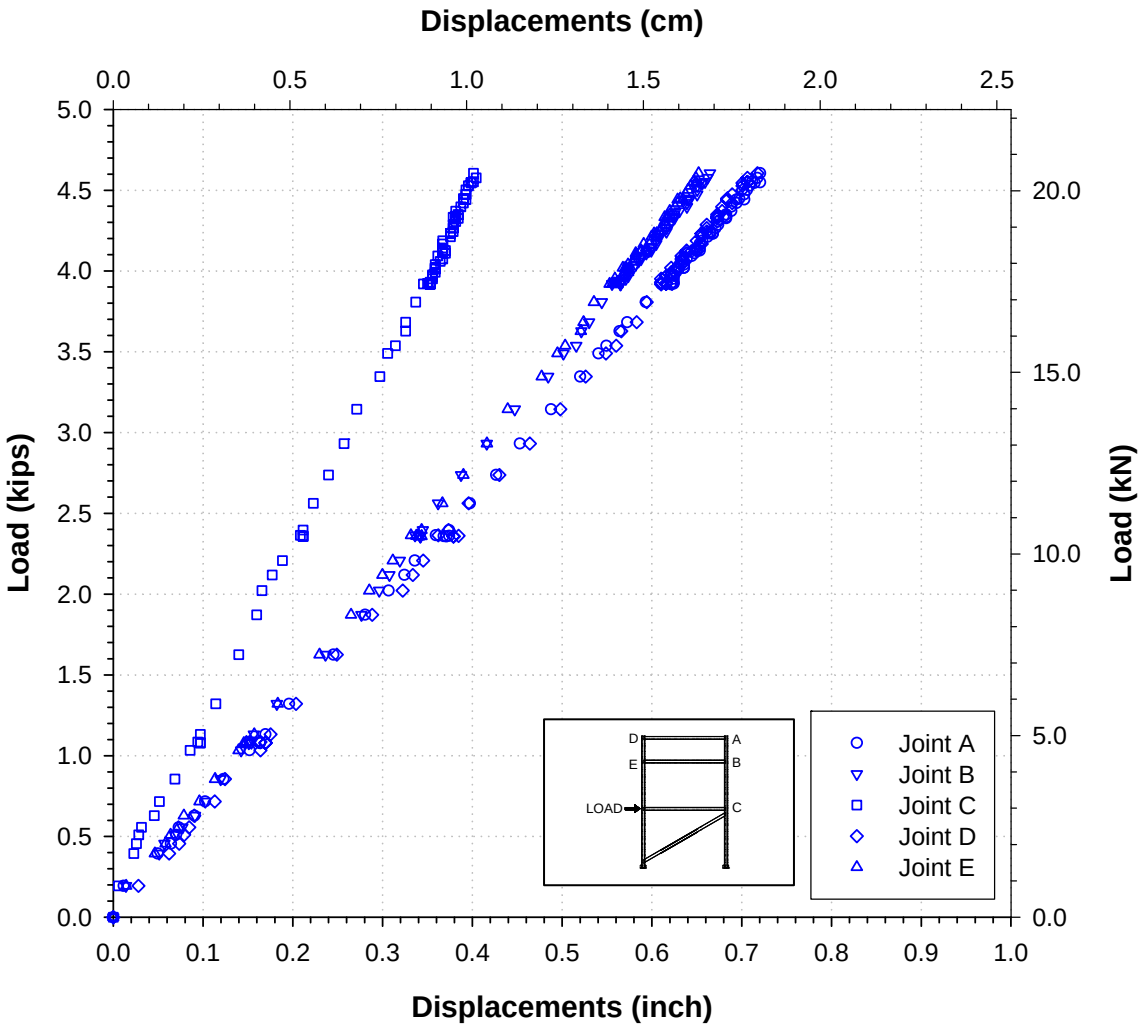

Figure 2.67: Typical loading-displacement curves result for test 'FR1-10-SA' (connections use steel angles)

2.8.4 'FR2-22' test series

Figure 2.68 shows loading and displacement measuring points for the 'FR2-22' test series (Table 2.9), where loading P was equal to 1.6 kips (Table 2.10). Tables 2.20, 2-21 and 2.22 present horizontal displacements of joints A, B, C, D, E, and F under a concentrated load P applied at joint D for three different beam-column connection types. Figures 2-69, 2-70 and 2-71 show typical load-displacement curves for test 'FR2-22-P', 'FR2-22-FA', and 'FR2-22-SA' respectively.

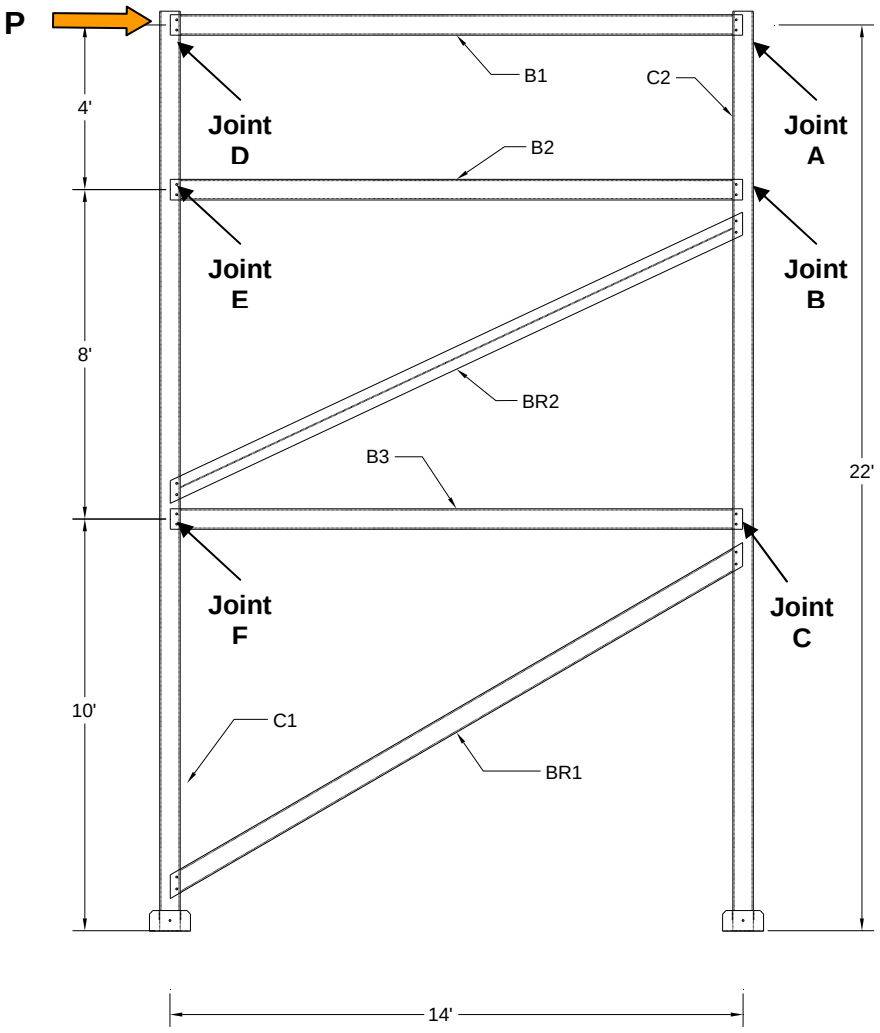

Figure 2.68: Loading and displacements measuring position for 'FR2-22' test series

Table 2.20: Measured displacement results under load P = 1.6 kips at level 22 ft. (Test 'FR2-22-P', connections use bolts only)

Test #	Displacement (inch) *		
	Joint A	Joint B	Joint C
1	0.853	0.409	0.150
2	0.815	0.381	0.177
3	0.821	0.389	0.167
4	0.813	0.384	0.170
5	0.808	0.384	0.164
6	0.812	0.389	0.167
7	0.809	0.388	0.170
8	0.812	0.392	0.177
9	0.814	0.393	0.171
10	0.811	0.390	0.152
Average	**0.817**	**0.390**	**0.167**
STD	0.013	0.008	0.009
COV (%)	1.624	2.017	5.566

* Displacement s of joints E and F were not measured.

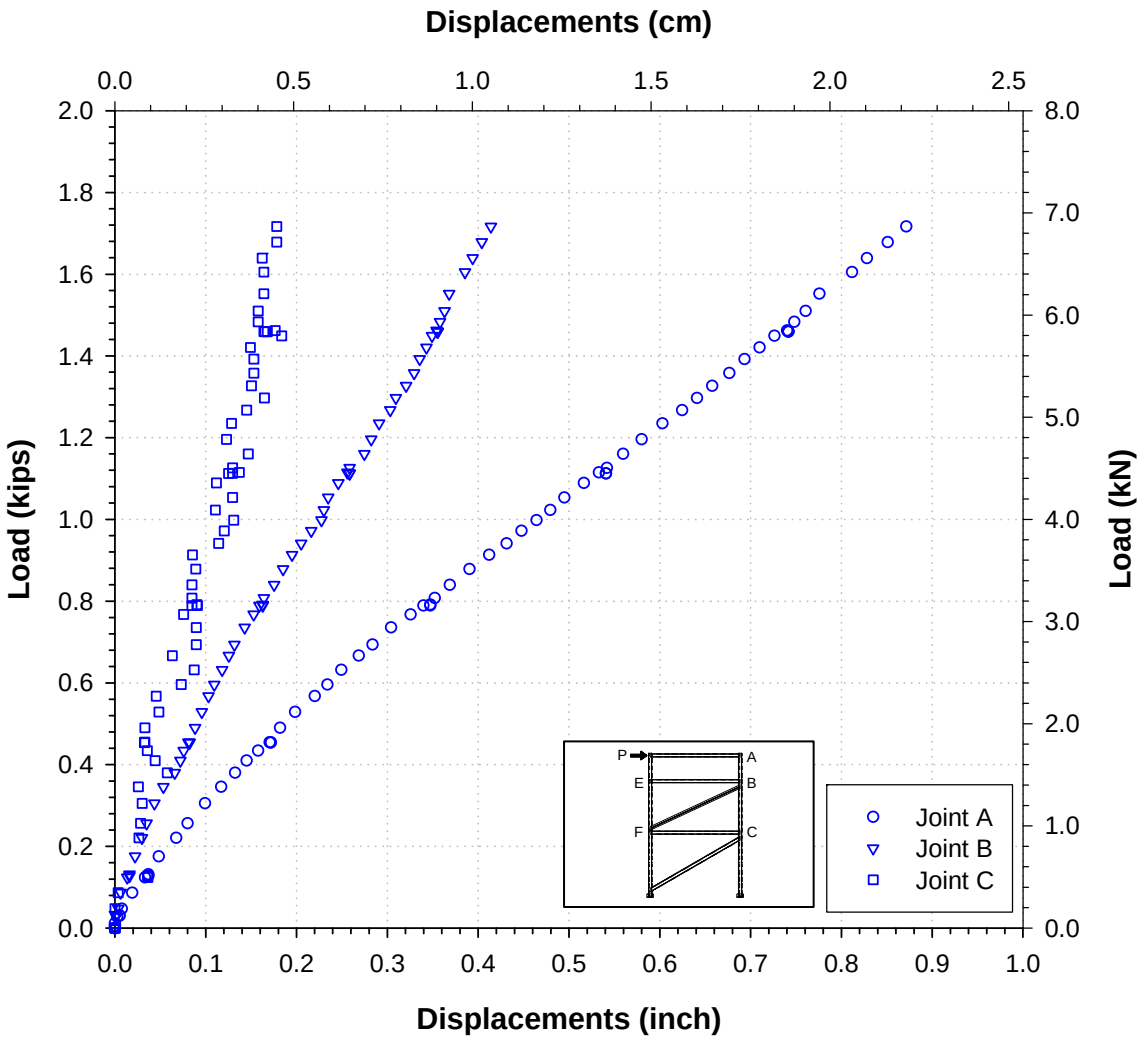

* Displacements of joints E and F were not measured

Figure 2.69: Typical loading-displacement curves result for test 'FR2-22-P' (connections use bolts only)

Table 2.21: Measured displacement results under load P = 1.6 kips at level 22 ft. (Test 'FR2-22-FA', connections use FRP angles)

Test #	Displacement (inch)				
	Joint A	Joint B	Joint C	Joint E	Joint F
1	0.763	0.409	0.173	0.420	0.184
2	0.712	0.387	0.157	0.413	0.182
3	0.733	0.381	0.157	0.407	0.172
4	0.736	0.387	0.153	0.403	0.178
5	0.711	0.390	0.157	0.401	0.175
6	0.709	0.374	0.150	0.402	0.166
7	0.728	0.384	0.158	0.403	0.173
8	0.724	0.390	0.153	0.411	0.179
9	0.734	0.391	0.157	0.410	0.176
10	0.712	0.369	0.147	0.389	0.172
Average	**0.726**	**0.386**	**0.156**	**0.406**	**0.176**
STD	0.017	0.011	0.007	0.008	0.005
COV (%)	2.292	2.732	4.432	2.034	2.992

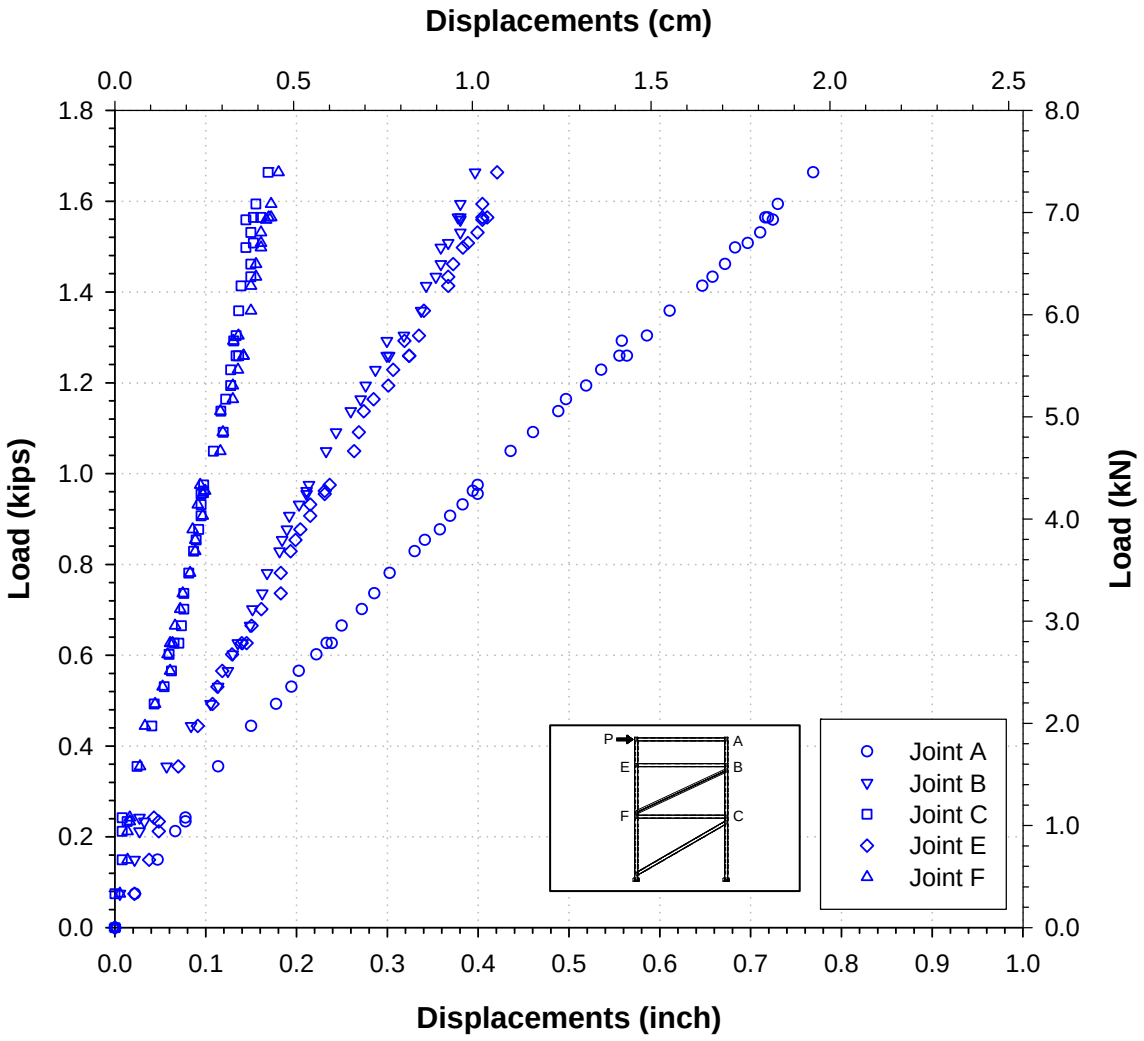

Figure 2.70: Typical loading-displacement curve result for test 'FR2-22-FA' (connections use FRP angles)

Table 2.22: Measured displacement results under load P = 1.6 kips at level 22 ft. (Test 'FR2-22-SA', connections use steel angles)

Test #	Displacement (inch)				
	Joint A	Joint B	Joint C	Joint E	Joint F
1	0.675	0.362	0.153	0.372	0.163
2	0.666	0.350	0.139	0.365	0.161
3	0.648	0.338	0.139	0.360	0.153
4	0.652	0.342	0.136	0.356	0.157
5	0.629	0.345	0.139	0.355	0.154
6	0.627	0.331	0.127	0.347	0.147
7	0.644	0.340	0.140	0.357	0.153
8	0.641	0.345	0.135	0.364	0.158
9	0.650	0.346	0.146	0.363	0.161
10	0.630	0.327	0.130	0.344	0.152
Average	**0.646**	**0.342**	**0.138**	**0.358**	**0.156**
STD	0.016	0.010	0.007	0.008	0.005
COV (%)	2.437	2.845	5.306	2.293	3.228

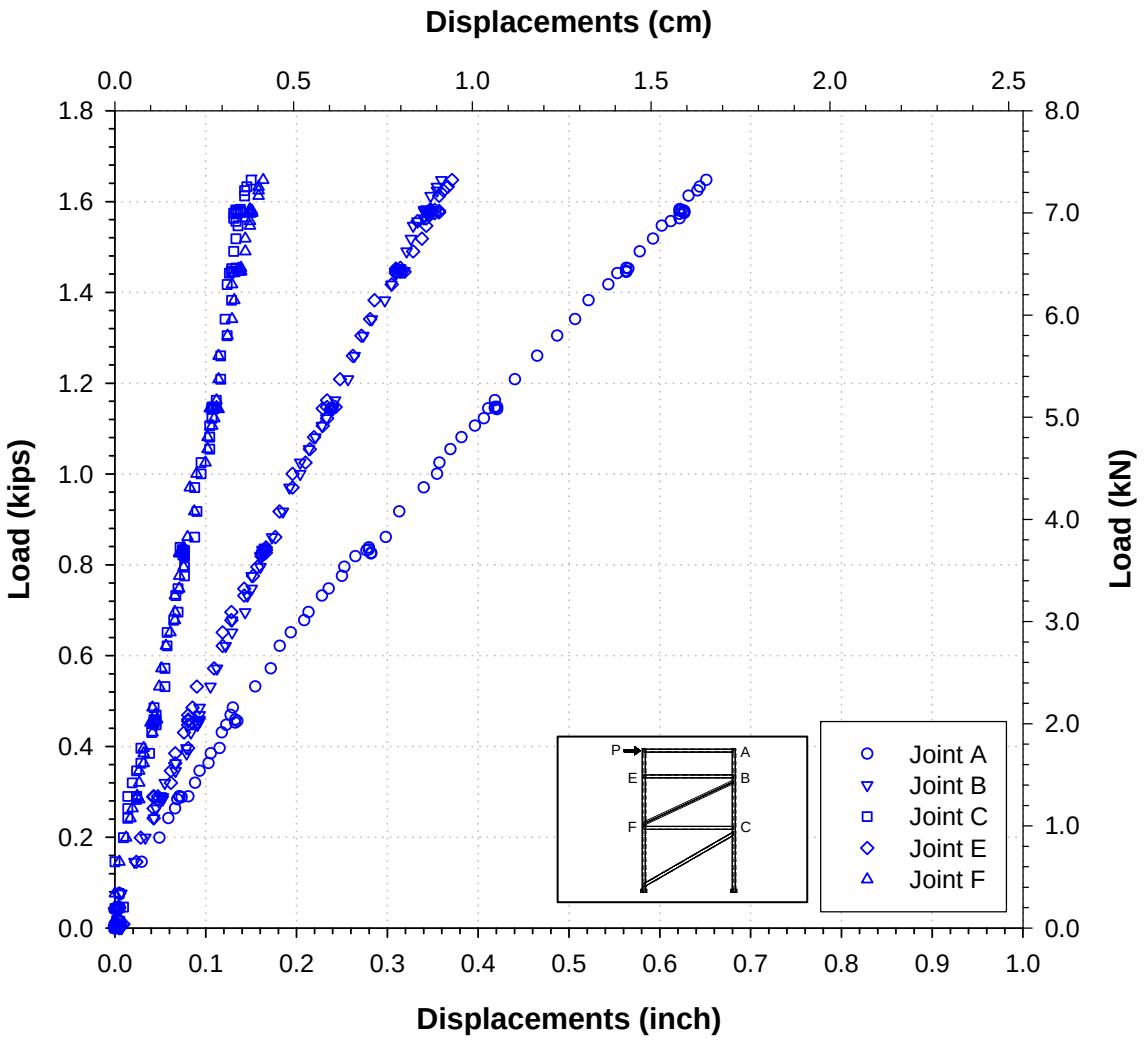

Figure 2.71: Typical loading-displacement curve result for test 'FR2-22-SA' (connections use steel angles)

2.8.5 'FR2-18' test series

Figure 2.72 shows loading and displacement measuring points for the 'FR2-18' test series (Table 2.9), where loading P was equal to 2.4 kips (Table 2.10). Tables 2.23, 2.24 and 2.25 present horizontal displacements of joints A, B, C, E, and F under a concentrated load P applied at joint E. Figures 2-73, 2-74 and 2-75 show typical load-displacement curves for test 'FR2-18-P', 'FR2-18-FA', and 'FR2-18-SA' respectively.

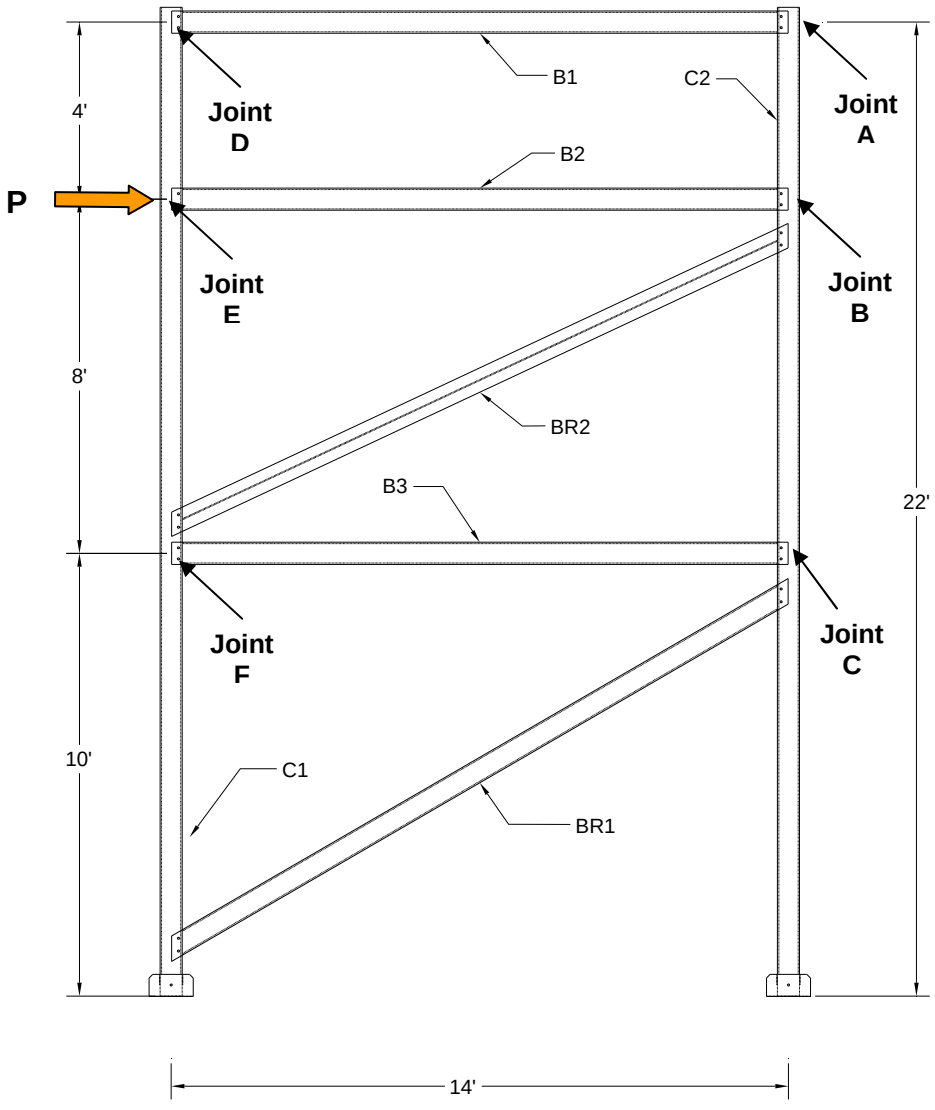

Figure 2.72: Loading and displacements measuring position for 'FR2-18' test series

Table 2.23: Measured displacement results under load P = 2.4 kips at level 18 ft. (Test 'FR2-18-P', connections use bolts only)

Test #	Displacement (inch.) *		
	Joint A	Joint B	Joint C
1	0.564	0.450	0.256
2	0.588	0.471	0.242
3	0.577	0.464	0.238
4	0.575	0.464	0.219
5	0.576	0.464	0.244
6	0.575	0.460	0.221
7	0.568	0.453	0.255
8	0.564	0.449	0.255
9	0.573	0.456	0.264
10	0.567	0.450	0.250
Average	**0.573**	**0.458**	**0.244**
STD	0.007	0.008	0.015
COV (%)	1.256	1.662	6.134

* Displacements of joints D and F were not measured.

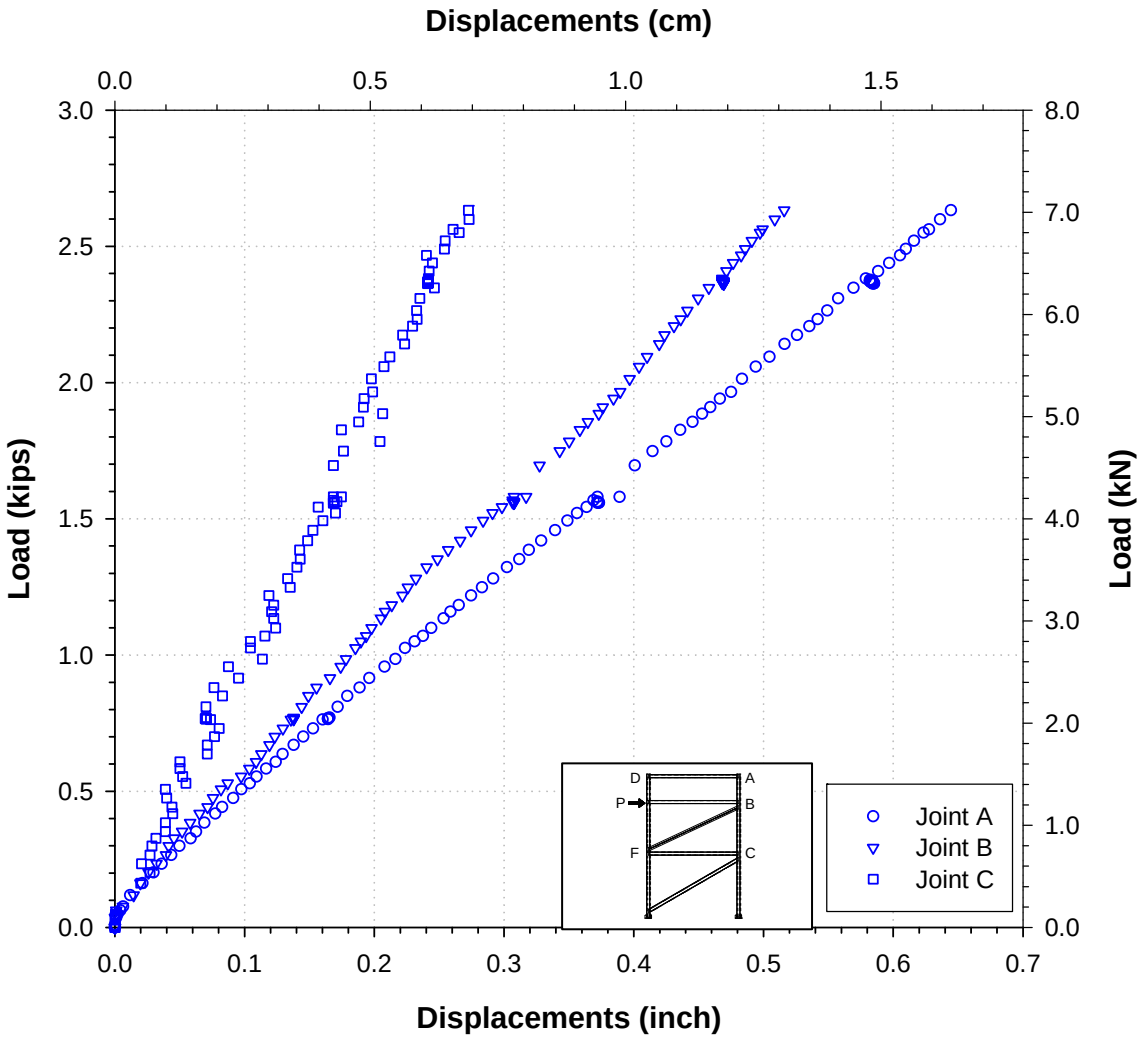

* Displacements of joints D and F were not measured

Figure 2.73: Typical loading-displacement curves result for test 'FR2-18-P' (connections use bolts only)

Table 2.24: Measured displacement results under load P = 2.4 kips at level 18 ft. (Test 'FR2-18-FA', connections use FRP angles)

Test #	Displacement (inch)				
	Joint A	Joint B	Joint C	Joint D	Joint F
1	0.544	0.431	0.219	0.554	0.241
2	0.550	0.446	0.233	0.543	0.250
3	0.544	0.431	0.219	0.554	0.241
4	0.531	0.429	0.219	0.533	0.241
5	0.531	0.425	0.223	0.547	0.248
6	0.534	0.424	0.216	0.538	0.228
7	0.548	0.445	0.233	0.530	0.241
8	0.545	0.434	0.221	0.545	0.245
9	0.535	0.430	0.219	0.531	0.236
10	0.542	0.447	0.226	0.574	0.252
Average	**0.540**	**0.434**	**0.223**	**0.545**	**0.242**
STD	0.007	0.009	0.006	0.013	0.007
COV (%)	1.276	1.987	2.653	2.462	2.983

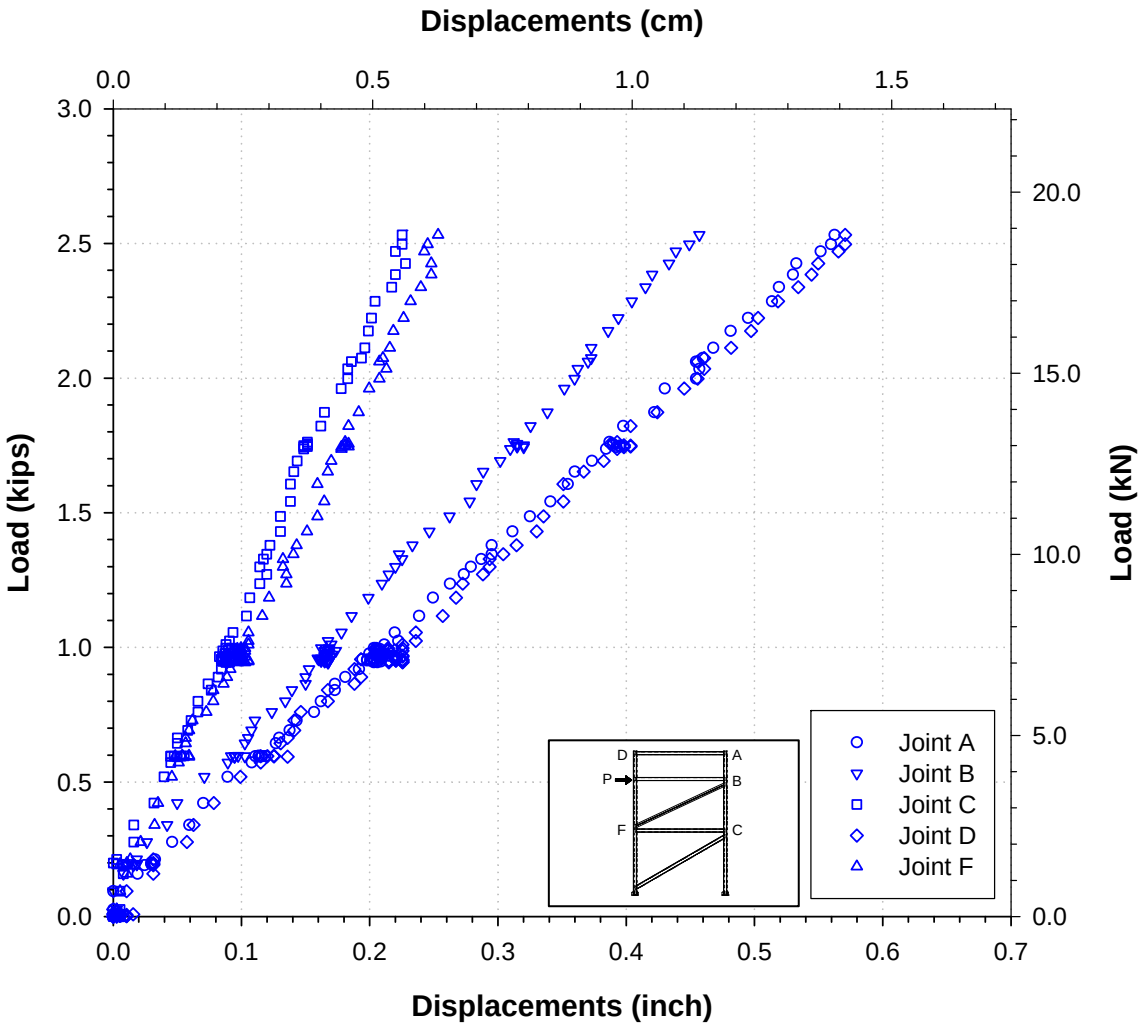

Figure 2.74: Typical loading-displacement curves result for test 'FR2-18-FA' (connections use FRP angles)

Table 2.25: Measured displacement results under load P = 2.4 kips at level 18 ft. (Test 'FR2-18-SA', connections use steel angles)

Test #	Displacement (inch)				
	Joint A	Joint B	Joint C	Joint D	Joint F
1	0.518	0.410	0.208	0.528	0.229
2	0.523	0.424	0.221	0.517	0.238
3	0.518	0.410	0.208	0.528	0.229
4	0.506	0.408	0.208	0.507	0.230
5	0.506	0.405	0.212	0.521	0.236
6	0.508	0.404	0.206	0.513	0.217
7	0.522	0.424	0.221	0.505	0.229
8	0.519	0.413	0.211	0.519	0.233
9	0.510	0.410	0.208	0.505	0.225
10	0.573	0.473	0.239	0.607	0.267
Average	**0.520**	**0.418**	**0.214**	**0.525**	**0.233**
STD	0.020	0.020	0.010	0.030	0.013
COV (%)	3.777	4.880	4.747	5.723	5.678

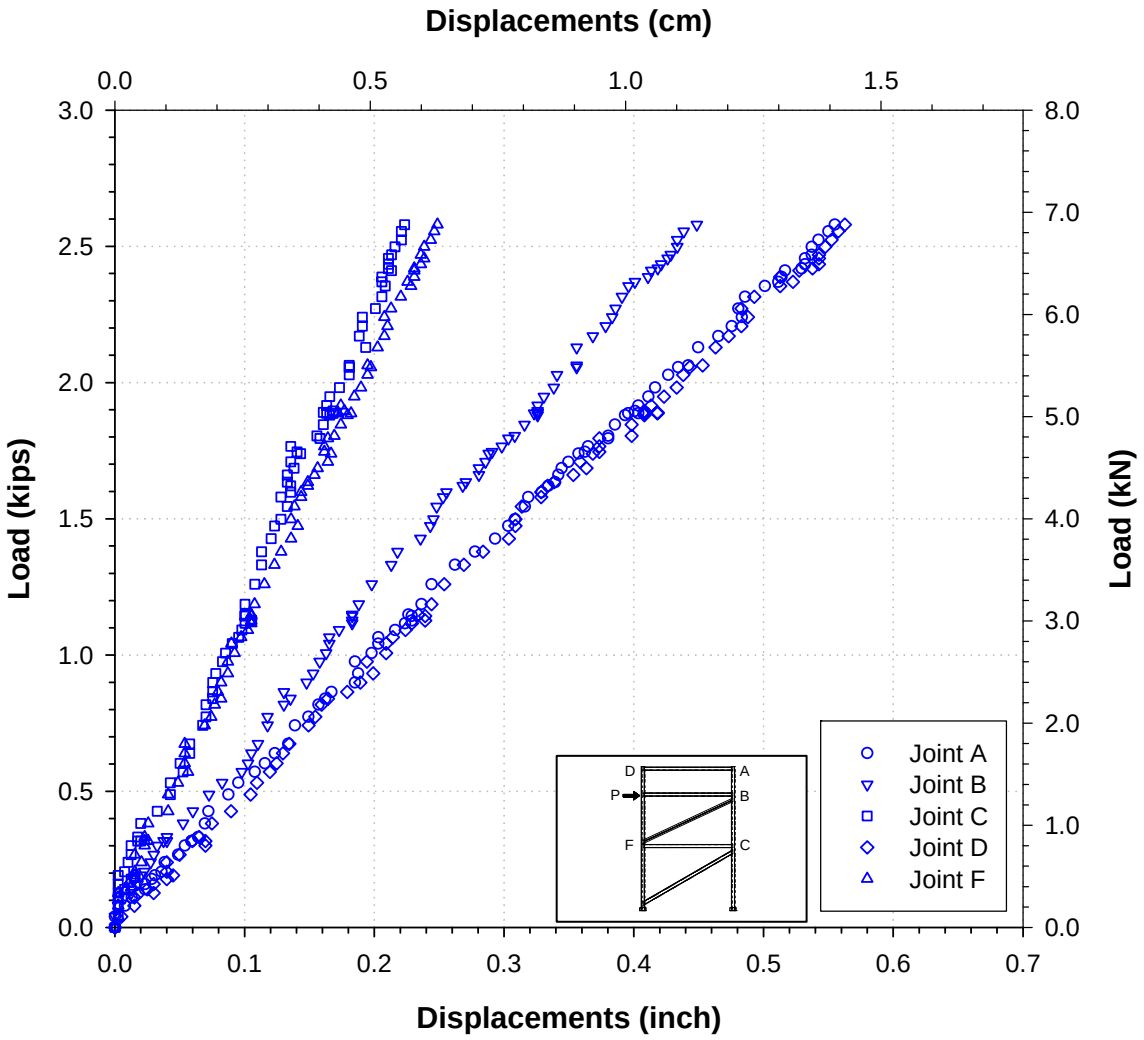

Figure 2.75: Typical loading-displacement curves result for test 'FR2-18-SA' (connections use steel angles)

2.8.6 'FR2-10' test series

Figure 2.76 shows loading and displacement measuring points for the 'FR2-10' test series (Table 2.9), where loading P was equal to 4.5 kips (Table 2.10). Tables 2.26, 2.27 and 2.28 present horizontal displacements of five joints A, B, C, D and E under a concentrated load P applied at joint F for three different beam-column connection types. Figures 2-77, 2-78 and 2-79 show typical load-displacement curves for 'FR2-10-P', 'FR2-10-FA', and 'FR2-10-SA' respectively.

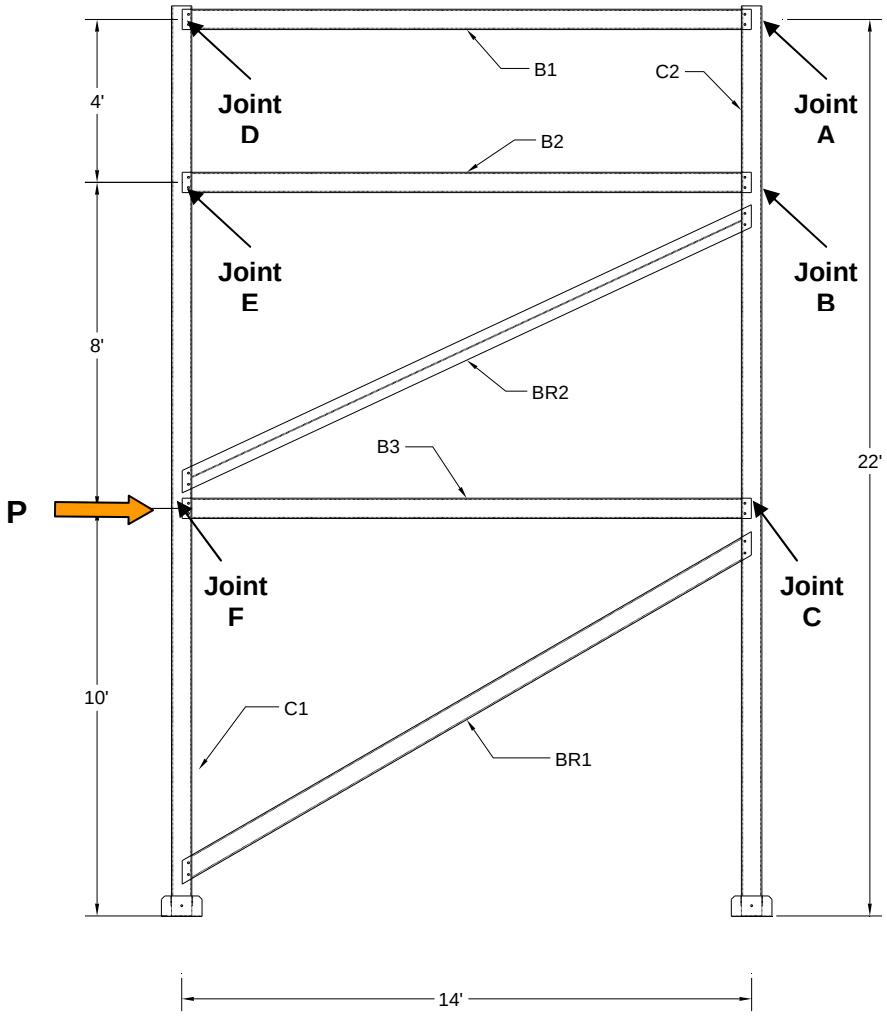

Figure 2.76: Loading and displacements measuring position for 'FR2-10' test series

Table 2.26: Measured displacement results under load P = 4.5 kips at level 10 ft. (Test 'FR2-10-P', connections use bolts only)

Test #	Displacement (inch) *		
	Joint A	Joint B	Joint C
1	0.547	0.520	0.368
2	0.549	0.518	0.397
3	0.543	0.520	0.380
4	0.545	0.516	0.406
5	0.548	0.522	0.409
6	0.547	0.522	0.369
7	0.545	0.523	0.360
8	0.538	0.512	0.368
9	0.538	0.510	0.385
10	0.543	0.515	0.386
Average	**0.545**	**0.518**	**0.383**
STD	0.004	0.004	0.017
COV (%)	0.730	0.832	4.422

* Displacements of joints D and E were not measured.

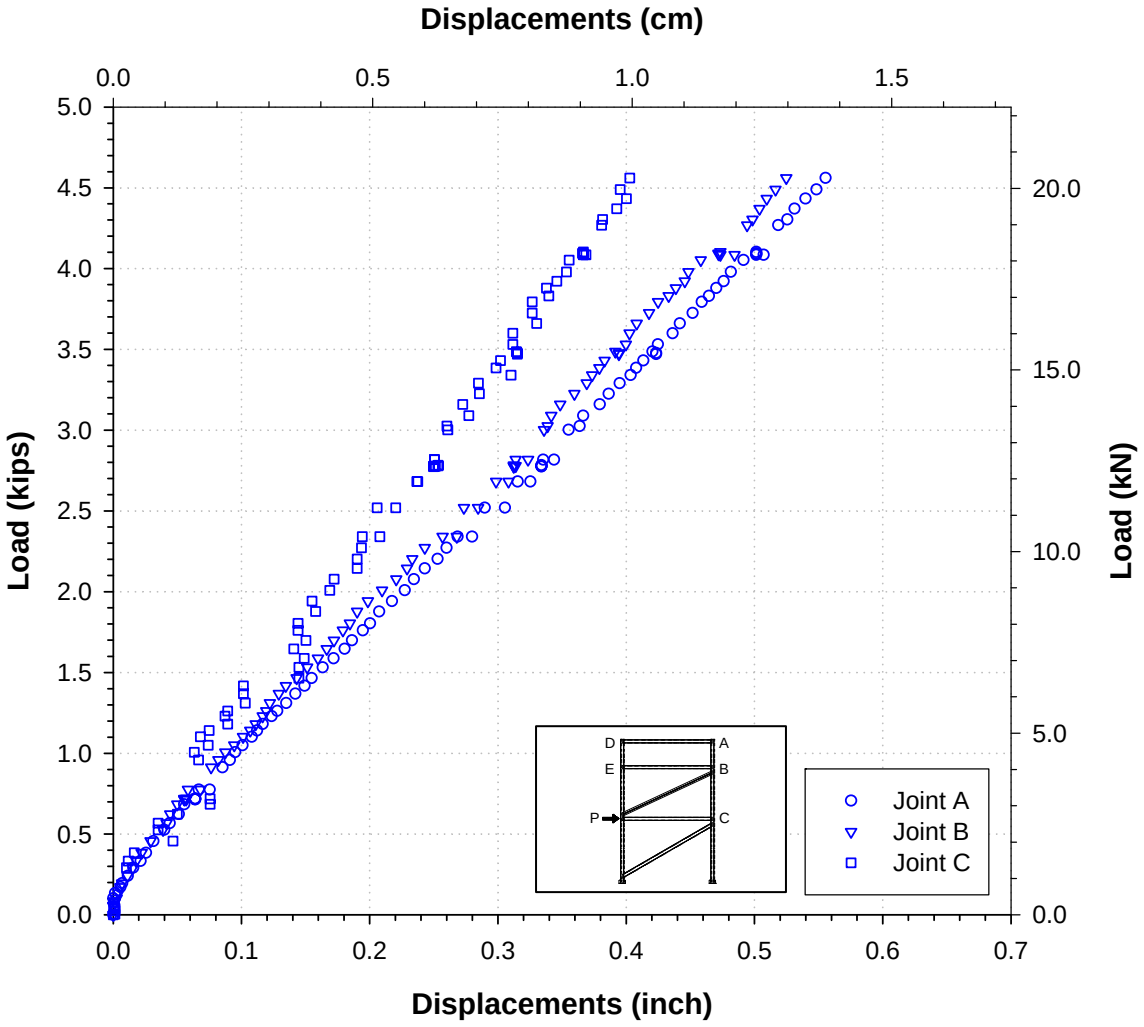

* Displacements of joints D and E were not measured

Figure 2.77: Typical loading-displacement curves result for test 'FR2-10-P' (connections use bolts only)

Table 2.27: Measured displacement results under load P = 4.5 kips at level 10 ft. (Test 'FR2-10-FA', connections use FRP angles)

Test #	Displacement (inch)				
	Joint A	Joint B	Joint C	Joint D	Joint E
1	0.554	0.501	0.371	0.540	0.498
2	0.525	0.492	0.368	0.522	0.492
3	0.517	0.492	0.363	0.538	0.494
4	0.523	0.485	0.360	0.523	0.495
5	0.517	0.487	0.358	0.531	0.491
6	0.517	0.476	0.349	0.517	0.479
7	0.521	0.500	0.366	0.522	0.490
8	0.521	0.492	0.360	0.542	0.489
9	0.517	0.489	0.348	0.548	0.488
10	0.515	0.486	0.355	0.537	0.490
Average	**0.523**	**0.490**	**0.360**	**0.532**	**0.491**
STD	0.012	0.007	0.007	0.010	0.005
COV (%)	2.208	1.497	2.080	1.957	1.017

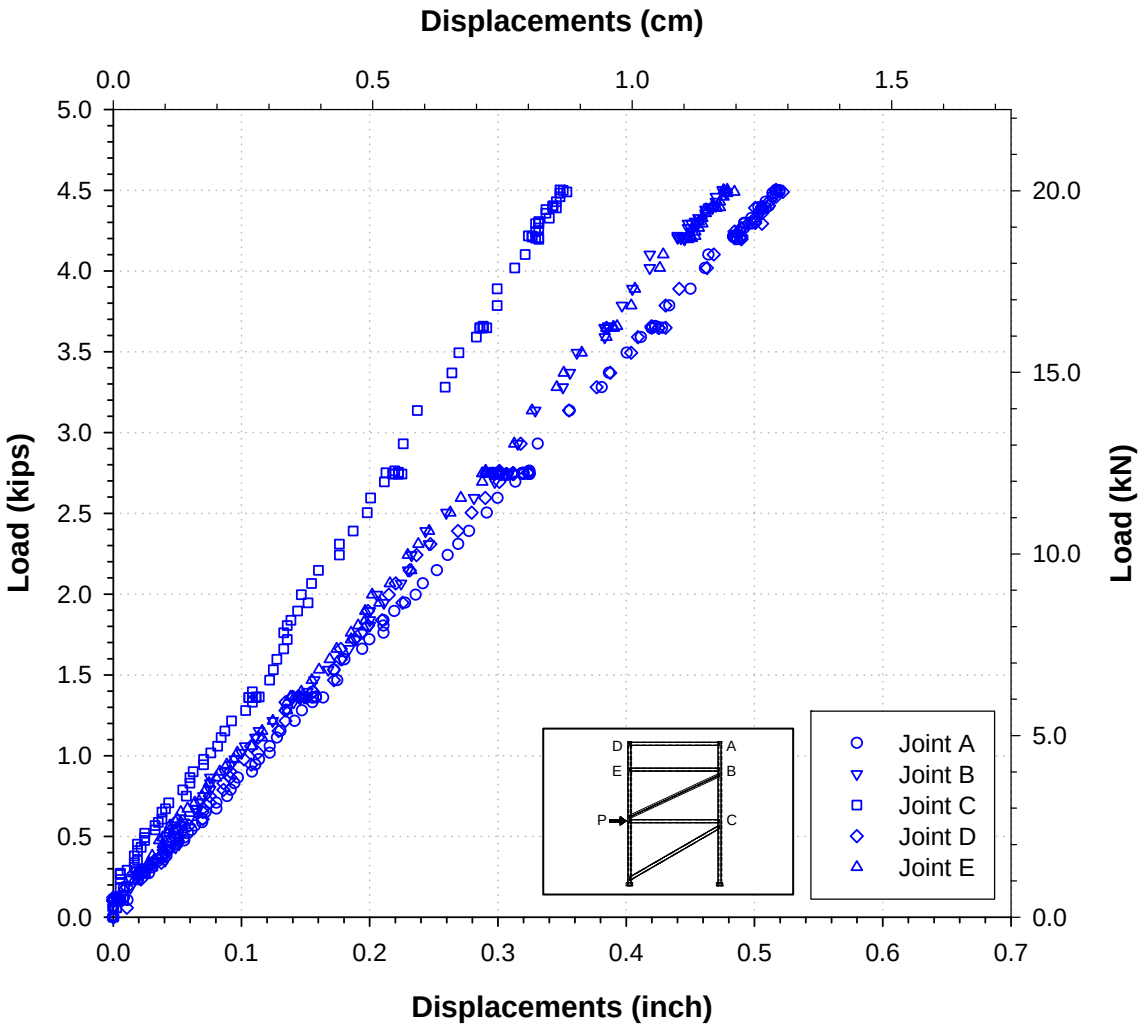

Figure 2.78: Typical loading-displacement curves result for test 'FR2-10-FA' (connections use FRP angles)

Table 2.28: Measured displacement results under load P = 4.5 kips at level 10 ft. (Test 'FR2-10-SA', connections use steel angles)

Test #	Displacement (inch)				
	Joint A	Joint B	Joint C	Joint D	Joint E
1	0.525	0.489	0.367	0.519	0.484
2	0.497	0.466	0.348	0.495	0.466
3	0.502	0.466	0.344	0.510	0.468
4	0.495	0.460	0.341	0.496	0.469
5	0.490	0.462	0.340	0.503	0.465
6	0.490	0.451	0.331	0.490	0.454
7	0.494	0.474	0.347	0.494	0.464
8	0.494	0.466	0.341	0.514	0.464
9	0.490	0.463	0.330	0.519	0.463
10	0.488	0.460	0.336	0.509	0.464
Average	**0.496**	**0.466**	**0.342**	**0.505**	**0.466**
STD	0.011	0.010	0.011	0.011	0.008
COV (%)	2.198	2.203	3.073	2.131	1.615

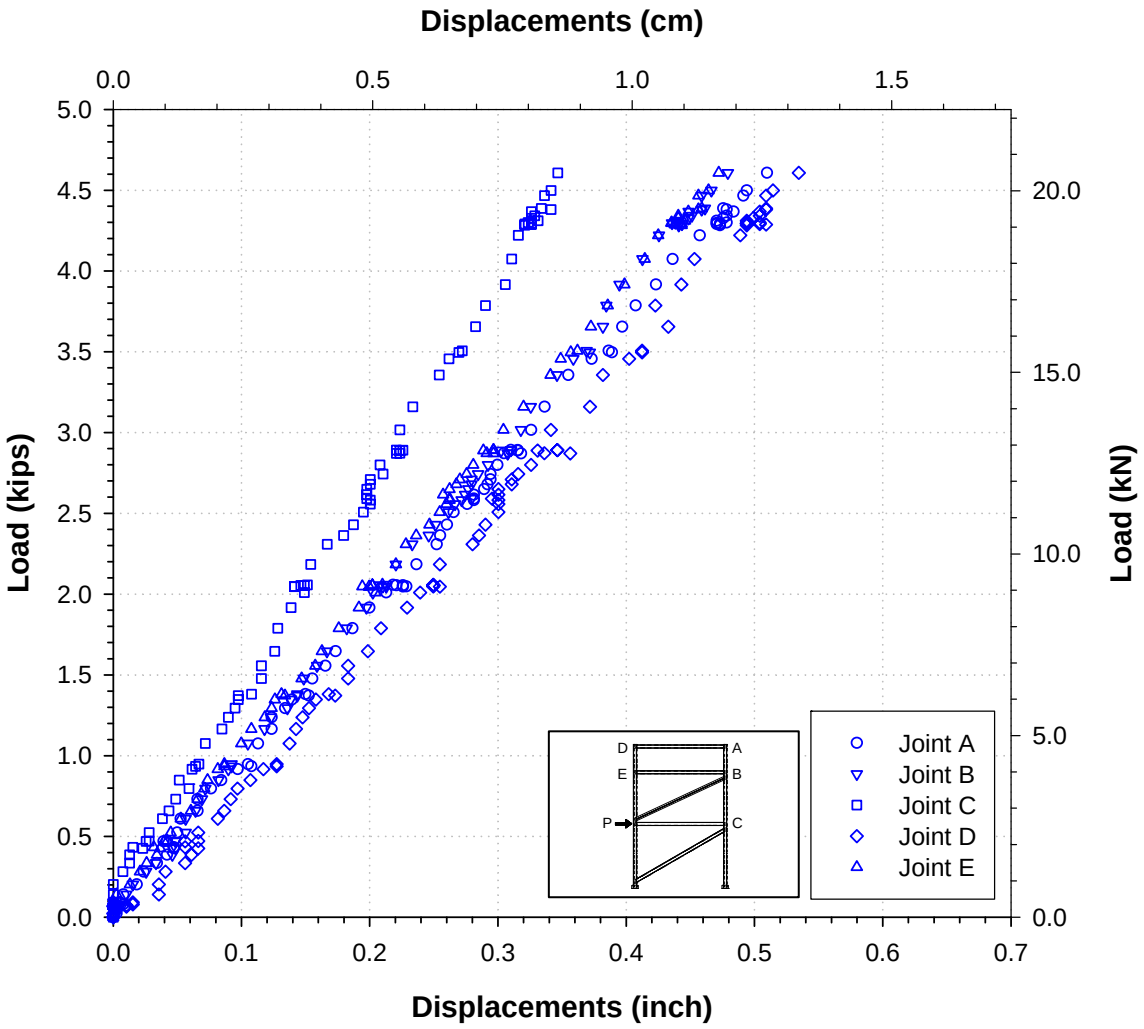

Figure 2.79: Typical loading-displacement curves result for test 'FR2-10-SA' (connections use steel angles)

ANALYTICAL PREDICTION OF STATIC LOAD DISPLACEMENT BEHAVIORS OF FRP COMPOSITE MATERIAL FRAME STRUCTURES

2.9 Introduction

In order to analytically predict the load-displacement response of structural frames composed of members fabricated from pultruded FRP composite materials, it is necessary to perform frame structural analyses based on analytical techniques that are different than those used to analyze frames composed of members fabricated from isotropic materials such as steel. The Fiber Reinforced Polymeric Frame Analysis (FRPFA) procedure developed in this thesis together with the Variational Asymptotic Beam Sectional (VABS) analysis method (Cesnik and Hodges, 1997) is used to analyze such frame structures.

In this study, the FRPFA procedure is developed and used as a numerical method in combination with the general finite element software system, GTSTRUDL, to analyze FRP frame structures. The FRPFA procedure is a procedure enables structural engineers to analyze 2D or 3D structural frames fabricated from pultruded FRP composite materials. In order to perform such analyses, it is essential to properly calculate the stiffness characteristics of FRP composite material members. The stiffness characteristics of members consisting of FRP composite materials should not be calculated using traditional methods based on cross-sectional area properties and isotropic material properties. Rather, a more specialized procedure that accounts for the detailed characteristics of FRP composite materials from which such members are fabricated must be used. The FRPFA procedure includes the following steps.

Fiber Reinforced Polymeric Frame Analysis (FRPFA) Procedure

Material Properties Preparation Stage

(1) Mechanical material properties of the constituents of composite materials such as fiber, resin and fillers can be measured experimentally or specified by the civil/structural engineer or by the manufacturer. Volume or weight fractions of the fiber, resin, and filler constituents can be specified or measured by the civil/structural engineer or the manufacturer.

(2) Effective mechanical material properties of the matrix (Figure 2.4(a)) which consists of some combination of resin, filler material and void can be calculated from the individual mechanical properties of the resin and filler materials and accounting for the voids. The Mori-Tanaka micro-mechanics model (Mori and Tanaka, 1973) was used to calculate the effective mechanical material properties of the matrix. Section 3.2.1 describes this step.

(3) Effective mechanical material properties of a single layer (Figure 2.4(c)) composed of a matrix and a fiber reinforcement system can be calculated from individual mechanical properties of the matrix and fiber. Two popular fiber reinforcement systems that are considered in this thesis are the roving fiber reinforcement and continuous strand mat fiber reinforcement systems (Figure 2.4(c)). Micro-mechanics models are used to calculate the effective mechanical material properties of these composite layers. The Halpin-Tsai model (Halpin and Tsai, 1969) was used for roving fiber reinforcement systems and the Tsai-Pagano model (Tsai and Pagano, 1968) was used for continuous strand mat fiber reinforcement systems. Sections 2.10.2 and 2.10.3 describe this step.

(4) (a) Effective mechanical material properties of the components of member cross-sections (e.g., flanges and webs) (Figure 2.4(d)) were calculated from the mechanical properties of the single layers. Components of member cross-sections

consist of multiple layers where each layers can have different material properties. Lamination theory (Jones, 1975) was used to calculate the effective mechanical material properties of the components of member cross-sections[6]. Section 2.10.4 describes this step (see Figure 2.4(d)).

(b) The effective mechanical material properties were also obtained by using experimental measurements of specimens taken from the components of the member cross-sections. Section 2.5 described this step and represented experimentally measured effective mechanical material properties of components (e.g. web and flange) of cross-sections.

Member Natural Stiffness and Member Fixed-End Forces Calculations

(5) Calculation of the 2D cross-sectional stiffness matrix of a member cross-section is performed next. A member cross-section is composed of several components (e.g., flanges and webs). The cross-sectional area of each such component is discretized using a finite element mesh. The effective mechanical material properties of the components of a member cross-section obtained in Step 4 above are used for a sectional analysis procedure. For the cross-sectional analysis, the Variational Asymptotic Beam Sectional analysis (VABS) procedure was used to perform cross-sectional stiffness matrix calculations (Appendix C).

(6) Calculation of the 1D space frame member natural stiffness matrix is performed next. The calculated cross-sectional stiffness matrix in Step 5 above is transformed into the space frame member natural stiffness sub-matrix $\mathbf{K}_{\mathbf{BB}}$ which is a sub-matrix of the space frame natural stiffness matrix $\mathbf{K}$. The sub-matrix $\mathbf{K}_{\mathbf{BB}}$ is then used as input for member properties in GTSTRUDL (Step 8). The transformation procedure from cross-sectional stiffness into $\mathbf{K}_{\mathbf{BB}}$ is presented in Appendix B.

[6] VABS can take 3D material properties directly without using the lamination theory to exactly calaulate the sectional stiffness. However, in the FRPFA procedure, the lamination theory is used to simplfy the cross-section modeling.

(7) Calculation of member fixed-end-forces is performed next. Applied member forces and moments are transformed into member fixed-end forces accounting for the special characteristics of anisotropic structural members. The theoretical formulation of this procedure is presented in Appendix E.

Frame System Analysis

(8) GTSTRUDL is used as the frame analysis program in this thesis. The $\mathbf{K}_{BB}$ matrix obtained in Step 6 above is input to GTSTRUDL as the member properties for members fabricated from FRP composite materials. Member fixed-end-forces computed in Step 7 above are used in order to account for applied member forces.

Figure 0.1 illustrates the flow of the FRPFA procedure.

It should be noted that, for the frame analysis used in this analysis, it was decided to use the effective mechanical material properties of the components of cross-sections that were determined experimentally (STEP 4 (b)). The reason that the experimentally measured values were used was that insufficient detailed material properties were available from the manufacturer of the FRP materials.

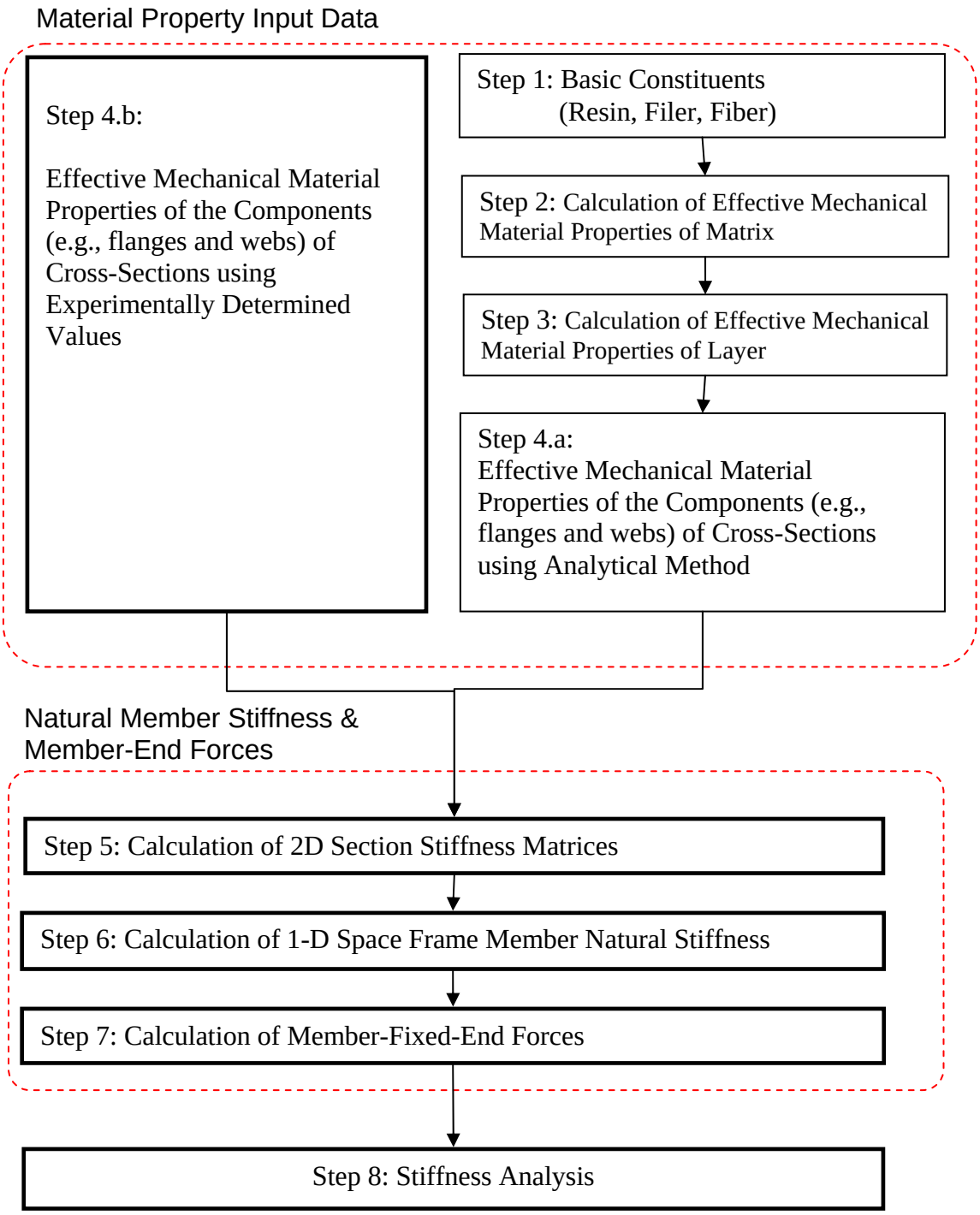

Figure 0.1: Flowchart of the FRPFA procedure

2.10 Calculation of Effective Mechanical Material Properties for Frame Analysis

The effective mechanical material properties of the matrix system, composite layers, and components of cross-section can be analytically determined herein.

2.10.1 Calculation of Effective Mechanical Material Properties of a Matrix System

The matrix system (Figure 2.4(a)) is composed of a resin material and fillers. Mori-Tanaka's formula (Mori and Tanaka, 1973) is used to analytically predict the effective mechanical material properties of a matrix system for pultruded composite structural member as follows. This procedure corresponds to Step 2 in Figure 0.1.

$$G_m = G_r\left\{1+\frac{\mathrm{v}^m_{filler}\left(G_{filler}-G_r\right)}{G_r+2S_{1212}\left(G_{filler}-G_r\right)}+\frac{\mathrm{v}^m_{void}\left(-G_r\right)}{G_r+2S_{1212}\left(-G_r\right)}\right\} \quad \textbf{(3.1)}$$

$$K_m = K_r\left\{1+\frac{\mathrm{v}^m_{filler}\left(K_{filler}-K_r\right)}{K_r+(1/3)S_{kkll}\mathrm{v}^m_{resin}\left(K_{filler}-K_r\right)}+\frac{\mathrm{v}^m_{void}\left(-K_r\right)}{K_r+(1/3)S_{kkll}\mathrm{v}^m_{resin}\left(-K_r\right)}\right\} \quad \textbf{(3.2)}$$

where

S_{1212} = $\dfrac{3K_r+6G_r}{15K_r+20G_r}$

S_{kkll} = $\dfrac{9K_r}{3K_r+4G_r}$

G_m = shear modulus of the matrix system.

G_{filler} = shear modulus of the filler.

G_r = shear modulus of the resin.

K_m = bulk modulus of the matrix.

K_{filler} = bulk modulus of the filler.

K_r = bulk modulus of the resin.

v^m_{filler} = volume fraction of the filler.

v_{void}^{m} = volume fraction of the void in the matrix system.

v_{resin}^{m} = volume fraction of the resin in the matrix system.

The Young's modulus E_m and Poisson's ratio ν_m of the matrix system can be computed using G_{m} and K_{m} from Equations (3.1) and (3.2) as follows:

$$E_{\mathrm{m}} = \frac{9K_{\mathrm{m}}}{1 + 3K_{\mathrm{m}} / G_{\mathrm{m}}} \tag{3.3}$$

$$\nu_m = \frac{E_m}{2G_m} - 1 \tag{3.4}$$

2.10.2 Calculation of Effective Mechanical Material Properties of a Single Roving Layer

A roving layer (Figure 2.4(c)) consists of the unidirectional roving fibers and matrix. The mechanical properties of the roving layer such as longitudinal modulus E_L^{RL}, transverse modulus E_T^{RL}, shear modulus G_{LT}^{RL} and Poisson's ratio ν_{LT}^{RL} can be obtained by using the Halpin-Tsai model (Halpin and Tsai, 1969) from a Young's modulus of a matrix E_m and a longitudinal modulus of anisotropic fiber E_f in the roving layers, where the superscript '*RL*' means a roving layer, as follows (This procedure corresponds to Step 3 in Figure 0.1):

$$E_L^{RL} = E_f \mathrm{v}_\mathrm{f}^{\mathrm{RL}} + E_m \mathrm{v}_\mathrm{m}^{\mathrm{RL}} \quad \textbf{(3.5)}$$

$$\nu_{LT}^{RL} = \nu_f \mathrm{v}_\mathrm{f}^{\mathrm{RL}} + \nu_m \mathrm{v}_\mathrm{m}^{\mathrm{RL}} \quad \textbf{(3.6)}$$

$$E_T^{RL} = \frac{1+\xi\eta_2 \mathrm{v}_\mathrm{f}^{\mathrm{RL}}}{1-\eta_2 \mathrm{v}_\mathrm{f}^{\mathrm{RL}}} E_m \ , \ \eta_2 = \frac{(E_f / E_m)-1}{(E_f / E_m)+\xi} \ , \ \xi = 2 \quad \textbf{(3.7)}$$

$$G_{LT}^{RL} = \frac{1+\xi\eta_G \mathrm{v}_\mathrm{f}^{\mathrm{RL}}}{1-\eta_G \mathrm{v}_\mathrm{f}^{\mathrm{RL}}} G_m \ , \ \eta_G = \frac{(G_f / G_m)-1}{(G_f / G_m)+\xi} \ , \ \xi = 1 \quad \textbf{(3.8)}$$

where

E_m	=	Young's modulus of a matrix
E_f	=	Young's modulus of a fiber
$\mathrm{v}_\mathrm{f}^{\mathrm{RL}}$	=	Volume fraction of fiber in roving layer
$\mathrm{v}_\mathrm{m}^{\mathrm{RL}}$	=	Volume fraction of matrix in roving layer
ξ	=	Empirical parameter.

2.10.3 Calculation of Effective Mechanical Material Properties of a Single Continuous Strand Mat (CSM) Layer

A continuous strand mat (CSM) layer (Figure 2.4(c)) consists of a randomly oriented fiber mat and matrix. The mechanical properties of the mat layer such as the modulus E^{CSM}, shear modulus G^{CSM}, and Poisson's ratio ν^{CSM} can be obtained by using the Tsai-Pagano model (Tsai and Pagano, 1968), where the superscript '*CSM*' means a continuous strand mat (CSM) layer, as follows (This procedure corresponds to Step 3 in Figure 0.1):

$$E^{CSM} = \frac{3}{8}E_L^* + \frac{5}{8}E_T^* \quad \textbf{(3.9)}$$

$$G^{CSM} = \frac{1}{8}E_L^* + \frac{1}{4}E_T^* \quad \textbf{(3.10)}$$

$$\nu^{CSM} = \frac{E^{CSM}}{2G^{CSM}} - 1 \quad \textbf{(3.11)}$$

where

$$E_L^* = E_f \mathrm{v}_\mathrm{f}^{\mathrm{CSM}} + E_m \mathrm{v}_\mathrm{m}^{\mathrm{CSM}}$$

$$E_T^* = \frac{1+2\eta_2 \mathrm{v}_\mathrm{f}^{\mathrm{CSM}}}{1-\eta_2 \mathrm{v}_\mathrm{f}^{\mathrm{CSM}}} E_m \ , \ \eta_2 = \frac{(E_f / E_m)-1}{(E_f / E_m)+\xi} \ , \ \xi = 2$$

E_m = Young's modulus of a matrix

E_f = Young's modulus of a fiber

$\mathrm{v}_\mathrm{f}^{\mathrm{CSM}}$ = Volume fraction of fiber in CSM layer.

$\mathrm{v}_\mathrm{m}^{\mathrm{CSM}}$ = Volume fraction of matrix in CSM layer.

2.10.4 Calculation of Effective Mechanical Material Properties of a Component of Cross-Section

The equivalent mechanical material properties of the components of an FRP member cross-section (e.g., web and flange) can be calculated using classical lamination theory (Figure 2.4(d)). Park (2001) simplified the classical lamination theory (Jones, 1975) to obtain an explicit form of equivalent mechanical material properties of components of an FRP member cross-section composed of roving layers and continuous strand mat (CSM) layers. The longitudinal modulus E_L , transverse modulus E_T , in-plane shear modulus G_{LT} , and in-plane Poisson's ratio ν_{LT} can be calculated using the following explicit forms (This procedure corresponds to Step 4.a in Figure 0.1).

$$E_L = \frac{E_L^{RL}}{\eta_{RL}}\nu_{RL} + \frac{E^{CSM}}{\eta_{CSM}}\nu_{CSM} - \frac{\left(\frac{\nu_{LT}^{RL}\cdot E_T^{RL}}{\eta_{RL}}\nu_{RL} + \frac{\nu^{CSM}\cdot E^{CSM}}{\eta_{CSM}}\nu_{CSM}\right)^2}{\frac{E_T^{RL}}{\eta_{RL}}\nu_{RL} + \frac{E_T^{CSM}}{\eta_{CSM}}\nu_{CSM}} \quad \textbf{(3.12)}$$

$$E_T = \frac{E_T^{RL}}{\eta_{RL}}\nu_{RL} + \frac{E^{CSM}}{\eta_{CSM}}\nu_{CSM} - \frac{\left(\frac{\nu_{LT}^{RL}\cdot E_T^{RL}}{\eta_{RL}}\nu_{RL} + \frac{\nu^{CSM}\cdot E^{CSM}}{\eta_{CSM}}\nu_{CSM}\right)^2}{\frac{E_T^{RL}}{\eta_{RL}}\nu_{RL} + \frac{E^{CSM}}{\eta_{CSM}}\nu_{CSM}} \quad \textbf{(3.13)}$$

$$G_{LT} = G_{LT}^{RL}\nu_{RL} + G^{CSM}\nu_{CSM} \quad \textbf{(3.14)}$$

$$\nu_{LT} = \frac{\frac{\nu_{LT}^{RL}\cdot E_T^{RL}}{\eta_{RL}}\nu_{RL} + \frac{\nu^{CSM}\cdot E^{CSM}}{\eta_{CSM}}\nu_{CSM}}{\frac{E_T^{RL}}{\eta_{RL}}\nu_{RL} + \frac{E^{CSM}}{\eta_{CSM}}\nu_{CSM}} \quad \textbf{(3.15)}$$

where

$$\eta_{RL} = 1 - \nu_{LT}^{RL}\nu_{TL}^{RL}$$

$$\eta_{CSM} = 1 - (\nu^{CSM})^2$$

v_{RL} and v_{CSM} are volume fraction of roving and continuous strand mat layers respectively. E_L^{RL} and E_T^{RL} are longitudinal and transverse moduli of roving layers calculated in Section 2.10.2 (Eqs. 3-5, 3-7). G_{LT}^{RL} and ν_{LT}^{RL} are shear modulus and Poisson's ratio of roving layer respectively (Eqs. 3-8, 3-6). E^{CSM}, G^{CSM}, and ν^{CSM} are Young's modulus, shear modulus, and Poisson's ratio of continuous strand mat layers respectively (see Section 2.10.3, Eqs. 3-9, 3-10, and 3-11).

However, as stated in step (4) in Section 2.9, the effective mechanical material properties of the components of a cross-section were directly measured through experimental procedures (e.g., coupon tests) as described in Section 2.5.

2.11 Frame Stiffness Analysis

2.11.1 Analytical Modeling of FRP Composite Frames

The FRP composite frames tested in Chapter 2 were analyzed by means of the computer program, GTSTRUDL (CASE Center, 2008). In such analyses, all member properties were input as member natural stiffness matrices computed by the FRPFA procedure (Section 2.9). Figures 3-3 and 3-4 illustrate two computer models showing the global coordinate system and the local coordinate systems of FRP composite structural members (Section 2.1). The following describes the FRP frames modeled for analysis purpose:

a. Columns, beams, and braces members are modeled using space frame members. Joint and member incidences are shown in Figures 3-3 and 3-4.

b. The mechanical materials properties of each component of the cross-section of structural members are determined based upon the experimental procedures performed in Section 2.5 and these results are used in the frame stiffness analysis (Step 4.b in FRPFA procedure (Section 2.9)). The next step is to calculate the 2D sectional stiffness of the cross-section. In order to calculate the 2D sectional stiffness of the cross-section based on the materials properties determined in Step 4.a or Step 4.b, all nine independent mechanical material properties are required. It is not intended to perform such experimental measurements of all nine mechanical material properties since such experiments are expensive and complex procedures. Rather, it is

intended to use mechanical material parameters showing high sensitivity to the load-displacement behavior of the frames (Section 2.11.2).

c. The column supports are modeled with finite elements using the GTSTRUDL Stretching and Bending Hybrid Quadrilateral (SBHQ6) plate finite elements in order to account for the stiffness characteristics of the column base support in the analysis (Figure 0.5). The detail of this column support was shown in Figure 2.22 in Section 2.4.

A sensitivity analysis was performed to determine the effect of each mechanical material property on the joint displacements results of FRP composite frames in Section 2.11.2. This analysis shows that only the longitudinal modulus, E_L, and the in-plane shear modulus, G_{LT}, are important to include in the analysis of the frames tested in this research. Therefore, the only mechanical material properties that were measured in the coupon tests were the longitudinal modulus, E_L, and the in-plane shear modulus, G_{LT} (Section 2.5.4) which were sufficient to analyze the FRP frame models.

In order to perform comparisons of analysis results and experimental results, a consideration of connection stiffness is necessary. However, the nature of the connection stiffness is unknown. Further, it was not intended in this research to experimentally determine the connection stiffness associated with the frames studied herein. In this study, bounds on the connection stiffness were used in the numerical calculations.

The member natural stiffness matrices of each structural member were calculated based on Step 5 and Step 6 in FRPFA procedure (Figure 0.1). The calculated member

stiffness matrices were input to GTSTRUDL to perform frame stiffness analysis. Member loads such as self-weight of members were converted into equivalent joint loads following Step.7.

Section 2.11.3 presents frame analysis results showing analytically calculated horizontal load-displacements results based on the FRPFA procedures. Figure 0.6 shows a typical deformed shape of a frame.

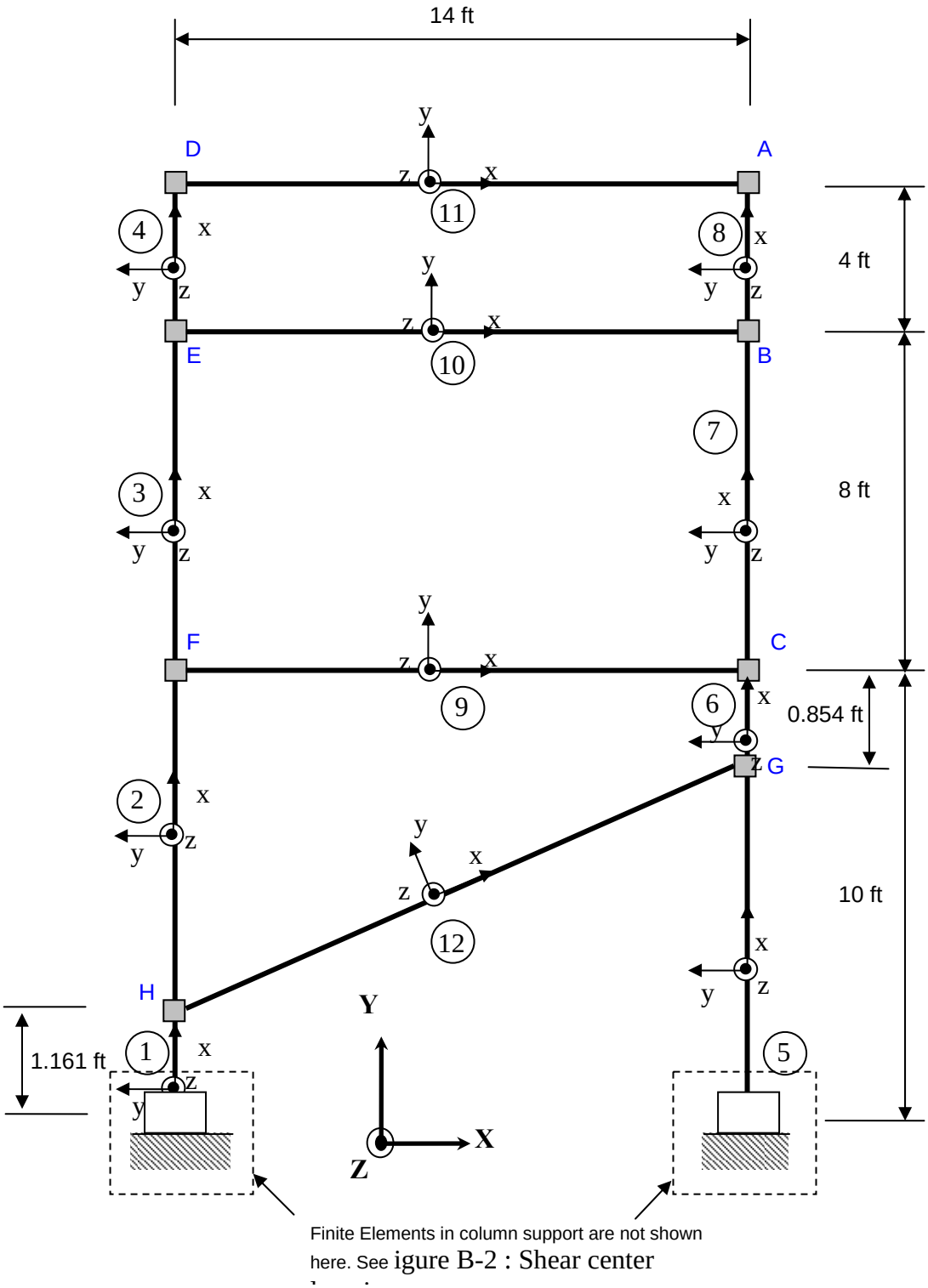

Figure 0.3: GTSTRUDL model for FRAME-1 series

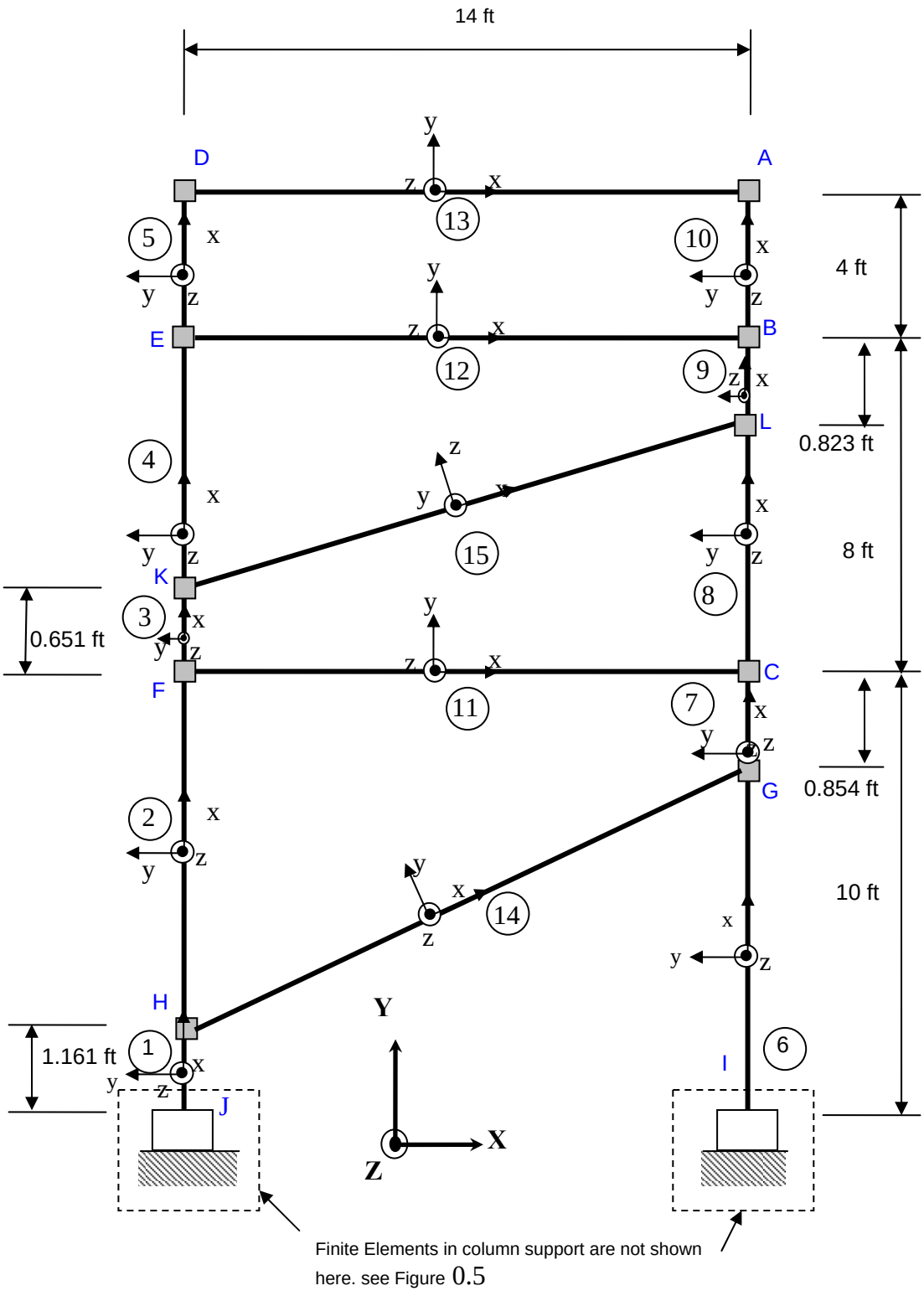

Figure 0.4: GTSTRUDL model for FRAME-2 series

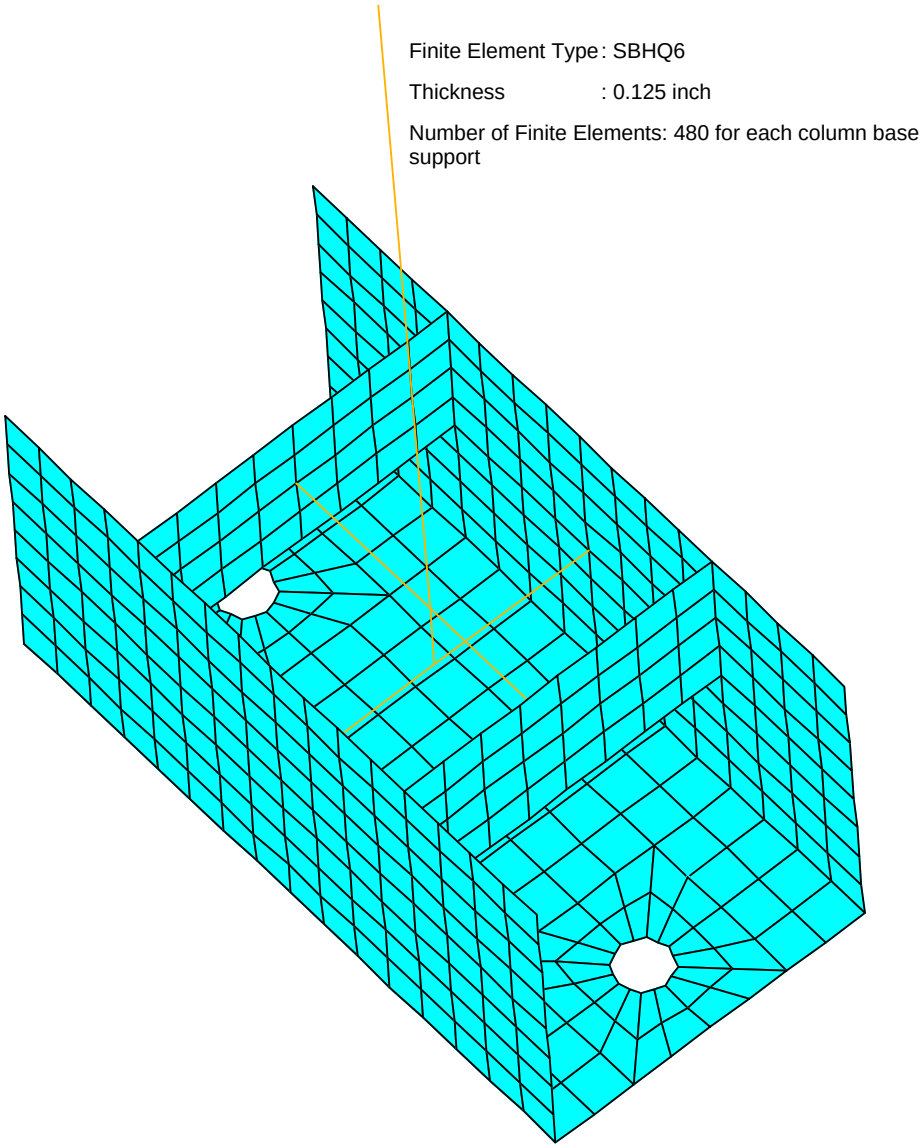

Figure 0.5: Column base support modeled with finite elements, SBHQ6

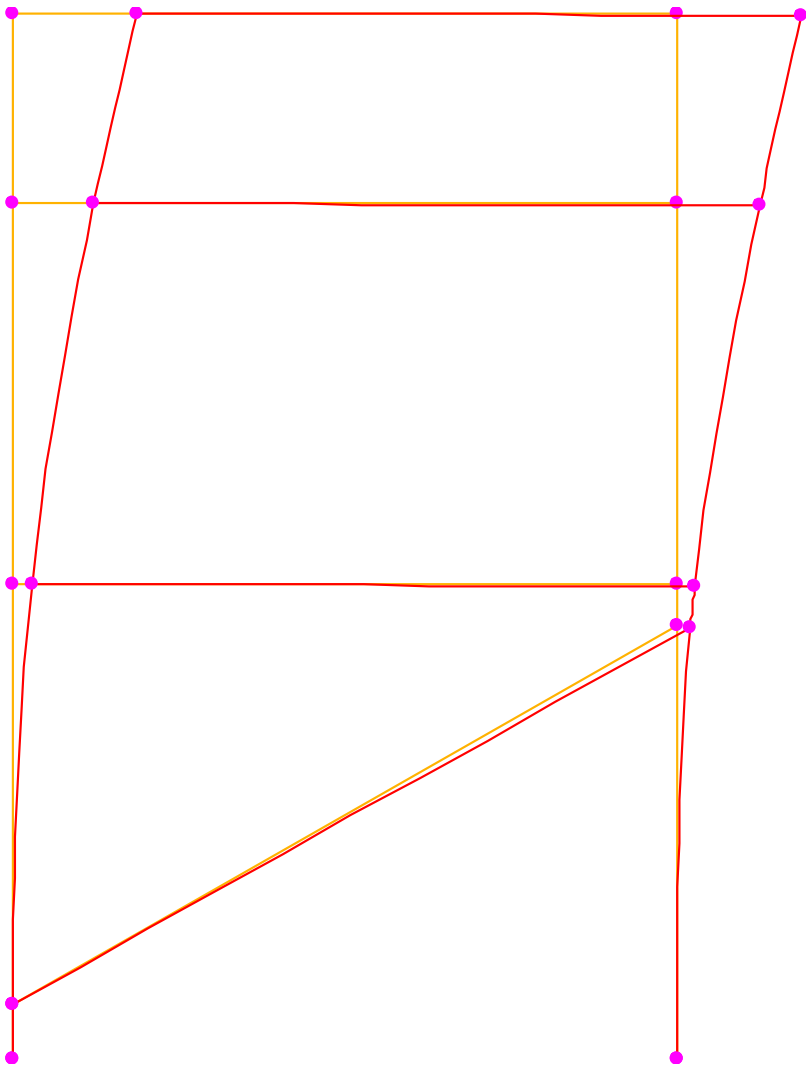

Figure 0.6: Typical deformed shape of the frame model

2.11.2 Mechanical Material Properties Sensitivity Analysis

The sensitivities of the joint displacements were evaluated with respect to the variations of mechanical material property input parameters for the frame analyses. Table 0.1 shows the reference material properties that were used in this sensitivity analysis. These values were taken from the material testing result in Section 2.5. To evaluate the effect of the nine mechanical material properties on the load-displacement behaviors in the frame analysis, all nine mechanical material properties inputs are required for the FRPFA procedures for the reference case. The longitudinal modulus E_L and in-plane Poisson's ratio ν_{LT} were taken from the tension and compression coupon tests. The in-plane shear modulus G_{LT} was taken from in-plane shear coupon tests. However, the other six material properties (E_T, E_N, G_{LN}, G_{TN}, ν_{TN}, and ν_{LN}) were not measured because of the difficulties of material testing.

For the initial material property inputs for a sensitivity analysis using FRPFA, transverse modulus, E_T, and normal modulus, E_N were assumed to be 65% of longitudinal modulus E_L. The ratio, 65%, was selected by using the previous mechanical material properties tests for the similar FRP composite material (E-glass/Vinylester) (Park, 2001). The through thickness shear moduli, G_{LN}, G_{TN}, and Poisson's ratios, ν_{TN}, ν_{LN}, were assumed to be the same as the in-plane properties, respectively. To evaluate the sensitivity of specific mechanical material property parameter on the joint displacement results, only one mechanical material property was decreased with 10% from a original reference mechanical material properties value with all other eight material parameter values fixed.

The analytically calculated joint displacement results for joint A in the test setup 'FR1-22' (Figure 0.7) was used for the sensitivity analysis. The beam-column connection condition was assumed as a pin connection in this analysis. Table 0.2 shows the sensitivity evaluation results of the joint displacements pertaining to the 10% decrease of each nine material input parameters. d_X represents the original joint displacements in global X direction. Δd_X represents the change of joint displacement in global X direction after specific material parameter is decreased by 10%. Therefore, $\Delta d_X / d_X$ is the ratio of a variation of joint displacement to the original joint displacements.

As expected, it was observed that the lateral displacement of the frames was most sensitive to the longitudinal modulus E_L. In addition, the in-plane shear modulus G_{LT} showed the second highest sensitivity respectively. The other parameters such as E_T, E_N, G_{TN}, G_{LN}, ν_{LT}, ν_{LN} and ν_{TN} showed insignificant sensitivities for the current frame system. Figure 0.8 shows the graphical presentation of sensitivity evaluations of joint displacement of joint A for the material input parameters for the frame analysis.

Table 0.1: Reference mechanical material properties used in sensitivity analysis

Parameter	COLUMNS (C1,C2) (t = 0.375 inch)	BEAMS (B1,B2,B3,BR1)	
		Flanges (t = 0.375 inch)	Webs (t = 0.25 inch)
E_L * (ksi)	5,300	5,249	4,262
E_T ** (ksi)	3,392	3,359	2,727
E_N ** (ksi)	3,392	3,359	2,727
G_{LT} (ksi)	550	677	681
G_{LN} (ksi)	550	677	681
G_{TN} *** (ksi)	550	677	681
ν_{LT}	0.26	0.25	0.25
ν_{TN}	0.26	0.25	0.25
ν_{LN} ***	0.26	0.25	0.25

Notes:

* Average of tensile and compressive moduli

** Assumed with 65% of longitudinal properties (for E-glass/Vinylester)

*** Assumed to be same with in-plane properties

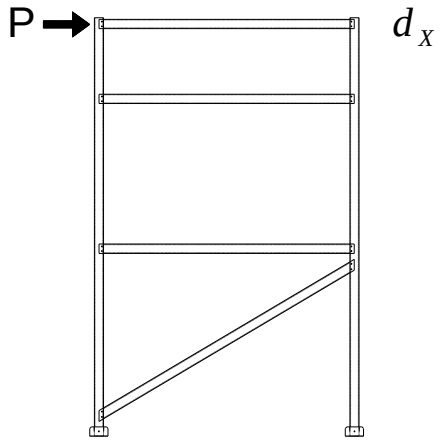

Figure 0.7: 'FR1-22' Test setup for the sensitivity analysis

Table 0.2: Displacement changes per 10% decrease of input parameters

	Joint A		Joint B		Joint C	
10% Decreased Input Parameter	Δd_X (in.)	$\frac{\Delta d_X}{d_X}$ (%)	Δd_X (in.)	$\frac{\Delta d_X}{d_X}$ (%)	Δd_X (in.)	$\frac{\Delta d_X}{d_X}$ (%)
E_L	0.112879	9.48	0.084737	9.38	0.009611	9.14
E_T	0.0	0.0	0.0	0.0	0.0	0.0
E_N	0.0	0.0	0.0	0.0	0.0	0.0
G_{LT}	0.006039	0.507	0.004439	0.492	0.001413	1.344
G_{LN}	0.000097	0.009	0.000050	0.006	0.000033	0.007
G_{TN}	0.0	0.0	0.0	0.0	0.0	0.0
ν_{LT}	0.0	0.0	0.0	0.0	0.0	0.0
ν_{TN}	0.0	0.0	0.0	0.0	0.0	0.0
ν_{LN}	0.0	0.0	0.0	0.0	0.0	0.0

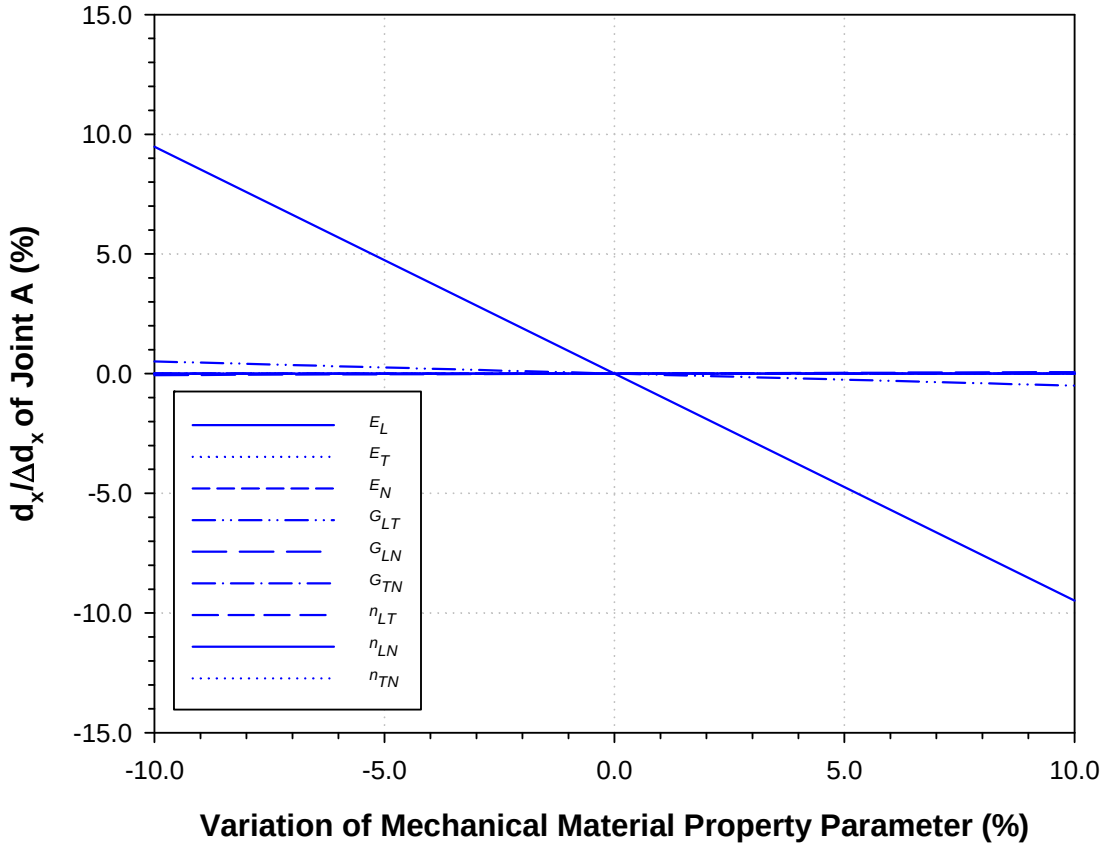

Figure 0.8: Variations of joint 'A' displacement to variation of mechanical material property parameter

2.11.3 Frame Analysis Results

The numerically calculated load-displacement results are presented in this Section along with experimentally measured test results. The analysis results include two analysis horizontal joint displacements results for frames using idealized 'pinned' and 'fixed' beam-column connection conditions. The comparisons of experimental and analytically calculated horizontal joint displacements are made to show that both analysis models with pinned and fixed beam/column boundary conditions form the bounds to the experimentally measured results. The test results presented in each chart in Figures 3-9 to 3-26 include the joint displacement results for frames with three different beam-column connection types. The details of the three beam-column connection types are shown in Figure 2.10 in Section 2.4.

The load-displacement results of FRAME-1 having one diagonal member are shown in Figures 3-9 to 3-17 and the load-displacement results of FRAME-2 having two diagonal members were shown Figures from 3-18 to 3-26. Table 0.3 shows five cases used in each figure for the load-displacement graphs.

Table 0.4 shows the normalized horizontal joint displacements, which mean the horizontal joint displacement under a unit loading of 1.0 kip.

Table 0.3: Compared load-displacement cases

Case	Meaning
Test (Type–P)	Test results of Frame with connection type ‘P’ (Figure 2.10a)
Test (Type–FA)	Test results of Frame with connection type ‘FA’ (Figure 2.10b)
Test (Type–SA)	Test results of Frame with connection type ‘SA’ (Figure 2.10c)
Analysis (Pin)	Frame analysis result for frames that all beam-columns connections at the beam ends are modeled as pinned connections
Analysis (Fix)	Frame analysis result for frames that all beam-columns connections at the beam ends are modeled as fixed connections

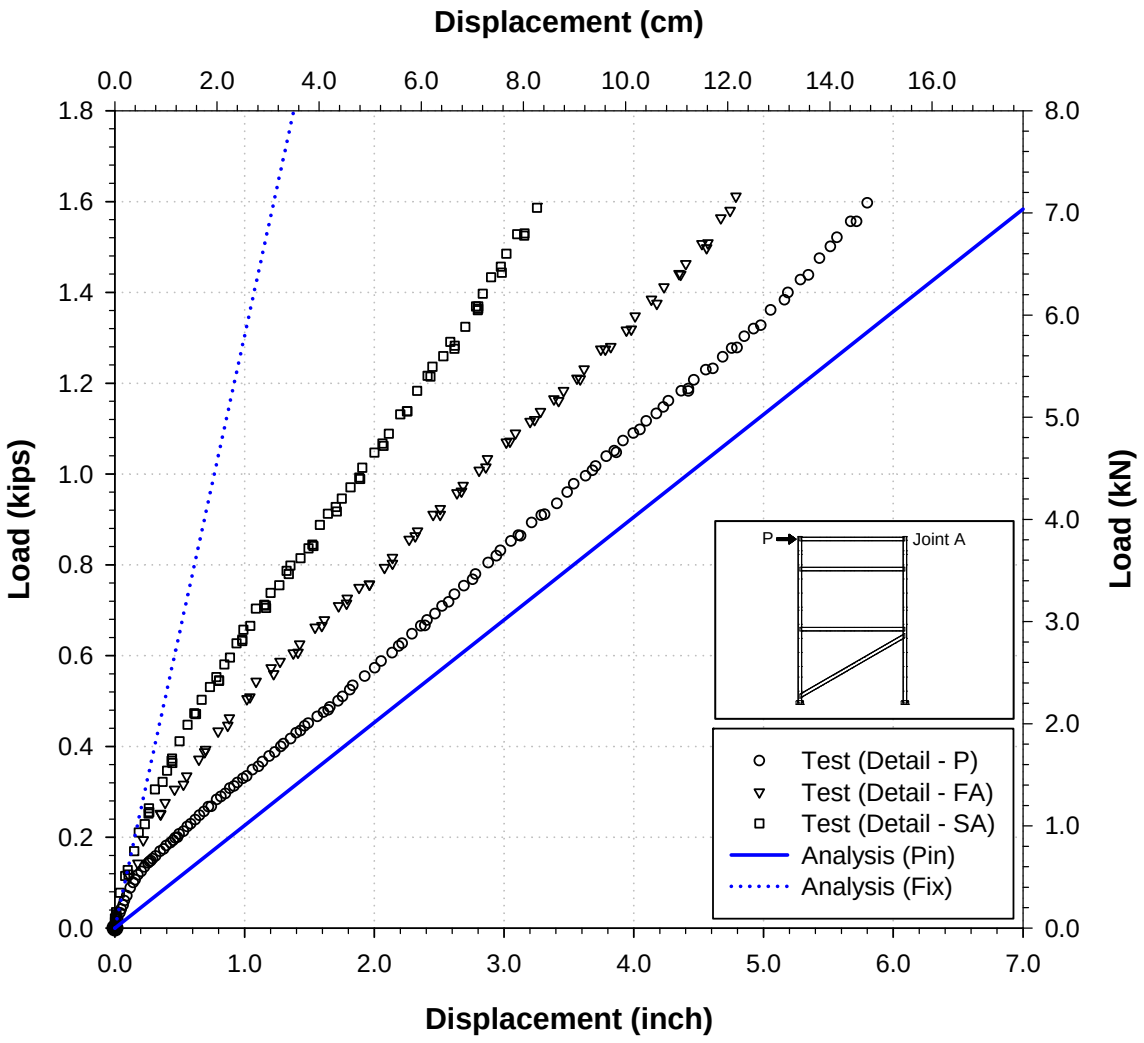

Figure 0.9: Load-displacement results of joint A for FRAME-1 with loading on 22 ft. level ('FR1-22' test series*)

* Table 2.9

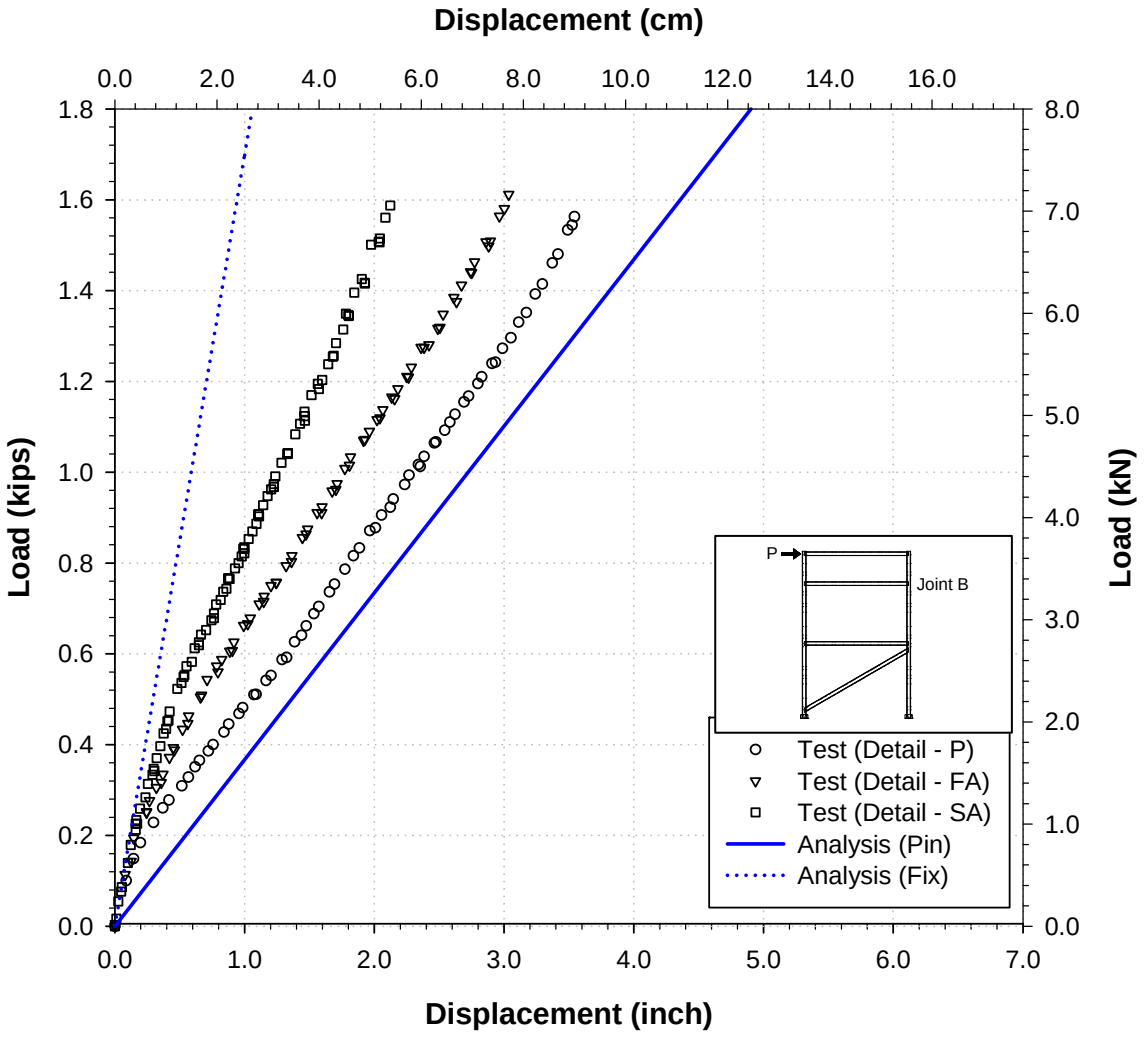

Figure 0.10: Load-displacement results of joint B for FRAME-1 with loading on 22 ft. level ('FR1-22' test series*)

* Table 2.9

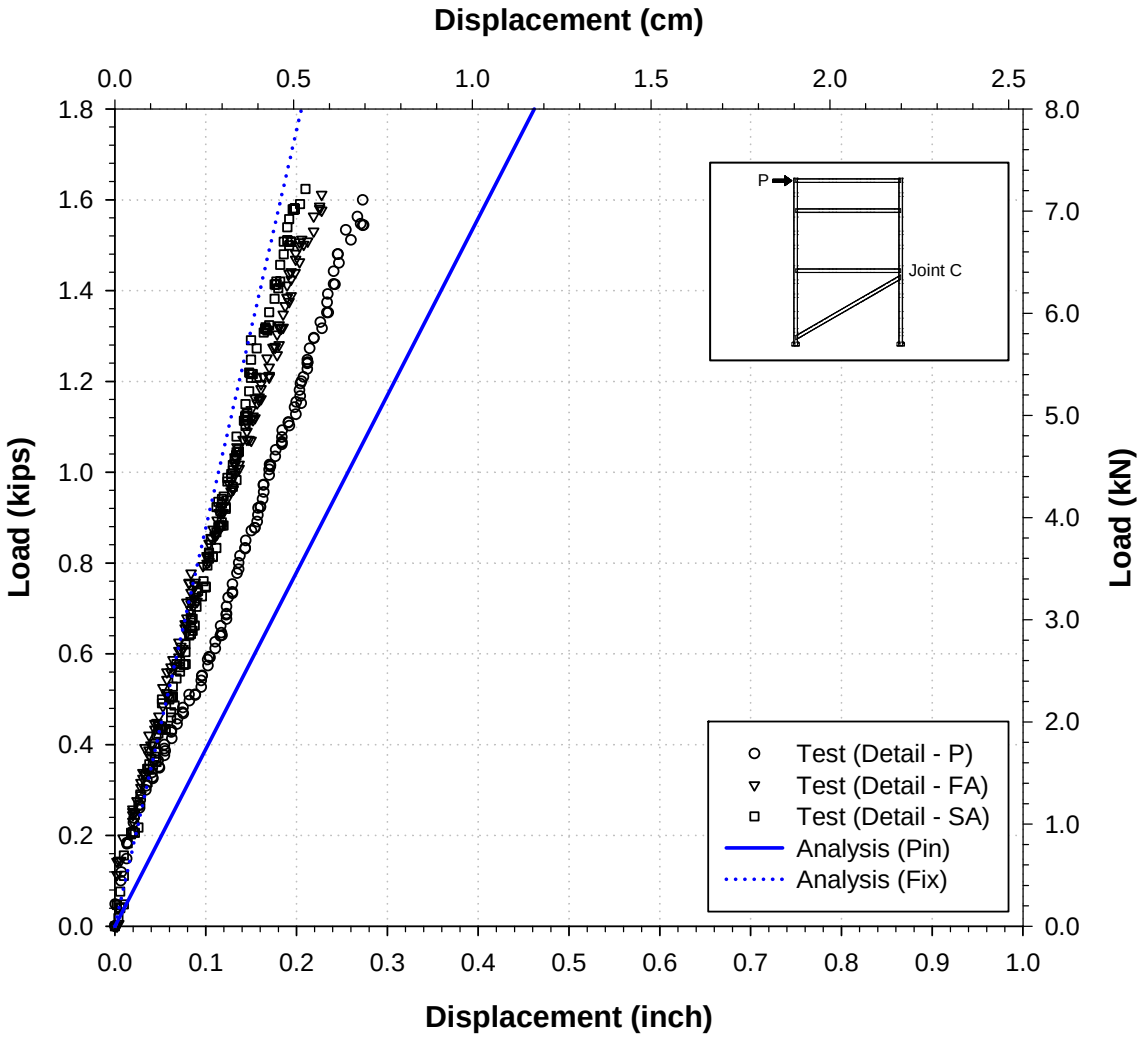

Figure 0.11: Load-displacement results of joint C for FRAME-1 with loading on 22 ft. level ('FR1-22' test series*)

* Table 2.9

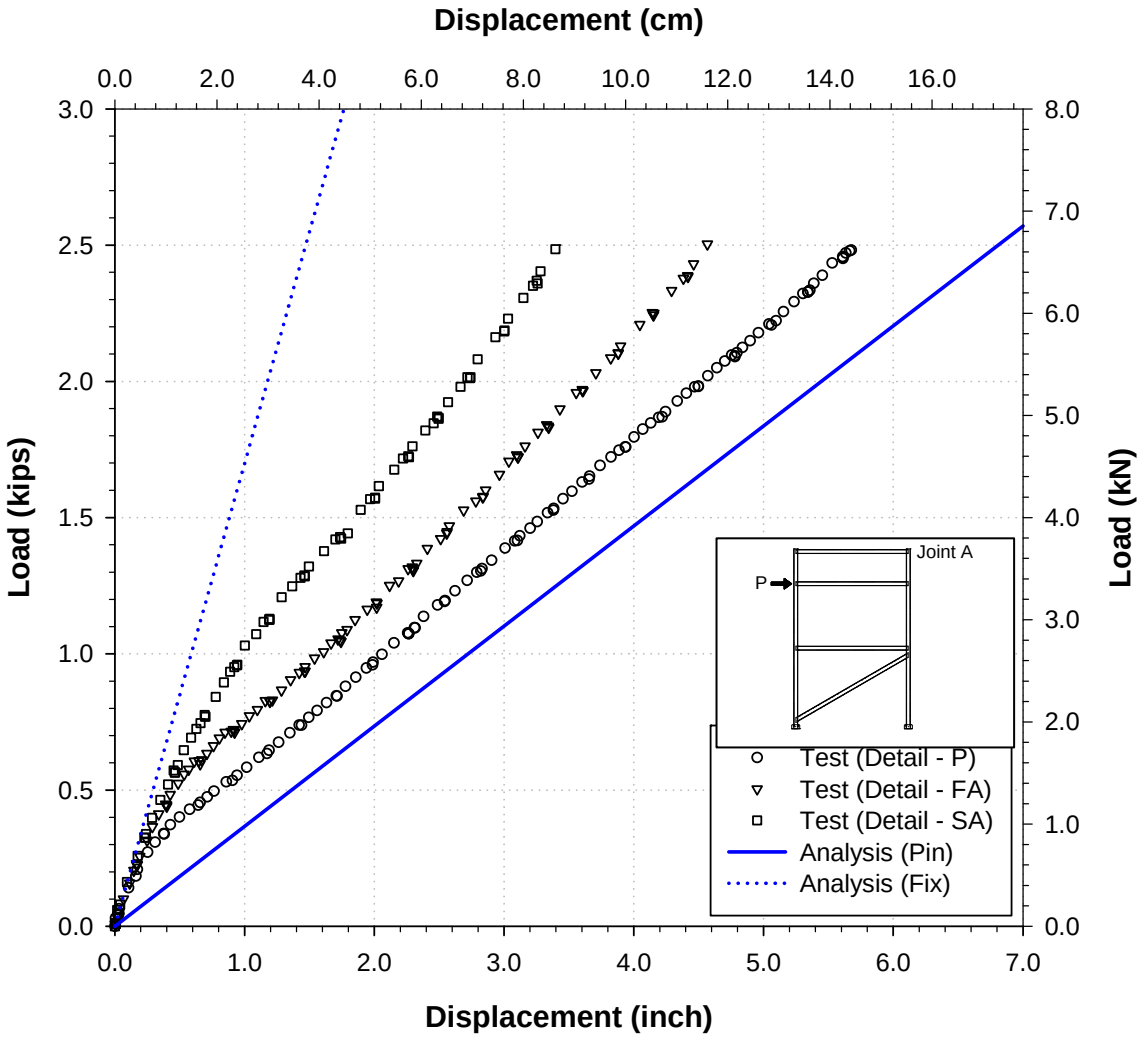

Figure 0.12: Load-displacement results of joint A for FRAME-1 with loading on 18 ft. level ('FR1-18' test series*)

* Table 2.9

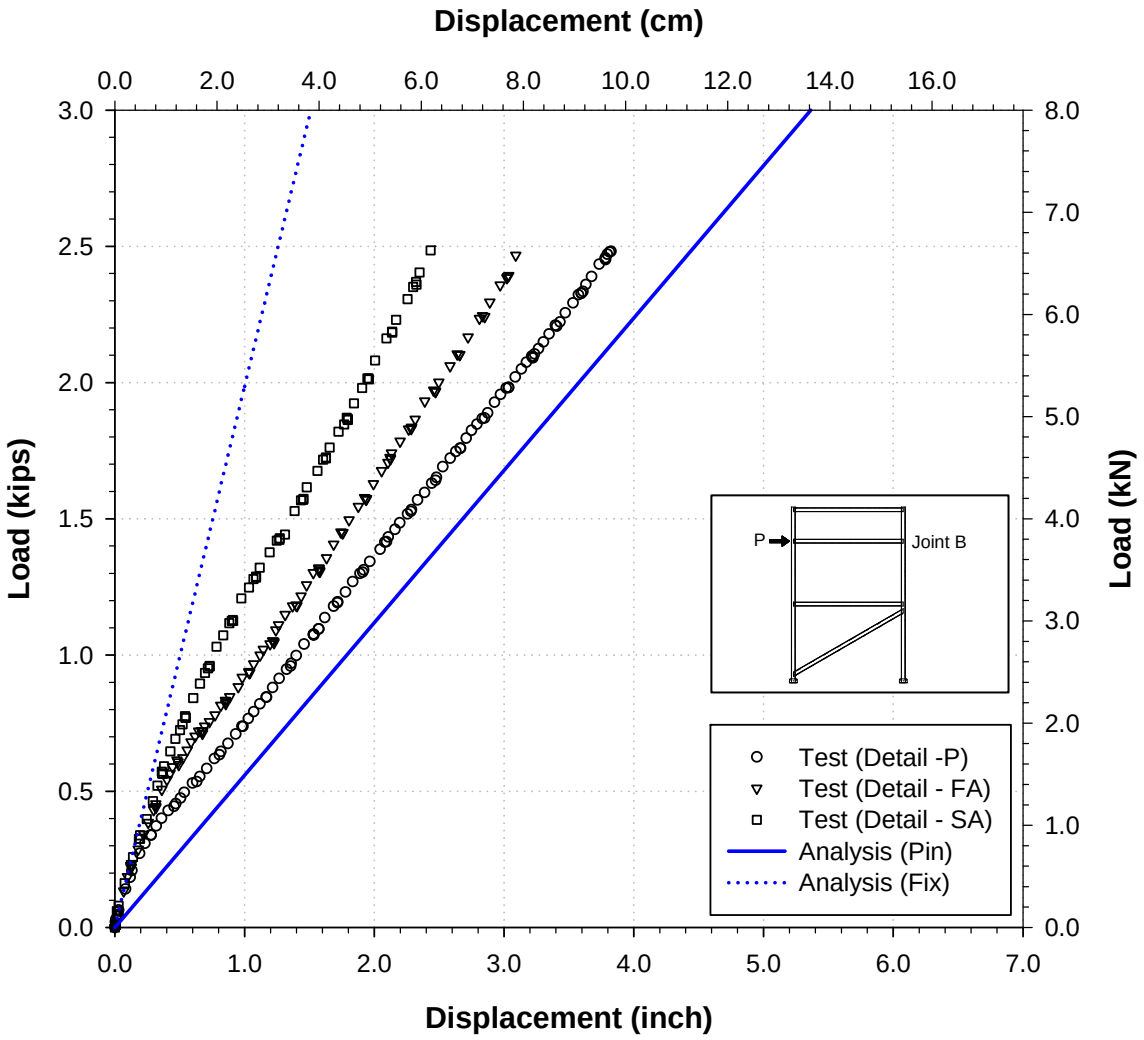

Figure 0.13: Load-displacement results of joint B for FRAME-1 with loading on 18 ft. level ('FR1-18' test series*)

* Table 2.9

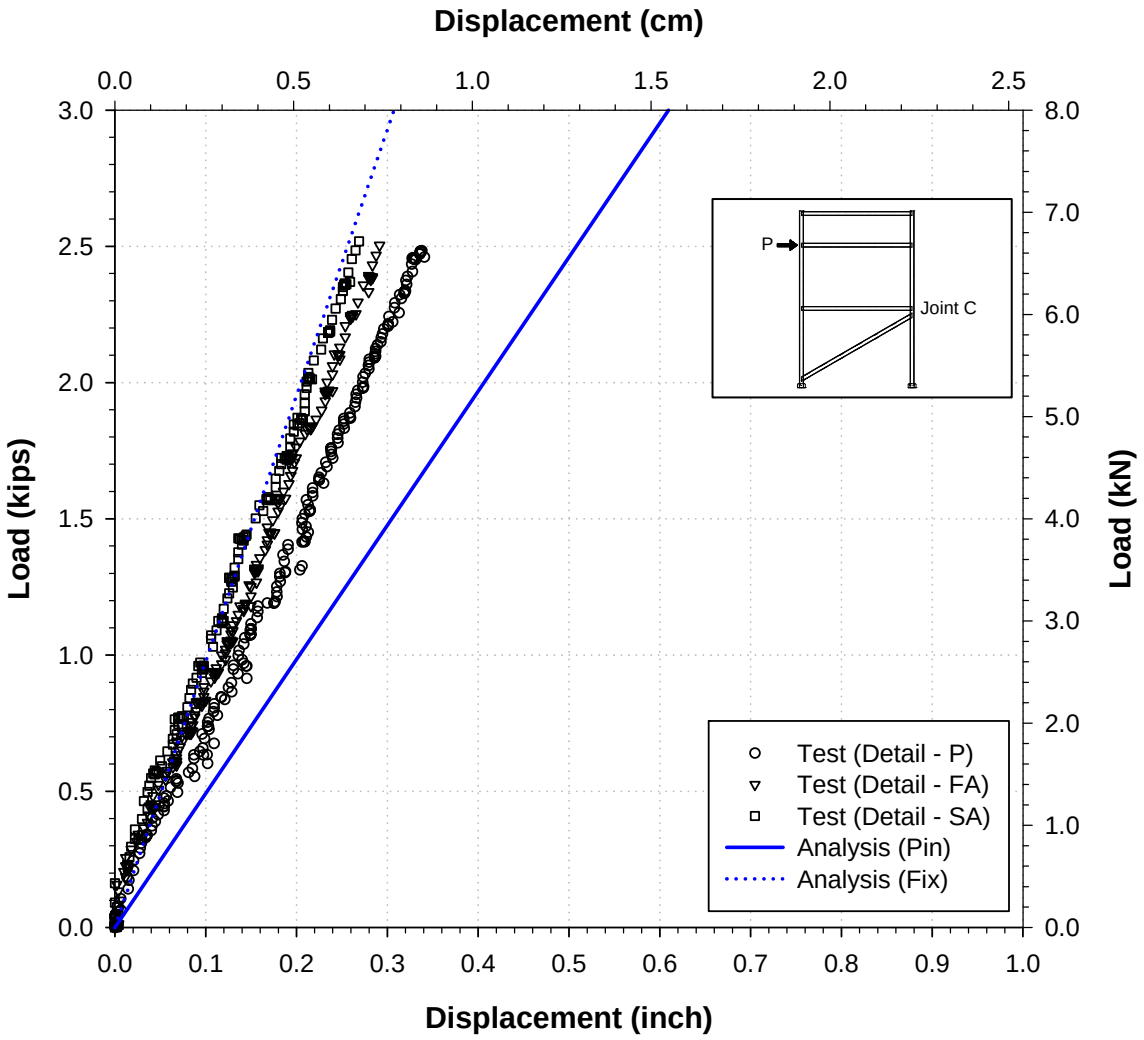

Figure 0.14: Load-displacement results of joint C for FRAME-1 with loading on 18 ft. level ('FR1-18' test series*)

* Table 2.9

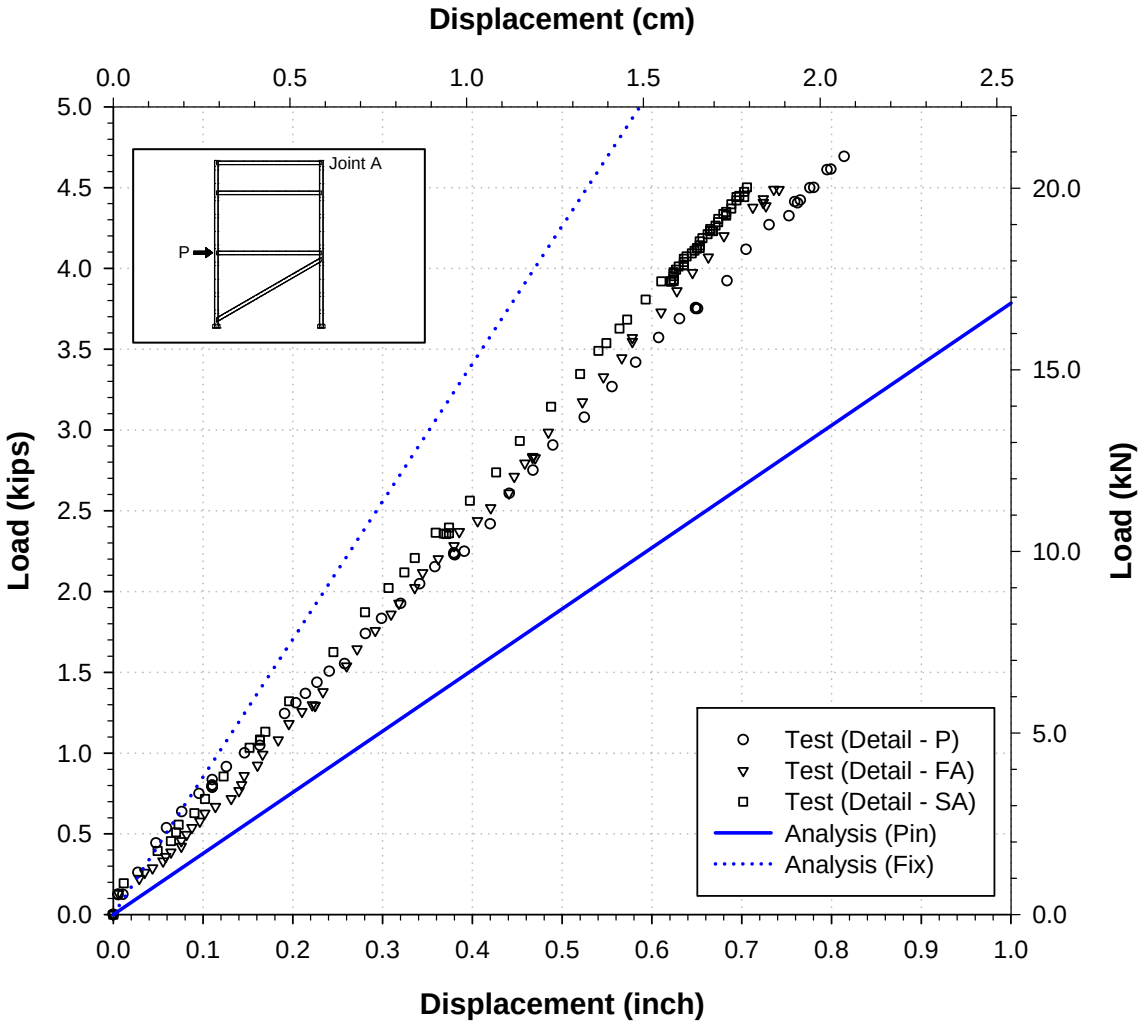

Figure 0.15: Load-displacement results of joint A for FRAME-1 with loading on 10 ft. level ('FR1-10' tests series*)

* Table 2.9

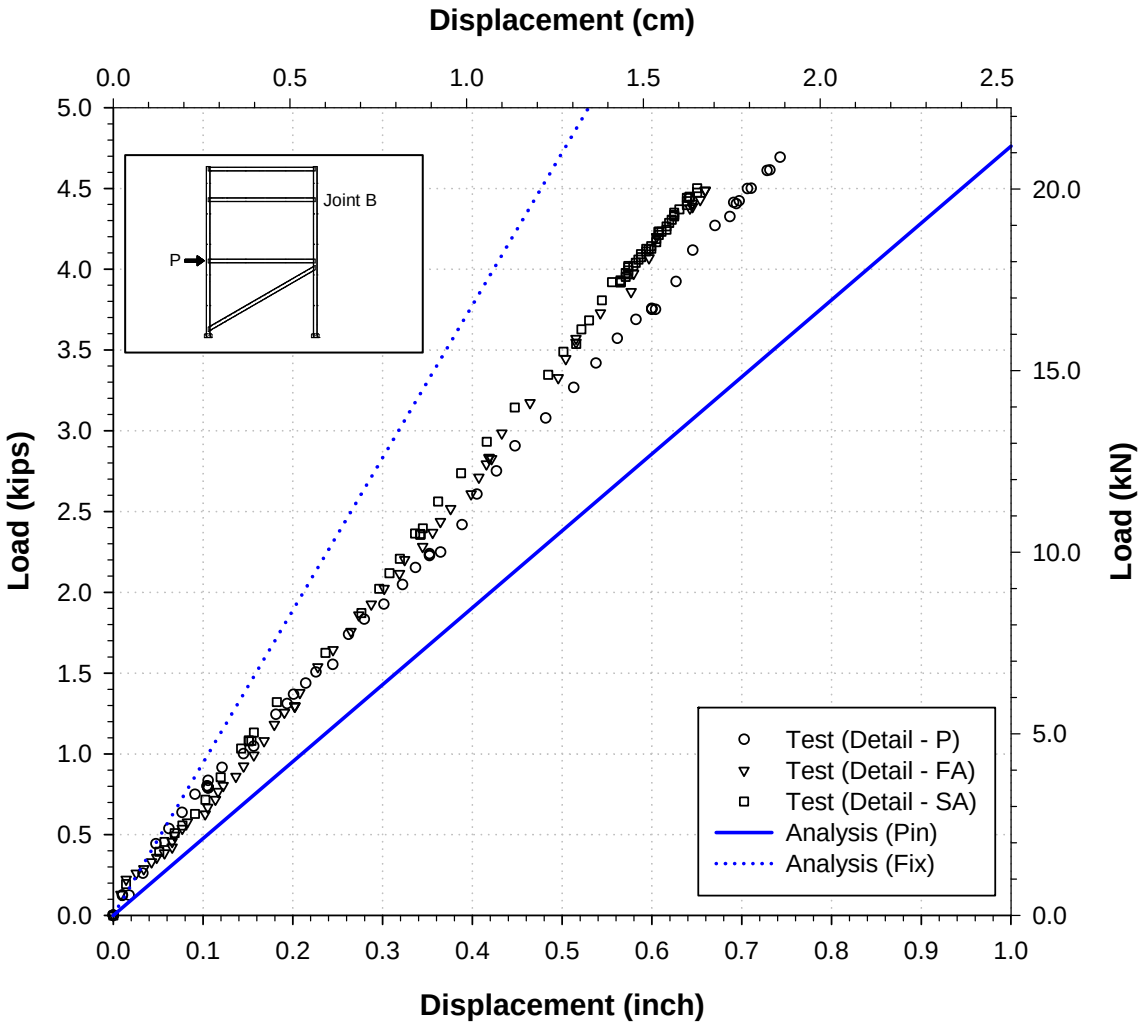

Figure 0.16: Load-displacement results of joint B for FRAME-1 with loading on 10 ft. level ('FR1-10' test series*)

* Table 2.9

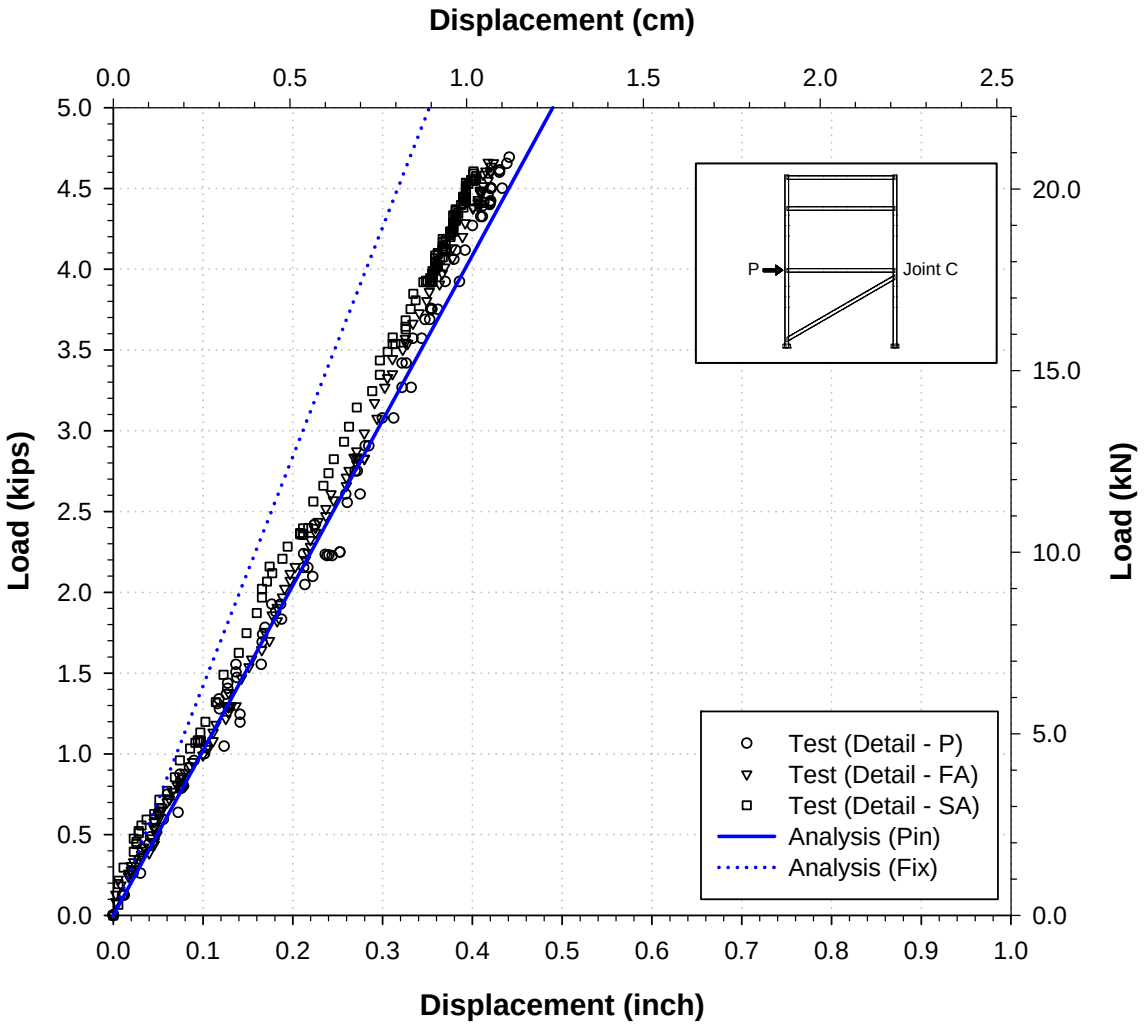

Figure 0.17: Load-displacement results of joint C for FRAME-1 with loading on 10 ft. level ('FR1-10' test series*)

* Table 2.9

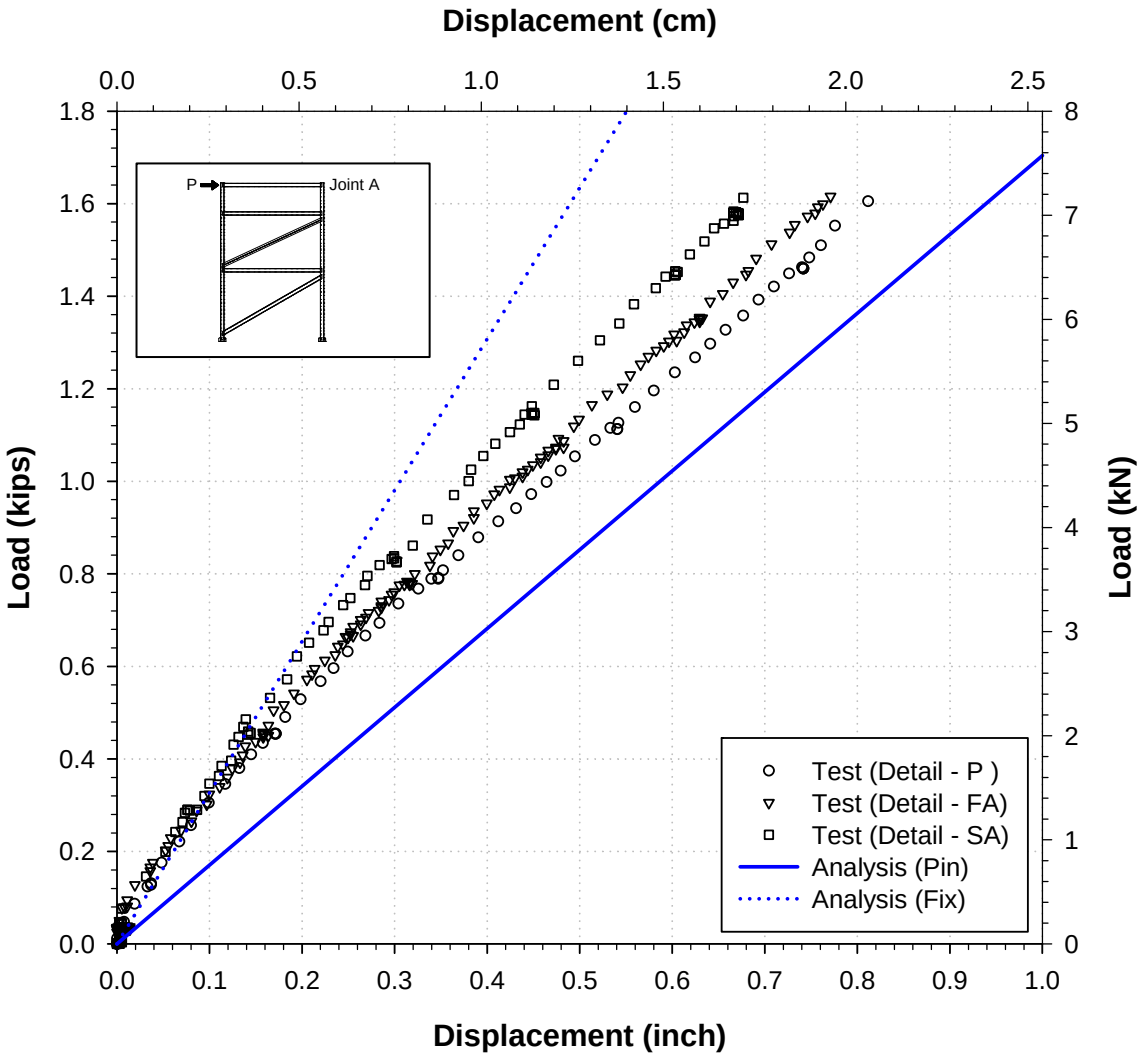

Figure 0.18: Load-displacement results of joint A for FRAME-2 with loading on 22 ft. level ('FR2-22' test series[*])

[*] Table 2.9

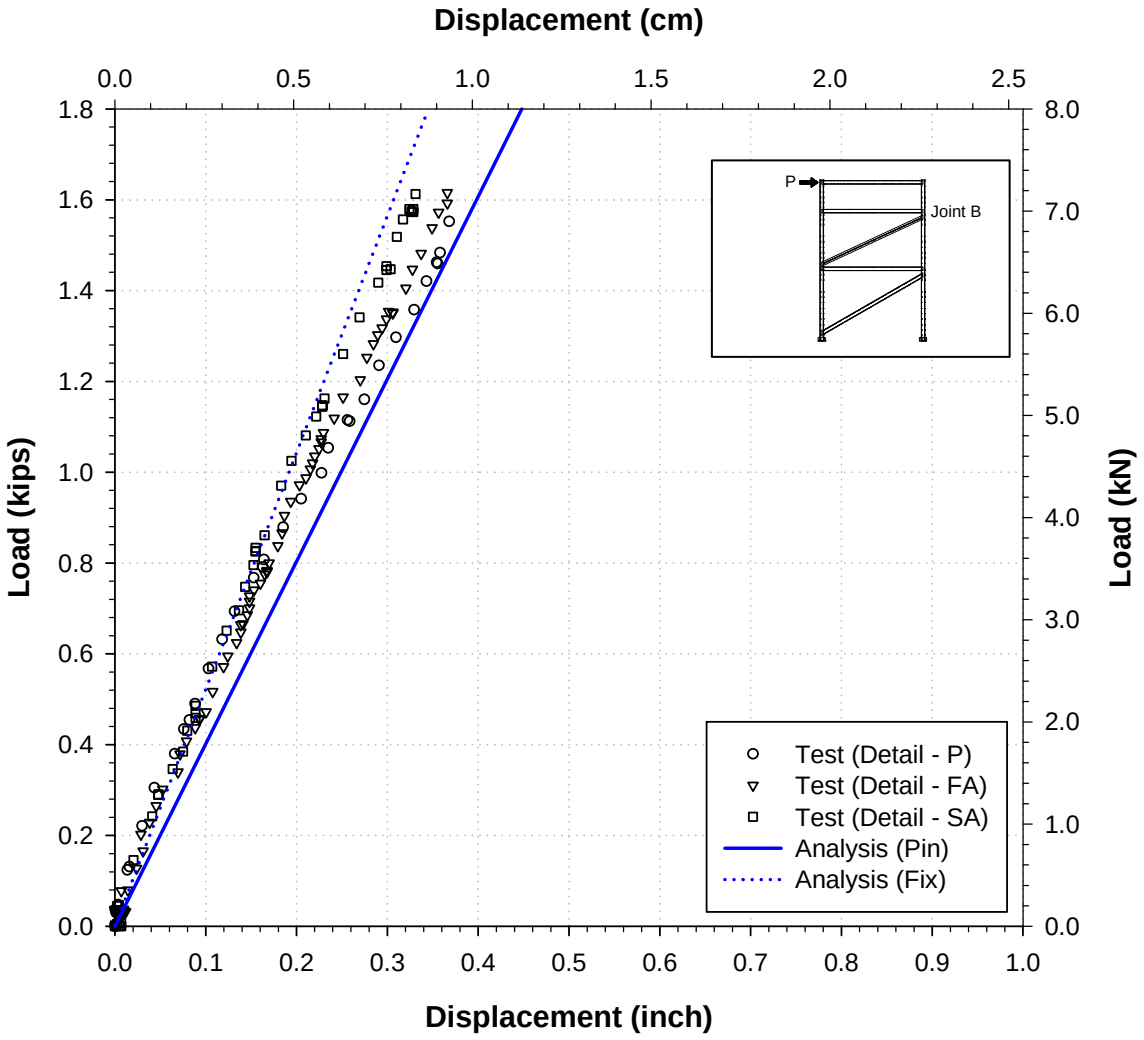

Figure 0.19: Load-displacement results of joint B for FRAME-2 with loading on 22 ft. level ('FR2-22' test series[*])

[*] Table 2.9

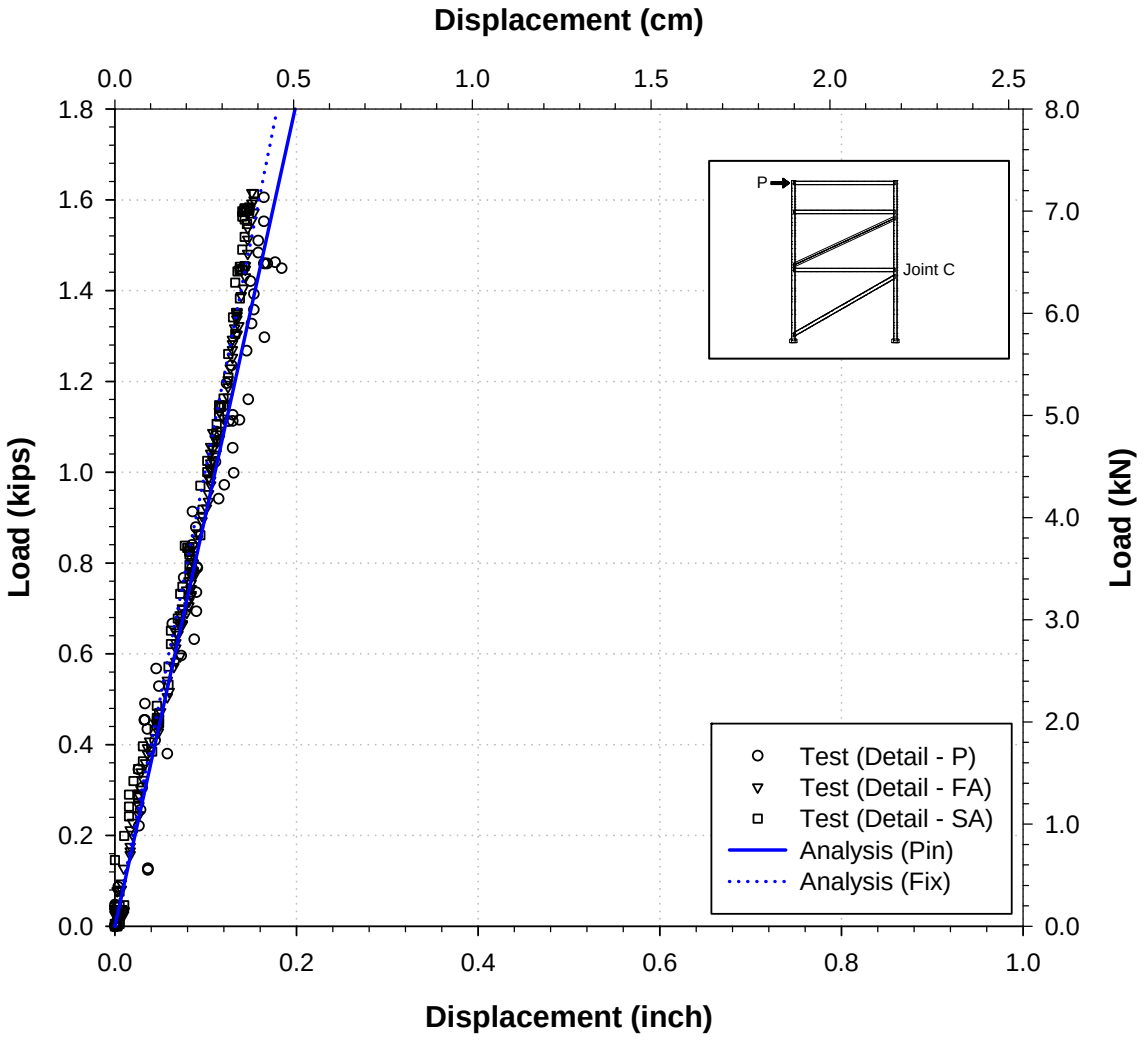

Figure 0.20: Load-displacement results of joint C for FRAME-2 with loading on 22 ft. level ('FR2-22' test series[*])

[*] Table 2.9

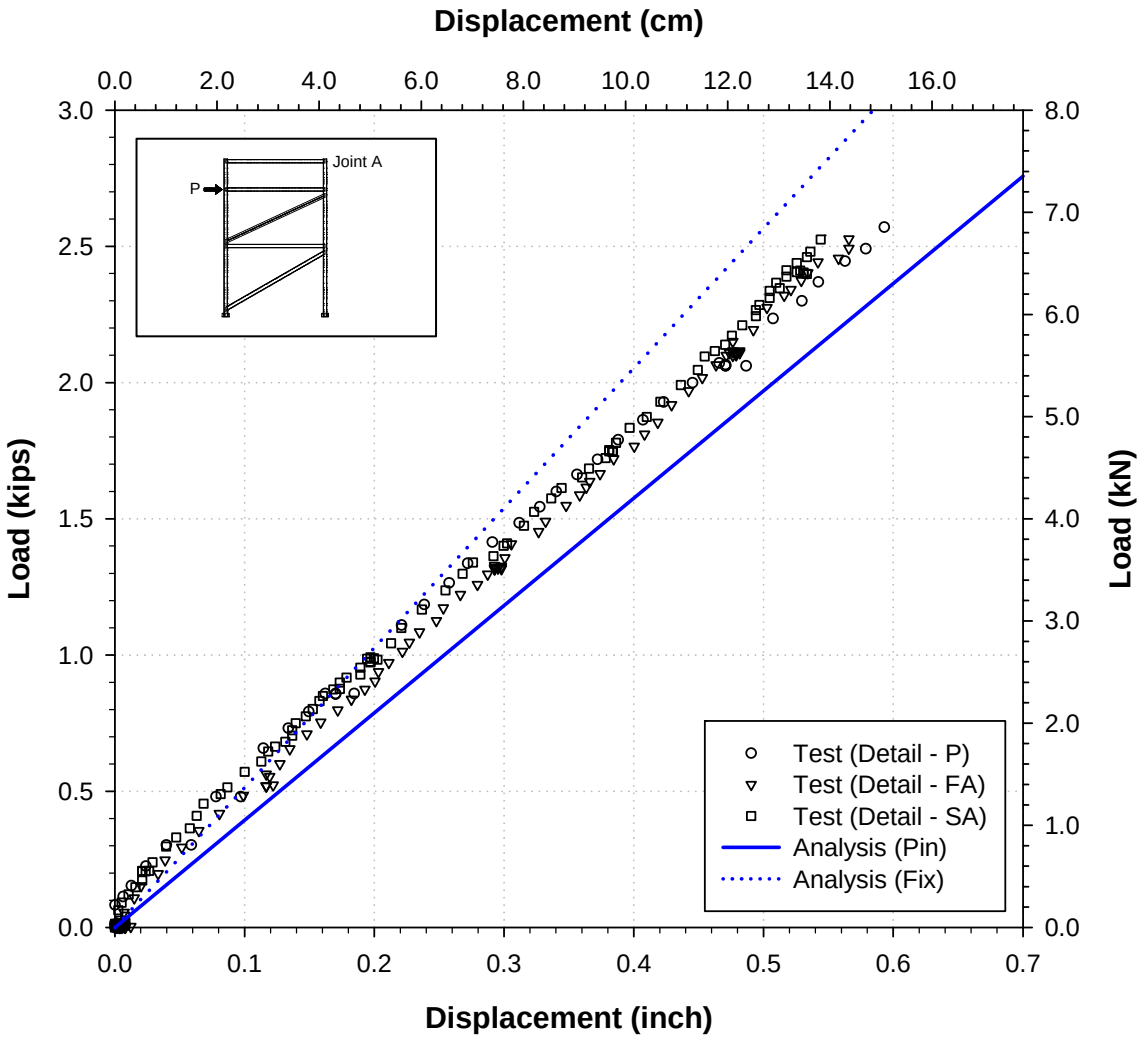

Figure 0.21: Load-displacement results of joint A for FRAME-2 with loading on 18 ft. level ('FR2-18' test series*)

* Table 2.9

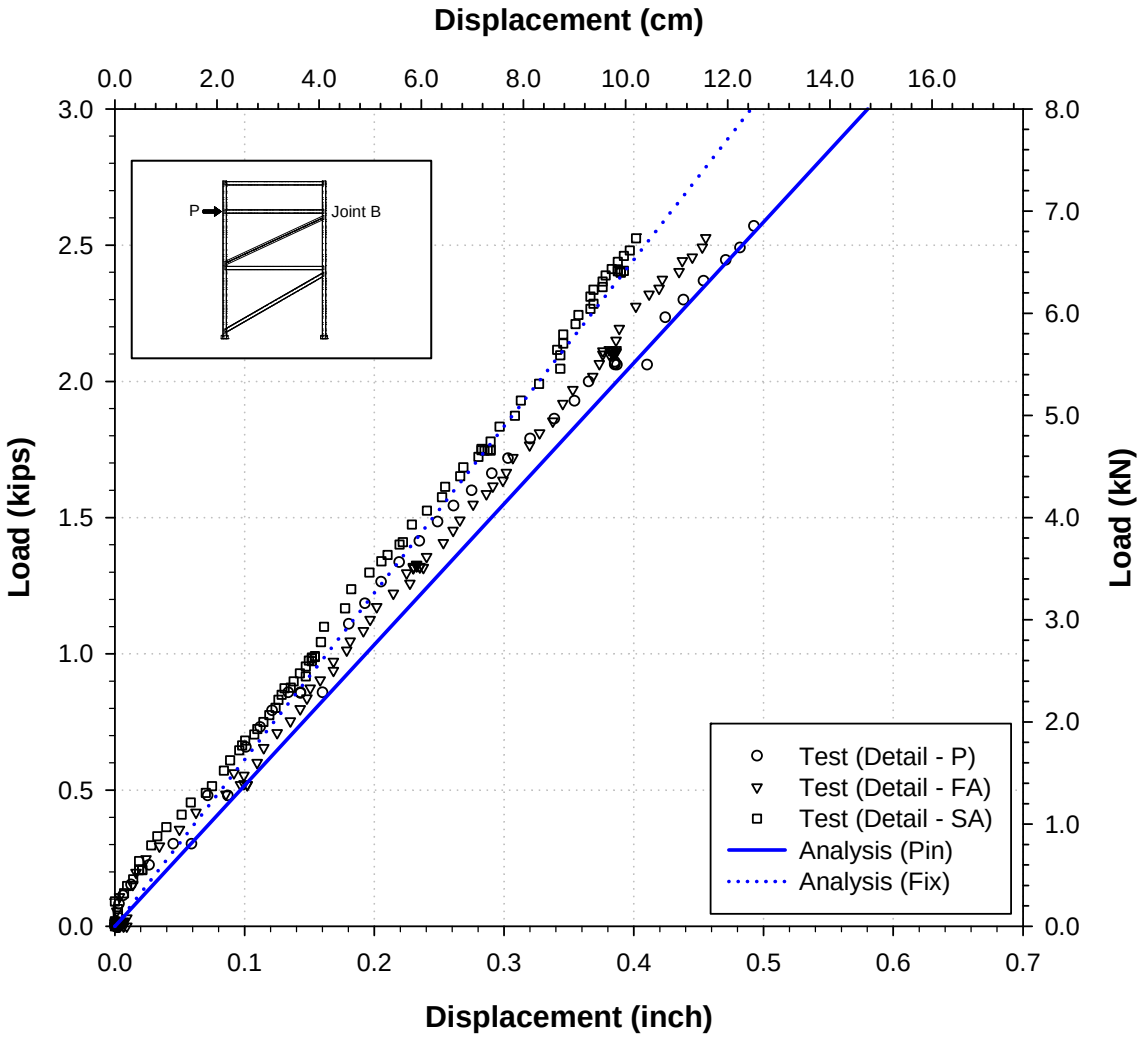

Figure 0.22: Load-displacement results of joint B for FRAME-2 with loading on 18 ft. level ('FR2-18' test series[*])

[*] Table 2.9

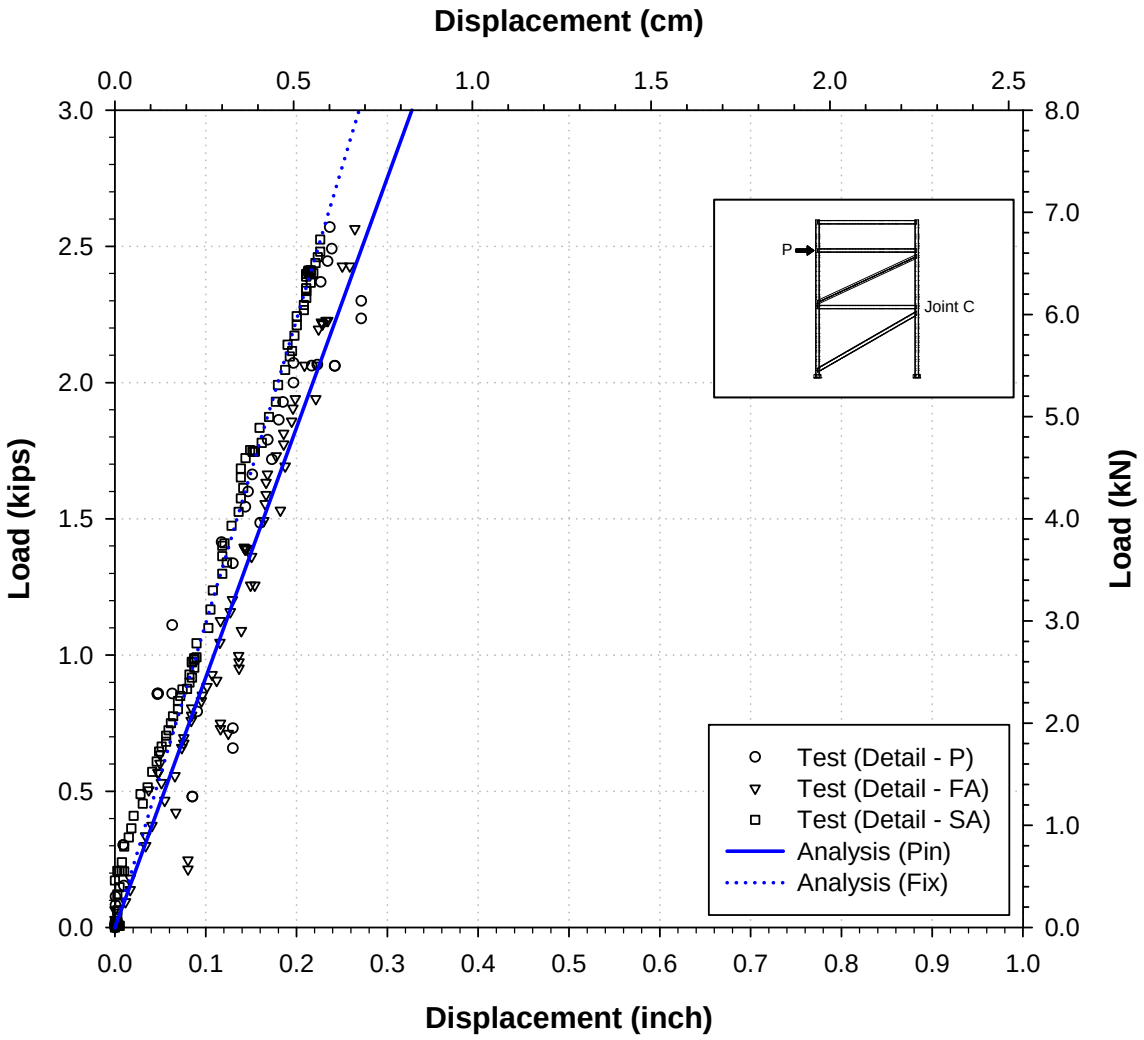

Figure 0.23: Load-displacement results of joint C for FRAME-2 with loading on 18 ft. level ('FR2-18' test series*)

* Table 2.9

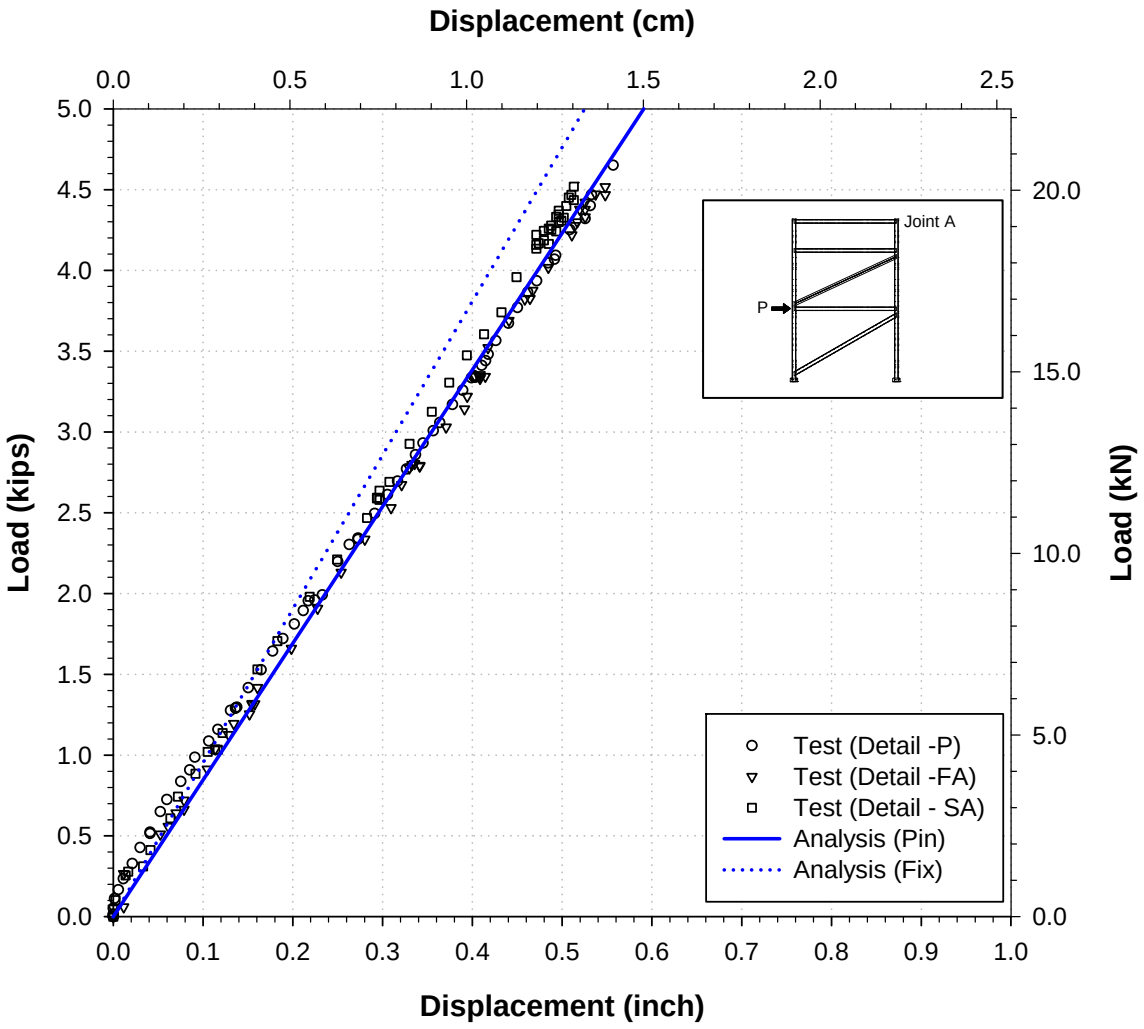

Figure 0.24: Load-displacement results of joint A for FRAME-2 with loading on 10 ft. level ('FR2-10' test series*)

* Table 2.9

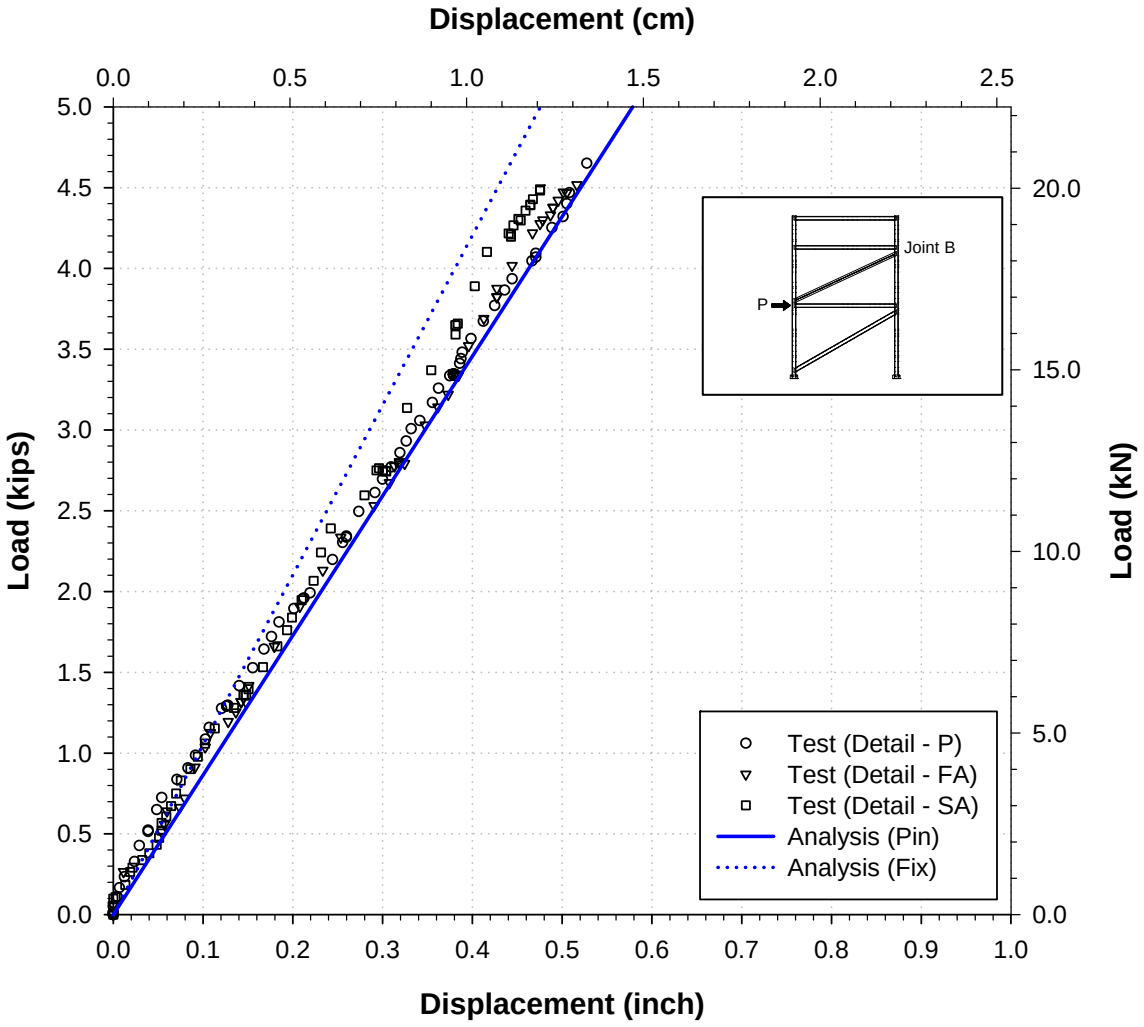

Figure 0.25: Load-displacement results of joint B for FRAME-2 with loading on 10 ft. level ('FR2-10' test series*)

* Table 2.9

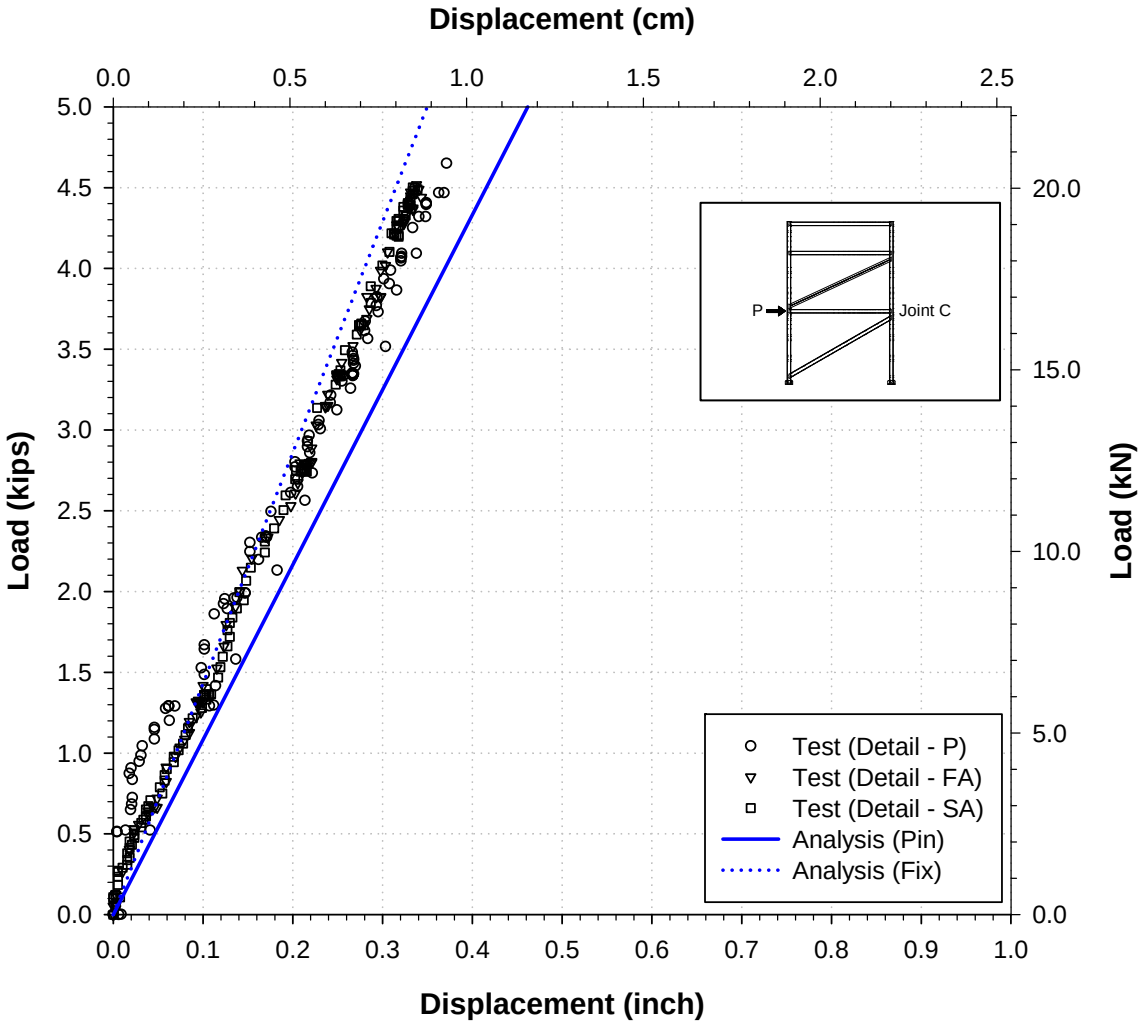

Figure 0.26: Load-displacement results of joint C for FRAME-2 with loading on 10 ft. level ('FR2-10' series tests[*])

[*] Table 2.9

Table 0.4: Joint displacements under horizontal unit loading

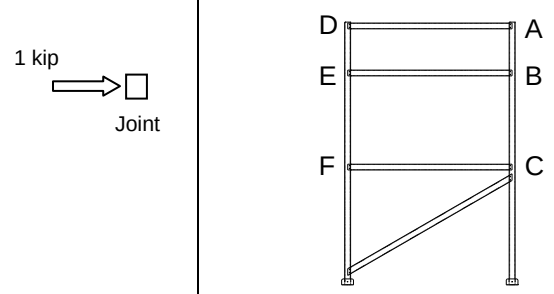

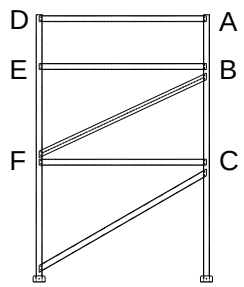

Loading Joint Applied to Joint	Boundary Condition	Horizontal Joint displacement under unit loading – Flexibility (inch/kips)											
		Joints						Joints					
		A	B	C	D	E	F	A	B	C	D	E	F
D	Analysis Pin	4.420	2.724	0.257	4.423	0.273	0.264	0.587	0.249	0.110	0.589	0.254	0.118
	TEST Type-P	3.570	2.314	0.241	-	-	-	0.511	0.244	0.104	-	-	-
	TEST Type-FA	2.954	1.875	0.207	-	1.924	0.204	0.454	0.241	0.098	-	0.254	0.110
	TEST Type-SA	2.087	1.361	0.184	-	1.408	0.184	0.404	0.214	0.086	-	0.224	0.098
	Analysis Fix	0.767	0.589	0.114	0.769	0.589	0.117	0.306	0.192	0.099	0.308	0.195	0.105
E	Analysis Pin	2.723	1.790	0.203	2.723	1.790	0.210	0.254	0.193	0.109	0.254	0.199	0.116
	TEST Type-P	2.281	1.575	0.191	-	-	-	0.239	0.191	0.102	-	-	-
	TEST Type-FA	1.922	1.322	0.175	1.952	-	0.171	0.225	0.181	0.093	0.227	-	0.101
	TEST Type-SA	1.429	1.025	0.162	1.453	-	0.163	0.217	0.174	0.089	0.219	-	0.097
	Analysis Fix	0.589	0.504	0.103	0.589	0.506	0.106	0.195	0.164	0.090	0.195	0.168	0.095
F	Analysis Pin	0.264	0.210	0.098	0.264	0.210	0.104	0.118	0.116	0.092	0.118	0.116	0.098
	TEST Type-P	0.172	0.156	0.091	-	-	-	0.121	0.115	0.085	-	-	-
	TEST Type-FA	0.164	0.147	0.092	0.166	0.148	-	0.116	0.109	0.080	0.118	0.109	-
	TEST Type-SA	0.156	0.143	0.088	0.155	0.142	-	0.110	0.104	0.076	0.112	0.104	-
	Analysis Fix	0.117	0.106	0.070	0.117	0.106	0.076	0.105	0.095	0.070	0.105	0.095	0.075

DISCUSSION OF TEST RESULTS

2.12 Structural Parameters Affecting Load-Displacement Response of FRP Composite Frames

Various structural parameters such as mechanical material properties of members, different beam-column connection types, and the number of diagonal members affect the joint load-displacement response of FRP composite frame systems. The effects of these parameters are discussed in this Section based on the experimental results and analysis results. The discussed parameters affecting the load-displacement response of the FRP composite frames studied herein are as follows:

- Effective mechanical material properties of components of a cross-section.
- Beam-column connection types.
- Diagonal members.

First, the relationship of effective mechanical material properties of components of a cross-section and the horizontal joint displacement of a frame were previously presented in Section 2.11.2 using a sensitivity analysis. The sensitivity analysis results showed that the longitudinal modulus E_L and in-plane shear modulus G_{LT} of the components of the member's cross-section has the dominant effect on the horizontal joint displacement results for the FRP composite frames.

Second, the effect of beam-column connection types on the horizontal joint displacements of the frames is compared. The horizontal joint displacement results of

frames having three different beam-column connection types (Figure 2.10) were observed to be between the horizontal joint displacements results of frame analysis based on ideal 'pinned' and 'fixed' beam-column boundary conditions.

The rotation stiffness characteristics of the beam-column connections were used to model different beam-column connection types, and these were modeled in GTSTRUDL using rotation member end springs. The rotation member end springs were located at each end of beam member, but not at the ends of the column and diagonal members. Figure 0.1 shows the variation of the horizontal joint displacement of Joint 'A' under a horizontal unit loading of 1.0 kip applied to the joint D as a function of beam-column rotational stiffnesses. The solid line in Figure 0.1 represents the analytically calculated results in terms of rotational stiffness values of the beam-column connections. The upper dot line and bottom dot lines are representing the analytically calculated joint displacement of frame having a ideal 'pinned' and 'fixed' beam-column boundary conditions, respectively. The experimentally measured displacements of Joint 'A' of the frames having three different beam/connection connection types (i.e., Detail-P, Detail-FA, and Detail-SA) are presented by three circles. By using this graph, the rotation stiffness values of the beam-column connection types could be estimated without performing actual beam-column connection tests. The rotation stiffness of connection with 'Type-P', 'Type-FA', and 'Type-SA' were estimated as 215 in-k/radian, 480 in-k/radian, and 1,380 in-k/radian respectively for the FRP composite frames tested. Among the several test cases, the 'FR1-22' series cases were used for this rotational stiffness estimation.

The estimated beam-column rotation stiffness can improve accuracy of the frame models. Table 0.1 shows the comparison of joint displacement result of tests and joint

displacement of frame accounting for the estimated beam-column rotational stiffness in Figure 0.1. For the cases that load was applied at joint D or E, the analytically calculated analysis result are close to the experimentally measured joint displacement with less than 5.3% difference. But, when the load was applied to joint F, the error was about 37%.

Table 0.2 presents the variation of horizontal joint displacements of joint A in terms of connection types. The displacement ratio of each cases are shown also using a Type-P (no angle case) as a reference case. As expeted, the results demonstrate that the Type-SA (steel angle) provides the stiffest connection properties.

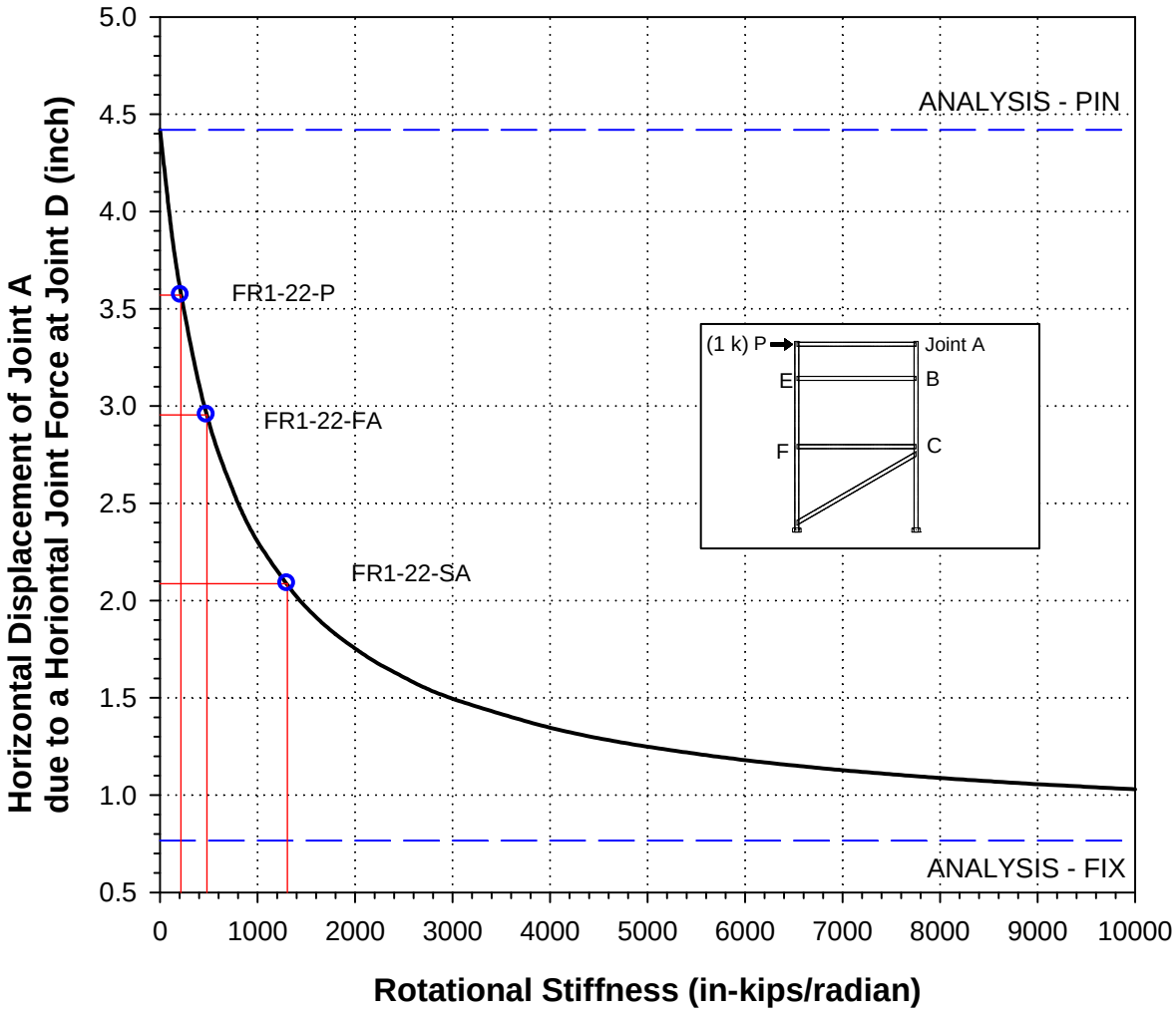

Figure 0.1: Variation of the horizontal displacement of joint A of FR1-22 case in terms of beam-column rotational stiffnesses

Table 0.1: Joint displacements comparison using frame with beam-column stiffness for FRAME-1

Loading Joint	Connection Type		Displacement (inch)					
			A	B	C	D	E	F
D (P=1.6k)	Type-P	Test	5.712	3.703	0.385	-	-	-
		Analysis	5.712	3.583	0.367	5.717	3.582	0.378
		Diff.(%)	0.021	-3.249	-4.805	-	-	-
	Type-FA	Test	4.727	3.000	0.331	-	3.079	0.326
		Analysis	4.724	3.016	0.333	4.728	3.015	0.343
		Diff.(%)	-0.057	0.537	0.604	-	-2.075	5.307
	Type-SA	Test	3.339	2.178	0.294	-	2.252	0.295
		Analysis	3.378	2.254	0.299	3.378	2.254	0.299
		Diff.(%)	1.174	3.476	1.803			
E (P=2.4k)	Type-P	Test	5.474	3.780	0.459	-	-	-
		Analysis	5.372	3.621	0.447	5.372	3.625	0.461
		Diff.(%)	-1.863	-4.198	-2.549	-	-	-
	Type-FA	Test	4.613	3.173	0.420	4.684	-	0.410
		Analysis	4.522	3.129	0.416	4.523	3.133	0.429
		Diff.(%)	-1.966	-1.399	-0.976	-3.444	-	4.610
	Type-SA	Test	3.429	2.459	0.388	3.486	-	0.391
		Analysis	3.379	2.473	0.387	3.379	2.473	0.387
		Diff.(%)	-1.467	0.586	-0.180	-3.078	-	-0.946
F (P=4.5k)	Type-P	Test	0.772	0.701	0.409	-	-	-
		Analysis	1.061	0.867	0.430	1.062	0.865	0.456
		Diff.(%)	37.461	23.666	5.159			
	Type-FA	Test	0.738	0.662	0.416	0.746	0.665	-
		Analysis	0.965	0.806	0.420	0.966	0.804	0.446
		Diff.(%)	30.759	21.767	1.034	29.424	20.932	-
	Type-SA	Test	0.701	0.644	0.394	0.699	0.640	-
		Analysis	0.866	0.751	0.425	0.866	0.751	0.425
		Diff.(%)	23.509	16.537	7.843	23.863	17.266	-

Note:

Type-P: K = 215 in-k/radian

Type-FA: K = 480 in-k/radian

Type-SA: K = 1,380 in-k/radian

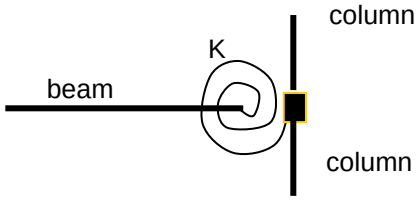

Table 0.2: Joint displacements comparison for frames having different beam-column connection types

Type-P (No Angle)	Type-FA (FRP Angle)	Type-SA (Steel Angle)
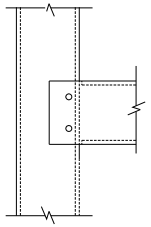	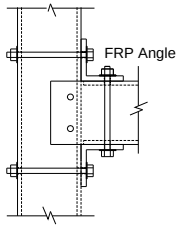	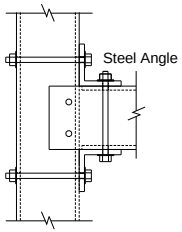

Loading Joints	Frame Type	Joint displacement under unit loading – Flexibility (inch/kips)									Displacement Ratio (%)					
		d_P			d_{FA}			d_{SA}			d_{FA}/d_P			d_{SA}/d_P		
		A	B	C	A	B	C	A	B	C	A	B	C	A	B	C
D	FRAME-1	3.570	2.314	0.241	2.954	1.875	0.207	2.087	1.361	0.184	82.8	81.0	86.0	58.5	58.8	76.4
	FRAME-2	0.511	0.244	0.104	0.454	0.241	0.098	0.404	0.214	0.086	88.9	99.0	93.4	79.1	87.7	82.6
E	FRAME-1	2.281	1.575	0.191	1.922	1.322	0.175	1.429	1.025	0.162	84.3	83.9	91.5	62.6	65.1	84.5
	FRAME-2	0.239	0.191	0.102	0.225	0.181	0.093	0.217	0.174	0.089	94.2	94.8	91.4	90.8	91.3	87.7
F	FRAME-1	0.172	0.156	0.091	0.164	0.147	0.092	0.156	0.143	0.088	95.6	94.4	101.7	90.8	91.9	96.3
	FRAME-2	0.121	0.115	0.085	0.116	0.109	0.080	0.110	0.104	0.076	96.0	94.6	94.0	91.0	90.0	89.3

Third, two frame systems having one diagonal member and two diagonal members are compared under the same loading conditions. Table 0.3 presents the joint displacements of FRAME-1 and FRAME-2 and ratios of joint displacement under the same horizontal unit loading conditions. As expected, it was observed that the joint displacements are significantly minimized by adding diagonal members to the FRP composite frame. The joint displacements at the top of the FRAME-2 having two diagonal members are from 14.3% to 19.3% of the joint displacement at the top FRAME-1 having only one diagonal member.

Table 0.3: Joint displacement comparisons for frames having different numbers of diagonal members

	FRAME-1	FRAME-2
	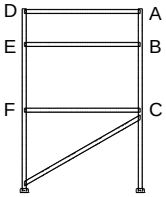	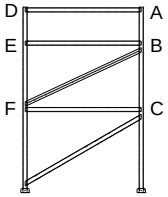

Loading Joints	Types	Joint displacement under unit loading – Flexibility (inch/kips)						Displacement Ratio (%)		
		d_{FR1}			d_{FR2}			d_{FR2} / d_{FR1} (%)		
		A	B	C	A	B	C	A	B	C
D	TEST Type-P	3.570	2.314	0.241	0.511	0.244	0.104	14.3	10.5	43.4
	TEST Type-FA	2.954	1.875	0.207	0.454	0.241	0.098	15.4	12.9	47.1
	TEST Type-SA	2.087	1.361	0.184	0.404	0.214	0.086	19.3	15.7	46.9
E	TEST Type-P	2.281	1.575	0.191	0.239	0.191	0.102	10.5	12.1	53.2
	TEST Type-FA	1.922	1.322	0.175	0.225	0.181	0.093	11.7	13.7	53.1
	TEST Type-SA	1.429	1.025	0.162	0.217	0.174	0.089	15.2	17.0	55.2
F	TEST Type-P	0.172	0.156	0.091	0.121	0.115	0.085	70.6	73.9	93.6
	TEST Type-FA	0.164	0.147	0.092	0.116	0.109	0.080	70.9	74.0	86.5
	TEST Type-SA	0.156	0.143	0.088	0.110	0.104	0.076	70.8	72.4	86.8

2.13 Load-Displacement Prediction Using Isotropic Material Assumption

Instead of using the FRPFA approach that can fully account for the anisotropic nature of FRP composite structural member, the classical analysis method for isotropic structural members was performed and is reported in this section. For the material properties for the analysis, the following assumptions were used.

a. The longitudinal modulus E_L was assumed as a Young's modulus for the components (e.g., web and flange) of the cross-section.

b. The in-plane modulus G_{LT} was assumed as a shear modulus for the components (e.g., web and flange) of the cross-section.

c. If the material properties of the components (e.g., web and flange) are different, the average values were used for the whole cross-section.

The assumed isotropic material properties used for the stiffness analysis are presented in Table 0.4.

This classical analysis using the assumption with isotropic materials was performed performed for FRAME-1 model (

Figure 0.3). The analysis results are presented along with the displacement results of FRPFA approach and the experimental results (Table 0.5). Table 0.6 shows the differences of the analytically predicted horizontal displacements of joints A, B, and C for both analytical models using a FRPFA approach and an equivalent isotropic material approach. The joint displacement results of an analytical model having pin beam-column connections are compared to the experimental results of a frame having Type-P (No angle) connection type. The Table 0.6 shows that a model based an FRPFA approach has

smaller error of horizontal joint displacement than the equivalent isotropic material approach in all cases.

It should be noted that the errors in the Table 4.6 are inceased by the nonlinear behavior of the frames in both cases (isotropic assumption and FRPFA). The main causes of the nonlinearity are thought to be (1) nonlinear in-plane shear modulus of the structural members (2) nonlinear beam-column connection stiffness.

Table 0.4: Assumed isotropic material properties for analysis

Member	***E*** (ksi)	***G*** (ksi)	Ref.
Column*	5,244	541	Table 2.4
Beams and Brace BR1**	4,756	681	Table 2.5 and Table 2.6
Brace BR2***	4,756	681	Table 2.7 and Table 2.8

Note:

* From GROUP-1 (see Section 2.5.4)
** From GROUP-2 and GROUP-3 (see Section 2.5.4)
** From GROUP-4 and GROUP-5 (see Section 2.5.4)

Table 0.5: Joint displacements results based on isotropic material assumption under unit loading (FRAME-1)

Loading Joint		Boundary condition	Joint					
			A	B	C	D	E	F
D	Analysis (Isotropic Assumption)	Pin	4.806	2.918	0.262	4.809	2.920	0.263
		Fix	0.834	0.631	0.116	0.834	0.631	0.120
	Analysis (FRPFA)	Pin	4.420	2.724	0.257	4.423	0.273	0.264
		Fix	0.767	0.589	0.114	0.769	0.589	0.117
	Experiments	Type-P	3.570	2.314	0.241	-	-	-
		Type-FA	2.954	1.875	0.207	-	1.924	0.204
		Type-SA	2.087	1.361	0.184	-	1.408	0.184
E	Analysis (Isotropic Assumption)	Pin	2.914	1.893	0.205	2.914	1.893	0.214
		Fix	0.631	0.533	0.104	0.631	0.535	0.108
	Analysis (FRPFA)	Pin	2.723	1.790	0.203	2.723	1.790	0.210
		Fix	0.589	0.504	0.103	0.589	0.506	0.106
	Experiments	Type-P	2.281	1.575	0.191	-	-	-
		Type-FA	1.922	1.322	0.175	1.952	-	0.171
		Type-SA	1.429	1.025	0.162	1.453	-	0.163
F	Analysis (Isotropic Assumption)	Pin	0.269	0.214	0.099	0.269	0.214	0.099
		Fix	0.120	0.108	0.070	0.120	0.108	0.076
	Analysis (FRPFA)	Pin	0.264	0.210	0.098	0.264	0.210	0.104
		Fix	0.117	0.106	0.070	0.117	0.106	0.076
	Experiments	Type-P	0.172	0.156	0.091	-	-	-
		Type-FA	0.164	0.147	0.092	0.166	0.148	-
		Type-SA	0.156	0.143	0.088	0.155	0.142	-

Table 0.6: Joint displacements relative errors with experimental results for analytical pin connection case (FRAME-1)

Loading Joint	Analysis Type	Joint		
		A	B	C
D	Isotropic Assumption	35 %	26 %	9 %
	FRPFA	24 %	18 %	7 %
E	Isotropic Assumption	28 %	20 %	7 %
	FRPFA	19 %	14 %	6 %
F	Isotropic Assumption	56 %	37 %	9 %
	FRPFA	53 %	35 %	8 %

Note:

The values in the table is determined as follows

Value = $(d_{ana} - d_{exp}) / d_{exp} \times 100$

d_{exp} = experimentally measured joint displacement

d_{ana} = analytically estimated horizontal joint displacement

2.14 Load-Displacement Prediction for Serviceability Design Consideration

In a typical civil frame structure design process, the frame structure is designed based on two factors: strength and stiffness. Member stiffnesses affect the stability and displacement of the structure. This thesis has focused on the load-displacement response of the FRP composite frame structure. A severe displacement can cause serviceability problem of the frame structure. This issue raised the need of limiting maximum interstory drift in many building design codes (e.g., ASCE7-05).

ASCE7-05, *Minimum Design Loads for Building and Other Structures* (ASCE, 2005) recommended the maximum story drift and a load combination for checking short-term effect for lateral loading. The ASCE7-05 cites common interstory drift limits of L/600 to L/400 and the commentary also notes that absolute interstory drift limit of 3/8 in (10mm) may often be appropriate to prevent damage to nonstructural elements in the structure. The commentary also provides the load combination with an annual probability of 5^{th} percentile of being exceeded for checking short-term effects as follows:

$$D + 0.5L + 0.7W \quad \textbf{(3.16)}$$

The characteristic value of mechanical material properties (Section 2.5.4) can provide statistically consistent way in analytically predicting the load-displacement prediction for design purpose. The characteristic value is defined as statistical property representing 80% lower confidence bound on 5^{th} percentile value of a specified population (ASTM, 2006). By using the characteristic values of mechanical material properties for the stiffness analysis of the FRP composite frame, the calculated corresponding horizontal joint displacements can be interpreted as a horizontal joint

displacement with 80% lower confidence bound on 5^{th} percentile displacements. This analytically calculated displacement results from the frame stiffness analysis and accounts for uncertainties associated with the mechanical materials properties obtained from the limited material test results.

The horizontal joint displacements presented in Section 2.8 are calculated from the analytical model that used the mean values. Table 0.4 presents the summary of the joint displacement results under unit loading.

Table 0.7 presents the horizontal joint displacement results for the analytical model with characteristic values with test results. The displacement results for the analytical model with characteristic values shows larger values than the joint displacements for model with the mean values.

Table 0.7: Joint displacements results based on characteristic value

		FRAME-1 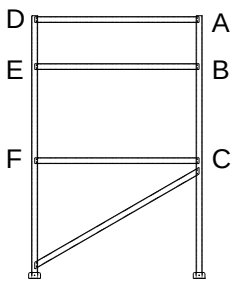						FRAME-2 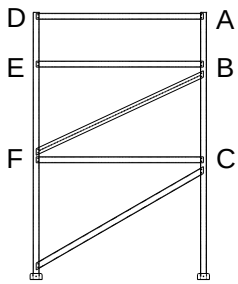					
Loading Joint	Boundary Condition	Joint displacement under unit loading – Flexibility (inch/kips)											
		Joints						Joints					
		A	B	C	D	E	F	A	B	C	D	E	F
D	Analysis Pin	4.917	3.025	0.278	4.920	3.024	0.287	0.648	0.271	0.116	0.650	0.277	0.126
	TEST Type-P	3.570	2.314	0.241	-	-	-	0.511	0.244	0.104	-	-	-
	TEST Type-FA	2.954	1.875	0.207	-	1.924	0.204	0.454	0.241	0.098	-	0.254	0.110
	TEST Type-SA	2.087	1.361	0.184	-	1.408	0.184	0.404	0.214	0.086	-	0.224	0.098
	Analysis Fix	0.856	0.655	0.122	0.859	0.655	0.126	0.334	0.207	0.105	0.336	0.210	0.112
E	Analysis Pin	3.024	1.981	0.220	3.024	1.983	0.228	0.277	0.210	0.116	0.277	0.216	0.124
	TEST Type-P	2.281	1.575	0.191	-	-	-	0.239	0.191	0.102	-	-	-
	TEST Type-FA	1.922	1.322	0.175	1.952	-	0.171	0.225	0.181	0.093	0.227	-	0.101
	TEST Type-SA	1.429	1.025	0.162	1.453	-	0.163	0.217	0.174	0.089	0.219	-	0.097
	Analysis Fix	0.655	0.558	0.110	0.655	0.561	0.114	0.210	0.176	0.095	0.210	0.182	0.102
F	Analysis Pin	0.287	0.228	0.106	0.287	0.228	0.113	0.126	0.124	0.099	0.126	0.124	0.106
	TEST Type-P	0.172	0.156	0.091	-	-	-	0.121	0.115	0.085	-	-	-
	TEST Type-FA	0.164	0.147	0.092	0.166	0.148	-	0.116	0.109	0.080	0.118	0.109	-
	TEST Type-SA	0.156	0.143	0.088	0.155	0.142	-	0.110	0.104	0.076	0.112	0.104	-
	Analysis Fix	0.126	0.114	0.076	0.126	0.114	0.082	0.112	0.102	0.075	0.112	0.102	0.082

CONCLUSIONS AND RECOMMENDATIONS

The static load-displacement response of a braced plane frame structure composed of fiber reinforced polymeric (FRP) composite material structural members is measured and studied. Effective computational procedures for the stiffness analysis of frame structures that can account for the anisotropic nature of FRP structural member are proposed to analytically predict the horizontal joint displacement behaviors of such frame systems.

The load-displacement results of frame analysis based on the proposed computational procedures are compared to the load-displacement results of the full-scale frames tests for the joint load-displacement results.

The effects of various structural parameters on the joint displacement of the FRP composite frame are examined. The results can be summarized as follows:

a. The longitudinal modulus is the most influential material property on the joint load-displacement of the frame composed of FRP composite members for the tested braced FRP frames.

b. The rotational stiffness of three beam-column connection types are analytically estimated based on the FRPFA procedures. The rotational stiffnesses of “Type-P”, “Type-FA”, and “Type-SA” are estimated as 215 in-k/radian, 480 in-k/radian, and 1,380 in-k/radian, respectively. Connection type “Type-P” has lrelatively low stiffness value and showed behavior close to that of pin connection condition.

Horizontal joint displacements predictions from two analytical models based on the FRPFA and the equivalent isotropic material approach are compared to the experimentally measured results, respectively. The horizontal displacements based on FRPFA approach showed less difference to experimentally measured results then than the results of the equivalent isotropic material approach.

Also, the characteristic value of mechanical material properties were used to estimate the displacement which is considering uncertainties associated with FRP composite material itself and limited samples for the material testing. The estimated displacement can be used for serviceability based building design code.

Finally, the FRPFA approach was implemented as a software application, which can be used for conventional stiffness analysis program such as GRSTRUDL.

Recommendations for Future work:

a. In this thesis, the experimentally obtained mechanical material properties of a component of cross-section are used for a frame analysis to get joint displacements analytically. Although, this method showed good agreement with the frame test results, the analytical method to get the mechanical material properties of the components of a cross section (i.e., web and flange) are suggested for future work.

b. The layers are suggested to be modeled for a cross-section mesh generation stage in order to reflect the different mechanical properties of each single layer instead of using lamination theory.

c. This research is based on 2D plane frame case. 3D frame analysis study is recommended as future study to examine three-dimensional behavior of a frame of fiber reinforced polymeric (FRP) composite material structural members.

d. Frames having other types of section profiles should be tested and studied as future research.

e. Extensive beam-column conection evaluation is recommended as future research.

APPENDIX A Software Implementation

The FRPFA computational procedure is implemented as a software application. The following features are implemented.

- Database which contains mechanical material properties of different types of basic constituent materials (e.g., fiber, matrix) is stored in the software for use by the engineer (Figures A-2 and A-3).
- Computation of the effective mechanical material properties for layers composed of the matrix with fiber reinforcement (Step 3 in Figure 0.1, see Sections 2.10.2 and 2.10.3) (Figure A-4).
- Computation of the effective engineering material properties for components (e.g., web and flange) of a cross-section and importing measured mechanical properties of components of cross-section (Step 4 in Figure 0.1, see Section 2.10.4) (Figure A-5).
- Computation of the 2D cross-sectional stiffness of a cross-section of member by using VABS (Steps 5 in Figure 0.1, see Appendix C) (Figure A-6).
- Computation of the one dimensional space frame member natural stiffness matrix of the structural member composed of multiple components (e.g., webs and flanges) having different material properties (Steps 6 in Figure 0.1, see Appendix B) (Figure A-7).
- Computation of the cross-sectional area properties such as centroidal location, principal axis orientation, cross-sectional area, principal axis

shear areas, principal axis moments of inertia, torsion constant, warping constant, shear center location, and member natural stiffness matrices for members composed of isotropic materials (see Appendix D) (Figure A-8).

- Computation of member end forces for structural member fabricated from FRP composite materials. (Step 7 in Figure 0.1, see Appendix E) (Figure A-9).
- Various cross-section shape generations for calculation of 1D space frame member natural stiffness matrix and area properties (Figure A-1).

The above computations are performed for, but not necessarily limited to, the cross-section shapes shown in Figure A-1. In combination with GTSTRUDL, the developed software can enable civil/structural engineers to perform a structural analysis of space frame structures whose members are composed of anisotropic FRP composite materials.

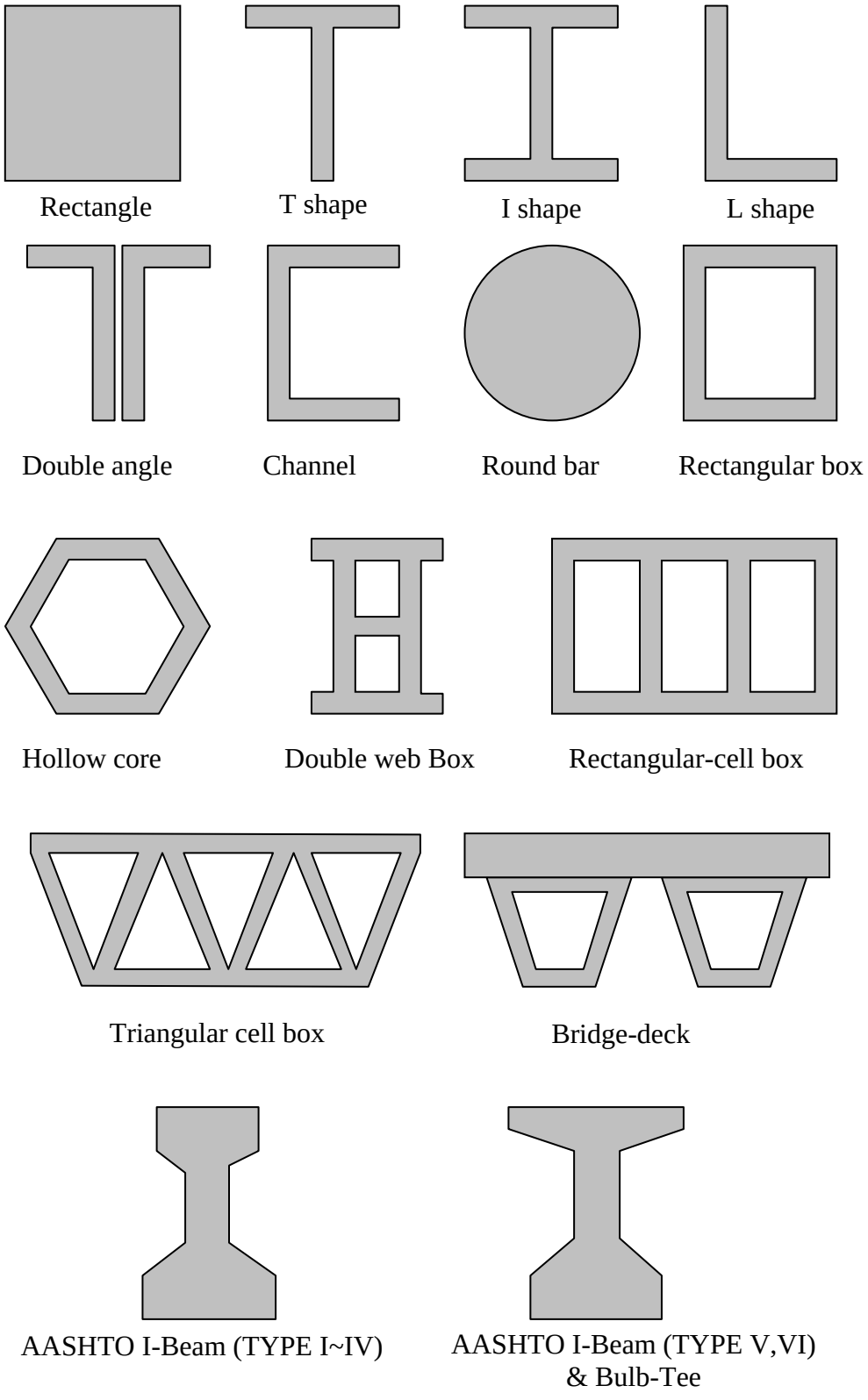

Figure A-1: Cross-section shapes included in the developed software

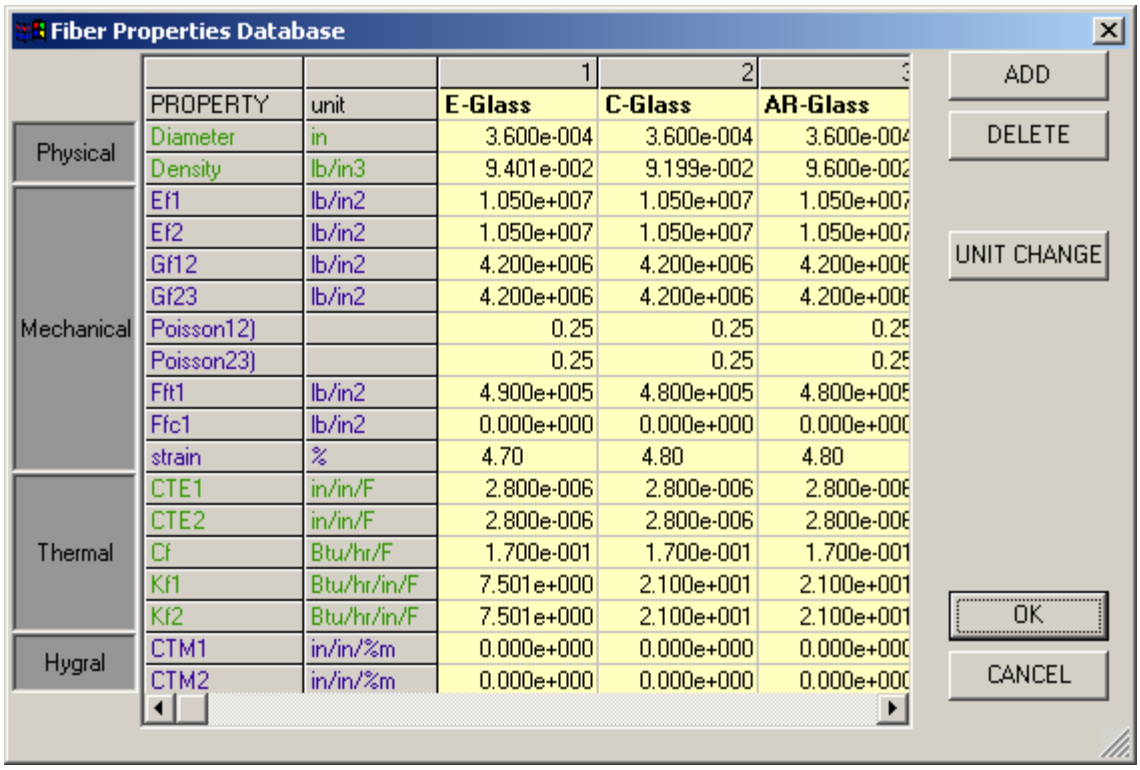

Figure A-2: Fiber properties database window

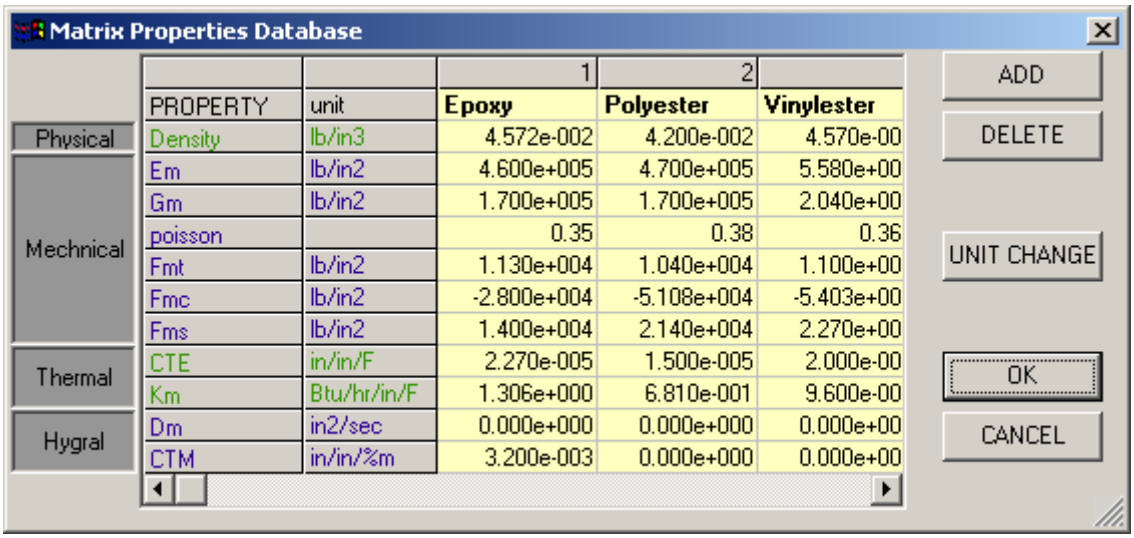

Figure A-3: Matrix properties database window

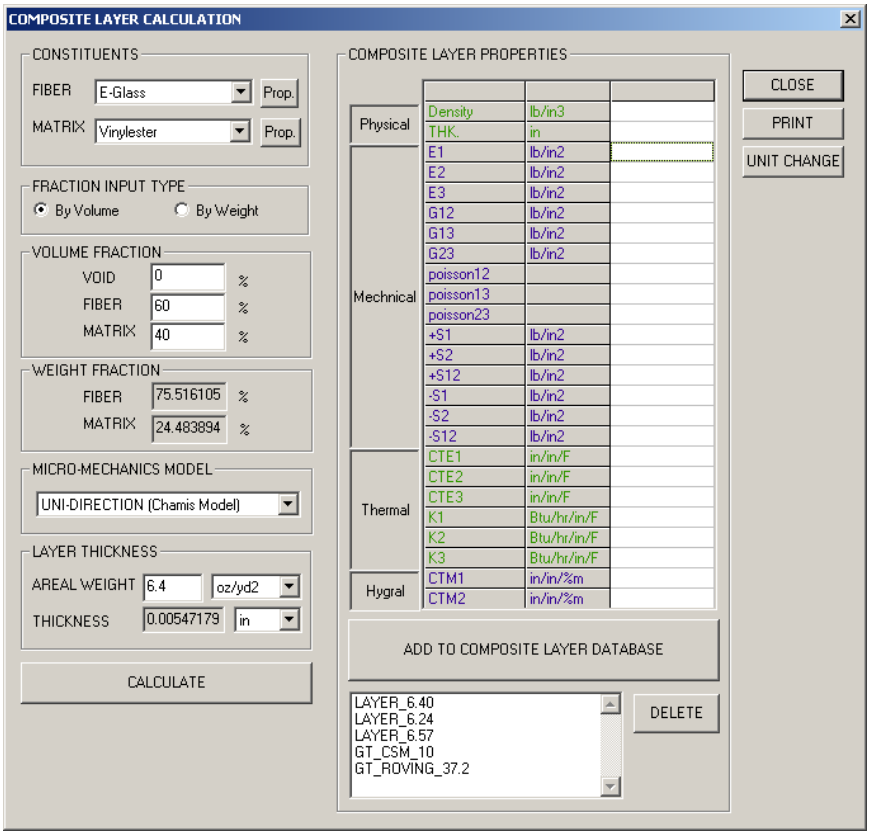

Figure A-4: Effective material properties of composite layer calculation window

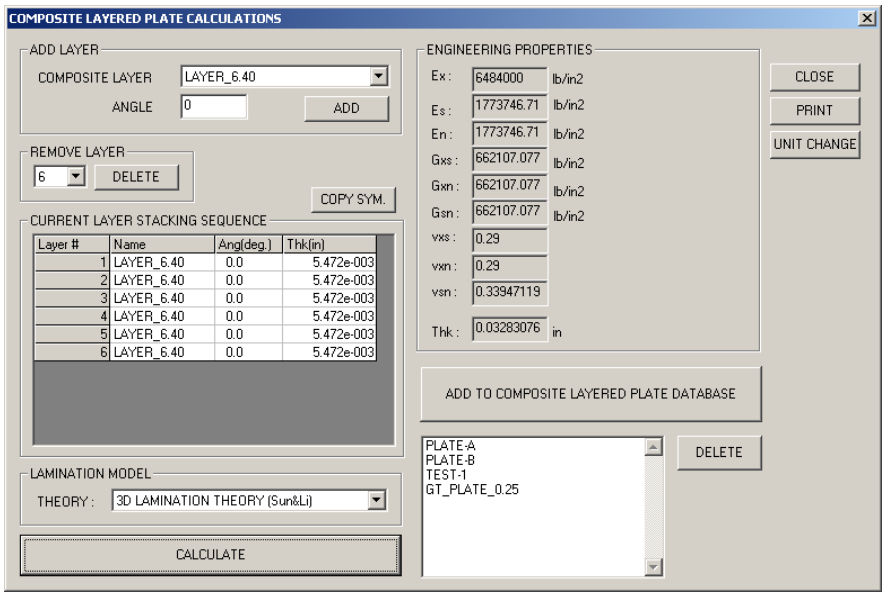

Figure A-5: Effective mechanical material properties of a component of a cross-section calculation window

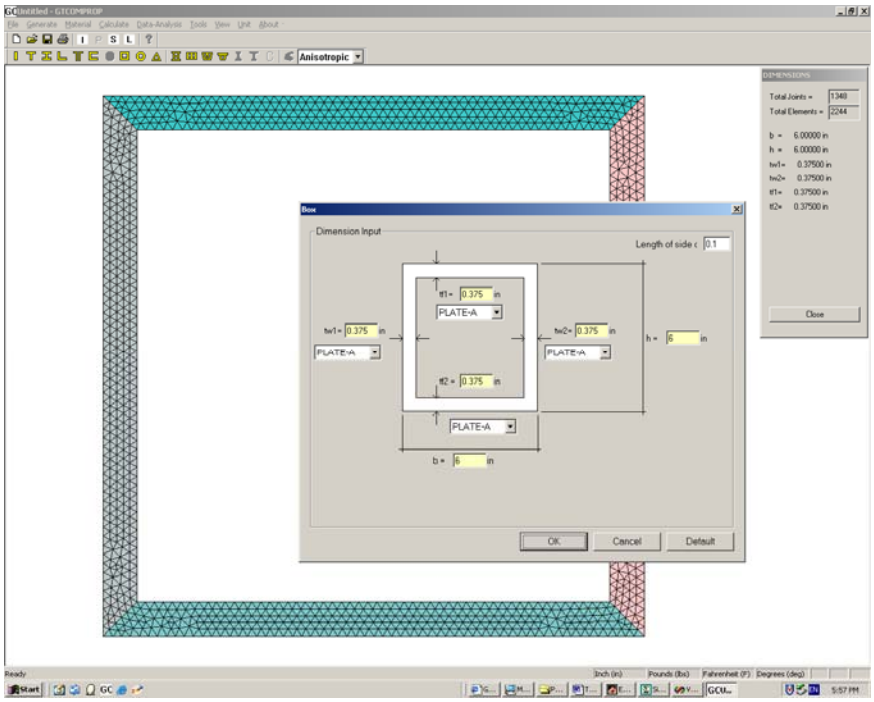

Figure A-6: 2D cross-section mesh generation with given dimensions

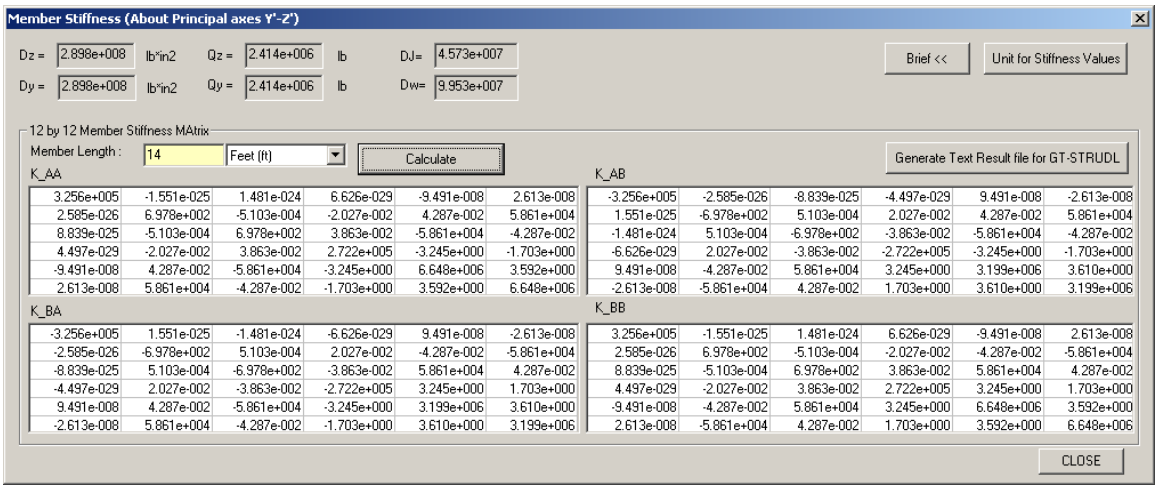

Figure A-7: 2D cross-sectional stiffness and 1D space frame member natural stiffness matrix calculation

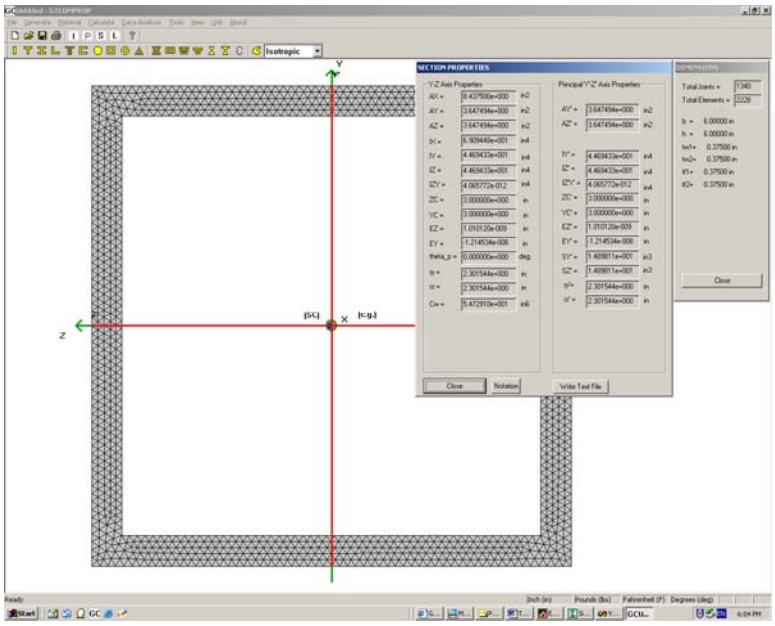

Figure A-8: Cross-sectional area properties calculation window

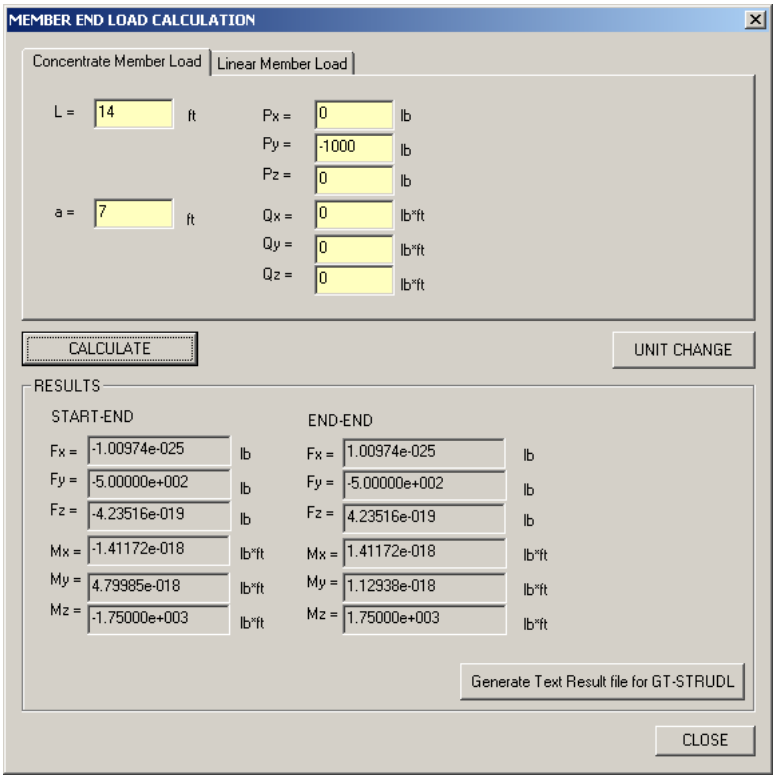

Figure A-9: Member-end-forces calculation window

APPENDIX B Member Natural Stiffness Formulation from a Sectional Stiffness

A stiffness analysis procedure uses the member natural stiffness matrix to define a member stiffness characteristic of space frame structural members, and the member natural stiffness matrix is a function of material properties, cross-sectional properties, and member length. The sectional stiffness calculated through VABS (Variational Asymptotic Beam Sectional analysis) must be converted into member natural stiffness for a conventional frame stiffness analysis procedure. First, displacement-forces relationship of a cantilever problem will be solved to get a 6 by 6 $\mathbf{K}_{BB}$ matrix in this Appendix B, which was originally presented by Hodges (2006). Once, the $\mathbf{K}_{BB}$ matrix results are available, the other stiffness $\mathbf{K}_{AB}$, $\mathbf{K}_{BA}$, $\mathbf{K}_{AA}$ can be formulated using a displacement transformation matrix and a force transformation matrix (Emkin, 1999). Finally, the 12 by 12 member natural stiffness matrix for a space frame member can be constructed.

Member internal force function must be represented in terms of externally applied member end forces for this derivation. In x_1-x_2 plane, reactions can be determined from equilibrium of entire member as follows:

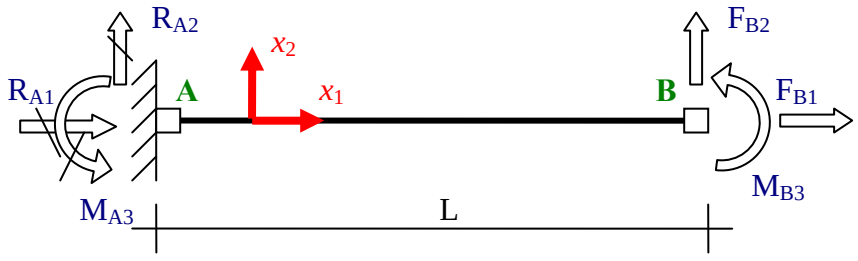

Figure B-1: FBD of cantilever in x_1-x_2 plane

$$R_{A1} = -F_{B1},\ R_{A2} = -F_{B2},\ M_{A3} = -M_{B3} - LF_{B2}$$

R_{A1}, R_{A2}, and M_{A3} represent reaction components at joints 'A'. F_{B1}, F_{B2} and M_{B3} represent the applied forces at the joint 'B', the L is a cantilever member length. By using the following free body diagram (Figure B-2), internal member forces functions for F_1, F_2, and M_3 can be represented with applied forces at joint 'B'.

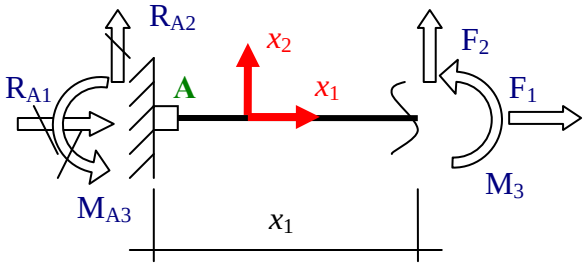

Figure B-2: FBD of left part of cutting line in x_1-x_2 plane

$$\sum F_{x1} = 0 \rightarrow F_1 = F_{B1}$$

$$\sum F_{x2} = 0 \rightarrow F_2 = F_{B2}$$

$$\sum M_{x3} = 0 \rightarrow M_3 = M_{B3} + (L - x_1)F_{B2}$$

In plane x_1-x_3, the reactions can be determined from the equilibrium

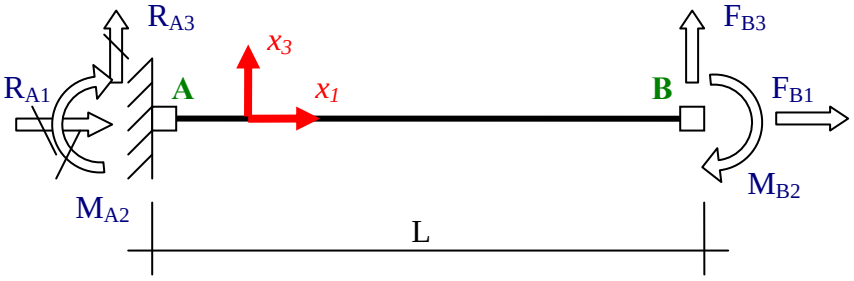

Figure B-3: FBD of cantilever in x_1-x_3 plane

$$R_{A1} = -F_{B1},\ \ R_{A3} = -F_{B3},\ \ M_{A2} = M_{B2} - LF_{B3}$$

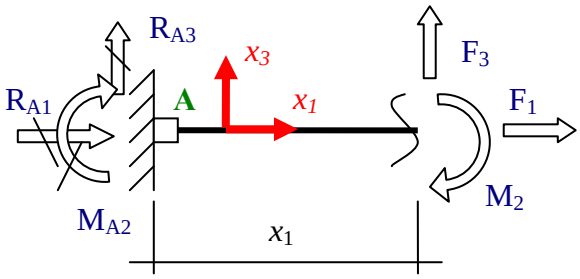

Figure B-4: FBD of left part of cutting line in x_1-x_3 plane

By using above free body diagram, the internal member forces functions for F_3, and M_2 can be represented as follows:

$$\sum F_{x1} = 0 \rightarrow F_1 = F_{B1}$$

$$\sum F_{x3} = 0 \rightarrow F_3 = F_{B3}$$

$$\sum M_{x2} = 0 \rightarrow M_2 = M_{B2} - (L - x_1)F_{B3}$$

About x_1 axis, the torsional force equilibrium must be satisfied. Therefore, the internal force function M_1 can be determined as follows:

$$\sum M_{x1} = 0 \rightarrow M_1 = F_{B1}$$

Finally, these six internal member force functions can be represented as follows:

$$F_1 = F_{B1}$$

$$F_2 = F_{B2}$$

$$F_3 = F_{B3}$$

$$M_1 = M_{B1}$$

$$M_2 = M_{B2} - (L - x_1)F_{B3}$$

$$M_3 = M_{B3} + (L - x_1)F_{B2}$$

In matrix form

$$\begin{Bmatrix} F_1 \\ F_2 \\ F_3 \\ M_1 \\ M_2 \\ M_3 \end{Bmatrix} = \begin{Bmatrix} F_{B1} \\ F_{B2} \\ F_{B3} \\ M_{B1} \\ M_{B2} \\ M_{B3} \end{Bmatrix} + \begin{Bmatrix} 0 \\ 0 \\ 0 \\ 0 \\ -F_{B3}(L - x_1) \\ F_{B2}(L - x_1) \end{Bmatrix}$$

or

$$\begin{Bmatrix} \overline{F} \\ \overline{M} \end{Bmatrix} = \begin{Bmatrix} \overline{F}_B \\ \overline{M}_B \end{Bmatrix} + \begin{Bmatrix} \overline{0} \\ (L - x_1)\bar{i} \times \overline{F}_B \end{Bmatrix}$$

By using the member sectional stiffness calculated from VABS procedure, the 1D deformation measures vector and the internal resultant forces vector can be related as follows:

$$\begin{Bmatrix} \bar{e} \\ \bar{k} \end{Bmatrix} = \begin{bmatrix} \mathbf{R} & \mathbf{Z} \\ \mathbf{Z}^T & \mathbf{T} \end{bmatrix} \begin{Bmatrix} \overline{F} \\ \overline{M} \end{Bmatrix} = \begin{bmatrix} \mathbf{R} & \mathbf{Z} \\ \mathbf{Z}^T & \mathbf{T} \end{bmatrix} \begin{Bmatrix} \overline{F}_B \\ \overline{M}_B + (L - x_1)\bar{i} \times \overline{F}_B \end{Bmatrix} \qquad \textbf{(B-1)}$$

$$= \begin{bmatrix} \mathbf{R} & \mathbf{Z} \\ \mathbf{Z}^T & \mathbf{T} \end{bmatrix} \begin{bmatrix} \mathbf{I} & \mathbf{O} \\ (L - x_1)\mathbf{C} & \mathbf{I} \end{bmatrix} \begin{Bmatrix} \overline{F}_B \\ \overline{M}_B \end{Bmatrix}$$

where

$$\mathbf{C} = \begin{bmatrix} 0 & 0 & 0 \\ 0 & 0 & -1 \\ 0 & 1 & 0 \end{bmatrix}$$

$$\begin{bmatrix} e_1 & e_2 & e_3 & k_1 & k_2 & k_3 \end{bmatrix}^T = \begin{Bmatrix} \bar{e} \\ \bar{k} \end{Bmatrix}$$

Above $\mathbf{R}$, $\mathbf{S}$, and $\mathbf{T}$ matrix are partitions of the sectional flexibility matrix that was calculated through the VABS analysis. For a linear case, the generalized 1D member strains are as follows:

$$\bar{e} = \bar{u}_{,1} + \bar{i} \times \bar{\omega} \tag{B-2a}$$

$$\bar{k} = \bar{\omega}_{,1} \tag{B-2b}$$

From equation (B-1), $\bar{k} = \left[\mathbf{Z}^T + (L - x_1)\mathbf{TC}\right]\bar{F}_B + \mathbf{T}\bar{M}_B$. By integrating $\bar{k}$ about x_1 and applying the boundary condition $\bar{\omega}(0) = \bar{0}$ and obtaines

$$\bar{\omega} = \left[x_1\mathbf{Z}^T + (Lx_1 - \frac{x_1^2}{2})\mathbf{TC} \right]\bar{F}_B + x_1\mathbf{T}\bar{M}_B \tag{B-3}$$

By using equations (B-1) and (B-2a), the following equation can be obtained.

$$\bar{u}_{,1} = \left[\mathbf{R} + (L - x_1)\mathbf{ZC}\right]\bar{F}_B + \mathbf{Z}\bar{M}_B - \bar{i} \times \bar{\omega} \tag{B-4}$$

Substituting equation (B-3) into equation (B-4), and finds that

$$\bar{u}_{,1} = \left[\mathbf{R} + (L - x_1)\mathbf{ZC}\right]\bar{F}_B + \mathbf{Z}\bar{M}_B - \bar{i} \times \left\{ \left[x_1\mathbf{Z}^T + (Lx_1 - \frac{x_1^2}{2})\mathbf{TC} \right]\bar{F}_B + x_1\mathbf{T}\bar{M}_B \right\}$$

$$= \left[\mathbf{R} + (L - x_1)\mathbf{ZC} - x_1\mathbf{CZ}^T - (Lx_1 - \frac{x_1^2}{2})\mathbf{CTC} \right]\bar{F}_B + \left[\mathbf{Z} - x_1\mathbf{CT}\right]\bar{M}_B \tag{B-5}$$

By integrating $\bar{u}_{,1}$ and applying of the boundary condition $\bar{u}(0) = \bar{0}$ and finds that

$$\bar{u} = \left[x_1\mathbf{R} + (Lx_1 - \frac{x_1^2}{2})\mathbf{ZC} - \frac{x_1^2}{2}\mathbf{CZ}^T - (L\frac{x_1^2}{2} - \frac{x_1^3}{6})\mathbf{CTC} \right]\bar{F}_B + \left[x_1\mathbf{Z} - \frac{x_1^2}{2}\mathbf{CT} \right]\bar{M}_B \tag{B-6}$$

By substituting $x_1 = L$ into equations (B-3) and (B-6), the displacement and rotation vector becomes

$$\begin{Bmatrix} \overline{u}_B \\ \overline{\omega}_B \end{Bmatrix} = \begin{bmatrix} L\mathbf{R} + \frac{L^2}{2}(\mathbf{ZC} - \mathbf{CZ}^T) - \frac{L^3}{3}\mathbf{CTC} & L\mathbf{Z} - \frac{L^2}{2}\mathbf{CT} \\ L\mathbf{Z}^T + \frac{L^2}{2}\mathbf{TC} & L\mathbf{T} \end{bmatrix} \begin{Bmatrix} \overline{F}_B \\ \overline{M}_B \end{Bmatrix} \qquad \textbf{(B-7)}$$

So,

$$\mathbf{F}_{BB} = \begin{bmatrix} L\mathbf{R} + \frac{L^2}{2}(\mathbf{ZC} - \mathbf{CZ}^T) - \frac{L^3}{3}\mathbf{CTC} & L\mathbf{Z} - \frac{L^2}{2}\mathbf{CT} \\ L\mathbf{Z}^T + \frac{L^2}{2}\mathbf{TC} & L\mathbf{T} \end{bmatrix}$$

Finally $\mathbf{K}_{BB}$ is found to be

$$\mathbf{K}_{BB} = \mathbf{F}_{BB}^{-1}$$

By using displacement and force transformation matrces, $\mathbf{K}_{AB}$, $\mathbf{K}_{BA}$, $\mathbf{K}_{AA}$ can be calculated as follows:

$$\mathbf{T}_F = \begin{bmatrix} 1 & 0 & 0 & 0 & 0 & 0 \\ 0 & 1 & 0 & 0 & 0 & 0 \\ 0 & 0 & 1 & 0 & 0 & 0 \\ 0 & W & -V & 1 & 0 & 0 \\ -W & 0 & U & 0 & 1 & 0 \\ V & -U & 0 & 0 & 0 & 1 \end{bmatrix}, \quad \mathbf{T}_F = \begin{bmatrix} 1 & 0 & 0 & 0 & 0 & 0 \\ 0 & 1 & 0 & 0 & 0 & 0 \\ 0 & 0 & 1 & 0 & 0 & 0 \\ 0 & W & -V & 1 & 0 & 0 \\ -W & 0 & U & 0 & 1 & 0 \\ V & -U & 0 & 0 & 0 & 1 \end{bmatrix} \qquad \textbf{(B-8)}$$

In this case, $U = L$, $V = 0$, and $W = 0$

$$\mathbf{K}^G = \begin{bmatrix} \mathbf{K}_{AA}^G & \mathbf{K}_{AB}^G \\ \mathbf{K}_{BA}^G & \mathbf{K}_{BB}^G \end{bmatrix}$$

where

$$\mathbf{K}_{BB}^G = \mathbf{R}^T \mathbf{K}_{BB} \mathbf{R}$$

$$\mathbf{K}_{AA}^G = \mathbf{T}_D^T \mathbf{K}_{BB} \mathbf{T}_D$$

$$\mathbf{K}_{AB}^G = \left(\mathbf{K}_{BA}^G\right)^T$$

APPENDIX C Member Sectional Stiffness Formulation using the "Member Sectional Analysis"

To get the exact sectional stiffness of general anisotropic space frame structural member, The Variational Asymptotic Beam Sectional method (Section 1.3.1, p. 8) was extensively used in this thesis. In this chapter, this theory was summarized based on several reference literatures regarding Variational Asymptotic Beam Sectional method (Cesnik, 1994; Hodges, 2006; Popescu and Hodges, 2000; Yu, 2002). However, some procedures were modified for practical purpose. Figure C-1 illustrates procedures to find a sectional stiffness/area property about principal axes for arbitrary cross-section shapes. It should be noted that, in this Appendix B, the member local reference, x_1-x_2-x_3, is used instead of *x*-*y*-*z* for a simplicity of mathematical formulation.

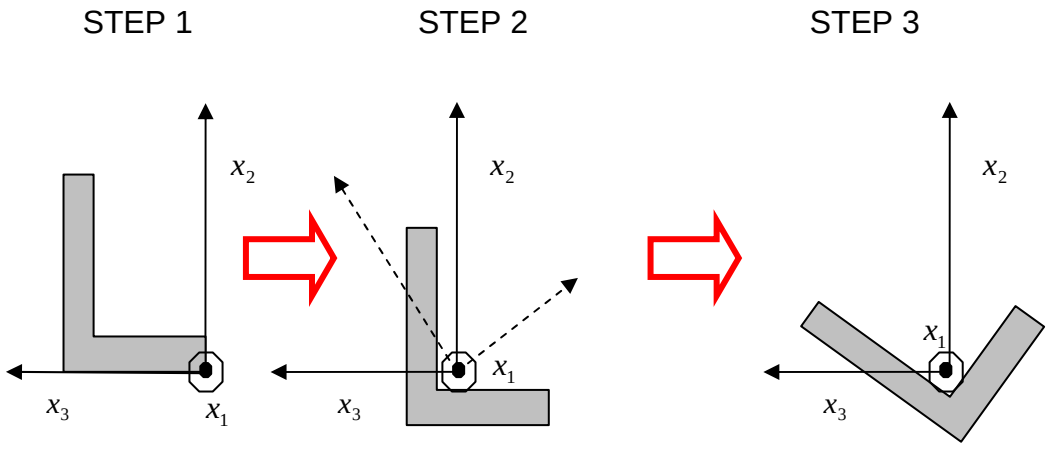

Figure C-1: Three steps to get sectional stiffness about principal axes

STEP 1: Centroid of the cross-section is calculated. The reference frame is relocated into the centroid.

STEP 2: Principal axes are calculated. Then, the calculated principal axes are redefined as a reference frame for next step.

STEP 3: Perform sectional analysis to find a sectional stiffness about principal axes.

STEP 1: Find centroid position and translate the reference frame

(1) Because the centroid location is unknown for the given cross-section, the local reference frame of the cross-section should be specified in an arbitrary position. In this thesis, a right-bottom corner is set as an origin of reference frame.

(2) The cross-section should be meshed with 2D elements. For current research, 3-node triangular elements are used. Then, the cross-sectional area A_1 can be calculated using typical gauss integration method as follows:

$$A_1 = \int_{A_1} dA_1 \tag{C-1}$$

(3) With this area result, the centroid coordinates x_{2c} , x_{3c} can be determined as follows:

$$x_{2c} = \frac{\int_{A_1} x_2 \, dA_1}{A_1} \text{ , } x_{3c} = \frac{\int_{A_1} x_3 \, dA_1}{A_1} \tag{C-2}$$

(4) Then, the original reference frame is relocated into the centroid position calculated in (4), making new centroid position as zero (Figure C-2).

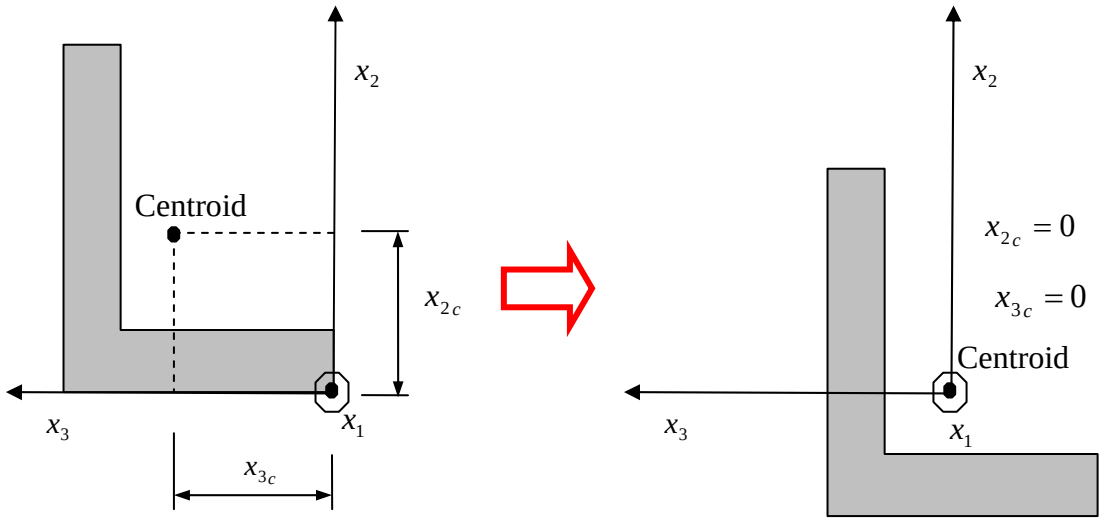

Figure C-2: Cross-section translation process

STEP 2: Calculate principal axes and set the principal axes as new reference frame

(1) In a civil/structure engineering practice, the cross-sectional properties such as cross-sectional area properties and member stiffness matrix about principal axes are mostly preferred cross-sectional properties. To get the cross-sectional properties about principal axes, the cross-section (cross-section determined in Step 1) should be rotated into the position making principal angle as zero. This new rotated geometry of the cross-section can be used to calculate the sectional stiffness and cross-sectional properties about the principal axes.

(2) To determine the principal angle, the flexural rigidities[9] about x_2, x_3, and coupling term[10] are required. And, these properties can be calculated from *classical sectional stiffness*[11] procedure without using *Timoshenko sectional stiffness*[12] calculation.

(3) The strain on the specific point of the cross-section can be represented in terms of 1D deformation measures on the centroid warping on each point in the cross-section. This new type of strain was introduced by Hodges (1987), It should be noted that it contains the 1D deformation measures at the centroid position. The gamma matrix Γ_h, Γ_ε are coefficient matrix for the strain vector and these matrix are defined as follows (Popescu and Hodges, 2000): For the classical stiffness calculations, matrix Γ_l is not required currently.

$$\overline{\Gamma} = \mathbf{\Gamma_h}\overline{w} + \mathbf{\Gamma_\varepsilon}\overline{\varepsilon} + \mathbf{\Gamma}_l\overline{w}' \qquad \textbf{(C-3)}$$

where

$$\mathbf{\Gamma}_h = \begin{bmatrix} 0 & 0 & 0 \\ \dfrac{\partial}{\partial x_2} & 0 & 0 \\ \dfrac{\partial}{\partial x_3} & 0 & 0 \\ 0 & \dfrac{\partial}{\partial x_2} & 0 \\ 0 & \dfrac{\partial}{\partial x_3} & \dfrac{\partial}{\partial x_2} \\ 0 & 0 & \dfrac{\partial}{\partial x_3} \end{bmatrix},$$

[9] For isotropic section, EI_2, EI_3 correspond to the flexural rigidities.
[10] For isotropic section, EI_{23} corresponds to the coupling rigidity.
[11] The term, *Classical sectional stiffness,* represents a 4 by 4 sectional stiffness without shear deformation effect (Hodges, 2006).
[12] However, the term, *Timoshenko like sectional stiffness,* represent a 6 by 6 sectional stiffness fully considering shear deformation (Hodges, 2006).

$$\mathbf{\Gamma}_{\varepsilon} = \begin{bmatrix} 1 & 0 & x_3 & -x_2 \\ 0 & -x_3 & 0 & 0 \\ 0 & x_2 & 0 & 0 \\ 0 & 0 & 0 & 0 \\ 0 & 0 & 0 & 0 \\ 0 & 0 & 0 & 0 \end{bmatrix}, \qquad \overline{w} = \begin{bmatrix} w_1 \\ w_2 \\ w_3 \end{bmatrix}, \text{ warping vector.}$$

$$\bar{\varepsilon} = \begin{bmatrix} e_1 \\ \kappa_1 \\ \kappa_2 \\ \kappa_3 \end{bmatrix}, \text{ 1D deformation measure vector on the centroid.}$$

(4) The warping vector, $\overline{w}$, can be represented with the nodal warping matrix $\mathbf{V}$ and shape function matrix $\mathbf{N}$ as follows:

$$\overline{w} = \mathbf{N}\,\mathbf{V} \qquad \textbf{(C-4)}$$

where

$$\mathbf{N} = \begin{bmatrix} N_1 & 0 & 0 & N_2 & 0 & 0 & N_3 & 0 & 0 \\ 0 & N_1 & 0 & 0 & N_2 & 0 & 0 & N_3 & 0 \\ 0 & 0 & N_1 & 0 & 0 & N_2 & 0 & 0 & N_3 \end{bmatrix}$$

$N_1 = 1 - r - s$, $N_2 = r$, $N_3 = s$

r, s: Iso-parametric coordinates for a triangle

It should be noted that each node have three degree of freedom for the strain without any restraint of direction.

(5) Then, the sectional strain energy, U should be represented with the strain defined at previous step (3) for the cross-section. This strain energy now can be represented as follows in terms of a strain vector and material rigidity matrix (Cesnik, 1994). Matrix $\mathbf{D}$ is a symmetric elastic constant matrix (Agarwal, et al. 1990).

$$U = \frac{1}{2}\int_{A_1} \overline{\Gamma}^T \mathbf{D}\overline{\Gamma} dA_1 \qquad \textbf{(C-5)}$$

where

$$\mathbf{D} = \begin{bmatrix} \frac{(1-\nu_{23}\nu_{32})}{\lambda}E_1 & 0 & 0 & \frac{(\nu_{12}+\nu_{13}\nu_{32})}{\lambda}E_2 & 0 & \frac{(\nu_{13}+\nu_{12}\nu_{23})}{\lambda}E_3 \\ & G_{12} & 0 & 0 & 0 & 0 \\ & & G_{13} & 0 & 0 & 0 \\ & & & \frac{(1-\nu_{31}\nu_{13})}{\lambda}E_2 & 0 & \frac{(\nu_{23}+\nu_{21}\nu_{13})}{\lambda}E_3 \\ & SYM. & & & G_{23} & 0 \\ & & & & & \frac{(1-\nu_{23}\nu_{32})}{\lambda}E_3 \end{bmatrix}$$

$$\lambda = 1-\nu_{12}\nu_{21}-\nu_{32}\nu_{23}-\nu_{13}\nu_{31}-2\nu_{21}\nu_{13}\nu_{32}$$

also, the following relations are valid (Jones, 1975)

$$G_{ij} = G_{ji} \qquad \textbf{(C-6a)}$$

$$\nu_{ij} = \nu_{ji}\frac{E_i}{E_j} \qquad \textbf{(C-6b)}$$

(6) The strain energy can be expanded in terms of nodal warping vector as follows:

$$\begin{aligned} U = {} & \mathbf{V}^T\left(\int_{A_1}(\boldsymbol{\Gamma}_h\mathbf{N})^T\mathbf{D}(\boldsymbol{\Gamma}_h\mathbf{N})dA_1\right)\mathbf{V} + \mathbf{V}^T\left(\int_{A_1}(\boldsymbol{\Gamma}_h\mathbf{N})^T\mathbf{D}(\boldsymbol{\Gamma}_\varepsilon)dA_1\right)\overline{\varepsilon} + \mathbf{V}^T\left(\int_{A_1}(\boldsymbol{\Gamma}_h\mathbf{N})^T\mathbf{D}(\boldsymbol{\Gamma}_l\mathbf{N})dA_1\right)\mathbf{V}' \\ & + \overline{\varepsilon}^T\left(\int_{A_1}(\boldsymbol{\Gamma}_h)^T\mathbf{D}(\boldsymbol{\Gamma}_h\mathbf{N})dA_1\right)\mathbf{V} + \overline{\varepsilon}^T\left(\int_{A_1}(\boldsymbol{\Gamma}_\varepsilon)^T\mathbf{D}(\boldsymbol{\Gamma}_\varepsilon)dA_1\right)\overline{\varepsilon} + \overline{\varepsilon}^T\left(\int_{A_1}(\boldsymbol{\Gamma}_\varepsilon)^T\mathbf{D}(\boldsymbol{\Gamma}_l\mathbf{N})dA_1\right)\mathbf{V}' \\ & + \mathbf{V}'^T\left(\int_{A_1}(\boldsymbol{\Gamma}_l\mathbf{N})^T\mathbf{D}(\boldsymbol{\Gamma}_h\mathbf{N})dA_1\right)\mathbf{V} + \overline{\varepsilon}^T\left(\int_{A_1}(\boldsymbol{\Gamma}_l\mathbf{N})^T\mathbf{D}(\boldsymbol{\Gamma}_\varepsilon)dA_1\right)\overline{\varepsilon} + \overline{\varepsilon}^T\left(\int_{A_1}(\boldsymbol{\Gamma}_l\mathbf{N})^T\mathbf{D}(\boldsymbol{\Gamma}_l\mathbf{N})dA_1\right)\mathbf{V}' \end{aligned} \qquad \textbf{(C-7)}$$

Now, the nodal warping matrix $\mathbf{V}$ that minimizes the sectional energy U should be found. A known analytical, closed-form solution of the equation (C-7) is not known. When the analytical solution is not available, the perturbation method can be used. To use the

perturbation method, the unknown solution, $\mathbf{V}$, should be represented with the series of small parameter '*h*' as follows:

$$\mathbf{V} = \mathbf{V}_0 + h\mathbf{V}_1^* + h^2\mathbf{V}_2^* + \cdots \qquad \textbf{(C-8)}$$

(7) First approximation can be performed neglecting the terms with higher order than h, reducing the equation (C-8) as follows:

$$\mathbf{V} = \mathbf{V}_0 \qquad \textbf{(C-9)}$$

This equation (C-9) is substituted into the sectional energy term (C-7). $\mathbf{V}_0$ and $\bar{\varepsilon}$ are assumed to be same order. $\mathbf{V}_1, \mathbf{V}_0^{'}$ and $\bar{\varepsilon}^{'}$ are assumed to same order with each other, but these are one level lower then $\mathbf{V}_0$ and $\bar{\varepsilon}$. Therefore, in the first approximation of (C-7), the terms with order of $(\mathbf{V}_0)^2$ or $(\bar{\varepsilon}_0)^2$ are determined to be used and all other terms with lower order are neglected. Then sectional energy term is reduced as follows (Popescu, 2000):

$$U_0 = \frac{1}{2}(\mathbf{V}_0^T\mathbf{E}\mathbf{V}_0 + 2\mathbf{V}_0^T\mathbf{D}_{h\varepsilon}\bar{\varepsilon} + \bar{\varepsilon}^T\mathbf{D}_{\varepsilon\varepsilon}\bar{\varepsilon}) \qquad \textbf{(C-10)}$$

where

$$\mathbf{E} = \int_{A_1}[\Gamma_h\mathbf{N}]^T\mathbf{D}[\Gamma_h\mathbf{N}]dA_1$$

$$\mathbf{D}_{\varepsilon\varepsilon} = \int_{A_1}\Gamma_\varepsilon{}^T\mathbf{D}\Gamma_\varepsilon dA_1$$

$$\mathbf{D}_{h\varepsilon} = \int_{A_1}[\Gamma_h\mathbf{N}]^T\mathbf{D}\Gamma_h dA_1$$

N = Shape function matrix. The following is a special case for 3 joints finite element.

$$\mathbf{N} = \begin{bmatrix} N_1 & 0 & 0 & N_2 & 0 & 0 & N_3 & 0 & 0 \\ 0 & N_1 & 0 & 0 & N_2 & 0 & 0 & N_3 & 0 \\ 0 & 0 & N_1 & 0 & 0 & N_2 & 0 & 0 & N_3 \end{bmatrix}$$

where

$$N_1 = 1 - r - s \ , \qquad N_2 = r \ , \qquad N_3 = s$$

r, s: Isoparametric coordinates or triangle

(8) Classical warping solution can be found by solving following equation.

This equation was derived by using the Lagrange-Multiplier method.

$$\mathbf{E}\hat{\mathbf{V}}_0^* = \left(\mathbf{H}\boldsymbol{\Psi}\ \boldsymbol{\Psi}^T - \mathbf{I}\right)\mathbf{D}_{h\varepsilon} \qquad \textbf{(C-11)}$$

where

$\mathbf{I}$ = Identity matrix.

$\boldsymbol{\Psi}$ = kernel matrix

$$\boldsymbol{\Psi} = \begin{bmatrix} 1 & 0 & 0 & 0 \\ 0 & 1 & 0 & -x_3^{(1)} \\ 0 & 0 & 1 & x_2^{(1)} \\ 1 & 0 & 0 & 0 \\ 0 & 1 & 0 & -x_3^{(2)} \\ 0 & 0 & 1 & x_2^{(2)} \\ & \vdots & & \vdots \\ 1 & 0 & 0 & 0 \\ 0 & 1 & 0 & -x_3^{(n)} \\ 0 & 0 & 1 & x_3^{(n)} \end{bmatrix}$$

$x_2^{(i)}$, $x_3^{(i)}$ = Coordinates of i$^{\text{th}}$ joint

N = Total number of joints in the discretized cross-section

(9) Then, the final solution $\hat{\mathbf{V}}_0$ can be calculated with following equation.

$$\hat{\mathbf{V}}_0 = \left(\mathbf{I} - \boldsymbol{\Psi}\boldsymbol{\Psi}^T\mathbf{H}\right)\hat{\mathbf{V}}_0^* \qquad \textbf{(C-12)}$$

where

$$\mathbf{H} = \int_{A_1} \mathbf{N}\mathbf{N}^T dA_1$$

Finally, the 4 by 4 classical sectional stiffness matrix can be calculated as follows:

$$\mathbf{A} = \mathbf{D}_{\varepsilon\varepsilon} + \hat{\mathbf{V}}_0^T \mathbf{D}_{h\varepsilon} \qquad \textbf{(C-13)}$$

$$\mathbf{A} = \begin{bmatrix} A_{11} & A_{12} & A_{13} & A_{14} \\ A_{21} & A_{22} & A_{23} & A_{24} \\ A_{31} & A_{32} & A_{33} & A_{34} \\ A_{41} & A_{42} & A_{43} & A_{44} \end{bmatrix}$$

$$\begin{Bmatrix} F_1 \\ M_1 \\ M_2 \\ M_3 \end{Bmatrix} = \begin{bmatrix} A_{11} & A_{12} & A_{13} & A_{14} \\ A_{21} & A_{22} & A_{23} & A_{24} \\ A_{31} & A_{32} & A_{33} & A_{34} \\ A_{41} & A_{42} & A_{43} & A_{44} \end{bmatrix} . \begin{Bmatrix} e_1 \\ \kappa_1 \\ \kappa_2 \\ \kappa_3 \end{Bmatrix}$$

(10) For a general cross-section, $A_{33} = (EI_2)_{equiv}$, $A_{44} = (EI_3)_{equiv}$, and $A_{34} = A_{43} = (EI_{23})_{equiv}$. Therefore, the principal axes, θ_p can be calculated from three sectional rigidity properties.

$$\theta_p = \frac{1}{2} \tan^{-1}\left(\frac{-2A_{34}}{A_{33} - A_{44}} \right) \qquad \textbf{(C-14)}$$

For next step, this cross-section must be rotated into position having principal angle zero (Figure C-3).

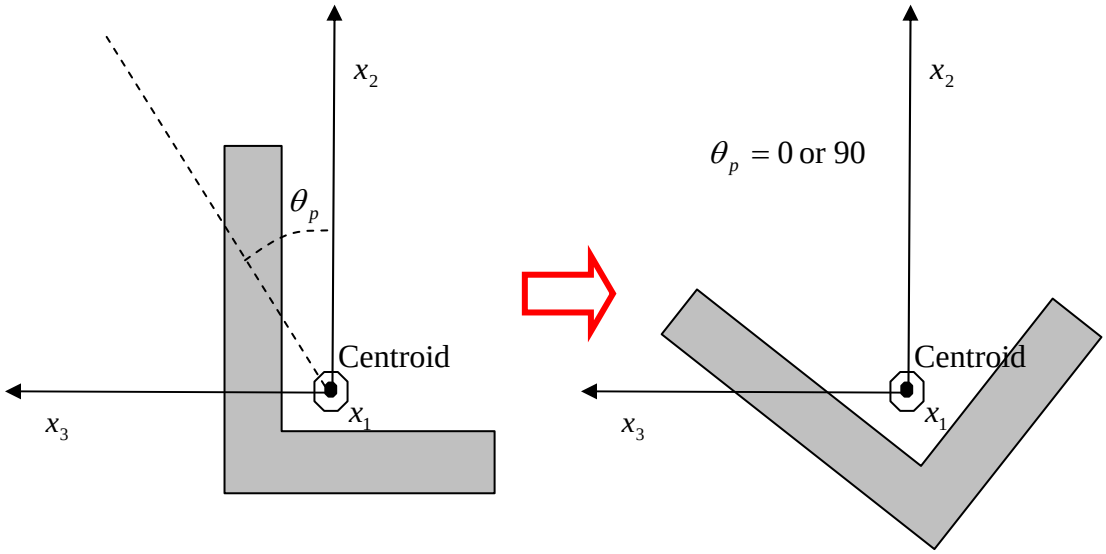

Figure C-3: Cross-section rotation process

Step 3: Calculate Timoshenko like Sectional Stiffness and Get Sectional Stiffness about Principal Axes

(1) With the new changed geometry of the cross-section, the calculation to find classical stiffness, **A** , must be performed again. This new classical stiffness, **A** , is a sectional stiffness about principal axes. Three intermediate matrices are additionally required to get the Timoshenko type sectional stiffness matrix as follows:

$$\mathbf{D}_{hl} = \int_{A_1} [\Gamma_h \mathbf{N}]^T \mathbf{D} [\Gamma_l \mathbf{N}] dA_1 \qquad \textbf{(C-15a)}$$

$$\mathbf{D}_{ll} = \int_{A_1} [\Gamma_l \mathbf{N}]^T \mathbf{D} [\Gamma_l \mathbf{N}] dA_1 \qquad \textbf{(C-15b)}$$

$$\mathbf{D}_{l\varepsilon} = \int_{A_1} [\Gamma_l \mathbf{N}]^T \mathbf{D} [\Gamma_\varepsilon] dA_1 \qquad \textbf{(C-15c)}$$

where

$\mathbf{\Gamma}_l = \begin{bmatrix} 1 & 0 & 0 \\ 0 & 1 & 0 \\ 0 & 0 & 1 \\ 0 & 0 & 0 \\ 0 & 0 & 0 \\ 0 & 0 & 0 \end{bmatrix}$, the other matrices were already calculated in

(2) The refined warping solution can be determined with the following equation

$$\mathbf{E}\hat{\mathbf{V}}_1^* = \left(\mathbf{H}\mathbf{\Psi}\ \mathbf{\Psi}^T - \mathbf{I}\right)\left(\mathbf{D}_{hl}\hat{\mathbf{V}}_0 - \mathbf{D}_{hl}^T\hat{\mathbf{V}}_0 - \mathbf{D}_{l\varepsilon}\right) \quad \textbf{(C-16)}$$

The solution of warping matrix can be calculated with similar way that was used for classical solutions in step.2. Then, the Timoshenko member like warping solution $\hat{\mathbf{V}}_1$ can be calculated with following equation.

$$\hat{\mathbf{V}}_1 = \left(\mathbf{I} - \mathbf{\Psi}\ \mathbf{\Psi}^T\mathbf{H}\right)\hat{\mathbf{V}}_1^* \quad \textbf{(C-17)}$$

(3) For prismatic member case, $\mathbf{A}$, $\mathbf{B}$, $\mathbf{C}$, and $\mathbf{D}$ matrix in VABS sectional analysis procedure can be calculated as follows:

$$U_1 = \frac{1}{2}(\bar{\varepsilon}^T\mathbf{A}\bar{\varepsilon} + 2\bar{\varepsilon}^T\mathbf{A}\mathbf{Q}\bar{\gamma}' + 2\bar{\varepsilon}^T\mathbf{B}\bar{\varepsilon}' + \bar{\varepsilon}'^T\mathbf{C}\bar{\varepsilon}' + 2\bar{\varepsilon}^T\mathbf{D}\bar{\varepsilon}'') \quad \textbf{(C-18)}$$

where

$$\mathbf{A} = \mathbf{D}_{\varepsilon\varepsilon} + \hat{\mathbf{V}}_0^T\mathbf{D}_{h\varepsilon}$$

$$\mathbf{B} = \hat{\mathbf{V}}_0^T\mathbf{D}_{hl}^T\hat{\mathbf{V}}_0 + \mathbf{D}_{l\varepsilon}^T\hat{\mathbf{V}}_0$$

$$\mathbf{C} = \hat{\mathbf{V}}_0^T\mathbf{D}_{hl}^T\hat{\mathbf{V}}_1 + \hat{\mathbf{V}}_1^T\mathbf{D}_{hl}^T\hat{\mathbf{V}}_0 + \hat{\mathbf{V}}_1^T\mathbf{D}_{l\varepsilon} + \hat{\mathbf{V}}_0^T\mathbf{D}_{hl}\hat{\mathbf{V}}_0$$

$$\mathbf{D} = \left(\mathbf{D}_{\mathbf{l\varepsilon}}^{\mathbf{T}} + \hat{\mathbf{V}}_{\mathbf{0}}^{\mathbf{T}}\mathbf{D}_{\mathbf{hl}}\right)\hat{\mathbf{V}}_1$$

$$\bar{\gamma} = \begin{bmatrix}\gamma_{12} & \gamma_{13}\end{bmatrix}^T$$

These $\mathbf{A}$, $\mathbf{B}$, $\mathbf{C}$, and $\mathbf{D}$ matrix are used for the following equations to relate the energy with 1D strain measures and its derivates. These $\mathbf{A}$, $\mathbf{B}$, $\mathbf{C}$, and $\mathbf{D}$ matrices are simplified results for the isotropic, homogenous, and prismatic beam problem for sectional properties calculation. The above equation should be transformed into a more familiar form having one dimensional strain measures without derivate of strain measures as follows:

$$2U = \bar{\varepsilon}^T\mathbf{X}\bar{\varepsilon} + 2\bar{\varepsilon}^T\mathbf{F}\bar{\gamma} + \bar{\gamma}^T\mathbf{G}\bar{\gamma} \qquad \textbf{(C-19)}$$

where

$$\mathbf{G} = \left(\mathbf{Q}^{\mathbf{T}}\mathbf{A}^{-\mathbf{1}}\mathbf{C}\mathbf{A}^{-\mathbf{1}}\mathbf{Q}\right)^{-\mathbf{1}}$$

$$\mathbf{F} = \mathbf{B}^{\mathbf{T}}\mathbf{A}^{-\mathbf{1}}\mathbf{Q}\mathbf{G}$$

$$\mathbf{X} = \mathbf{A} + \mathbf{F}\mathbf{G}^{-\mathbf{1}}\mathbf{F}^{\mathbf{T}}$$

$$\mathbf{Q} = \begin{bmatrix}0 & 0\\ 0 & 0\\ 0 & -1\\ 1 & 0\end{bmatrix}$$

(4) After reordering these 3 matrices, the 6 by 6 sectional stiffness can be calculated as follows. This sectional stiffness matrix will be transformed into 1D space frame member natural stiffness matrix.

$$\begin{Bmatrix} F_1 \\ F_2 \\ F_3 \\ M_1 \\ M_2 \\ M_3 \end{Bmatrix} = \begin{bmatrix} C_{11} & C_{12} & C_{13} & C_{13} & C_{13} & C_{13} \\ & C_{22} & C_{23} & C_{24} & C_{25} & C_{26} \\ & & C_{33} & C_{34} & C_{35} & C_{36} \\ & & & C_{44} & C_{45} & C_{46} \\ & Sym. & & & C_{55} & C_{56} \\ & & & & & C_{66} \end{bmatrix} \cdot \begin{Bmatrix} e_1 \\ e_2 \\ e_3 \\ \kappa_1 \\ \kappa_2 \\ \kappa_3 \end{Bmatrix} \qquad \textbf{(C-20)}$$

(5) After inversing the stiffness matrix above, a sectional flexibility matrix also can be found. With the flexibility matrix, a shear center by using the equilibrium condition to prevent no twisting for arbitrary forces on section.

$$\begin{Bmatrix} e_1 \\ e_2 \\ e_3 \\ \kappa_1 \\ \kappa_2 \\ \kappa_3 \end{Bmatrix} = \begin{bmatrix} S_{11} & S_{12} & S_{13} & S_{13} & S_{13} & S_{13} \\ & S_{22} & S_{23} & S_{24} & S_{25} & S_{26} \\ & & S_{33} & S_{34} & S_{35} & S_{36} \\ & & & S_{44} & S_{45} & S_{46} \\ & Sym. & & & S_{55} & S_{56} \\ & & & & & S_{66} \end{bmatrix} \cdot \begin{Bmatrix} F_1 \\ F_2 \\ F_3 \\ M_1 \\ M_2 \\ M_3 \end{Bmatrix} \qquad \textbf{(C-21)}$$

$$sc_2 = -\frac{S_{34}}{S_{44}}$$

$$sc_3 = \frac{S_{24}}{S_{44}}$$

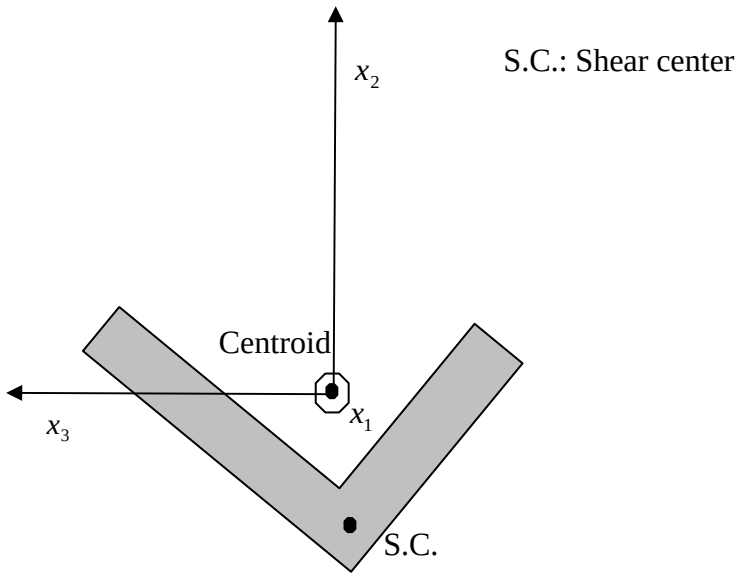

Figure C-4: Shear center location

APPENDIX D Area Properties Calculation using VABS method

The sectional stiffness presented in Appendix C can be used for a general anisotropic member cross-section. However, if the entire cross-section is composed with isotropic material, various cross-sectional properties can be obtained with highly exact accuracy.

The material rigidity matrix for an orthotropic material can be defined as follows:

$$\mathbf{D}=\begin{bmatrix} \frac{(1-\nu_{23}\nu_{32})}{\lambda}E_1 & 0 & 0 & \frac{(\nu_{12}+\nu_{13}\nu_{32})}{\lambda}E_2 & 0 & \frac{(\nu_{13}+\nu_{12}\nu_{23})}{\lambda}E_3 \\ & G_{12} & 0 & 0 & 0 & 0 \\ & & G_{13} & 0 & 0 & 0 \\ & & & \frac{(1-\nu_{31}\nu_{13})}{\lambda}E_2 & 0 & \frac{(\nu_{23}+\nu_{21}\nu_{13})}{\lambda}E_3 \\ & SYM. & & & G_{23} & 0 \\ & & & & & \frac{(1-\nu_{23}\nu_{32})}{\lambda}E_3 \end{bmatrix} \quad \textbf{(D-1)}$$

where $\lambda = 1-\nu_{12}\nu_{21}-\nu_{32}\nu_{23}-\nu_{13}\nu_{31}-2\nu_{21}\nu_{13}\nu_{32}$

If the material for the cross-section is isotropic material, the matrix **D** can be presented as follows:

$$\mathbf{D}=\begin{bmatrix} \frac{(1-\nu^2)}{\lambda}E & 0 & 0 & \frac{\nu(1+\nu)}{\lambda}E & 0 & \frac{\nu(1+\nu)}{\lambda}E \\ & G & 0 & 0 & 0 & 0 \\ & & G & 0 & 0 & 0 \\ & & & \frac{(1-\nu^2)}{\lambda}E & 0 & \frac{\nu(1+\nu)}{\lambda}E \\ & SYM. & & & G & 0 \\ & & & & & \frac{(1-\nu^2)}{\lambda}E \end{bmatrix} \quad \textbf{(D-2)}$$

where $\lambda = 1-3\nu^2-2\nu^3$

Except this material definition, all calculation procedures are same with those of anisotropic case. From the final sectional stiffness matrix obtained in Appendix C, various cross-sectional area properties can be derived by utilizing material properties. These calculated cross-sectional area properties are about principal axes:

$$\begin{Bmatrix} F_1 \\ F_2 \\ F_3 \\ M_1 \\ M_2 \\ M_3 \end{Bmatrix} = \begin{bmatrix} C_{11} & C_{12} & C_{13} & C_{13} & C_{13} & C_{13} \\ & C_{22} & C_{23} & C_{24} & C_{25} & C_{26} \\ & & C_{33} & C_{34} & C_{35} & C_{36} \\ & & & C_{44} & C_{45} & C_{46} \\ & \textit{Sym.} & & & C_{55} & C_{56} \\ & & & & & C_{66} \end{bmatrix} \cdot \begin{Bmatrix} e_1 \\ e_2 \\ e_3 \\ \kappa_1 \\ \kappa_2 \\ \kappa_3 \end{Bmatrix} \qquad \textbf{(D-3)}$$

Area $A_1 = \dfrac{C_{11}}{E}$

Shear area along *y* axis $A_2 = \dfrac{C_{22}}{G}$

Shear area along *z* axis $A_3 = \dfrac{C_{33}}{G}$

St. Venant torsional constant $J = I_1 = \dfrac{C_{44}}{G}$

Moment of inertia about axis x_2 $I_2 = \dfrac{C_{55}}{E}$

Moment of inertia about axis x_3 $I_3 = \dfrac{C_{66}}{E}$

Cross product of moment $I_{23} = \dfrac{C_{56}}{E}$

APPENDIX E Fixed-End-Forces Formulation for an Anisotropic Structural Member

In this Section, an explicit equation for fixed-end-forces for general anisotropic structural members is presented. A fixed-end-force is a key concept to account for applied member force in the stiffness analysis procedure. Member forces applied to general anisotropic structural members whose stiffnesses are represented by the 6 by 6 cross-sectional stiffness matrix, **S** (Appendix C), can be transformed into equivalent joint forces on the joints to which the member ends are connected. The explicit forms for a concentrated force and moment and a linearly distributed force and moment are presented in this Section.

The Fixed-End-Member forces can be obtained by solving for the reactions of a fixed-fixed member. To solve for the reactions of the fixed-fixed member, one end of the member (all six degrees of freedom) can be selected as 'redundant' forces and then released to create a cantilever member. This cantilever member corresponds to the 'primary structure' in a general indeterminate frame analysis solution. Section E-1 describes member end displacement of the cantilever (primary structure). Section E-2 presents the Fixed-End-Member force solution for a member with concentrated member forces and moments. Section E-3 presents the fixed-end-member forces solution for a member with lineally distributed member forces and moments.

E-1 Member End Displacements for a Cantilever Member Using the Member Sectional Stiffness Approach

One-dimensional deformation measures and resultant forces in the cross-section of a structural member can be related with so called a 'Sectional Stiffness', **S** (Appendix C). This 6 by 6 cross-sectional stiffness matrix, **S**, can be fully populated with non-zero values in case of structural members composed of anisotropic materials (Hodges, 2006). However, a sectional stiffness of cross-section composed of isotropic materials always has multiple zero terms in this sectional stiffness.

$$\begin{Bmatrix} F_x \\ F_y \\ F_z \\ M_x \\ M_y \\ M_z \end{Bmatrix} = \mathbf{S} \cdot \begin{Bmatrix} e_x \\ e_y \\ e_z \\ k_x \\ k_y \\ k_z \end{Bmatrix} \qquad \textbf{(E-1)}$$

where

$$\mathbf{S} = \begin{bmatrix} S_{11} & S_{12} & S_{13} & S_{14} & S_{15} & S_{16} \\ & S_{23} & S_{24} & S_{24} & S_{25} & S_{26} \\ & & S_{33} & S_{34} & S_{35} & S_{36} \\ & & & S_{44} & S_{45} & S_{46} \\ & & & & S_{55} & S_{56} \\ & & & & & S_{66} \end{bmatrix} : \text{Sectional stiffness matrix}$$

e_x: axial deformation measure along axis x

e_y, e_z: shear deformation measure along axes y and z.

k_x: rotation rate about axis x.

k_y, k_z: curvatures about axes y and z.

F_x: axial force resultant along axis x.

F_y, F_z: shear force resultants along axes y, z.

M_x: torsional force resultant about axis x.

M_y, M_z: moment resultant about axes y and z.

To derive displacement along member, the cross-sectional flexibility matrix, $\mathbf{\Phi}$, is calculated by inverting the sectional stiffness matrix in Eq. E-1 resulting in:

$$\begin{Bmatrix} e_x \\ e_y \\ e_z \\ k_x \\ k_y \\ k_z \end{Bmatrix} = S^{-1} \cdot \begin{Bmatrix} F_x \\ F_y \\ F_z \\ M_x \\ M_y \\ M_z \end{Bmatrix} = \mathbf{\Phi} \cdot \begin{Bmatrix} F_x \\ F_y \\ F_z \\ M_x \\ M_y \\ M_z \end{Bmatrix} \qquad \textbf{(E-2)}$$

where

$$\mathbf{\Phi} = \begin{bmatrix} \Phi_{11} & \Phi_{12} & \Phi_{13} & \Phi_{14} & \Phi_{15} & \Phi_{16} \\ & \Phi_{23} & \Phi_{24} & \Phi_{24} & \Phi_{25} & \Phi_{26} \\ & & \Phi_{33} & \Phi_{34} & \Phi_{35} & \Phi_{36} \\ & & & \Phi_{44} & \Phi_{45} & \Phi_{46} \\ & & & & \Phi_{55} & \Phi_{56} \\ & & & & & \Phi_{66} \end{bmatrix}$$

Eq. E-2 can be expressed with simple form as follows:

$$\begin{Bmatrix} \bar{e} \\ \bar{k} \end{Bmatrix} = \mathbf{\Phi} \cdot \begin{Bmatrix} \bar{F} \\ \bar{M} \end{Bmatrix} = \begin{bmatrix} \mathbf{R} & \mathbf{Z} \\ \mathbf{Z}^T & \mathbf{T} \end{bmatrix} \cdot \begin{Bmatrix} \bar{F} \\ \bar{M} \end{Bmatrix} \qquad \textbf{(E-3)}$$

where

$$\bar{e} = \begin{Bmatrix} e_x \\ e_y \\ e_z \end{Bmatrix},\ \bar{k} = \begin{Bmatrix} k_x \\ k_y \\ k_z \end{Bmatrix},\ \bar{F} = \begin{Bmatrix} F_x \\ F_y \\ F_z \end{Bmatrix},\ \bar{M} = \begin{Bmatrix} M_x \\ M_y \\ M_z \end{Bmatrix}$$

R, **Z**, and **T** matrices are 3 by 3 sub-matrices from the 6 by 6 cross-sectional flexibility matrix, $\mathbf{\Phi}$, in Eq. E-2.

The member end displacement vector, $\begin{bmatrix} u_x & u_y & u_z & \omega_x & \omega_y & \omega_z \end{bmatrix}^T$, of a cantilever member with arbitrary length, x, under a member end concentrated force

vector $\begin{bmatrix} P_x & P_y & P_z & Q_x & Q_y & Q_z \end{bmatrix}^T$ can be represented as a function of the length of x (Figure E-1). The relationship of a member end displacement and a member end forces of a cantilever member are represented by using Sectional Analysis Procedures for anisotropic structural member (Hodges, 2006, page 117) as follows:

$$\begin{Bmatrix} \bar{u}(x) \\ \bar{\omega}(x) \end{Bmatrix} = \begin{bmatrix} x\mathbf{R} + \frac{x^2}{2}\left(\mathbf{ZC} - \mathbf{CZ}^T\right) - \frac{x^3}{3}\mathbf{CTC} & x\mathbf{Z} - \frac{x^2}{2}\mathbf{CT} \\ x\mathbf{Z}^T + \frac{x^2}{2}\mathbf{TC} & x\mathbf{T} \end{bmatrix} \cdot \begin{Bmatrix} \bar{P} \\ \bar{Q} \end{Bmatrix} \qquad \textbf{(E-4)}$$

where

$$\mathbf{C} = \begin{bmatrix} 0 & 0 & 0 \\ 0 & 0 & -1 \\ 0 & 1 & 0 \end{bmatrix}$$

$\bar{u}(x)$: vector of displacement of member end

$\bar{\omega}(x)$: vector of rotation of member end

$\bar{P}$: vector of applied force at the root end

$\bar{Q}$: vector of applied moment root end

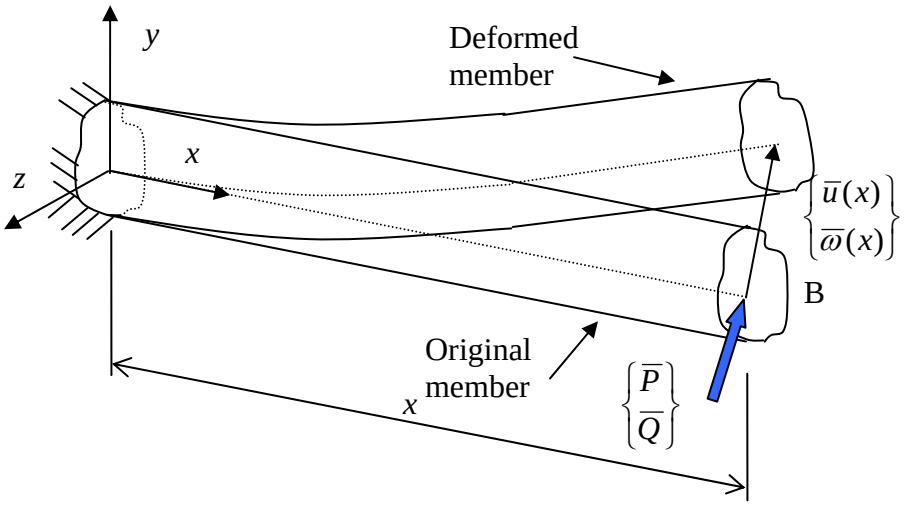

Figure E-1: End loaded prismatic cantilever member

E-2 Fixed-End-Forces for Concentrated Member Forces and Moments

Fixed-end-forces for concentrated member forces and moments are calculated in this section utilizing the cantilever problem described in previous Section E-1. Figure E-2 presented a cantilever with concentrated forces and moments $\left[\overline{P}_a^T \quad \overline{Q}_a^T\right]^T$ at distance 'a' from fixed support of the cantilever member. Figure E-3 shows the cross-section of the member in Figure E-2. The procedure to find the displacement of the cantilever member end corresponds to a 'CASE 0' procedure in a general indeterminate method of superposition frame analysis procedure.

The displacement vector $\left[\overline{u}_a^T \quad \overline{\varpi}_a^T\right]^T$ at the point under the applied concentrated member force vector $\left[\overline{P}_a^T \quad \overline{Q}_a^T\right]^T$ can be calculated by replacing the variable *x* in Eq. E-4 with *a*, the location of the concentrated member forces and moments as follows:

$$\begin{Bmatrix} \overline{u}(x) \\ \overline{\varpi}(x) \end{Bmatrix} = \begin{bmatrix} x\mathbf{R} + \frac{x^2}{2}(\mathbf{ZC} - \mathbf{CZ}^T) - \frac{x^3}{3}\mathbf{CTC} & x\mathbf{Z} - \frac{x^2}{2}\mathbf{CT} \\ x\mathbf{Z}^T + \frac{x^2}{2}\mathbf{TC} & x\mathbf{T} \end{bmatrix} \begin{Bmatrix} \overline{P}(x) \\ \overline{Q}(x) \end{Bmatrix} \qquad \textbf{(E-5)}$$

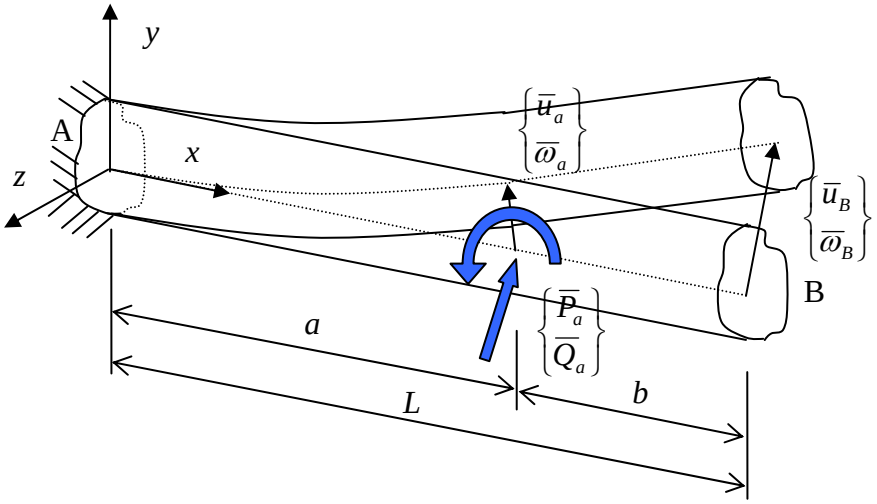

Figure E-2: Cantilever member under a member concentrated forces and moments

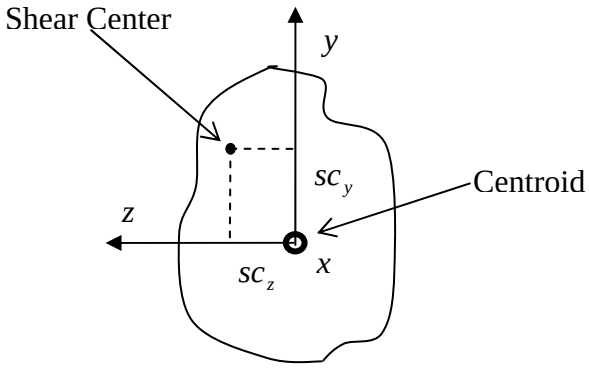

where sc_x, sc_y are coordinates of the shear-center in terms of member local axes *y* and *z*

Figure E-3: Cross-section of a structural member

Because the member is straight in a range between x = *a* and x = *L* (member end-end) (Figure E-2), the displacement vector $\left[\bar{u}_B^T \quad \bar{\varpi}_B^T\right]^T$ can be calculated from a geometry relationship of displacements as follows (Eq. E-6). u_x^B , u_y^B , u_z^B are displacements at the end of the cantilever, while ω_x^B , ω_y^B , ω_z^B are the rotations at the end of the cantilever in the Equation E-21.

$$u_x^B = u_x^a \qquad \textbf{(E-6a)}$$

$$u_y^B = u_y^a + b\omega_z^a \qquad \textbf{(E-6b)}$$

$$u_z^B = u_z^a - b\omega_y^a \qquad \textbf{(E-6c)}$$

$$\omega_x^B = \omega_x^a \qquad \textbf{(E-6d)}$$

$$\omega_y^B = \omega_y^a \qquad \textbf{(E-6e)}$$

$$\omega_z^B = \omega_z^a \qquad \textbf{(E-6f)}$$

Equations E-6a to E-6f can be represented in matrix form as follows:

$$\begin{Bmatrix} \bar{u}_B \\ \bar{\omega}_B \end{Bmatrix} = \begin{Bmatrix} \bar{u}_a \\ \bar{\omega}_a \end{Bmatrix} + \begin{Bmatrix} -b\bar{i} \times \bar{\omega}_a \\ \bar{0} \end{Bmatrix} = \begin{bmatrix} \mathbf{I} & -b\mathbf{C} \\ \mathbf{O} & \mathbf{I} \end{bmatrix} \begin{Bmatrix} \bar{u}_a \\ \bar{\omega}_a \end{Bmatrix} \qquad \textbf{(E-7)}^{13}$$

where

$$\bar{u}_B = \begin{Bmatrix} u_x^B \\ u_y^B \\ u_z^B \end{Bmatrix}, \quad \bar{\varpi}_B = \begin{Bmatrix} \omega_x^B \\ \omega_y^B \\ \omega_z^B \end{Bmatrix}, \quad \bar{i} = \begin{Bmatrix} 1 \\ 0 \\ 0 \end{Bmatrix}, \quad \bar{0} = \begin{Bmatrix} 0 \\ 0 \\ 0 \end{Bmatrix}, \quad \mathbf{O} = \begin{Bmatrix} 0 & 0 & 0 \\ 0 & 0 & 0 \\ 0 & 0 & 0 \end{Bmatrix}, \; b = L - a \,,$$

The following procedure corresponds to the ‘CASE 1’ of general indeterminate method of superposition frame analysis procedure. Considering compatibility condition of the cantilever, the following condition is satisfied.

13 : × is a cross product operator

$$\begin{Bmatrix} \overline{u}_B \\ \overline{\omega}_B \end{Bmatrix} + \begin{Bmatrix} \overline{u}_B \\ \overline{\omega}_B \end{Bmatrix}_{\mathrm{Re}.B} = \begin{Bmatrix} \overline{0} \\ \overline{0} \end{Bmatrix}$$

where

$\begin{Bmatrix} \overline{u}_B \\ \overline{\omega}_B \end{Bmatrix}$ = 6 by 1 displacements and rotations vector of member end 'B' under member loading as described in previous page.

$\begin{Bmatrix} \overline{u}_B \\ \overline{\omega}_B \end{Bmatrix}_{\mathrm{Re}.B}$ = 6 by 1 displacements and rotations vector of member end 'B' under force and moment under member end 'B' (which is same with reaction at joint at member end 'B').

This vector corresponds to the displacements and rotations vector of the cantilever member end for 'CASE 1' in a general indeterminate method of frame analysis procedure.

$$\begin{Bmatrix} \overline{u}_B \\ \overline{\omega}_B \end{Bmatrix}_{\mathrm{Re}.B} = -\begin{Bmatrix} \overline{u}_B \\ \overline{\omega}_B \end{Bmatrix}$$

However, reactions at the joint where the member end 'B' and fixed-end-forces at member end 'B' are 'equal and opposite forces'.

A member flexibility matrix $\mathbf{F}_{BB}$ can be obtained by substituting L for x in Equation E-4 The member flexibility matrix $\mathbf{F}_{BB}$ relates an applied member concentrated force vector at B, $\begin{bmatrix} \overline{F}_B^T & \overline{M}_B^T \end{bmatrix}^T$ and displacement vector $\begin{bmatrix} \overline{u}_B^T & \overline{\omega}_B^T \end{bmatrix}^T$ at member end B as follows:

$$\begin{Bmatrix} \overline{u}_B \\ \overline{\omega}_B \end{Bmatrix} = \mathbf{F}_{BB} \begin{Bmatrix} \overline{F}_B \\ \overline{M}_B \end{Bmatrix} \qquad \textbf{(E-8)}$$

where

$$\mathbf{F}_{BB} = \begin{bmatrix} L\mathbf{R} + \frac{L^2}{2}(\mathbf{ZC} - \mathbf{CZ}^T) - \frac{L^3}{3}\mathbf{CTC} & L\mathbf{Z} - \frac{L^2}{2}\mathbf{CT} \\ L\mathbf{Z}^T + \frac{L^2}{2}\mathbf{TC} & L\mathbf{T} \end{bmatrix}$$

By combining Equations E-7 and E-8, the applied concentrated member force vector at cantilever member end 'B' can be represented in terms of displacement vector at loading point at 'a'.

$$\begin{Bmatrix} \overline{F}_B \\ \overline{M}_B \end{Bmatrix} = \mathbf{F}_{BB}^{-1} \begin{bmatrix} \mathbf{I} & -b\mathbf{C} \\ \mathbf{O} & \mathbf{I} \end{bmatrix} \begin{Bmatrix} \overline{u}_a \\ \overline{\omega}_a \end{Bmatrix} \qquad \textbf{(E-9)}$$

By using Equation E-5, the fixed-member end forces and moment vector can be represented with a given applied member concentrated force and moment vector $\begin{bmatrix} \overline{P}_a^T & \overline{Q}_a^T \end{bmatrix}^T$ as follows:

$$\begin{Bmatrix} \overline{F}_B \\ \overline{M}_B \end{Bmatrix} = \mathbf{F}_{BB}^{-1} \begin{bmatrix} \mathbf{I} & -b\mathbf{C} \\ \mathbf{O} & \mathbf{I} \end{bmatrix} \begin{bmatrix} a\mathbf{R} + \frac{a^2}{2}\left(\mathbf{ZC} - \mathbf{CZ}^T\right) - \frac{a^3}{2}\mathbf{CTC} & a\mathbf{Z} - \frac{a^2}{2}\mathbf{CT} \\ a\mathbf{Z} + \frac{a^2}{2}\mathbf{TC} & a\mathbf{T} \end{bmatrix} \begin{Bmatrix} \overline{P}_a \\ \overline{Q}_a \end{Bmatrix} \qquad \textbf{(E-10)}$$

Equation E-10 can be simplified to the following form and this result can be used to get fixed-end forces at member end 'B' when a member has an arbitrary concentrated force on fixed-fixed member.

$$\begin{Bmatrix} \overline{F}_B \\ \overline{M}_B \end{Bmatrix} = \mathbf{F}_{BB}^{-1} \cdot \begin{bmatrix} \mathbf{D}_{11} & \mathbf{D}_{12} \\ \mathbf{D}_{21} & \mathbf{D}_{22} \end{bmatrix} \begin{Bmatrix} \overline{P}_a \\ \overline{Q}_a \end{Bmatrix} \qquad \textbf{(E-11)}$$

where

$$\mathbf{D}_{11} = a\mathbf{R} + \frac{a^2}{2}\mathbf{ZC} + \left(\frac{a^2}{2} - La\right)\mathbf{CZ}^T + \left(\frac{a^3}{6} - \frac{La^2}{2}\right)\mathbf{CTC}$$

$$\mathbf{D}_{12} = a\mathbf{Z} + \left(\frac{a^2}{2} - La\right)\mathbf{CT}$$

$$\mathbf{D}_{21} = a\mathbf{Z}^T + \frac{a^2}{2}\mathbf{TC}$$

$$\mathbf{D}_{22} = a\mathbf{T}$$

and where the size of $\mathbf{D}_{ij}$ (i=1,2, j=1,2) matrices is 3 by 3

Now, the other end of the original indeterminate structure has to be calculated. A fixed-end force vector at member end 'A' can be obtained from a force translation relationship. The fixed-end-forces vector at member end 'B' and a applied member concentrated force vector $\left[\overline{P}_a^T \quad \overline{Q}_a^T\right]^T$ must be transformed to member end 'A'.

General force transformation matrix is represented as follows:

$$\mathbf{T}_F = \begin{bmatrix} 1 & 0 & 0 & 0 & 0 & 0 \\ 0 & 1 & 0 & 0 & 0 & 0 \\ 0 & 0 & 1 & 0 & 0 & 0 \\ 0 & W & V & 1 & 0 & 0 \\ -W & 0 & U & 0 & 1 & 0 \\ V & -U & 0 & 0 & 0 & 1 \end{bmatrix} \qquad \textbf{(E-12)}$$

where

U,*V*, and *W* are translations along *x*,*y*, and *z* axes respectively.

Previously calculated member end forces vector at member end 'B' (Eq. E-11) can be transformed into equivalent force vector at member end 'A' by using Eq. E-12. For that purpose, the parameters *U*,*V*, and *W* in Eq. E-12 can be specified as –*L*, 0, and 0, respectively. The equation can be represented as follows:

$$\mathbf{T}_F^B = \begin{bmatrix} \mathbf{I} & \mathbf{O} \\ L\mathbf{C} & \mathbf{I} \end{bmatrix} \tag{E-13}$$

Similarly, the force transformation vector for the applied member concentrated forces and moments applied at $x = a$ on the member can be transformed into equivalent force vector by using following force transformation matrix

$$\mathbf{T}_F^a = \begin{bmatrix} \mathbf{I} & \mathbf{O} \\ a\mathbf{C} & \mathbf{I} \end{bmatrix} \tag{E-14}$$

Because the summation of all forces at member end 'A' must satisfy the equilibrium condition, the unknown member-end forces at member end 'A' can be determined from the following equation.

$$\begin{Bmatrix} \overline{F}_A \\ \overline{M}_A \end{Bmatrix} + \mathbf{T}_F^B \begin{Bmatrix} \overline{F}_B \\ \overline{M}_B \end{Bmatrix} + \mathbf{T}_F^a \begin{Bmatrix} \overline{F}_B \\ \overline{M}_B \end{Bmatrix} = \overline{0} \tag{E-15}$$

In summary, the fixed-end-force vectors at member ends 'A and 'B' for externally applied member concentrated forces and moments on a general anisotropic structural member can be defined as follows (Figure E-4). At member end 'B':

$$\begin{Bmatrix} \overline{F}_B \\ \overline{M}_B \end{Bmatrix} = \mathbf{F}_{BB}^{-1} \cdot \begin{bmatrix} \mathbf{D}_{11} & \mathbf{D}_{12} \\ \mathbf{D}_{21} & \mathbf{D}_{22} \end{bmatrix} \begin{Bmatrix} \overline{P}_a \\ \overline{Q}_a \end{Bmatrix} \tag{E-16}$$

where

$$\mathbf{D}_{11} = a\mathbf{R} + \frac{a^2}{2}\mathbf{ZC} + \left(\frac{a^2}{2} - La\right)\mathbf{CZ}^T + \left(\frac{a^3}{6} - \frac{La^2}{2}\right)\mathbf{CTC}$$

$$\mathbf{D}_{12} = a\mathbf{Z} + \left(\frac{a^2}{2} - La\right)\mathbf{CT}$$

$$\mathbf{D}_{21} = a\mathbf{Z}^T + \frac{a^2}{2}\mathbf{TC}$$

$$\mathbf{D}_{22} = a\mathbf{T}$$

At member end ‘A’:

$$\begin{Bmatrix} \overline{F}_A \\ \overline{M}_A \end{Bmatrix} = -\mathbf{T}_F^B \begin{Bmatrix} \overline{F}_B \\ \overline{M}_B \end{Bmatrix} - \mathbf{T}_F^a \begin{Bmatrix} \overline{F}_B \\ \overline{M}_B \end{Bmatrix} \qquad \textbf{(E-17)}$$

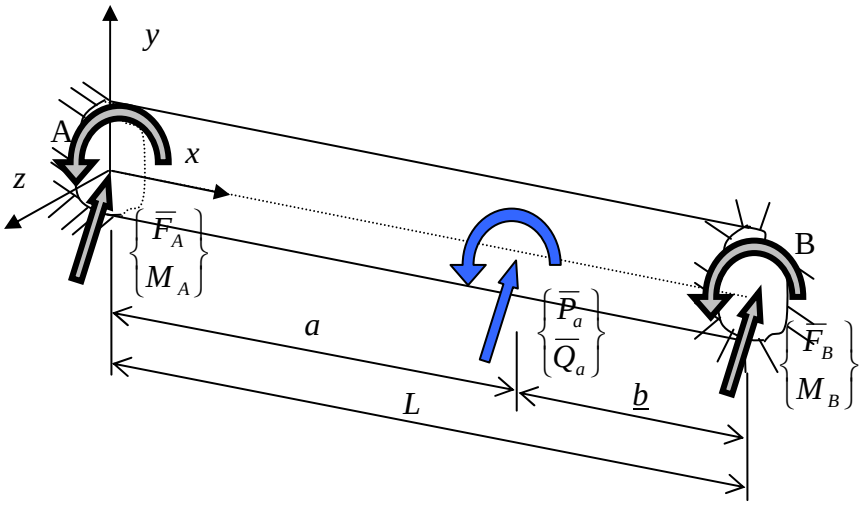

Figure E-4: Fixed-end-forces for concentrated member forces and moment under anisotropic structural member

E-3 Fixed-End-Forces for Linearly Distributed Member Forces and Moments

Fixed-end-forces for linearly distributed member forces and moments can be calculated by extending a previously presented case associated with fixed-end-forces for concentrated member forces and moments. The forces and moments at the specific point of member can be treated as a function of x ($\bar{p}(x)$ and $\bar{q}(x)$ respectively), and the function can be integrated to obtain the member end displacement at 'B'. Figure E-5 represents the primary structure of both fixed member case.

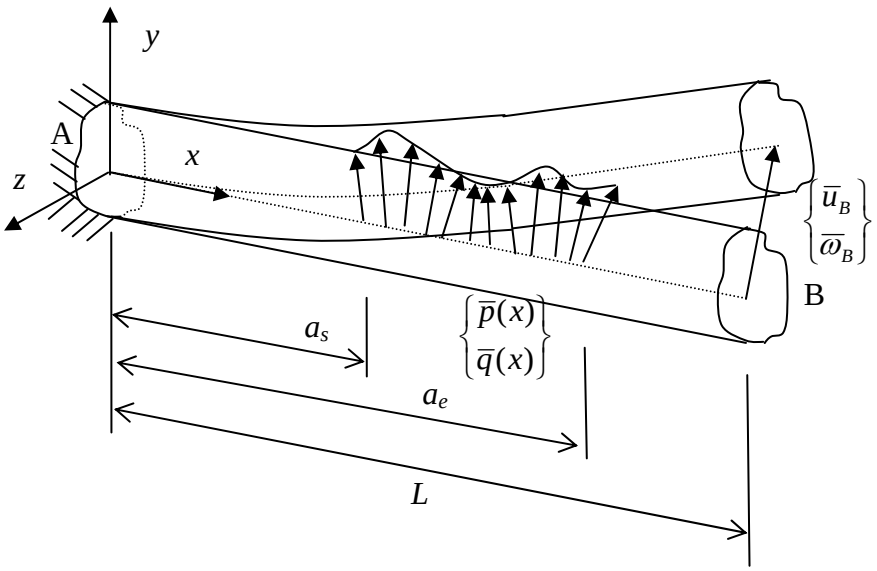

Figure E-5: Cantilever member with an arbitrary distributed member forces and moments

The displacement of member end 'B' can be determined by integrating the displacements caused by an applied member concentrated forces and moments in a specific range of the member. In this case, the fixed-end-forces vector at member end 'B' can be represented as a function in terms of x. Then, Equation E-11 can be presented as a function of x as follows:

$$\begin{Bmatrix} \overline{F}_B \\ \overline{M}_B \end{Bmatrix} = \mathbf{F}_{BB}{}^{-1} \begin{bmatrix} \mathbf{D}_{11}(x) & \mathbf{D}_{12}(x) \\ \mathbf{D}_{21}(x) & \mathbf{D}_{22}(x) \end{bmatrix} \begin{Bmatrix} \overline{P}(x) \\ \overline{Q}(x) \end{Bmatrix} \quad \textbf{(E-18)}$$

where

$$\mathbf{D}_{11}(x) = x\mathbf{R} + \frac{x^2}{2}\mathbf{ZC} + \left(\frac{x^2}{2} - Lx\right)\mathbf{CZ}^T + \left(\frac{x^3}{6} - \frac{Lx^2}{2}\right)\mathbf{CTC}$$

$$\mathbf{D}_{12}(x) = x\mathbf{Z} + \left(\frac{x^2}{2} - Lx\right)\mathbf{CT}$$

$$\mathbf{D}_{21}(x) = x\mathbf{Z}^T + \frac{x^2}{2}\mathbf{TC}$$

$$\mathbf{D}_{22}(x) = x\mathbf{T}$$

If external member forces and moments are applied in a range between a_s and a_e along x, the fixed-end-force in the member end 'B' can be represented as following integration equation.

$$\begin{Bmatrix} \overline{F}_B \\ \overline{M}_B \end{Bmatrix} = \mathbf{F}_{BB}^{-1} \int_{a_s}^{a_e} \left(\begin{bmatrix} \mathbf{D}_{11}(x) & \mathbf{D}_{12}(x) \\ \mathbf{D}_{21}(x) & \mathbf{D}_{22}(x) \end{bmatrix} \begin{Bmatrix} \overline{p}(x) \\ \overline{q}(x) \end{Bmatrix} \right) dx \quad \textbf{(E-19)}$$

If external linearly distributed member forces and moments are applied between a_s and a_e, the external member forces function vector for the linearly distributed member force vector $\begin{bmatrix} \overline{p}(x)^T & \overline{q}(x)^T \end{bmatrix}^T$ can be determined as (Eq. E-21). $\begin{bmatrix} \overline{p}_s^T & \overline{q}_s^T \end{bmatrix}^T$, $\begin{bmatrix} \overline{p}_e^T & \overline{q}_e^T \end{bmatrix}^T$ are vectors with magnitudes of applied member forces and moments at the loading starting and ending location a_s and a_e respectively.

$$\begin{Bmatrix} \overline{p}(x) \\ \overline{q}(x) \end{Bmatrix} = \left(\frac{x - a_s}{a_e - a_s}\right) \begin{Bmatrix} \overline{p}_e \\ \overline{q}_e \end{Bmatrix} - \left(\frac{x - a_e}{a_e - a_s}\right) \begin{Bmatrix} \overline{p}_s \\ \overline{q}_s \end{Bmatrix} \quad \textbf{(E-20)}$$

By using above member loading function, the Equation E-19 turns into as follows:

$$\begin{Bmatrix} \overline{F}_B \\ \overline{M}_B \end{Bmatrix} = \mathbf{F}_{BB}^{-1} \begin{Bmatrix} \overline{G}_1 \\ \overline{G}_2 \end{Bmatrix} \qquad \textbf{(E-21)}$$

where

$$\begin{aligned}
\overline{G}_1 = \quad & \mathbf{R}\frac{1}{c_1}\left[\left(\frac{c_3}{3}-\frac{a_s c_2}{2}\right)\overline{p}_e-\left(\frac{c_3}{3}-\frac{a_e c_2}{2}\right)\overline{p}_s\right] + \\
& \mathbf{ZC}\frac{1}{2c_1}\left[\left(\frac{c_4}{4}-\frac{a_s c_3}{3}\right)\overline{p}_e-\left(\frac{c_4}{4}-\frac{a_e c_3}{3}\right)\overline{p}_s\right] + \\
& \mathbf{CZ}^T\frac{1}{c_1}\left\{\left[\frac{c_4}{8}-\frac{(L+a_s/2)c_3}{3}+\frac{La_s c_2}{2}\right]\overline{p}_e-\left[\frac{c_4}{8}-\frac{(L+a_e/2)c_3}{3}+\frac{La_e c_2}{2}\right]\overline{p}_s\right\} + \\
& \mathbf{CTC}\frac{1}{2c_1}\left\{\left[\frac{c_5}{15}-\frac{(L+a_s/3)c_4}{4}+\frac{La_s c_3}{3}\right]\overline{p}_e-\left[\frac{c_5}{15}-\frac{(L+a_e/3)c_4}{4}+\frac{La_e c_3}{3}\right]\overline{p}_s\right\} + \\
& \mathbf{Z}\frac{1}{c_1}\left[\left(\frac{c_3}{3}-\frac{a_s c_2}{2}\right)\overline{q}_e-\left(\frac{c_3}{3}-\frac{a_e c_2}{2}\right)\overline{q}_s\right] + \\
& \mathbf{CT}\frac{1}{c_1}\left\{\left[\frac{c_4}{8}-\frac{(L+a_s/2)c_3}{3}+\frac{La_s c_2}{2}\right]\overline{q}_e-\left[\frac{c_4}{8}-\frac{(L+a_e/2)c_3}{3}+\frac{La_e c_2}{2}\right]\overline{q}_s\right\}
\end{aligned}$$

$$\begin{aligned}
\overline{G}_2 = \quad & \mathbf{Z}^T\frac{1}{c_1}\left[\left(\frac{c_3}{3}-\frac{a_s c_2}{2}\right)\overline{p}_e-\left(\frac{c_3}{3}-\frac{a_e c_2}{2}\right)\overline{p}_s\right] + \\
& \mathbf{TC}\frac{1}{2c_1}\left[\left(\frac{c_4}{4}-\frac{a_s c_3}{3}\right)\overline{p}_e-\left(\frac{c_4}{4}-\frac{a_e c_3}{3}\right)\overline{p}_s\right] + \\
& \mathbf{T}\frac{1}{c_1}\left[\left(\frac{c_3}{3}-\frac{a_s c_2}{2}\right)\overline{q}_e-\left(\frac{c_3}{3}-\frac{a_e c_2}{2}\right)\overline{q}_s\right]
\end{aligned}$$

$$c_i = (a_e)^i - (a_a)^i \quad (i = 1,2,3,4,5)$$

A fixed-end-force vector at member end ‘A’ can be calculated from a force translation relationship as follows:

$$\begin{Bmatrix} \overline{F}_A \\ \overline{M}_A \end{Bmatrix} = -\mathbf{T}_F^B \begin{Bmatrix} \overline{F}_B \\ \overline{M}_B \end{Bmatrix} - \int_{a_s}^{a_e} \left(\mathbf{T}_F^a(x) \begin{Bmatrix} \overline{p}(x) \\ \overline{q}(x) \end{Bmatrix} \right) dx \qquad \textbf{(E-22)}$$

$$\begin{Bmatrix} \overline{F}_A \\ \overline{M}_A \end{Bmatrix} = -\mathbf{T}_F^B \begin{Bmatrix} \overline{F}_B \\ \overline{M}_B \end{Bmatrix} - \int_{a_s}^{a_e} \left(\begin{bmatrix} \mathbf{I} & \mathbf{O} \\ x\mathbf{C} & \mathbf{I} \end{bmatrix} \begin{Bmatrix} \overline{p}(x) \\ \overline{q}(x) \end{Bmatrix} \right) dx \qquad \textbf{(E-23)}$$

Then, fixed-end-force vector at member end 'A' for linear distributed member loading can be calculated as follows:

$$\begin{Bmatrix} \overline{F}_A \\ \overline{M}_A \end{Bmatrix} = -\mathbf{T}_F^B \begin{Bmatrix} \overline{F}_B \\ \overline{M}_B \end{Bmatrix} - \begin{Bmatrix} \overline{P}_{Lin} \\ \overline{Q}_{Lin} \end{Bmatrix} \qquad \textbf{(E-24)}$$

where

$$\overline{P}_{Lin} = \frac{1}{c_1}\left[\left(\frac{c_2}{2} - a_s c_1\right)\overline{p}_e - \left(\frac{c_2}{2} - a_e c_1\right)\overline{p}_s\right]$$

$$\overline{Q}_{Lin} = \mathbf{C}\frac{1}{c_1}\left[\left(\frac{c_3}{3} - \frac{a_s c_2}{2}\right)\overline{p}_e - \left(\frac{c_3}{3} - \frac{a_e c_2}{2}\right)\overline{p}_s\right] + \frac{1}{c_1}\left[\left(\frac{c_2}{2} - a_s c_1\right)\overline{q}_e - \left(\frac{c_2}{2} - a_e c_1\right)\overline{q}_s\right]$$

$$c_i = (a_e)^i - (a_a)^i \quad (\ i = 1,2\ )$$

Finally, the fixed-end-force vectors at member end 'A and 'B' for linearly distributed member forces and moments applied to general anisotropic structural member, can be defined as follows (Figure E-6) at member end 'B':

$$\begin{Bmatrix} \overline{F}_B \\ \overline{M}_B \end{Bmatrix} = \mathbf{F}_{BB}^{-1} \begin{Bmatrix} \overline{G}_1 \\ \overline{G}_2 \end{Bmatrix} \qquad \textbf{(E-25)}$$

where

$$\begin{aligned}
\overline{G}_1 = \quad & \mathbf{R}\frac{1}{c_1}\left[\left(\frac{c_3}{3} - \frac{a_s c_2}{2}\right)\overline{p}_e - \left(\frac{c_3}{3} - \frac{a_e c_2}{2}\right)\overline{p}_s\right] + \\
& \mathbf{ZC}\frac{1}{2c_1}\left[\left(\frac{c_4}{4} - \frac{a_s c_3}{3}\right)\overline{p}_e - \left(\frac{c_4}{4} - \frac{a_e c_3}{3}\right)\overline{p}_s\right] + \\
& \mathbf{CZ}^T\frac{1}{c_1}\left\{\left[\frac{c_4}{8} - \frac{(L + a_s/2)c_3}{3} + \frac{L a_s c_2}{2}\right]\overline{p}_e - \left[\frac{c_4}{8} - \frac{(L + a_e/2)c_3}{3} + \frac{L a_e c_2}{2}\right]\overline{p}_s\right\} + \\
& \mathbf{CTC}\frac{1}{2c_1}\left\{\left[\frac{c_5}{15} - \frac{(L + a_s/3)c_4}{4} + \frac{L a_s c_3}{3}\right]\overline{p}_e - \left[\frac{c_5}{15} - \frac{(L + a_e/3)c_4}{4} + \frac{L a_e c_3}{3}\right]\overline{p}_s\right\} + \\
& \mathbf{Z}\frac{1}{c_1}\left[\left(\frac{c_3}{3} - \frac{a_s c_2}{2}\right)\overline{q}_e - \left(\frac{c_3}{3} - \frac{a_e c_2}{2}\right)\overline{q}_s\right] +
\end{aligned}$$

$$\mathbf{CT}\frac{1}{c_1}\left\{\left[\frac{c_4}{8}-\frac{(L+a_s/2)c_3}{3}+\frac{La_sc_2}{2}\right]\overline{q}_e-\left[\frac{c_4}{8}-\frac{(L+a_e/2)c_3}{3}+\frac{La_ec_2}{2}\right]\overline{q}_s\right\}$$

$$\overline{G}_2 = \mathbf{Z}^T\frac{1}{c_1}\left[\left(\frac{c_3}{3}-\frac{a_sc_2}{2}\right)\overline{p}_e-\left(\frac{c_3}{3}-\frac{a_ec_2}{2}\right)\overline{p}_s\right]+$$

$$\mathbf{TC}\frac{1}{2c_1}\left[\left(\frac{c_4}{4}-\frac{a_sc_3}{3}\right)\overline{p}_e-\left(\frac{c_4}{4}-\frac{a_ec_3}{3}\right)\overline{p}_s\right]+$$

$$\mathbf{T}\frac{1}{c_1}\left[\left(\frac{c_3}{3}-\frac{a_sc_2}{2}\right)\overline{q}_e-\left(\frac{c_3}{3}-\frac{a_ec_2}{2}\right)\overline{q}_s\right]$$

$$c_i=(a_e)^i-(a_a)^i \quad (\ i=1,2,3,4,5\ )$$

At member end ‘A’:

$$\begin{Bmatrix}\overline{F}_A\\ \overline{M}_A\end{Bmatrix}=-\mathbf{T}_F^B\begin{Bmatrix}\overline{F}_B\\ \overline{M}_B\end{Bmatrix}-\begin{Bmatrix}\overline{P}_{Lin}\\ \overline{Q}_{Lin}\end{Bmatrix} \qquad \textbf{(E-26)}$$

where

$$\overline{P}_{Lin}=\frac{1}{c_1}\left[\left(\frac{c_2}{2}-a_sc_1\right)\overline{p}_e-\left(\frac{c_2}{2}-a_ec_1\right)\overline{p}_s\right]$$

$$\overline{Q}_{Lin}=\mathbf{C}\frac{1}{c_1}\left[\left(\frac{c_3}{3}-\frac{a_sc_2}{2}\right)\overline{p}_e-\left(\frac{c_3}{3}-\frac{a_ec_2}{2}\right)\overline{p}_s\right]+\frac{1}{c_1}\left[\left(\frac{c_2}{2}-a_sc_1\right)\overline{q}_e-\left(\frac{c_2}{2}-a_ec_1\right)\overline{q}_s\right]$$

$$c_i=(a_e)^i-(a_a)^i \quad (\ i=1,2\ )$$

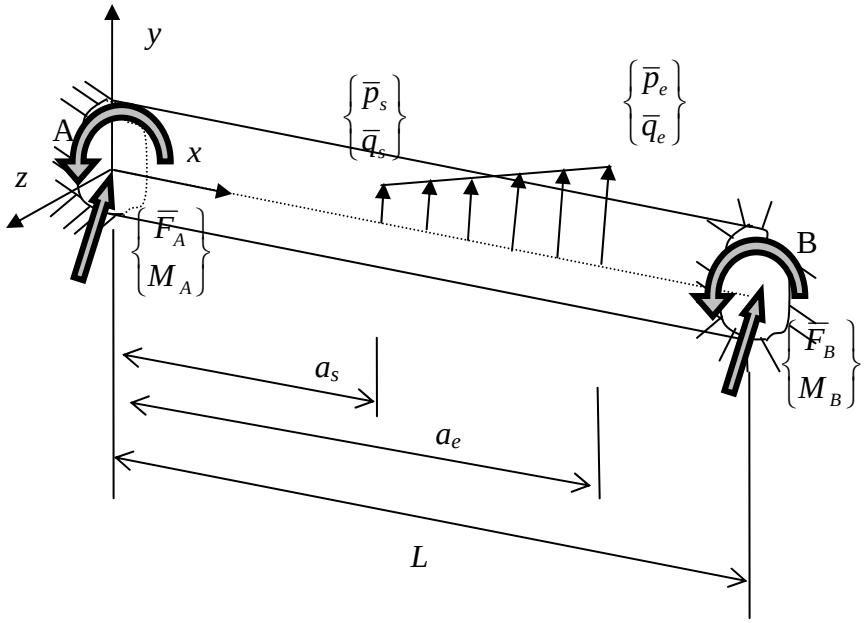

Figure E-6: Fixed-end-forces for anisotropic structural member undergoing linearly distributed member forces and moments

REFERENCES

ASCE. (2005). *Minimum Design Loads for Buildings and Other Structures,* American Society of Civil Engineers

ASTM. (1993). "Standard Test Method for Tensile Properties of Polymer Matrix Composite Materials", American Society for Testing and Materials.

ASTM. (1995). "Standard Test Method for Compressive Properties of Polymer Matrix Composite Materials with Unsupported Gage Section by Shear Loading", American Society for Testing and Materials.

ASTM. (2006). "Standard Practice for Evaluating Material Property Characteristic Values for Polymeric Composite for Civil Engineering Structural Application", American Society for Testing and Materials.

Bank, L. C. (1987). "Shear Coefficient for Thin-Walled Composite Beams" *Composite Structures*, 8(1), 47-61.

Bank, L. C. (1989). "Properties of Pultruded Fiber Reinforced Plastic Structural Members" *Transportation Research Record*, 1223, 117-124.

Bank, L. C., Mosallam, A. S., and Gonsiors, H. E. (1990) "Beam-to-Column Connections for Pultruded FRP Structures." *Servicebility and Durability of Construction Materials, Proceddings of the 1st Materials Engineering Congress*, 804-813.

Barbero, E. J., Lopez-Anido, R., and Davalos, J. F. (1993). "On the Mechanics of Thin-Walled Laminated Composite Beams" *Journal of Composite Materials*, 11(4), 806-829.

Bass, A. J., and Mottram, J. T. (1994). "Behavior of Connections in Frames of Fibre Reinforced-Polymer Section" *The Structural Engineer*, 72(17), 280-285.

Bauld, N. R., and Tzeng, L. S. (1983). "A Vlasov Theory for Fiber-Reinforced Beams with Thin-Walled Open Cross Sections" *Int. Journal of Solids Structures* 20(3), 277-297.

Berdichevsky, V. L. (1981). "On the Energy of an Elastic Rod" *Prikl. Matern. Mekhan*, 45(4), 518-529.

CASE Center, G. T. (2008). *ANALYSIS - GTSTRUDL User Guide.*

Cesnik, C. E. S. (1994). "Cross-Sectional Analysis of Initially Twisted and Curved Composite Beams", Doctoral Thesis, Aerospace Engineering, Georgia Institute of Technology.

Cesnik, C. E. S., and Hodges, D. H. (1997). "VABS: A New Concept for Composite Rotor Blade Cross-Sectional Modeling" *Journal of the American Helicopter Society*, 42(1), 27-38.

Cowper, C. R. (1966). "The Shear Coefficient in Timoshenko's Beam Theory" *Journal of Applied Mechanics*, 33, 335-340.

Creative Pultrusion, I. (2005). "Quality Assurance Test Summary Report", Creative Pultrusion, Inc.

Emkin, L. Z. (1999). "Class Notes for Matrix Analysis of Structure Course".

Gjelsvik, A. (1981). *The Theory of Thin Walled Bars*, John Wiley & Sons Inc.

Haj-Ali, R., H, K., and Muliana, A. (2007). "Nested Nonlinear Micromechanical and Structural Models for the Analysis of Thick-Section Composite Materials and Structures" *Composite Science and Technology*, 67, 1993-2004.

Haj-Ali, R., Kilic, H., and Zureick, A. H. (2001). "Three-Dimensional Micromechanics-Based Constitutive Framework for Analysis of Pultruded Composite Structures" *Journal of Engineering Mechanics*, 127(7), 653-660.

Halpin, J. C., and Tsai, S. W. (1969). "Effect of Environmental Factors on Composite Materials", Air Force Material Research Laboratory.

Hodges, D. H. (2006). *Nonlinear Composite Beam Theory*, AIAA.

Hodges, D. H., Atilgan, A. R., and Cesnik, C. E. (1992). "On a Simplified Strain Energy Function for Geometrically Nonlinear Behavior of Anisotropic Beams" *Composites Engineering*, 2, 513-526.

Hodges, D. H., and Danielson, D. A. (1987). "Nonlinear Beam Kinematics for Small Strains and Finite Rotations" *Vertica*, 11(3), 573-589.

Jones, R. M. (1975). *Mechanics of Composite Materials*, Scripta Book Company, Washington D.C.

Liu, X., Mosallam, A. S., and Kreiner, J. (1998) "A Numerical Investigation on Static Behavior of Pultruded Composite (PFRP) Portal Frame Structures." *43rd International SAMPE Symposium*, 1838-1846.

Mori, T., and Tanaka, T. (1973). "Average Stress in Matrix and Average Energy of Materials with Misfitting Inclusion" *Act. Metal*, Vol.21, 571-574.

Mosallam, A. S., and Bank, L. C. (1992). "Short-Term Behavior of Pultruded Fiber-Reinforced Plastic Frame" *Journal of Structural Engineering*, 118(7), 1937-1954.

Mottram, J. T., and Zheng, Y. (1996). "State-of-the-art Review on the Design of Beam-to-Column Connections for Pultruded Frames" *Composite Structures*, 35, 357-401.

Park, J. Y. (2001). "Pultruded Composite Materials under Shear Loading", Doctoral Thesis, Civil and Environmental Engineering, Georgia Institute of Technology.

Popescu, B., and Hodges, D. H. (2000). "On Asymptotically Correct Timoshenko-Like Anisotropic Beam Theory" *Int. Journal of Solids Structures*, 37, 535-558.

Rehfield, L. W., and Murthy, P. L. N. (1982). "Toward a New Engineering Theory of Bending: Fundamentals" *AIAA Journal*, 20(5), 693-699.

Saint-Venant, B. d. (1855). *Mjmoire sur la Torsion des Prismes. Paris: Mémoire des Savants Strangers*.

Smith, S. J., Parsons, I. D., and Hjelmstad, K. D. (1999). "Experimental Comparisons of Connections for Pultruded Frames" *Journal of Composite for Construction*, 3(1), 20-26.

Timoshenko, S. P. (1922). "On the Correction for Shear of Differential Equation for Transverse Vibration of Prismatic Bars" *Philosophical Magazine*, 41, 744-746.

Timoshenko, S. P. (1953). *History of Strength of Materials*.

Tsai, W. T., and Pagano, N. J. (1968). *Invariant Properties of Composite Materials*, Technomic Publishing Co., Stamford. Conn.

Turvey, G. J. (1996). "Testing of Pultruded GRP Pinned Base Rectangular Portal Frame for the EUROCOMP Project." EUROCOMP Design code and Handbook, J. L. Clarke, and Spon, F.N., ed., London, 719-741.

Turvey, G. J. (2000) "Bolted Connections in PFRP Structures." *Progress in Structural Engineering and Materials*, 146-156.

Turvey, G. J. (2001). "Pultruded GRP Frames: Simple (Conservative) Approach to Design, a Rational Alternative and Research Needs for Improved Design" Composite in Construction: A Reality.

Turvey, G. J., and Cooper, C. (2004). "Review of Tests on Bolted Joints Between Pultruded GRP Profiles" *Structures & Buildings*, 157(SB3), 211-233.

Vlasov, V. Z. (1961). *Thin-Walled Elastic Beams*, National Science Foundation and Department of Commerce.

Yu, W. (2002). "Variational Asymptotic Modeling of Composite Dimensionally Reducible Structure", Doctoral Thesis, Aerospace Engineering, Georgia Institute of Technology.

Yu, W., and Hodges, D. H. (2005). "Generalized Timoshenko Theory of the Varational Asymptotic Beam Sectional Analysis" *Journal of the American Helicopter Society*, 50, 46~55.

Yu, W., Hodges, D. H., Volovoi, V., and Cesnik, C. E. S. (2002). "On Timoshenko-Like Modeling of Initially Curved and Twisted Composite Beams" *International Journal of Solids and Structures*, 39(19), 5101-5121.

Zhang, S. (2000). "Lateral-Torsional Buckling of Simply Supported and Cantilevered Fiber Reinforced Polymeric I-Beams", Doctoral Thesis, Civil and Environmental Engineering, Georgia Institute of Technology.

Zureick, A. H. (1998). "FRP Pultruded Structural Shapes" *Progress in Structural Engineering and Materials*, 1(2), 143-149.

VITA

Gwang-Seok Na was born on March 11, 1969 in Seoul, South Korea. He received his Bachelor of Science in Architectural Engineering from Yonsei University, Seoul, South Korea in 1993. He has two Master of Science degrees. One is in the field of Architectural Engineering from Yonsei University, Seoul, South Korea in 1995, and the other is in the field of Civil Engineering from Georgia Institute of Technology, Atlanta, Georgia in 2005. He worked as a structural engineer with Samsung Engineering & Construction and Yunwoo Structural Engineering in Seoul, South Korea from 1995 to 2002, where he performed design and analysis of various types of commercial and industrial structures. He joined the School of Civil and Environmental Engineering at Georgia Institute of Techology to pursue a Doctorate in Structural Engineering in 2002. He began to work as a structural engineer in 2007 at Atlanta, Georgia. He is married to Hye-Sook Lim and they have two daughters, Hyun-Jin and Ashley.